

# **MOLECULAR MIGRATION IN COMPLEX INDUSTRIAL FORMULATIONS**

by

**KATARZYNA MAJERCZAK**

A thesis submitted to the University of Birmingham for the degree of DOCTOR  
OF PHILOSOPHY

School of Chemical Engineering  
University of Birmingham  
August 2021

UNIVERSITY OF  
BIRMINGHAM

**University of Birmingham Research Archive**

**e-theses repository**

This unpublished thesis/dissertation is copyright of the author and/or third parties. The intellectual property rights of the author or third parties in respect of this work are as defined by The Copyright Designs and Patents Act 1988 or as modified by any successor legislation.

Any use made of information contained in this thesis/dissertation must be in accordance with that legislation and must be properly acknowledged. Further distribution or reproduction in any format is prohibited without the permission of the copyright holder.



## Abstract

Understanding migration of small molecules within polymer matrices (either additives already in the matrix or those infiltrating from adjacent media) is a challenge in many industrial systems. Migration can lead to undesirable changes in product properties, reduced shelf-lives and increased material wastage that is harmful for the environment. Herein, this challenge is addressed by studying the migration characteristics of model additives (surfactants of various head group chemistry, plasticiser, and fluorophore) in poly(vinyl alcohol) (PVA) films that are widely used in single unit detergent applications. The aim of this project is to investigate how lateral migration (x,y-migration) and vertical migration (z-migration) of small molecules affect film behaviour, establishing the mechanisms that influence this phenomenon, the molecular interactions associated, and their timescales.

To fully address the complex, multi-component nature of PVA-based films, complexity was introduced stepwise into the system. First, the migration mechanisms of a model additive (rhodamine B, RhB) were tracked through aqueous solutions of PVA, glycerol (a plasticiser) and surfactants of various head group chemistry (cationic, nonionic, and anionic) using fluorescence correlation spectroscopy. Specific intermolecular interactions and steric effects were revealed to be the primary factors influencing migration in formulations containing ionic surfactants and nonionic surfactants, respectively. Presence of the plasticiser was shown to decrease the diffusivity of the tracer, chiefly due to increased viscosity in the system. These solutions were then spin-coated, and RhB diffusion through the resultant films was tracked using fluorescence recovery after photobleaching. In films, an additional mechanism of migration was identified – compatibility of the components in the system, with phase separation of glycerol from the PVA matrix lowering the overall tracer diffusivity; again, intermolecular interactions and steric effects controlled tracer diffusivity in the surfactant-doped systems.



Third, the mechanism of surfactant migration was studied as films were aged under various environmental conditions (primarily relative humidity, RH). The plasticising effect of atmospheric water was demonstrated, with films restructuring to reach equilibrium molecular conformation. The nature and speed of the restructuring was dependent on surfactant concentration and its compatibility with the other components of the system. The properties of the PVA-based matrix were then measured upon exposing it to elevated temperature, with system compatibility overall increasing as the glass transition temperature was exceeded. A significant dependence on compatibility was observed while changing the properties of the matrix (increased degree of hydrolysis (DH) and molecular weight ( $M_w$ ) of the polymer) as well as introducing a second surfactant to the system. However, the molecular arrangement of surfactant within the polymer matrix remained the same independent of polymer DH and  $M_w$ . Overall, observed changes could be explained by the compatibility of the four components with one another, their hydrogen bonding, and other intermolecular interactions in the system.

Finally, wetting of PVA-based film by water, dodecane, or aqueous surfactant solutions of various head group chemistry were examined. Variations in solvophilic behaviour were observed upon changing the polymer crystallinity, crystallite size, size of the free volume cavities, and polymer entanglement, regardless of liquid medium. Further, matrix hydrophilicity was identified as an important factor controlling infiltration of surfactant solutions into the polymer matrix.

Through this work, importance of environmental conditions and chemical environment on molecular migration is highlighted, providing a set of variables that need to be controlled while designing migration in industrially relevant systems as well as future directions for further investigations.

## Acknowledgements

This thesis summarises a very important chapter of my life. I would like to take this opportunity to acknowledge people without whom this journey would not have been possible.

First and foremost, I would like to give my thanks to my supervisor, Dr Zhenyu Jason Zhang, for providing me with this unique opportunity to be a member of his group. His support and dedication have provided me with invaluable lessons and helped me widen my perspectives, for which I am very grateful.

I would like to extend these thanks to the whole Molecular Migration Research Consortium – collaborators from Procter & Gamble, Mondelez, AkzoNobel, as well as University of Durham and University of Sheffield – for the helpful discussions and challenging directions in the project. I gratefully acknowledge Royal Society of Chemistry for funding my research project in Procter & Gamble in Mason – although the project did not go as planned due to the pandemic, it was a very valuable experience for me, both professionally and personally.

Thanks must go to my family and friends from all over the world. Special acknowledgements should go to my partner Joe for his patience, help, and believing in me when I did not believe in myself; my brother Przemek, who has always been my role model and taught me that goals are there to be achieved; my parents, for constant approval of my life decisions; and my friend Lena, who has never fully understood why I decided to do a PhD, but was with me for better and for worse.

Finally, I would like to thank all fellow PhD students with whom I shared lab shifts, lunch breaks as well as all the joys and worries of PhD life – it would be impossible to name everyone here, but without these people this experience would have been much less enjoyable.

# Contents

Abstract .....	i
Acknowledgements .....	iii
Contents .....	iv
Chapter 1. Introduction .....	1
1.1. Project scope.....	1
1.2. Poly(vinyl alcohol).....	3
1.2.1. Crystalline region.....	7
1.2.2. Interfacial region.....	9
1.2.3. Amorphous region .....	10
1.3. Phase transitions of polymers.....	11
1.4. Additives in polymer systems .....	12
1.4.1. Plasticisers .....	12
1.4.2. Surfactants .....	22
1.5. Mechanisms of molecular migration.....	27
1.5.1. Effect of surface free energy.....	28
1.5.2. Effect of entropy .....	29
1.5.3. Effect of compatibility .....	29
1.5.4. Small molecule migration.....	32
1.5.5. Specific aspects of diffusion in thin films .....	35
1.5.6. Migration of molecules in PVA films from surrounding liquid medium .....	36
1.6. Thesis outline .....	38
Chapter 2. Materials and methods.....	40
2.1. Materials.....	40
2.2. Solution preparation .....	41
2.3. Film preparation .....	42
2.4. Atomic force microscopy .....	43
2.4.1. Operating principle .....	43
2.4.2. Contact mode .....	45
2.4.3. Dynamic modes .....	46
2.4.4. Force spectroscopy .....	47
2.4.5. Experimental procedure.....	52

2.5. Fluorescence recovery after photobleaching .....	52
2.5.1. Operating principle.....	52
2.5.2. Experimental procedure .....	54
2.6. Fluorescence correlation spectroscopy .....	56
2.6.1. Operating principle.....	56
2.6.2. Experimental procedure .....	58
2.7. Dynamic light scattering .....	59
2.7.1. Operating principle.....	59
2.7.2. Experimental procedure .....	61
2.8. Rheometry.....	61
2.8.1. Operating principle.....	61
2.8.2. Experimental procedure .....	62
2.9. Dynamic vapour sorption.....	63
2.9.1. Operating principle.....	63
2.9.2. Experimental procedure .....	64
2.10. Contact angle goniometry .....	64
2.10.1. Operating principle.....	64
2.10.2. Experimental procedure .....	66
2.11. Fourier-transform infrared spectroscopy .....	67
2.11.1. Operating principle.....	67
2.11.2. Experimental procedure .....	71
Chapter 3. Molecular diffusion in tertiary poly(vinyl alcohol) solutions.....	72
3.1. Introduction.....	72
3.2. Materials and methods .....	74
3.3. Results and discussion .....	76
3.3.1. Determining the appropriate model for PVA diffusion in solution .....	76
3.3.2. Molecular diffusion in PVA solutions .....	78
3.3.3. Molecular diffusion in PVA/glycerol binary solutions .....	81
3.3.4. Molecular diffusion in PVA/glycerol/surfactant tertiary solutions.....	86
3.4. Conclusions.....	94
Chapter 4. Kinetics of molecular migration in thin poly(vinyl alcohol)-based films.....	95
4.1. Introduction.....	95
4.2. Materials and methods .....	97
4.3. Results and discussion .....	98

4.3.1. Effect of glycerol concentration .....	98
4.3.2. Investigations into migration mechanisms in thin polymer films .....	104
4.3.3. Modelling fluorophore migration .....	108
4.3.4. RhB migration in thin films prepared from filtered solutions .....	110
4.3.5. Effect of surfactant of various head group chemistry addition.....	112
4.3.6. Modelling fluorophore migration in surfactant-doped films .....	117
4.3.7. RhB migration in surfactant-doped films prepared from filtered solutions .....	118
4.4. Conclusions .....	119
Chapter 5. Humidity- and surfactant-accelerated aging of thin polymer films .....	120
5.1. Introduction .....	120
5.2. Materials and methods.....	122
5.3. Results and discussion.....	123
5.3.1. Films aged at ambient RH .....	124
5.3.2. Films aged at various RH conditions.....	138
5.4. Conclusions .....	146
Chapter 6. Aging of surfactant-doped poly(vinyl alcohol) films at elevated temperatures ...	149
6.1. Introduction .....	149
6.2. Materials and methods.....	151
6.3. Results .....	152
6.3.1. Effect of temperature and humidity on surfactant migration.....	152
6.3.2. Anionic surfactant formulations .....	154
6.3.3. Cationic surfactant formulations.....	156
6.3.4. Nonionic surfactant formulations .....	157
6.4. Binary surfactant mixtures .....	161
6.4.1. CTAB + C <sub>12</sub> E <sub>10</sub> system .....	161
6.4.2. SDS + C <sub>12</sub> E <sub>10</sub> system .....	162
6.4.3. SDS + CTAB system.....	163
6.5. Chemical characteristics of the films .....	164
6.5.1. Single surfactant systems.....	167
6.5.2. Binary surfactant systems .....	169
6.6. Discussion .....	173
6.6.1. General remarks.....	173
6.6.2. Effect of aging conditions on migration in single surfactant systems .....	175
6.7. Conclusions .....	182

Chapter 7. Kinetics of water migration in PVA-based formulations .....	184
7.1. Introduction.....	184
7.2. Materials and methods .....	187
7.3. Results and discussion .....	187
7.3.1. Wetting models .....	187
7.3.2. General remarks on film structure.....	190
7.3.3. Effect of composition change on water spreading behaviour for thin films .....	192
7.3.4. Effect of composition change on water spreading behaviour for thick films .....	196
7.3.5. FTIR characterisation of crystallinity in PVA-based formulations .....	199
7.3.6. Effect of liquid medium change on water spreading behaviour.....	201
7.3.7. Effect of aging RH conditions on the water spreading behaviour of thick films..	215
7.4. Conclusions.....	224
Chapter 8. Conclusions.....	227
8.1. Motivation.....	227
8.2. Main findings .....	227
8.3. Final remarks .....	229
Chapter 9. Future work.....	231
Bibliography .....	234
Chapter 10. Appendices.....	251
Appendix A.....	251
Appendix B .....	254
B1. Effect of sonicating spin coating solutions on eventual film properties.....	256
Appendix C .....	258
Appendix D.....	270
D1. FTIR spectroscopy of PVA-based thick films .....	271
D2. Trends in $\Delta A$ and $\Delta V$ during ionic surfactant solution wetting .....	282
D3. Trends in $\Delta A$ and $\Delta V$ during nonionic surfactant solution wetting .....	283
Appendix E – Migration of molecules from adjacent media into PVA-based films.....	288
E1. Introduction.....	288
E2. Materials and methods .....	289
E3. Results and discussion .....	290
E4. Conclusions.....	299

## List of figures

<b>Figure 1.1.</b> Fully (a) and partially (b) hydrolysed PVA. ....	4
<b>Figure 1.2.</b> Hydrogen bonding in PVA. ....	5
<b>Figure 1.3.</b> Polymer structure that consists of amorphous and crystalline regions.....	6
<b>Figure 1.4.</b> Schematic diagram for intramolecular hydrogen bonding in the triad sequences of PVA.....	8
<b>Figure 1.5.</b> Changes of the amorphous and semicrystalline state with temperature.. ....	12
<b>Figure 1.6.</b> Schematic illustration of three-layers model. ....	36
<b>Figure 2.1.</b> AFM operating principle.. ....	44
<b>Figure 2.2.</b> Lennard-Jones potential and force distance dependence versus tip-surface separation. ....	45
<b>Figure 2.3.</b> Exemplary force curves showing cantilever deflection as a function of z-piezo displacement, demonstrating hard and soft surfaces.....	50
<b>Figure 2.4.</b> Schematic diagram of SAM–surfactant bloom interactions.....	51
<b>Figure 2.5.</b> FRAP operating principle. ....	53
<b>Figure 2.6.</b> Positions used to calculate scaled fluorescence intensity .....	56
<b>Figure 2.7.</b> (a) FCS operating principle, (b) changes of the autocorrelation function shape with concentration and diffusion coefficient, and (c) characteristic fluorescence timescales.. ....	58
<b>Figure 2.8.</b> Changes of light intensity dependent on the size of the particle and resultant autocorrelation functions.....	60
<b>Figure 2.9.</b> Graphical representation of shear flow.....	62
<b>Figure 2.10.</b> Graphical representation of a DVS experimental setup. ....	63
<b>Figure 2.11.</b> Forces influencing wetting behaviour of the system. ....	66
<b>Figure 2.12.</b> FTIR operating principle. ....	68
<b>Figure 3.1.</b> Chemical structure of compounds used in this study. ....	74
<b>Figure 3.2.</b> Preparation method for test solutions of various compositions.....	75
<b>Figure 3.3.</b> Normalised diffusion coefficient of RhB as a function of PVA concentration without and with glycerol. ....	79
<b>Figure 3.4.</b> Distribution of hydrodynamic diameter for solutions of various PVA concentration with the addition of water, glycerol stock solution and pure glycerol.....	80
<b>Figure 3.5.</b> Diffusion coefficient of RhB in PVA solution with the addition of pure glycerol. ....	85
<b>Figure 3.6.</b> Average diffusion coefficient of RhB in PVA solutions with the addition of surfactant and water or glycerol solution, compared against control samples with no surfactants .....	87
<b>Figure 3.7.</b> Possible interactions between RhB and both cationic and anionic surfactants; PVA –surfactant tail group interactions, using SDS molecule as an example. ....	89
<b>Figure 3.8.</b> Particle size distribution for PVA/water/surfactant, PVA/glycerol/surfactant solutions and PVA/pure glycerol/pure surfactant solutions.....	90
<b>Figure 3.9.</b> Average diffusion coefficients of RhB in PVA solutions with the addition of pure glycerol and surfactant compared against equivalent samples with the addition of glycerol and surfactant solutions and corresponding control solutions containing no surfactant .....	93

<b>Figure 4.1.</b> Morphology and height profile of compositions (a,b) A, (c,d) C and (e,f) D investigated using AFM. ....	99
<b>Figure 4.2.</b> Recorded diffusion coefficients of RhB in samples A-F. ....	100
<b>Figure 4.3.</b> (a) FRAP recovery curve for representative position for pure glycerol sample, (b,c) AFM image and surface profile of pure glycerol sample (scratch region).....	103
<b>Figure 4.4.</b> Fluorescence recovery curve for samples of compositions (a) C, (b) D, (c) C with increased bleach size, and (d) C prepared from filtered solutions (dots) and fits to Equation 4.1 (lines).....	105
<b>Figure 4.5.</b> Graphic representation of diffusion-uncoupled mechanism and diffusion-coupled mechanism. ....	107
<b>Figure 4.6.</b> Comparison of average diffusion coefficient for filtered and non-filtered solutions A–F. ....	111
<b>Figure 4.7.</b> Average diffusion coefficient and its distribution for surfactant-doped films prepared from filtered and non-filtered solutions.....	113
<b>Figure 4.8.</b> Morphology and surface profiles of sample G (a,b) in the absence of RhB and (c,d) containing RhB; sample H doped with RhB: (e,f) background morphology and (g,h) surface features.....	115
<b>Figure 5.1.</b> Morphology and height profile of: (a,b) PVA film and (c,d) glycerol-plasticised PVA film on day 0.....	125
<b>Figure 5.2.</b> AFM image and height profile of plasticised PVA film with CTAB addition..	126
<b>Figure 5.3.</b> AFM image and height profile of plasticised PVA containing SDS.....	129
<b>Figure 5.4.</b> AFM images and height profiles of (a,b) spin-coated, glycerol-plasticised film with 20 wt% C <sub>12</sub> E <sub>10</sub> on day 0 and (c,d) day 7 (exhibiting chequerboard pattern of surfactant blooms); (e,f) solution cast thick film with 1 wt% C <sub>12</sub> E <sub>10</sub> , and (g,h) SDS blooms on the surface of plasticised PVA thick film with 1 wt% SDS.....	133
<b>Figure 5.5.</b> CFM measurements on areas without surfactant blooms: (a) day 0, and (b) day 7; surfactant blooms/crystals on: (c) day 0, and (d) day 7.....	135
<b>Figure 5.6.</b> Exemplary force curves obtained from (a) acid- and (b) methyl-terminated cantilevers. Bg stands for background – regions without surfactant blooms. ....	137
<b>Figure 5.7.</b> Equilibrium water sorption versus RH for (a,c,e) absorption and (b,d,f) desorption processes.....	140
<b>Figure 5.8.</b> AFM image and height profile of a bloom on the surface of plasticised PVA film containing 1 wt% SDS stored at 55% RH for 3 days. ....	144
<b>Figure 5.9.</b> AFM image and height profile of plasticised PVA doped with SDS stored at various RH conditions.....	145
<b>Figure 6.1.</b> Morphology and height profile of: (a,b) 87PVA film plasticised with glycerol and (c,d) 99PVA film plasticised with glycerol on day 0. ....	154
<b>Figure 6.2.</b> Morphology and height profile of plasticised 87PVA film containing 1 wt% SDS .....	155
<b>Figure 6.3.</b> Morphology and height profile of plasticised 99PVA film containing 1 wt% SDS stored at elevated temperature on day 0 .....	155
<b>Figure 6.4.</b> Morphology and height profile of plasticised 87PVA films containing 5 wt% CTAB. ....	156
<b>Figure 6.5.</b> Morphology and height profile of plasticised 87PVA films containing C <sub>12</sub> E <sub>10</sub> ..	158



<b>Figure 6.6.</b> Morphology and height profile of plasticised 99PVA films containing 10 wt% C <sub>12</sub> E <sub>10</sub> .....	159
<b>Figure 6.7.</b> Morphology and height profile of plasticised 99PVA films containing 10 wt% C <sub>12</sub> E <sub>10</sub> stored at low RH conditions. ....	160
<b>Figure 6.8.</b> Morphology and height profile of plasticised 87PVA films containing 5 wt% CTAB and 10 wt% C <sub>12</sub> E <sub>10</sub> .....	162
<b>Figure 6.9.</b> Morphology and height profile of plasticised 87PVA films containing 1 wt% SDS and 10 wt% C <sub>12</sub> E <sub>10</sub> .....	163
<b>Figure 6.10.</b> Morphology and height profile of plasticised 87PVA films containing 5 wt% CTAB and 1 wt% SDS.....	164
<b>Figure 6.11.</b> AFM force curve measurements on samples prepared with 99PVA.....	166
<b>Figure 6.12.</b> Representative force curves for: (a,c) acid-terminated cantilever, measurements on samples on day 0 and day 7, respectively; (b,d) methyl-terminated cantilever, measurements on plasticised 99PVA samples on day 0 and day 7, respectively; (e,f) acid- and methyl-terminated cantilever 87PVA on samples doped with two surfactants.....	168
<b>Figure 6.13.</b> (a,e) Height and (c,g) friction channels for SDS+CTAB samples for acid-terminated cantilever with corresponding height profiles; (i,k) height and friction channels, respectively, for SDS+CTAB samples for methyl-terminated cantilever with corresponding height profiles. ....	171
<b>Figure 7.1.</b> Morphology and height profile of: (a,b) spin-coated plasticised 87PVA film, (c,d) solution cast 87PVA film, (e,f) solution cast plasticised 87PVA film, (g,h) spin-coated 99PVA film, (i,j) solution cast 99PVA film, and (k,l) solution cast plasticised 99PVA film.....	191
<b>Figure 7.2.</b> (a) CA evolution for spin-coated PVA films of various composition. (b) Corresponding geometrical investigations for spin-coated samples prepared using 1000 rpm spin speed.....	192
<b>Figure 7.3.</b> Fitted values to the model by Farris et al for parameters (a) <i>k</i> and (b) <i>n</i> for spin-coated and solution cast films. ....	195
<b>Figure 7.4.</b> (a) CA evolution for solution cast PVA-based films of various composition prepared from solutions of 10% (w/v) concentration (400 μl). (b) Corresponding geometrical investigations for these samples.....	197
<b>Figure 7.5.</b> FTIR spectra of PVA-based films of various composition prepared from solutions of 10% (w/v) concentration (400 μl). ....	200
<b>Figure 7.6.</b> Fitted values to the model by Farris et al for parameters (a,c) <i>k</i> and (b,d) <i>n</i> for solution cast and spin-coated formulations, respectively, during spreading of surfactant solutions and dodecane compared against water. ....	205
<b>Figure 7.7.</b> CA evolution with time and corresponding geometrical investigations for solution cast films prepared from solutions of 10% (w/v) concentration (400 μl).....	207
<b>Figure 7.8.</b> CA evolution with time and corresponding geometrical investigations for spin-coated films prepared from solutions of 4% (w/v) concentration (1209 μl).....	209
<b>Figure 7.9.</b> Box and whisker graphs of Farris model fits for parameter (a) <i>k</i> and (b) <i>n</i> for spreading of water on samples stored at various RH conditions. ....	216
<b>Figure 7.10.</b> CA evolution with time and corresponding geometrical investigations for solution cast films. ....	218

<b>Figure 7.11.</b> FTIR spectra of solution cast PVA-based films stored at various RH conditions, compared against freshly prepared samples.....	220
<b>Figure 10.1.</b> FCS autocorrelation functions of PVA solutions of various concentrations (compositions 2-6).....	251
<b>Figure 10.2.</b> DLS autocorrelation functions of (a) PVA solutions of compositions 2-6 and (b) PVA/glycerol solution compositions 2a-5a.....	252
<b>Figure 10.3.</b> Average size distribution for C <sub>12</sub> E <sub>10</sub> stock solution investigated by DLS. ....	253
<b>Figure 10.4.</b> Sample preparation procedure used for FRAP measurements.....	254
<b>Figure 10.5.</b> Films of composition D containing (a) Alexa 488 C5 Maleimide at 3.4 nM in the spin coating solution – image size 214 μm and (b) Alexa 488 carboxylic acid at 3.4 nM in the spin coating solution – image size 60.7 μm. ....	254
<b>Figure 10.6.</b> Morphology of the pure glycerol films doped with RhB –image obtained from optical microscope connected with AFM. ....	256
<b>Figure 10.7.</b> Optical microscope image of the bloom region (framed) in a plasticised PVA film containing 3 wt% CTAB after two months of sample storage. The length of the protruding cantilever is ca. 125 μm.....	258
<b>Figure 10.8.</b> Optical microscope image of the bloom region (framed) for a film containing 4 wt% CTAB after 2 weeks of sample storage.....	258
<b>Figure 10.9.</b> Optical microscopy image of surfactant blooms and crystals visible on the surface of a film containing 5 wt% CTAB .....	258
<b>Figure 10.10.</b> Optical microscope image of bloom region for a sample containing 2 wt% SDS on day 0. ....	258
<b>Figure 10.11.</b> Optical microscope image of a bloom region (framed) for a sample containing 5 wt% SDS on day 0.....	259
<b>Figure 10.12.</b> Optical microscope image of a bloom region for a sample containing 20 wt% C <sub>12</sub> E <sub>10</sub> on day 7.....	259
<b>Figure 10.13.</b> FTIR spectra of solution-cast PVA films, comparing between different thicknesses. (a) 87PVA, (b) plasticised 87PVA, (c) 99PVA, and (d) plasticised 99PVA.....	274
<b>Figure 10.14.</b> Raman spectroscopy operating principle. Reproduced from reference 440. ...	290
<b>Figure 10.15.</b> Mass change over time for PVA films stored at various solvents. ....	291
<b>Figure 10.16.</b> Raman spectra for pure components (solvent, PVA film and surfactant) and solutions of surfactant in non-aqueous solvent for investigated compositions. ....	293
<b>Figure 10.17.</b> AFM images and surface profiles of 87PVA-based films in contact with non-aqueous solvent (control samples).....	296
<b>Figure 10.18.</b> Images from the optical microscope connected to the AFM instrument: (a) solvent visible on the surface of the sample, (b) surface features after drying the film surface with compressed air, and (c) morphology of the film created from fully hydrolysed PVA...	297
<b>Figure 10.19.</b> AFM images and surface profiles of 99PVA-based films in contact with non-aqueous solvent with 15 wt% SDS addition.....	298

## List of Tables

<b>Table 1.1.</b> Lattice parameters of the two crystal structures of PVA (adapted from reference 62). .....	7
<b>Table 2.1.</b> Details of the chemicals used in this thesis. ....	40
<b>Table 3.1.</b> Compositions used to investigate the dependence of RhB diffusion coefficient on PVA concentration.....	78
<b>Table 3.2.</b> Composition of PVA-based solutions with the addition of glycerol. ....	81
<b>Table 3.3.</b> Viscosity and average hydrodynamic diameter of PVA solutions with the addition of glycerol and surfactant of various head group chemistry. ....	86
<b>Table 4.1.</b> Compositions and thickness of investigated thin films. Calculations of the glycerol content in the films do not include water present in the films. ....	98
<b>Table 4.2.</b> Immobile molecules data and bleaching data for samples A-F. ....	102
<b>Table 4.3.</b> Half recovery times for different bleach radii as a function of film composition. ....	106
<b>Table 4.4.</b> Average $\tau_{1/2}$ and normalised amplitude for fast and slow migrating molecules for investigated samples. ....	110
<b>Table 5.1.</b> Average SFE values for freshly prepared formulations and those aged for one week. .....	136
<b>Table 5.2.</b> Experimental plan for investigation into effect of RH conditions on morphology of the thin films. ....	143
<b>Table 6.1.</b> Average SFE values for freshly prepared formulations on day 0 and day 7, and thickness for freshly prepared investigated samples. ....	153
<b>Table 7.1.</b> CMC and $N_{agg}$ values for surfactants used in this study. ....	206
<b>Table 10.1.</b> Average diffusion coefficient of Rhodamine B in samples of various compositions ( $T \approx 28^\circ\text{C}$ ). ....	251
<b>Table 10.2.</b> Images obtained from confocal microscope for PVA/glycerol/surfactant films doped with RhB. ....	255
<b>Table 10.3.</b> Average radius of FRAP bleach for samples A-I. ....	256
<b>Table 10.4.</b> The average diffusion coefficient for the sample C prepared from solution with and without sonication. ....	257
<b>Table 10.5.</b> Average half recovery times and normalised amplitude for fast and slow migrating molecules for investigated samples prepared from filtered solutions. ....	257
<b>Table 10.6.</b> Thickness of PVA-based samples doped with surfactants of various head group chemistry and concentration investigated using AFM scratch test. ....	260
<b>Table 10.7.</b> Thickness (% changes) of the PVA-based samples doped with surfactants of various head group chemistry and concentration investigated as in Table 10.6. ....	261
<b>Table 10.8.</b> Thickness of PVA-based samples doped with surfactants of various head group chemistry and concentration investigated using AFM scratch test. ....	262
<b>Table 10.9.</b> Thickness (% changes) of PVA-based samples doped with surfactants of various head group chemistry and concentration investigated as in Table 10.8. ....	264
<b>Table 10.10.</b> Average thickness and thickness range of solution cast PVA-based samples doped with surfactants of various head group chemistry and concentration. ....	267
<b>Table 10.11.</b> Time required to reach equilibrium (in minutes) for thick PVA-based samples doped with surfactants of various head group chemistry and concentration investigated using DVS. ....	268

<b>Table 10.12.</b> Thickness, roughness, SFE, and fit parameters to Equation 7.1 for PVA films with various compositions. ....	270
<b>Table 10.13.</b> CA evolution parameters for investigated compositions using water as the medium. ....	271
<b>Table 10.14.</b> FTIR absorption bands of PVA films. ....	272
<b>Table 10.15.</b> Average DC values for all investigated compositions. ....	273
<b>Table 10.16.</b> Fit parameters to Equation 7.1 for spreading of SDS solution on the surface of the films of various compositions. ....	275
<b>Table 10.17.</b> Fit parameters to Equation 7.1 for spreading of CTAB solution on the surface of the films of various compositions. ....	276
<b>Table 10.18.</b> Fit parameters to Equation 7.1 for spreading of C <sub>12</sub> E <sub>10</sub> solution on the surface of the films of various compositions. ....	277
<b>Table 10.19.</b> Fit parameters to Equation 7.1 for spreading of dodecane on the surface of the films of various compositions. ....	278
<b>Table 10.20.</b> CA evolution parameters for investigated compositions using CTAB solution as the medium. ....	279
<b>Table 10.21.</b> CA evolution parameters for investigated compositions using SDS solution as the medium. ....	280
<b>Table 10.22.</b> CA evolution parameters for investigated compositions using C <sub>12</sub> E <sub>10</sub> solution as the medium. ....	281
<b>Table 10.23.</b> CA evolution parameters for investigated compositions using dodecane as the medium. ....	282
<b>Table 10.24.</b> Average DC values for all investigated compositions after one week of storage at controlled RH. ....	284
<b>Table 10.25.</b> Fit parameters to Equation 7.1 for spreading of water on the surface of the films of various compositions after storing at 4% RH conditions. ....	285
<b>Table 10.26.</b> Fit parameters to Equation 7.1 for spreading of water on the surface of the films of various compositions after storing at 45% RH conditions. ....	285
<b>Table 10.27.</b> Fit parameters to Equation 7.1 for spreading of water on the surface of the films of various compositions after storing at 100% RH conditions. ....	286
<b>Table 10.28.</b> CA evolution parameters for investigated compositions stored at 4% RH using water as the medium. ....	286
<b>Table 10.29.</b> CA evolution parameters for investigated compositions stored at 45% RH using water as the medium. ....	287
<b>Table 10.30.</b> CA evolution parameters for investigated compositions stored at 100% RH using water as the medium. ....	287

## List of symbols and abbreviations

$\tau_{1/2}$	Fluorescence half recovery time
$\Delta A$	Changes in droplet surface area
$\Delta V$	Changes in droplet volume
(w/v)%	Weight per volume percent
AFM	Atomic force microscopy
$c^*$	Overlap concentration
$C_{12}E_{10}$	Decaethylene glycol monododecyl ether
CA	Contact angle
CAC	Critical aggregation concentration
CFM	Chemical force microscopy
CM	Contact mode
CMC	Critical micelle concentration
CTAB	Hexadecyltrimethylammonium bromide
$D$	Diffusion coefficient
DC	Degree of crystallinity
$D_{DLS}$	Diffusion coefficient of the particle obtained from DLS
$D_{FRAP}$	Effective diffusion coefficient of the fluorophore in the thin film
DH	Degree of hydrolysis
$d_H$	Hydrodynamic diameter
DLS	Dynamic light scattering
DSC	Differential scanning calorimetry
DVS	Dynamic vapour sorption
FCS	Fluorescence correlation spectroscopy
FRAP	Fluorescence recovery after photobleaching
FTIR	Fourier-transform infrared spectroscopy
$G(\tau)$	Autocorrelation function
HLB	Hydrophilic-lipophilic balance
HPLC	High performance liquid chromatography
ICM	Intermittent contact mode
$I_N$	Normalised fluorescence intensity

$I_{N,fast}$	Normalised amplitudes of the fraction of fast migrating molecules
$I_{N,slow}$	Normalised amplitudes of the fraction of slow migrating molecules
$k$	Rate of contact angle evolution
$m$	Isotactic (meso) tacticity
$M_w$	Molecular weight
$n$	Parameter describing the dominant wetting phenomenon
NCM	Non-contact mode
$n_{FCS}$	Scaling parameter related to the polymer chain excluded volume
NMR	Nuclear magnetic resonance
PEG	Poly(ethylene glycol)
PVA	Poly(vinyl alcohol)
PVAc	Poly(vinyl acetate)
$r$	Syndiotactic (racemic) tacticity
$R_g$	Radius of gyration
RH	Relative humidity
RhB	Rhodamine B
$R_q$	Root mean square roughness
SAXS	Small angle X-ray scattering
SDS	Sodium dodecyl sulfate
SFE	Surface free energy
$T_{cp}$	Cloud point
$T_g$	Glass transition temperature
$T_k$	Krafft point
$T_m$	Melting temperature
wt%	Weight percent
XRD	X-ray diffraction



# Chapter 1. Introduction

## 1.1. Project scope

Complex polymer formulations have become an almost indispensable part of everyday life in the form of hygiene products, paints, and food. Due to the presence of many constituents (small molecules) within these systems, however, unintended changes in material structure (e.g. blooming, segregation, leaching, or even release of toxic additives into the atmosphere) may occur. These changes are a consequence of molecular movement – both lateral (within the x, y plane relative to the material surface) and vertical (within the z direction) migration – that is dependent on many factors including compatibility with matrix constituents, component surface tension, and ability to self-assemble into mesophases. Moreover, they are further influenced by environmental factors during aging (e.g. relative humidity (RH), temperature, or chemical environment). As a result, these systems can exhibit long term non-equilibrium behaviour that is difficult to predict due to complexity of the system, potentially affecting their operational life cycle.

An exemplary complex mixture where these phenomena are of utmost importance is water-soluble poly(vinyl alcohol) (PVA)-based films used in packaging applications. PVA exhibits a range of industrially desirable properties – characterised by good film forming capability,<sup>1,2</sup> low toxicity,<sup>2</sup> excellent barrier properties,<sup>3,4</sup> and biodegradability.<sup>5,6</sup> However, other properties of pure PVA such as brittleness and low flexibility<sup>7</sup> need to be improved before its application to many sectors of industry. Finished artificial products use formulations of polymer and several property-enhancing additives (e.g. plasticisers, antioxidants, or reinforcements).<sup>8</sup> While mechanical properties of the material are improved, the presence of many additives included in the formulation leads to substantial issues during aging, as described



above. Paving a way to understand these difficult to predict systems can therefore result in environmentally friendly, functionalised to purpose products with enhanced performance and prolonged shelf life.

PVA films commonly used in the packaging industry are ca. 70  $\mu\text{m}$  thick (e.g. the plastic film surrounding a single unit laundry pod). Due to the long time scales for migration in these micron-thick films and limited experimental techniques that can analyse migration within the bulk solid, simplified systems must first be investigated. Understanding migration phenomena in thin (ca. 100 nm thick) films and on shorter time scales will enable conclusions to be drawn about general trends that can then be translated to more industrially relevant formulations. Similarly, adding new chemical species piecemeal will enable important insight to be gained into the action of individual components and combinations of additives on the system behaviour. In real-world applications, the chemical species can be either in contact with a polymer film (in the case of single unit laundry pods, contact with washing water or surfactant solutions enclosed within the pouch) or be already incorporated in the matrix (e.g. surfactants and plasticisers improving film forming properties). This is of particular importance when considering the process of pouch preparation: the seal is formed by partial dissolution of PVA film, followed by two films being placed together. Sealing between these two films is a result of interdiffusion of polymer chains, that can be significantly influenced by migration of other components in the system and film aging. Therefore, by sequentially investigating the action of each additive in the system, molecular migration can be described from nano- to microscale, enabling further extension to multi-component systems in contact with various media.

This project aims to understand the migration behaviour of model additives (surfactants of various head group chemistry, fluorophore, and plasticiser) in PVA films to establish

migration mechanisms, timescales, and factors influencing this phenomenon. Specifically, this is achieved by:

1. Developing the methodology to probe molecular migration using advanced microscopy techniques.
2. Investigating the kinetics of molecular migration both in 2- and 3-dimensional contexts.
3. Evaluating the effect of environmental conditions on molecular migration in complex mixtures.
4. Identifying the factors controlling migration.

## **1.2. Poly(vinyl alcohol)**

PVA is the quintessential example of a broadly used polymer. Its high degree of water solubility in combination with adhesive properties and resistance to oil, grease and other nonaqueous solvents lead to application in many industries.<sup>9-11</sup> PVA is biocompatible,<sup>12</sup> nontoxic, noncarcinogenic, bioadhesive, and shows low acute oral toxicity.<sup>13</sup> Further, it is the only known polyolefin that can be biodegraded.<sup>14</sup> Combined, these properties create an opportunity for PVA to be increasingly used in the medical,<sup>4,12,13,15,16</sup> food packaging,<sup>4</sup> and consumer goods industries.<sup>17</sup> However, due to its low decomposition temperature and high glass transition temperature ( $T_g$ ), PVA needs to be modified to mitigate its disadvantages and maintain desired properties. This can be achieved using modification methods e.g. carboxymethylation<sup>18</sup> or introduction of additives to the system.<sup>16</sup> For example, in applications where the brittleness and flexibility of PVA needs to be improved while retaining satisfactory tensile and shear stress, addition of compatible plasticisers was shown to give desirable result.

The monomer of PVA (vinyl alcohol) does not exist in a stable form,<sup>19,20</sup> rearranging spontaneously to its tautomer, acetaldehyde.<sup>21</sup> Hence, PVA is produced by hydrolysing

poly(vinyl acetate) (PVAc). This reaction usually does not convert all the acetate groups into hydroxyl groups, producing PVA resins of various degrees of hydrolysis (DH, Figure 1.1) – percent conversion of acetate groups to hydroxyl groups that is dependent on extent of the reaction.

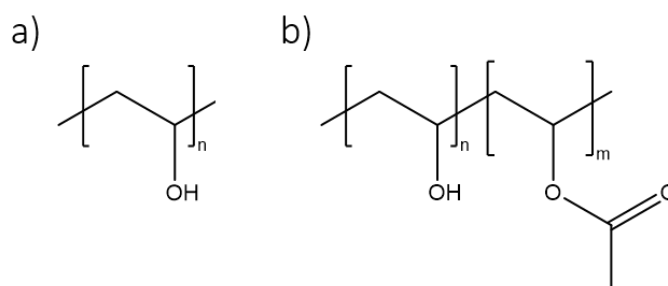


**Figure 1.1.** Fully (a) and partially (b) hydrolysed PVA.

Many unique properties of PVA, for instance the ability to exhibit high crystallinity, are caused by the presence of hydroxyl groups on the backbone and consequent hydrogen bonding.<sup>22</sup> Being weaker than ionic bond and covalent bonds (generally  $> 300$  kJ/mol each),<sup>23</sup> but much stronger than Van der Waals interactions (ca. 2 kJ/mol),<sup>23</sup> hydrogen bonding (ca. 20 kJ/mol)<sup>23</sup> is responsible for unique properties of some chemicals. Hydrogen bonds form between atoms in the same or different molecules where one atom of the pair (donor) – usually fluorine, nitrogen, or oxygen – is covalently bonded to a hydrogen atom (FH, -NH, -OH) across which electrons are shared unequally. Therefore, slight positive charge is taken by hydrogen due to its lower electronegativity. At the same time, fluorine, nitrogen, or oxygen exhibit negative charges because of the higher electronegativity and presence of electron lone pairs. Hydrogen bonding is formed at the confluence of two of these electronegative elements, ‘sandwiching’ the hydrogen atom between them (seen in Figure 1.2).

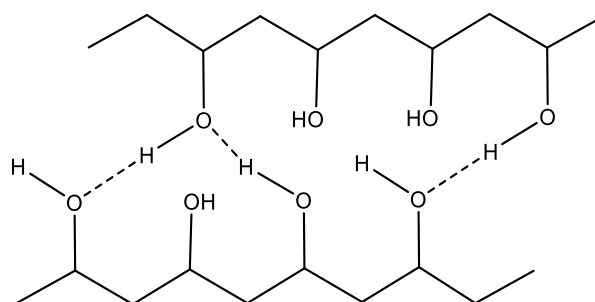


**Figure 1.2.** Hydrogen bonding in PVA.

Hydrogen bonding and DH are intimately linked in PVA polymers. With increasing DH, two effects are observed: firstly, the resin solubility in water decreases.<sup>24</sup> Residual acetate groups disrupt polymer-polymer inter- and intrachain hydrogen bonds, leading to preferential polymer-solvent interactions. Conversely, in almost fully hydrolysed PVA, physical entanglements due to higher hydrogen bond density retards dissolution in the solvent. While for resins of lower DH solubility does not depend on the polymer molecular weight ( $M_w$ ), solubility of highly hydrolysed PVA decreases while  $M_w$  increases.<sup>25</sup> Secondly, increased DH facilitates PVA crystallisation – measured by the degree of crystallinity (DC) – leading to a more homogeneous distribution of crystallites.<sup>5,26</sup> However, while higher DC may suggest improved regularity of the matrix structure, this conclusion is not valid for PVA due to possible changes in the head/tail chain configurations.<sup>27</sup> Chain mobility in samples with higher crystallinity is decreased, resulting in higher  $T_g$ <sup>28</sup> and melting temperature ( $T_m$ ).<sup>29</sup> Similarly, changes in polymer  $M_w$  and DH result in differences in swelling, Young's modulus,<sup>13</sup> and surface activity for otherwise moderately surface active PVA.<sup>30</sup> In addition to the previously mentioned parameters, the amount, distribution and nature of crystallites are also dependent on pre- and post- processing conditions. Possible ways to change PVA crystallinity include:

- A) Crosslinking (chemical,<sup>31–33</sup> physical,<sup>24,34–36</sup> or irradiative<sup>37,38</sup>)
- B) Thermal annealing<sup>36,39,40</sup>
- C) Changes in film drying rates<sup>32,41–44</sup>

- D) Changes in RH<sup>42</sup>
- E) Choice of solvent for film preparation<sup>40,45,46</sup>
- F) Mechanical stretching<sup>47-49</sup>
- G) Introducing additives into the matrix<sup>50,51</sup>

PVA films have a semicrystalline nature regardless of DH or  $M_w$ , with lack of long-range order and stiffness typical for a crystal, but only short-range order and stiffness (Figure 1.3).<sup>52</sup> There is still ongoing discussion about the best model to represent PVA film morphology. A three-phase model assumes that there are three solid states that this polymer can exhibit: amorphous, interfacial (a “rigid amorphous” layer of less mobile non-crystalline chains), and crystalline, hence, making the term ‘crystallinity’ an approximate one.<sup>53</sup> While this model was confirmed by nuclear magnetic resonance (NMR) measurements,<sup>54-56</sup> recent differential scanning calorimetry (DSC) and fluorescence correlation spectroscopy (FCS) analysis found no evidence of a third phase, showing that the polymer can instead be described using a two-phase model.<sup>57</sup> The latter model is more frequently used<sup>58</sup> due to its simplicity. Below, descriptions of crystalline, interfacial, and amorphous region of PVA are given.

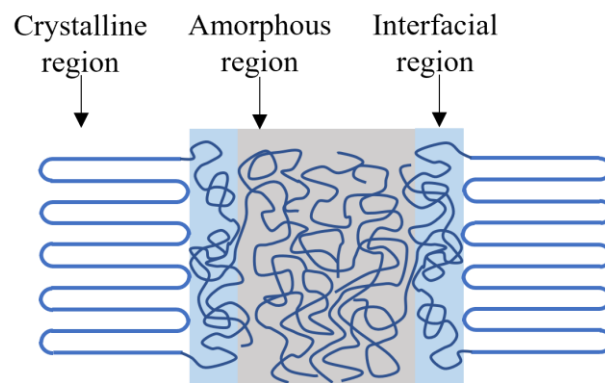


**Figure 1.3.** Polymer structure that consists of amorphous and crystalline regions.

### 1.2.1. Crystalline region

PVA chains in the crystalline region have a zigzag planar conformation with molecular repeat distance equal to  $2.52 \text{ \AA}$ <sup>59,60</sup> and hydroxyl groups distributed in isotactic, atactic or syndiotactic manner (Figure 1.4). Based on a detailed X-ray diffraction (XRD) investigation, Colvin<sup>61</sup> postulated that PVA has two crystal polymorphs: monoclinic and orthorhombic (lattice parameters given in Table 1.1), with a structural preference for the monoclinic system. Indeed, this structure in PVA was discovered in 1948 by Bunn,<sup>60</sup> who suggested that monoclinic unit cell is packed by chains in a lamellar, trans-planar conformation. Small crystallites dispersed in an amorphous region of the matrix are created via folding of the chain.<sup>62</sup> Hence, there is a minimum chain length of PVA necessary to create those crystalline lamellar structures.<sup>63</sup> Strong hydrogen bonds hold together the double layer of molecules, while Van der Waals forces of weaker nature operate between the double layers.<sup>60</sup> Lamellar structures created this way usually have lateral dimensions much larger than their thicknesses and often build up in stacks.<sup>64</sup> Because of this, a two-phase PVA model with one-dimensional crystalline stacks is normally applied for the polymers morphology, especially for small angle X-ray scattering (SAXS) measurements.<sup>65</sup>

**Table 1.1.** Lattice parameters of the two crystal structures of PVA (adapted from reference 61).

<b><math>\alpha</math> form (monoclinic)</b>	<b><math>\beta</math> form (orthorombic)</b>
$a = 15.58 \text{ \AA} \pm 0.02 \text{ \AA}$	$a = 15.86 \text{ \AA} \pm 0.03 \text{ \AA}$
$b = 7.59 \text{ \AA} \pm 0.01 \text{ \AA}$	$b = 5.95 \text{ \AA} \pm 0.02 \text{ \AA}$
$c = 10.65 \text{ \AA} \pm 0.02 \text{ \AA}$	$c = 10.54 \text{ \AA} \pm 0.03 \text{ \AA}$
$\beta = 96^\circ 00' \pm 10'$	—

A similar model of PVA crystal topology was suggested by Sakurada.<sup>59</sup> While his model suggested corrections to the Bunn model (in orientation of the molecules and directions of intermolecular hydrogen bonding within crystal lattices of similar parameters), it corresponds

to higher packing energy and was confirmed experimentally<sup>66</sup> and computationally<sup>67,68</sup> to be less appropriate compared to the Bunn model.

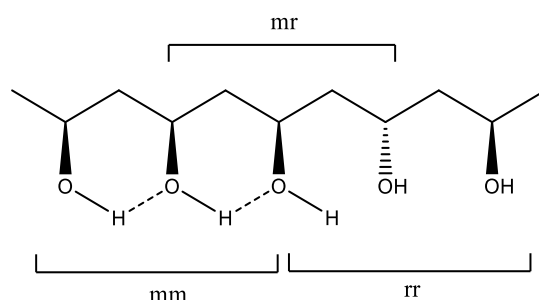


**Figure 1.4.** Schematic diagram for intramolecular hydrogen bonding in the triad sequences of PVA. Symbols stand for: m – isotactic (meso) tacticity, r – syndiotactic (racemic) tacticity. Adapted from reference 54.

The overall tacticity of the polymer (determined by the percentage of *m* or *r* dyads – Figure 1.4) plays an important role in resultant crystallinity of the polymer sample. Increased regularity in hydroxyl group arrangement (associated with both isotacticity and syndiotacticity) do not lead to increase in crystallinity of the polymer film, with crystallinity decreasing in the following order:<sup>69</sup>

$$\text{Atactic} \geq \text{syndiotactic-rich} \gg \text{isotactic-rich}$$

Naturally, one may expect that syndiotactic polymers would crystallise more easily due to the perfectly alternating nature of the hydroxyl groups. A possible explanation for the preference towards crystallisation of atactic chains may come from imperfections in chain folding, itself a consequence of the film preparation method. Stereoregularity of PVA chains also influences the character of the created hydrogen bonding (intra- or intermolecular), both in crystalline and non-crystalline regions, in turn affecting crystallite structure. For instance, it was proven that probability of intra- and intermolecular hydrogen bond creation is nearly equal for *mm* sequences,<sup>54</sup> syndiotactic samples predominantly create intermolecular hydrogen bonds, while isotactic samples – intramolecular hydrogen bonds.<sup>69</sup> This fact, and consequent changes in chain mobility, were used to explain differences in water resistance of PVA samples

of different tacticities. While atactic material has the highest degree of crystallinity, syndiotactic-rich and isotactic-rich PVA are more water-resistant.<sup>69</sup>

Regardless of chain tacticity, bulk PVA melts between 220°C and 240°C.<sup>24</sup> Normally, crystalline fraction in polymer films does not exceed 40 wt%.<sup>32</sup> However, by applying changes (multiple freeze-thaw cycles<sup>35</sup> or very slow drying at high RH<sup>32</sup>) in the polymer film preparation, it is possible to reach crystallinity of above 70 wt%.

### **1.2.2. Interfacial region**

Aside from crystalline and amorphous regions, a less mobile non-crystalline region was distinguished and associated with interfacial areas between the lamellar crystals and the fully amorphous phase. Interfacial regions have been identified in PVA by NMR measurements, where <sup>13</sup>C spin-lattice relaxation analyses suggested three components with various relaxation times existing in each polymer film.<sup>54</sup> Such a definition of the so-called rigid amorphous region enables polymer morphology to be described using a one-dimensional layer stack model. However, assumptions need to be made about the thickness of both interfacial layer and crystal lamellae. It was proven that assumption of constant layer thickness independent of the lamellae thickness gives satisfactory results.<sup>65</sup>

Although interfacial regions are amorphous, they are in the glassy state.<sup>65</sup> Therefore, their presence is not identifiable by DSC in the usual conditions used for investigating  $T_g$ .<sup>70</sup> The fraction of rigid amorphous region within a polymer matrix is dependent on many factors, including:<sup>71</sup>

- chain flexibility and crystallization conditions (high temperature and increasing chain flexibility decreases its prevalence),
- crystal size (at low crystallization temperatures, the main mechanism of crystal formation is via branching, creating small crystallites with large interfacial area. Hence,



fraction of rigid amorphous region will increase),

– the degree of irregularity of the lamellar crystal stacking.

Due to the metastable nature of the rigid amorphous fraction, reorganisation and recrystallization can occur during analysis.<sup>72</sup>

### 1.2.3. Amorphous region

The amorphous state is characterised by a presence of only short-range order, providing elasticity and flexibility. In the absence of cross-linking agents, large rotational barriers, or strong inter-chain interactions, low tensile strength is exhibited by amorphous polymers.<sup>73</sup>  $T_g$  of amorphous PVA films is within the range of 70-85°C, with a value of 85°C reported for dry films that decreases in the presence of solvents.<sup>74</sup> Hence, in ambient conditions, PVA is in its glassy state.

There is ongoing discussion about the appropriate model to describe the long-range order of polymer chains within the amorphous region. All established models, however, seem to contain elements suggested by random coil<sup>75</sup> and Kargin<sup>76</sup> models. In the random coil model, conformations of the chains are similar to those present in the perfect (or theta) solvent. Conversely, the Kargin model claims that the polymer chains in amorphous region exist as aggregates in parallel alignment.<sup>76</sup> In atactic PVA amorphous regions, like in the crystalline region, intra- and intermolecular hydrogen bonds are formed according to a statistical distribution. However, unlike in the crystalline region, two conformations are present: trans and gauche, and are randomly distributed along the chains.<sup>77</sup>

The overall percentage of amorphous region is very important when considering transport of any molecular species (water, additives etc.) in PVA films, as well as transport of charge.<sup>28</sup> This transport takes place almost exclusively in the amorphous region due to its flexible molecular structure. Hence, the greater overall rate of amorphous region, the higher

migration rate of guest molecules present in the system. In this thesis, any migration is therefore going to be considered as taking place in the amorphous region.

### 1.3. Phase transitions of polymers

To determine the main polymer properties, phase transitions of polymers as well as the temperatures at which they take place need to be known. Due to their very long molecular structure, polymers cannot be divided into the traditional gas-solid-liquid states. They decompose before boiling, are only rarely purely crystalline in solid phase and show only thermodynamically metastable states in liquid phase.

At low temperatures, polymer molecules in the amorphous region do not show the tendency for significant movement, but only for slight vibration. In this state, called the glassy state, the polymer is brittle, rigid and hard. The glassy state is also characterised by the presence of both short-range order and stiffness. Once the polymer is heated, its backbone atoms are free to rotate around the carbon-carbon bond axis, increasing the overall material flexibility and decreasing hardness (rubbery state). Polymers in the rubbery state show only short-range order and have all property of liquids except short-timescale fluidity. The state of the polymer matrix influences many properties of polymers, such as diffusion coefficient resulting in much slower diffusion in glassy polymers than rubbery ones.<sup>78</sup>

The amorphous region of polymer makes a transition from the glassy to the rubbery state at  $T_g$ . As the glassy state is not in equilibrium, this value is not unique and is influenced by multiple factors such as measurement method, rate of heating and cooling as well as polymer  $M_w$ .  $T_m$  of the polymer, similarly to  $T_g$ , is not fully discrete – it increases with the size of individual crystallites, the presence of the side groups that confine the backbone flexibility (e.g. aromatic groups), as well as with the presence of double bonds. Because the polymer is usually

a combination of both crystalline and amorphous phases, polymer materials show both  $T_m$  and  $T_g$  (Figure 1.5). Every polymer has a  $T_g$ , although not every polymer possesses a  $T_m$ .

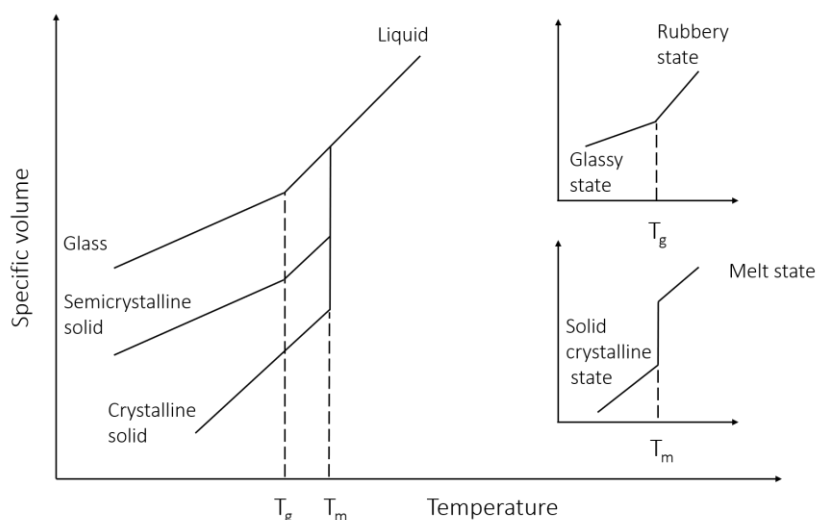


**Figure 1.5.** Changes of the amorphous and semicrystalline state with temperature. Adapted from reference 79.

## 1.4. Additives in polymer systems

Nowadays changing the polymer matrix to obtain the desired characteristics of a product has become a very important field of science since it enables tailoring of final properties. Additives present in the polymer matrix can alter either the chemical or physical behaviour of the matrix, e.g. by chemical reaction with the polymer, noncovalent interactions with the matrix, or by directly affecting the matrix free volume. Among the substances used to improve the polymer properties are plasticisers, antioxidants, heat stabilisers, slip agents, light stabilisers, thermal stabilisers, lubricants, colorants, reinforcements, surfactants and antistatic agents. Below, the specific additive types used within this thesis are discussed.

### 1.4.1. Plasticisers

Plasticisers – one of the most commonly additives in PVA matrices – in general act as a lubricant between polymer chains, facilitating their movement across one another by increasing their free volume. Plasticisation typically lowers  $T_g$  and elastic modulus, reduces the

melt viscosity, and decreases tensile strength. The addition of plasticisers to the system may also lead to change in substance odour, biodegradability, flammability, and cost of the resultant product. Because of the growing importance of plasticisers in industry, analytical methods and models to describe their diffusion in various systems are required during product development. Equilibrium-based methods are not convenient to use as they generally require long experimental timescales with unchanged conditions. To mitigate the costs associated with waiting for a film to reach equilibrium, alternative environments that result in the same film behaviour over short timescales (e.g. by increasing the environment temperature or RH) have been developed.

Among the most popular plasticisers in PVA matrices are glycerol,<sup>17,80</sup> propylene glycol,<sup>51</sup> polyethylene glycol, sorbitol, polyether polyols and ethanolamines.<sup>81</sup> Plasticisation and consequent changes to DC in the PVA system is further dependent on the chemistry of the plasticiser. Glycerol, having higher –OH group density than e.g. propylene glycol will more readily form hydrogen bonds with the –OH groups of the PVA chains,<sup>51</sup> leading to a more pronounced effect on the system. In formulations where partially hydrolysed PVA is mixed with fully hydrolysed PVA, partially hydrolysed PVA plays the role of the plasticiser and decreases overall DC.<sup>82</sup>

In this thesis, glycerol was used as the plasticiser of choice. Glycerol is characterised by low molecular weight, high polarity, non-toxicity, and high potential for molecular bonding. Due to these properties, it has been extensively studied in PVA with and without other guest molecules.<sup>22,80,83–85</sup> Glycerol changes the nanostructure of PVA due to PVA-plasticiser hydrogen bonding, resulting in increased flexibility as well as lower tensile strength of the plasticised materials compared to their non-plasticised counterparts. For polymer blends, glycerol addition can change the compatibility and miscibility between the components of the

system.<sup>83,84</sup> As a result, properties of the PVA/glycerol system such as  $T_m$ , hardness, and elastic modulus are reduced proportional to the glycerol content.<sup>80</sup>

Glycerol influences the size and aggregation behaviour of the polymer, entanglement behaviour of the polymer chains as well as DC (decreasing with increasing plasticiser content).<sup>83</sup> Although no effect on crystallite size distribution is apparent for partially hydrolysed PVA upon glycerol addition (despite gradual decrease in crystallization rate with increasing glycerol content), plasticiser disrupts the chain regularity in fully hydrolysed PVA, increasing the activation energy of homogeneous nucleation and resulting in a greater range in crystallite sizes.<sup>82</sup> Indeed,  $T_g$  of the polymer is dependent both on the DH (increases with increasing DH due to higher DC) and plasticiser content (decreases with increasing amount of plasticiser in the system due to increasing free volume in the system).<sup>51,82</sup> The relationship between plasticiser amount and  $T_g$  of PVA systems can be obtained from the Kelly-Bueche equation,<sup>85</sup> with equivalent models able to describe plasticiser influence on  $T_m$ .<sup>82</sup>

The impact of glycerol on DC is correlated with its concentration, becoming more prominent until the compatibility limit is reached (reported as 40 wt% glycerol<sup>82</sup> for fully hydrolysed PVA and values of 65 wt%<sup>82</sup> or 39 wt%<sup>51</sup> for partially hydrolysed PVA), whereupon phase separation occurs. Glycerol-glycerol interactions become much more important at the point of phase separation, leading to different trends in matrix behaviour compared to those observed before phase separation. For fully hydrolysed PVA, after reaching phase separation DC decreases up until the miscibility limit after which no significant further changes in DC are observed. Conversely, for partially hydrolysed PVA, DC continues to decrease slowly after phase separation followed by a sharp reduction at 65 wt% glycerol.<sup>82</sup>

### 1.4.1.1. Plasticisation theories

Despite the advent of complex computational methods over the last 100 years, the two initial theories of plasticisation (lubricity theory and gel theory) remain popular today due to their simplicity and generality. The first claims that plasticisers reduce the intermolecular friction between polymer molecules without changes in polymer arrangement due to solvent action and/or simple lubrication of the plastic matrix. The latter theory assumes rigidity of a matrix is due to the dynamic bonds between randomly arranged polymer chains. Plasticiser molecules interrupt this network in two ways: by reducing attachments between polymer molecules to let the matrix deform without changing its structure, and by changing the local equilibria in the film due to local variations in plasticiser concentration.<sup>86,87</sup>

Free-volume theory was developed after the first attempts to explain change of the polymer properties – viscosity, thermal expansion coefficient and specific volume – with temperature.<sup>86</sup> The free volume was first defined by Fox and Flory for temperatures above  $T_g$  as:<sup>86</sup>

$$V_f = V_{T_g} - V_{0s} \quad 1.1.$$

where  $V_f$  is the free volume of the polymer above  $T_g$ ,  $V_{T_g}$  is the polymer specific volume above  $T_g$  and  $V_{0s}$  is the solid specific volume extrapolated to the same temperature above the transition temperature. Given that this definition suggests that for all temperatures below the  $T_g$  free volume is equal to 0, other definitions have been suggested. However, they still contain parameters that are difficult to obtain (e.g. specific volume at 0 K).<sup>88</sup>

Free-volume theory is applied to explain some properties of plasticised polymers. Plasticisers have the tendency to increase the polymer free volume because of disruption of noncovalent interactions between polymer chains. The motion of the polymer backbone, side chains, and chain ends are the principal sources of free volume. Accordingly, free volume can

be increased by internal plasticisation, increasing temperature, and lowering the molecular weight of polymer.<sup>86</sup> Changes in  $T_g$  with varying polymer molecular weight are described by Flory-Fox equation:

$$T_g = T_{g,\infty} - \frac{K}{M_w} \quad 1.2.$$

where  $T_{g,\infty}$  is the maximum glass transition temperature that can be achieved at a theoretical infinite molecular weight, and  $K$  is an empirical parameter related to free volume. Therefore, increasing the molecular weight of the polymer leads to higher  $T_g$ .

Free volume theory has become the base theory for many mathematical models connecting  $T_g$  of each component with  $T_g$  of the plasticised matrix, for instance the Gordon-Taylor equation:<sup>11</sup>

$$\frac{1}{T_g} = \frac{w_1}{T_{g1}} + \frac{w_2}{T_{g2}} \quad 1.3.$$

where  $T_{g1}$  and  $T_{g2}$  are the glass transition temperatures of the component 1 and component 2, respectively, and  $w_1$ ,  $w_2$  are the mass fractions of components 1 and 2, respectively. However, Equation 1.3 assumes that components create a single amorphous phase with components ideally mixed. Because of this, plasticisation effects predicted by this equation are associated only with the amorphous region of the polymer. The composition of this region must be corrected when one of the components undergoes a freezing transition.<sup>11</sup>

For a compatible polymer blends,  $T_g$  can be expressed using Couchman's relation.<sup>89,90</sup> However, for systems with polymer-plasticiser phase separation, the individual  $T_g$  of each phase needs to be taken into consideration. For the first polymer-rich phase, the glass transition temperature is higher, while for the latter, plasticiser-rich phase – lower. Couchman's relation can hence be rewritten as:<sup>89</sup>

$$T_{g_{\text{mix},a}} = \frac{\sum X_{i,a} \Delta C_{pi} T_{gi}}{\sum X_{i,a} \Delta C_{pi}} \quad 1.4.$$

where  $X_{i,a}$  is a molar fraction of the constituent  $i$  within phase  $a$ ,  $T_{gi}$  is the glass transition temperature of the pure constituent  $i$  in the phase  $a$ , and  $\Delta C_{pi}$  is the change in heat capacity at  $T_g$  of the pure constituent  $i$ .

#### 1.4.1.2. Antiplasticisation

An antiplasticiser is a substance that, like a plasticiser, reduces  $T_g$  of the polymer. However, adding antiplasticisers to glassy polymers leads to increase in material stiffness or bulk modulus.<sup>91</sup> Antiplasticisation occurs when the additive strongly interacts with the polymer matrix (e.g. via polar interactions), decreasing segmental chain mobility and consequently increasing steric hindrance within the film. Antiplasticisation can also occur through the addition of a small amount of plasticiser, as the increased chain mobility leads to increased DC, decreasing the free volume in the matrix.<sup>92</sup> Antiplasticisation can be a desired process that leads to increased scratch resistance in polymer films and controls material brittleness as well as nonlinear mechanical properties.

Depending on the  $M_w$  of the polymer, the same additive can have plasticising properties for one chain length and antiplasticising properties for the other. This behaviour can be explained by considering the effect of free volume on additive compatibility in those polymers. High  $M_w$  polymers have significantly less chain ends when compared to low  $M_w$  polymers, reducing the number of voids within the matrix significantly. As plasticiser molecules initially fill those voids, a lower amount is necessary to saturate a high  $M_w$  polymer. Once the polymer is saturated and the compatibility limit is reached, phase separation occurs, leading to antiplasticisation.<sup>93</sup>



### 1.4.1.3. Plasticiser loss and migration

Plasticiser loss from the polymeric matrix is a significant problem, as even a small reduction in plasticiser content leads to change in overall system properties. Plasticisers may be removed from the system due to evaporation from the surface-air interface, migration to adjacent polymers or extraction due to contact with solvent media.<sup>94</sup> When considering plasticised polymer films in contact with solvents, it was proven that plasticiser molecules do not migrate into water; however, they were found in products like shower gels,<sup>93</sup> making plasticiser loss very relevant to the formulations considered in this thesis.

For stand-alone polymer films, evaporation of the plasticiser is the only possible mechanism of plasticiser loss. The amount of plasticiser that evaporates from the surface is dependent on the plasticiser surface concentration, itself affected by the plasticiser migration rate and solubility limit.<sup>93</sup> For plasticiser concentrations above the solubility limit, deposition and accumulation on the material surface (i.e. blooming) can occur. For concentrations below that level, however, rate of additive loss is only controlled by volatility and plasticiser diffusion rate.

In the latter case, plasticiser loss to the atmosphere is a two-step process (migration in the matrix followed by evaporation), with diffusion coefficient expressed by the dependence of concentration of plasticiser ( $C$ , Equation 1.5) or its free volume ( $f$ , Equation 1.6), itself function of plasticiser content:

$$D(C) = D_{C0}e^{\alpha C} \quad 1.5.$$

$$D = Ae^{-\frac{B}{f}} \quad 1.6.$$

where  $D_{C0}$  is the zero-concentration diffusion coefficient,  $\alpha$  describes the plasticisation efficiency of the plasticiser, and  $A$ ,  $B$  are empirical constants.<sup>95</sup> Plasticiser excess on the surface

occurs in the case of plasticiser loss where evaporation, rather than diffusion, is the rate-limiting step.

The mass transfer theory (evaporation from stationary liquid into a stirred gas) can be used to calculate the rate of evaporation of the plasticiser in the second step of the process:

$$v_0 = 0.33 \left( \frac{u^{0.5}}{l^{0.5}} \right) S_g D_g^{0.66} \left( \frac{\rho}{\mu_g} \right)^{0.17} \quad 1.7.$$

where  $v_0$  is the rate of evaporation,  $l$  is the width of the surface,  $u$  is the velocity of the gas flowing perpendicular to said surface,  $S_g$  is the concentration of the plasticiser in the gas phase,  $D_g$  is the diffusion coefficient in the gas phase, and  $\rho$  and  $\mu_g$  are density and viscosity of the gas phase, respectively. Naturally, this model is invalid in the case of perfectly still air.<sup>96</sup>

Given that plasticiser migration, polymer relaxation, and plasticiser vapour pressure are temperature-dependent, the relative rates of the two stages of plasticiser loss are temperature-dependent. In general, for polymer-plasticizer systems at low temperatures, plasticiser loss is limited by evaporation, while at high temperatures – by diffusion; transition temperatures are specific to each given system.<sup>95</sup> Rates of plasticiser loss are further controlled by properties of the surrounding air as well as shape of the plasticiser molecule.<sup>95</sup>

To calculate the rate of evaporation from the plasticiser partial vapour pressure ( $p$ ), the Hertz equation can be applied, using temperature, plasticiser molecular weight and the rate constant of plasticiser transfer from the material ( $k_p$ ):<sup>93</sup>

$$v_0 = \frac{p}{\sqrt{2M_w k_p T}} \quad 1.8.$$

according to this equation, molecules with high boiling point (high enthalpy of vaporisation) should be characterised by slow evaporation rate. However, in the case of glycerol used in this

thesis (boiling point 290 °C),<sup>97</sup> plasticiser loss within a week of aging has been identified, therefore this phenomenon is of particular importance.

#### 1.4.1.4. Plasticising properties of water

Water vapour permeation plays an important role in the packaging industry. This phenomenon can change the quality of products as well as affect their shelf life<sup>98</sup> because water also can act as a plasticiser; it interacts with macromolecules via hydrogen bonds and removes further barriers for polymer chains to move.<sup>4</sup> The extent of water permeation is determined by polymer-water affinity, itself a function of the properties of the polymer (e.g. DH). In the case of water soluble polymer films, refractive index,<sup>99</sup>  $T_g$ , DC, film thickness, free volume and, as a consequence, molecular mobility<sup>11</sup> all change upon the uptake of water. As PVA is considered to be the simplest hydrophilic polymer, it has become a convenient system to investigate the influence of water content in water soluble polymers.<sup>11</sup>

Water present in PVA can be both bound and free. The possible water states were divided into three groups:<sup>11,100,101</sup>

1. Nonfreezing water, which is bound so strongly to hydroxyl groups that it shows no thermal transition by DSC. It was proven to have the most significant plasticising effect on PVA.
2. Freezable water, which can be weakly bound both to nonfreezing water and polymer chain. Because of those interactions, in atmospheric pressure it melts on temperatures above 0 °C.
3. Free water, which behaves like bulk water with the same phase behaviour.

Water dissolves crystalline regions increasing the amorphous regions, however, it is not present in the regions of intact crystallites.<sup>101</sup> Therefore, overall water content is equal to water content in the amorphous regions. At least two types of interaction between the polymer and

water can be distinguished.<sup>102</sup> For low water quantities (<10%), the polymer-water system is more compact than a pure polymer-polymer system. Increasing water concentration forms a looser network as water-water interactions occur.

Equilibrium water content in polymeric materials increases with RH.<sup>16</sup> As a result, tensile strength and Young's modulus are both inversely proportional to RH, while elongation increases with RH.<sup>103,104</sup> In biaxially-oriented PVA films, water vapour and oxygen transmission rate as well as swelling rate grow exponentially with increasing RH, even though temperature has little effect on these properties.<sup>98</sup> Moisture sorption of polymer films is also dependent on film thickness,<sup>99,105</sup> a fact which can be taken advantage of in polymer humidity sensors as most other RH-dependent properties are also temperature-dependent.<sup>99</sup> While choosing the best polymer film thickness for a particular application, one needs to make a compromise: thinner films have better humidity sensitivity but longer time for water absorption.

If another plasticiser is present in the system, the water uptake is dependent on the quantity and chemistry of the other plasticiser in the matrix. If this other plasticiser creates strong hydrogen bonds with the polymer backbone, some sites initially occupied by water molecules are later occupied by the plasticiser. When plasticiser concentration rises above a threshold limit, all the sites surrounding polymeric units are occupied by plasticiser and water molecules. Any further plasticiser or water addition leads to plasticiser-plasticiser interactions, more mobile additive species, and eventually increased sensitivity to atmospheric water.<sup>89</sup>

Because of all aforementioned variations in polymer properties with changes in RH, attempts have been made to produce polymers with improved moisture resistance<sup>18</sup> or create controlled RH environment during testing.<sup>106-114</sup> A very common method to achieve constant RH is by using saturated salt solutions in sealed vessels<sup>115,116</sup> as the water vapour concentration

and therefore the RH over the salt solution is lower than over pure water.<sup>117</sup> A second strategy involves bubbling dry gases through a container with controlled water level.<sup>107</sup> RH is controlled in this case by the amount of water entering the gas during bubbling, therefore lower gas flow and higher water level results in high RH content in the outflow.

### 1.4.2. Surfactants

Surfactants (surface active agents) reduce the surface tension of a system, improving its wetting properties. They are of great importance to industry, used in processes where mixing or contact between various phases is desired e.g. dyeing of textiles, dispersing aqueous suspensions of insoluble dyes or perfumes, wetting, coating, emulsification, or cleaning.<sup>118</sup>

Structurally, a surfactant molecule consists of a hydrophilic head group and hydrophobic tail group. Usually, this tail group is a hydrocarbon chain that consists of more than 10 carbons in length, which makes it lipophilic. The hydrophobicity difference between head and tail group is of great importance in detergents, in which lipophilic groups show affinity to oil molecules, while the head groups show good compatibility with polar solvents e.g. water. Four major groups of surfactant head groups can be distinguished: anionic, cationic, non-ionic and zwitterionic. In this thesis, the behaviour of the first three groups in PVA-based systems will be investigated, with more detailed description given in relevant chapters. Specifically, sodium dodecyl sulfate (SDS), hexadecyltrimethylammonium bromide (CTAB), and decaethylene glycol monododecyl ether ( $C_{12}E_{10}$ ) were used. While the hydrophobic tail length of SDS and  $C_{12}E_{10}$  is shorter compared to that of CTAB (12 and 16 carbons, respectively), these surfactant species are the most commonly utilised in consumer goods (as opposed to the higher-priced dodecyltrimethylammonium bromide). Moreover, using nonionic surfactant of high  $M_w$

enables to draw a conclusion about the behaviour of a species with significantly larger hydrophilic chain compared to its ionic counterparts.

An important parameter for describing the suitable usage (water/oil or oil/water emulsions) of a surfactant is the hydrophilic-lipophilic balance (HLB), describing the balance of the strength and size of the hydrophilic and lipophilic moieties of a surfactant molecule.<sup>119</sup> According to Griffin,<sup>120,121</sup> HLB values range between 0 and 20, with surfactants of HLB between 3.5 and 6.0 proven to be more suitable in water/oil emulsions,<sup>119</sup> and those of HLB from 8 to 18 in oil/water emulsions. Using HLB as a way of characterising surfactant species is, however, limited as it does not provide the accurate description of various chemistries (e.g. hydrocarbon versus fluorocarbon tail)<sup>122</sup> and it cannot be used for charged surfactant moieties. To include these various chemical nuances, Davies<sup>123</sup> developed a group contribution method to estimate HLB. However, as with all other group contribution methods for chemical thermodynamics, the Davies method requires dedicated studies to determine the contribution values of the relevant moiety, and therefore cannot calculate the HLB values for large groups of cationic and zwitterionic surfactants.<sup>122</sup>

One of the characteristic features of surfactants is their tendency to create aggregates in solutions, mainly micelles, with their arrangement dependent on the character of the environment (water- or oil-based). Non-polar tails have low solubility in water, resulting in their preference to aggregate with other non-polar molecules.<sup>124</sup> The main driving force for such arrangement are hydrophobic interactions, which in aqueous solvents result in repulsive interactions between the non-polar tail group and the surrounding water. As a result of such arrangement into micelles, entropy is minimised in the system. The shape of the resultant micelle is dependent on the relative size of the head group compared to tail group, with

possibilities of spherical, ellipsoidal shapes, rods, as well as lyotropic crystalline phases (lamellar, hexagonal, and cubic phases).

The formation of these structures for a given surfactant usually occurs at a critical micelle concentration (CMC), dependent on the temperature and solvent type. Unfavourable electrostatic interactions are responsible for much higher CMCs of ionic surfactants compared to nonionic surfactants (as the surfactant head groups repel one another).<sup>125</sup> Moreover, the CMC decreases with increasing hydrophobic chain length.<sup>122</sup> Above the CMC, the activity of the surfactant in liquid medium becomes practically independent of its concentration, which enables investigation of CMC based on surface tension measurements.

Another very important parameter that rules ionic surfactant behaviour in solution is temperature. For each surfactant, micelles will not form if characteristic temperature (Krafft point,  $T_k$ ) is not reached. This temperature defines solubility of the surfactant that is equal to CMC and therefore micelles will not form for temperatures that are below  $T_k$ . For temperatures above the  $T_k$  and concentrations above the CMC, increasing the temperature leads to increase in surfactant solubility. For nonionic surfactants, however, their solubility decreases with increasing temperature until reaching cloud point ( $T_{cp}$ )<sup>122,126</sup> – the temperature at which phase separation of the solution becomes visible (solution becomes cloudy) – as dissolution of the surfactant in the solvent is no longer complete.

### **1.4.2.1. Polymer-surfactant interactions**

In this thesis, PVA-based films were prepared from aqueous solutions where both polymer and surfactants can interact prior to film preparation, including a dedicated study for their migration in the solution phase. As the polymer and surfactant are therefore in constant contact throughout preparation and film characterisation, understanding polymer-surfactant

interactions are of particular importance to predict the behaviour of molecules in solid polymer films.

In general, weakly amphiphilic, uncharged cosolutes and electrolytes can lower the CMC as they reduce the electrostatic penalty for self-assembly. Because of the additive effect of their many functional groups, polymers also depress the CMC when present in surfactant solutions. This effect may be insignificant for polymer-nonionic surfactant solutions as stabilisation of the surfactant micelles by the polymer is less prominent. However, in cases where favourable electrostatic interactions between the polymer and surfactant can be formed, the CMC can be lowered by orders of magnitude through surfactant-polymer complex formation.<sup>125</sup> The concentration at which such a surfactant-polymer complex is formed is called critical aggregation concentration (CAC).<sup>127</sup> Polymer-surfactant interactions can also result in creation of films at the air-water interface that contain an ordered micelle phase encapsulated in a polymer gel matrix.<sup>128,129</sup>

As with pure surfactant self-assembly, aggregation in aqueous polymer-surfactant systems is largely driven by the reduction of hydrophobic interactions between the solvent and aliphatic groups, balanced with the maximisation of favourable electrostatic interactions.<sup>122</sup> On this basis, these mixtures can be characterised by three types of water-soluble polymer-surfactant interactions:

- Systems containing polymers with hydrophobic groups where surfactant micellization occurs prior to aggregation with polymer.
- Systems containing polymers with hydrophilic groups. Here, polymer-surfactant binding occurs below the CMC. The polymer becomes saturated with surfactant prior to micellization, leading to creation of complexes that behave like association



polyelectrolytes<sup>130</sup> with the necklace model used to describe the structure of the aggregate.<sup>131</sup>

– Complex intermediate behaviour between these two extremes, exhibited by systems depending on the strength of the polymer-surfactant interactions.

As PVA is a neutral polymer, it can exhibit any of the three cases described (dependent on the surfactant length, charge, and presence of other cosolutes in the system), hence the relevant case for mixtures in this thesis cannot be predetermined. Accordingly, one must consider all possible interaction types to interpret the behaviour of aqueous PVA-surfactant mixtures.

While ionic surfactants in general associate with polymers starting at the CAC, nonionic surfactants show weak interactions with most homopolymers.<sup>125</sup> The shape of the adsorption curve of surfactant on suspended polymers also differ, generally presenting as a Langmuir isotherm for nonionic surfactants and sigmoidal for ionic surfactants, without a clear dependence on temperature.<sup>132</sup>

For ionic surfactant-nonionic polymer systems, hydrophobic interactions further influence system behaviour, with oriented aggregation of the surfactant tail groups onto hydrophobic parts of the polymer. For that reason, polymer-surfactant assembly is dependent on the type and structure of the surfactant itself, pH of the system,<sup>122</sup> degree of polymer branching,<sup>133</sup> hydrophobicity of the polymer<sup>130,134</sup> as well as presence of polar groups in its surface.<sup>132</sup> While the interaction mechanism of anionic and cationic surfactants is expected to show very similar behaviour, the latter group shows in general lower affinity for neutral water-soluble polymers. This can be explained by the size of the hydrated head group of the surfactants used that, in general, is larger for cationic and non-ionic surfactants compared to anionic ones.<sup>122</sup>

Surfactants introduced to polymer systems strengthen the junctions in the polymer network and increase osmotic pressure in the network. As a consequence, the  $T_{cp}$  of polymer increases.<sup>130</sup> In PVA systems, this behaviour is more pronounced for polymers of lower DH due to higher amount of hydrophobic acetate groups hence stronger polymer-surfactant tail group interactions.<sup>134</sup> Indeed, SDS forms polyelectrolytes with PVA of lower DH thereby disrupting interactions between polymer chains in a more pronounced way compared to PVA of higher DH.<sup>135,136</sup>

For nonionic polyol surfactants, a similar tendency was shown – increasing amount of -CH<sub>2</sub>CH<sub>2</sub>O- groups causes unfavourable interactions, while -CH<sub>2</sub>- groups cause favourable ones. Cationic surfactants do not show significant dependence of surfactant association with the polymer with increasing tail group length (and hence hydrophobicity), as the polar head group plays a more important role in the binding affinity.<sup>122</sup> However, CTAB has shown similar behaviour to SDS while in contact with PVA, creating polymer-surfactant complexes based on tail group interactions.<sup>130</sup>

### **1.5. Mechanisms of molecular migration**

Additive migration and segregation in polymer blends, block copolymers or end-functionalised polymers has been previously reported.<sup>137,138</sup> Migration of small molecules, especially in solid films, received relatively little attention, though.

Molecular migration within the polymeric matrix is dependent on many factors, such as component surface energies, compatibility between the components, and entropy. When considering individual migration mechanisms, behaviour of the molecules present in the system can be easily predicted. However, only rarely does a situation like this take place; the behaviour of the migrant is typically the result of many variables, thus difficult to predict.

### 1.5.1. Effect of surface free energy

Surface energy can be defined by considering the interaction between molecules in the system. In the bulk, molecules interact with all adjacent neighbours. Molecules at surfaces, however, have fewer neighbours – only on the surface and below it – inducing a surface free energy (SFE). The magnitude of this SFE is related to the cohesive forces binding constituents together. The component with the lowest surface energy tends to migrate to the surface and create areas rich in this component to minimise the overall system SFE.<sup>138</sup> The reduction in the overall SFE increases with the differences in surface tension following the Gibbs equation:

$$\Gamma_i = -\frac{1}{RT} \left( \frac{\partial \gamma}{\partial \ln c_i} \right)_T \quad 1.9.$$

where  $\Gamma_i$  is the SFE of component  $i$  at an interface,  $\gamma$  is surface tension,  $c_i$  is the concentration of component  $i$  at the interface,  $R$  is molar gas constant, and  $T$  is temperature. Equation 1.9 was further corrected for the case of charged molecules where both molecule and counterion adsorb at the interface:<sup>139</sup>

$$\Gamma_i = -\frac{1}{2RT} \left( \frac{\partial \gamma}{\partial \ln c_i} \right)_T \quad 1.10.$$

The difference in SFE of the components is an important factor for migration within polymer blends<sup>140</sup> and can be used to predict additive distribution within more complex polymer blends, either through group contribution methods<sup>141</sup> or through the relationship between component interfacial tensions.<sup>142</sup> These approaches have been successfully applied to explain migration processes of the plasticiser in the polyvinyl butyral/polypropylene system, enabling prediction of plasticiser enrichment at the interface between the two polymers.<sup>143</sup> However, as interfacial surface tensions are not readily experimentally accessible, methods to estimate these quantities are required to determine SFE. The most widely applied method to estimate

interfacial tension is through contact angle goniometry and Young's method, which will be discussed in Section 2.10.

### 1.5.2. Effect of entropy

For polymer systems where polymer species of different  $M_w$  are present, entropic effects may cause molecular migration. As species of lower  $M_w$  encounter lower entropic penalty for being on the interface compared to higher  $M_w$  counterparts, they are likely to diffuse there to lower the system SFE. Moreover, as the free volume associated with the chain ends increases with decreasing  $M_w$  of the polymer, the smaller species adds mobility and configurational freedom to the surface.<sup>140</sup>

The enrichment of the surface with additives is a result of a balance between the reduction in SFE and gain in translational entropy. This mechanism is also responsible for creation of surfactant micelles as described by the Gibbs-Helmholtz equation:

$$\Delta G = \Delta H_m - T\Delta S_m \quad 1.11.$$

where  $\Delta G$  is the Gibbs free energy of micellization,  $\Delta H_m$  is the enthalpy of micellization,  $T$  is the temperature, and  $\Delta S_m$  is the entropy of micellization. Formation of micelles generally leads to both increased enthalpy and conformational entropy in the system. As a consequence, the Gibbs free energy of the system is lower and the system is more stable because the unfavourable interactions are reduced. Further increase in surfactant concentration may lead to creation of liquid crystal phases.<sup>144</sup>

### 1.5.3. Effect of compatibility

In polymer systems, 'compatibility' can have several meanings, albeit all bearing similarity to the lay definition of the term.<sup>145</sup> In this thesis, this term is used to describe

formulations where no phase separation takes place, i.e. discussed system components are miscible on molecular scale.

### 1.5.3.1. Flory-Huggins theory

Flory-Huggins solution theory is commonly used for investigating the compatibility between polymer and the solvent. In this lattice theory of polymer solutions, molecules are assumed to be placed within a lattice composed of cubic cells of volume equal to that of an individual solvent molecule (or segment of polymer chain). The total number of lattice sites is equal to the number of solvent molecules and segments of polymer chain occupying a continuous sequence of cells. The free energy of mixing in the system is a product of three types of interactions: solvent-solvent, solvent-polymer segment and polymer segment-polymer segment interactions. From these considerations, the Flory-Huggins solubility parameter ( $\chi$ ) can be expressed by the equation:

$$\chi = (z - 2) \frac{\Delta g_{12}}{k_B T} \quad 1.12.$$

where  $z$  is the number of nearest neighbours of a cell in a lattice,  $\Delta g_{12}$  is the Gibbs free energy change for the formation of the solvent-polymer segment contact, and  $k_B$  is a Boltzmann constant. In a good solvent the polymer will swell because of favourable polymer-solvent interactions while in a poor solvent the polymer will shrink, reducing mixing with the surrounding medium. If  $\chi$  exceeds a threshold value (typically between 0.5 and 0.55), phase separation will take place. However, due to the simplicity of this model the behaviours predicted can only ever be approximate. For instance, because of the mobility of small plasticiser molecules, they may be lost to the atmosphere after some time, even when the semi-empirical constant is lower than 0.5.

In Flory-Huggins theory, all interactions are assumed to be isotropic and the system to be incompressible. Therefore, to apply this theory to strongly interacting systems (like the polymer/charged surfactant systems discussed in this thesis), additional terms need to be included to account for these effects.<sup>146</sup> Despite its drawbacks, this theory can successfully be used to predict thermodynamic properties of polymers (swelling equilibria, solubility/miscibility, formation of a ‘wetting layer’, bulk phase separation), as well as polymer-plasticiser and polymer-solvent compatibility.

### 1.5.3.2. Solubility parameters

For discussing compatibility in the polymer/additive system, two parameters are usually considered: Hildebrand and Hansen solubility parameters. The former parameter is defined as:

$$\delta = \sqrt{c_E} = \sqrt{\frac{\Delta H_v - RT}{V_m}} \quad 1.13.$$

where  $\delta$  is the Hildebrand parameter,  $c_E$  is cohesive energy density,  $\Delta H_v$  is the heat of vaporisation, and  $V_m$  is the molar volume for a given component. This parameter can be widely used for polymers and other non-polar materials as a tool to predict the degree of the interactions within mixtures. Furthermore, it can be a solubility indicator as when values of Hildebrand for two species are similar, materials are likely to be miscible.<sup>147</sup>

Based on Hildebrand solubility parameters, the Hildebrand-Scatchard equation is used to estimate the heat of mixing of two-component solutions:

$$\frac{\Delta H_{\text{mix}}}{V_{\text{mix}}} = (\delta_1 - \delta_2)^2 \phi_1 \phi_2 \quad 1.14.$$

where  $\Delta H_{\text{mix}}$  and  $V_{\text{mix}}$  are the heat of mixing and molar volume of the mixture, respectively, and  $\phi_i$  is the volume fractions of component  $i$ . In miscible systems,  $(\delta_1 - \delta_2)^2$  is small.

However, due to its assumptions, Equation 1.14 cannot be used for polar solutions with a negative enthalpy of mixing.

Providing more detail to the Hildebrand parameter, Hansen solubility parameters help to predict the tendency of one material present in another material to form a solution. It splits the Hildebrand solubility parameter into three components:

$$\delta = \sqrt{(\delta_d^2 + \delta_p^2 + \delta_h^2)} \quad 1.15.$$

where  $\delta_d$ ,  $\delta_p$ ,  $\delta_h$  are the Hansen dispersion, polar, and hydrogen bonding parameters, respectively. Hansen parameters work best predicting solvation of spherical molecules but can also be applied to predict the behaviour of elongated molecules, including polymers. They can therefore be used to choose the best plasticiser for a polymer to improve its properties. The more similar each Hansen parameter is for two substances, the more compatible they are. However, when considering industrial applications one needs to remember that other properties of the substance, for example toxicity, must also be considered.

### 1.5.4. Small molecule migration

When surface active additives are present in small amount in the polymer system during typical processing, it may be transported to the surface by physical processes such as spontaneous surface segregation, shear, or diffusion.<sup>140</sup> Spontaneous surface segregation is a result of the factors mentioned in the previous section, therefore will not be discussed in further detail here. Moreover, while shear effects may be important because of the film preparation method (spin coating), migration of suspended particles due to shear has only been proven in cases of micron-sized additives,<sup>148</sup> and in simulations of polymer chain aggregation.<sup>149</sup> Further, as in-depth evidence of shear-induced additive migration has only been

studied in systems using different flow conditions to those studied here,<sup>150</sup> these effects will be disregarded.

This project aims to understand the timescales of migration in parallel to their mechanisms, hence a general description of diffusion models will be given, with more information about each system provided in the introduction to the relevant experimental chapter.

#### 1.5.4.1. Fickian and non-Fickian diffusion

Fick's laws are broadly used for determination of the macroscopic diffusion coefficient of a component in the system as a result of a concentration gradient. In polymer formulations, they have applied to describe absorption<sup>151</sup> and release<sup>152</sup> of additives from the matrix, which is especially important in the food industry.<sup>78,153,154</sup>

Fick's first law describes the linear dependence of diffusion over time, described by equation:<sup>155</sup>

$$J = -D\left(\frac{\partial c}{\partial x}\right) \quad 1.16.$$

where  $J$  is the diffusion flux in the  $x$  direction (per unit area),  $c$  is the concentration of the diffusing species, and  $D$  is the diffusion coefficient. The change of diffusion coefficient over time is described using Fick's second law. For the 1-dimensional case it is expressed using equation:

$$\frac{\partial c}{\partial t} = -D\left(\frac{\partial^2 c}{\partial x^2}\right) \quad 1.17.$$

Contrasting with Fickian diffusion, case II diffusion describes molecular transport typically involving a front propagating at a constant velocity, with consequent swelling of the polymer and linear dependence of diffusion rates on time (proportional to  $t^{0.5}$  for Fickian



diffusion).<sup>156–158</sup> Due to the variety of factors that influence diffusion in polymer system, diffusion rates can differ from Fickian behaviour or case II diffusion and display time dependence following  $t^n$ , where  $n \in \langle 0.5; 1 \rangle$  – i.e. anomalous diffusion. Moreover, in more complicated systems, chemical reactions and convection need to be considered.

### 1.5.4.2. Other models

In addition to the macroscopic description of diffusion, there are many models that describe the migration of single molecule in polymer systems, primarily Einstein's work<sup>159</sup> (Stokes-Einstein equation, Section 2.7), considered as foundation of molecular diffusion processes. In this case – diffusion in homogeneous systems – the mean-square displacement of the diffusing particle increases in a proportional manner with diffusion time.<sup>160</sup> Polymer formulations cannot be considered as homogeneous systems, however. As has been previously shown, solvent (in the case of polymer solutions), polymer, and diffusing molecules should be considered as separate components, characteristics of which need to be included to accurately describe their behaviour.<sup>161,162</sup> That led to creation of a number of diffusion models based on various physical concepts.

For dilute polymer solutions (defined in Section 3.3.1), the polymer can be modelled as a hard sphere (following the Stokes-Einstein relation), a series of connected beads interacting independently with the solvent (the Rouse model), and a series of connected beads interacting both with one another and the solvent (the Zimm model).<sup>163</sup> Here, only the latter model can accurately describe the system behaviour as the Rouse model consistently overestimates the influence of polymer length on diffusivity.

In the case of semi-dilute polymer solutions and polymer gels, more complex models considering the restricted diffusion paths available are required. These include:

- Obstruction,<sup>164,165</sup> where the polymer is considered as a rigid obstacle for diffusing substances.
- Hydrodynamics,<sup>166</sup> where the polymer network indirectly interacts with the diffusing molecules, without acting as a rigid obstacle.
- Free volume,<sup>167,168</sup> where particles may only diffuse into cavities between solvent molecules.
- Reptation,<sup>163</sup> where the polymer chains diffuse as a tube rather than hard sphere, with unconstrained motion only at the chain ends.
- Entropic trapping,<sup>163</sup> where the polymer network is considered as a series of interconnected pores constrained by narrow paths.

Despite the variety of models described, the specific assumptions in each case limit their applicability, resulting in limited general predictability in these systems.<sup>169,170</sup> Moreover, these models consider only geometric aspects of the system, and there is still ongoing discussion about physical meaning of the model parameters.<sup>171</sup> The systems considered here are complicated further by their network density, glassy state, and multicomponent nature. Indeed, the free volume of polymer, size and shape of migrant, and migrant-polymer intermolecular interactions are important for diffusion in glassy polymer films.<sup>172</sup>

### **1.5.5. Specific aspects of diffusion in thin films**

Thin polymer films are broadly used for device miniaturisation<sup>173</sup> as well as sensors and show different behaviour than solution cast films. For these systems, diffusivity, temperature-dependent properties<sup>173</sup> and  $T_g$  are different than those for bulk. The prevailing explanation for these phenomena was presented as a three layer model, according to which polymer films can

be divided into three layers that are distinguished because of the variant nature of the interactions within them<sup>105</sup> (visualised in Figure 1.6):

1. The layer next to the solid substrate, where properties are dependent on polymer-substrate interactions.
2. The middle layer, which behaves in a similar way to bulk polymer.
3. The layer near polymer-air interface, which has reduced packing density and enhanced mobility when compared to bulk polymer.

While considering micron-thick films, the thickness of the first and the third layers are too small to contribute significantly to polymer properties. However, when the thickness decreases, they have an overriding influence on the interactions present in the system.

The properties of thin films are therefore highly dependent on polymer-substrate interactions and solvent-substrate interactions. Hence, homogeneous thin polymer films can be obtained in cases when there is no preferential interactions between components, or when substrate-solvent interactions are weaker than polymer-substrate ones.<sup>174</sup>

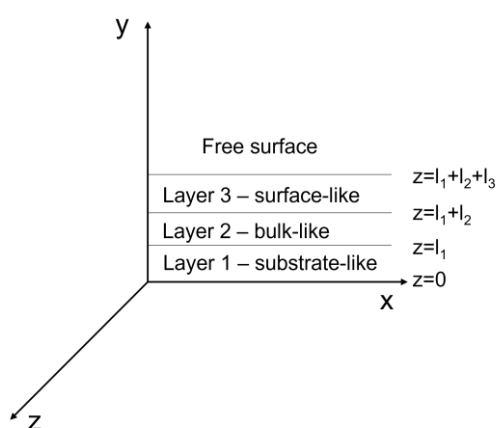


**Figure 1.6.** Schematic illustration of three-layers model.

### 1.5.6. Migration of molecules in PVA films from surrounding liquid medium

Infiltration of water and other compounds into PVA is of great importance to this thesis (i.e. in Chapter 5, Chapter 7, and Appendix E); here, a brief overview is provided.

While in contact with a polar solvent (e.g water), hydrogen bonding present in the PVA chain will interact with incoming solvent molecules, leading to swelling of the material, increased free volume, and increased diffusion coefficient of infiltrants inside the polymer matrix. In general, infiltration of solvent or solute molecules into a semicrystalline PVA film from fluid environments is determined by the distance between crystallites, polymer entanglement,<sup>175</sup> film-liquid medium partition coefficient,<sup>175</sup> DC, and  $M_w$ . Polar solvent uptake is negatively correlated with DC, while positively correlated with  $M_w$ <sup>25</sup> as the higher amount of crystallites within the matrix significantly increases the diffusion path length (tortuosity factor) and restricts the movement of the chain in the amorphous region (chain-immobilization factor).<sup>29</sup> Moreover, DC and  $M_w$  also control the swelling in the system upon infiltration by solvent molecules.<sup>25</sup>

One of the main reasons for studying solvent infiltration into PVA is its influence on the eventual release of additives into the surrounding media. Like many other mass transfer processes, this release can be divided into three steps: solvent diffusion into the film network, relaxation of the polymer matrix, and finally diffusion of the active compound from the swollen polymeric network into the surrounding medium.<sup>29</sup> This is particularly important when considering infiltration of solvents from vapours i.e. aging of PVA films at elevated RH.

While large body of literature has been dedicated to study water infiltration into PVA formulations, substantially fewer studies are dedicated to migration from other solvents. In alcohol-water mixtures, it was proven that DH influences the degree of polymer interactions with the solute – the higher the DH, the higher the affinity of the polymer to negatively charged molecules.<sup>29</sup> In this system, presence of ethanol modifies the amount of water molecules interacting with polymer, hence slowing down the relaxation of the polymer matrix<sup>176,177</sup> and lowering swelling of the matrix. In studies of dye release from PVA films prepared from resins

of different  $M_w$  and DH, the release profiles were similar for all polymers studied and depended on the rate of crystal dissolution in the solvent. Total release is therefore only possible in systems where the crystalline phase is completely dissolved.<sup>29</sup>

Additive release from films was proven to follow Higuchi's diffusion model:<sup>178,179</sup>

$$Q = [DC_d(2C_0 - C_d)t]^{0.5} \quad 1.18.$$

where  $Q$  is the amount of relaxed component per unit area of the matrix,  $C_0$  is the initial amount of the component per unit volume of the matrix, and  $C_d$  is the solubility limit of the component in the matrix. Moreover, the importance of heat-treatment was underlined: release kinetics were similar for both films heat-treated below  $T_g$  and untreated films. For films heated above  $T_g$ , however, retardation of diffusant release was correlated with increasing DC,<sup>178,179</sup> implying its encapsulation in polymer crystallites.

### 1.6. Thesis outline

Within this project, the migration of three types of surfactants (cationic, nonionic and anionic) as well as one type of plasticiser and fluorophore in PVA matrices is studied. All five species studied represent model additives, with the surfactants additionally emulating the concentrated detergent solutions contained within single unit laundry pods.

As was outlined in Section 1.1, complexity is introduced stepwise into the system. In Chapter 3, migration of a fluorescent probe through PVA-based solutions is investigated as a function of plasticiser content and surfactant head group chemistry. This is then extended to spin-coated PVA-based films in Chapter 4, where the importance of overall system compatibility and migration mechanisms are demonstrated.

Then, the effect of environmental conditions (i.e. RH and temperature) as well as concentration of the additive on migration of surfactants within the film to the air-film interface is addressed. In Chapter 5, the migration behaviour of surfactants with various head group

chemistry in thin PVA-based films is investigated by aging these formulations both in ambient conditions (as a function of surfactant concentration) or in controlled RH conditions (as a function of RH). In parallel, surfactant influence on water vapour sorption as well as investigations into surfactant molecular arrangement (tail-up or head-up) in mesophases on the polymer surface are provided.

Building on these findings, the migration behaviour under various temperatures is investigated using partially- and fully hydrolysed PVA as a matrix in Chapter 6. Accordingly, the effect of temperature and RH on migration behaviour in the system as well as the effect of physical properties of the matrix can be compared. The influence of temperature on aging and migration of the additive is also investigated in films doped with binary surfactant mixtures, followed by investigation into molecular arrangement and hydrophilicity changes using chemical force microscopy.

A different perspective of migration is presented in Chapter 7. Here, the migration of adjacent medium (water or surfactant solution) is investigated, establishing kinetics of liquid wetting (spreading and infiltration) on PVA-based films of various composition. More industrially relevant formulations (thick films) are compared to thin films to introduce further complexity into the system, highlighting different phenomena that must be considered at each length scale. Insight into changes in DC with changes in composition as well as influence of DC on migration behaviour in the system are discussed alongside a comparison of film morphology versus preparation method.

Finally, the thesis is summarised in Chapter 8. Then, future research directions are presented in Chapter 9. Preliminary data on migration of surfactants from adjacent nonaqueous media is presented in Appendix E.

## Chapter 2. Materials and methods

### 2.1. Materials

The following chemicals (Table 2.1) were purchased and used as received. Their specific use is described in the relevant experimental chapter.

**Table 2.1.** Details of the chemicals used in this thesis.

Material reference	Product	Supplier	$M_w$ (g/mol)	Purity (%)
87PVA	P8136	Sigma-Aldrich	30 000-70 000	87-90 (DH)
99PVA	341584	Sigma-Aldrich	89 000-98 000	99+ (DH)
Glycerol	G9012	Sigma-Aldrich	92.09	>99.5
SDS	BP8200	Fisher Scientific	288.38	>99
Decaethylene glycol monododecyl ether (C <sub>12</sub> E <sub>10</sub> )	P9769	Sigma-Aldrich	626.86	>98
CTAB	H5882	Sigma-Aldrich	364.45	>98
Rhodamine B (RhB)	R6626	Sigma-Aldrich	479.02	>95
HPLC water	34877-M	Sigma-Aldrich	18.02	HPLC Plus
Ethanol	200-578-6	Fisher Scientific	46.07	99.8
16-Mercaptohexadecanoic acid	674435	Sigma-Aldrich	288.49	99
1-Hexadecanethiol	674516	Sigma-Aldrich	258.51	99
Trifluoroacetic acid	74564	Sigma-Aldrich	114.02	Analytical standard
Hydrogen peroxide	UN2014	Fisher Scientific	34.01	30 (w/v)
Sulfuric acid	S/9240/PB 17	Fisher Scientific	98.07	≥95
Ammonium hydroxide	UN2672	Fisher Scientific	35.05	25=30
Lithium chloride	CHE 2360	Scientific Laboratory Supplies	42.40	99
Potassium acetate	217105000	Acros Organics	98.15	99+
Magnesium chloride	197530010	Acros Organics	95.21	99
Potassium carbonate	P/4080/60	Fisher Scientific	138.21	Extra pure
Magnesium nitrate	A10329	Alfa Aesar	148.3	98
Silica gel	S/0762/53	Fisher Scientific	60.08	HPLC grade
Poly(ethylene glycol) (PEG) 200	P3015	Sigma-Aldrich	190-210	99
2-ethoxyethanol	A16100	Alfa Aesar	90.12	99
Ethylene glycol	102466	Sigma-Aldrich	62.07	>99
Dipropylene glycol	D215554	Sigma-Aldrich	134.17	99
Butyl carbitol	579963	Sigma-Aldrich	162.23	>98
2-methyl-1-propanol	I0094	Tokyo Chemical Industry UK Ltd.	74.12	>99
2-butanone	L13185	Alfa Aesar	72.11	99
2-undecanone	U1303	Sigma-Aldrich	170.29	99
Oleic acid	A16663	Alfa Aesar	282.47	90

## 2.2. Solution preparation

Polymer films discussed in this thesis were prepared by spin coating (thin films) or solution casting (thick films) from aqueous PVA-based solutions. Water was used as a solvent of choice due to its wide application in industrial applications of PVA as well as poor solubility or lack of solubility in other non-toxic solvents (e.g. ethanol).<sup>180</sup> Moreover, water dissolves the other additives used in this thesis, enabling preparation of homogeneous solutions.

PVA powder was dissolved in HPLC water by heating up to 75°C (87PVA) or 100°C (99PVA) with continuous stirring (for ca. 2 hours or until completely dissolved) to obtain a concentration of 4% or 10% (w/v). Then, the solution was stirred while cooling to room temperature. Solutions of plasticiser (glycerol) of 4% (w/v), and ionic surfactant (SDS or CTAB) of 1% (w/v) were prepared by dissolving required amount of substance and stirring at room temperature for ca. 4 hours. Nonionic surfactant (C<sub>12</sub>E<sub>10</sub>) solutions of 1% (w/v) were prepared by dissolving it at 30°C with continuous mixing for ca. 2 hours, then stirring at room temperature until the temperature equilibrated. As prepared, all stock solutions were below the solubility limits for the corresponding chemical.

Aqueous solutions used for film preparation were created by mixing the above stock solutions in the appropriate polymer/plasticiser/surfactant volume ratio. To avoid creation of surfactant mesophases, PVA/glycerol/surfactant test solutions were heated up to 50°C for 15 minutes under stirring before cooling to ambient and stirring overnight. In addition, for some contact angle (CA) measurements, pure glycerol was added to 10% (w/v) to achieve solutions of PVA such that PVA/glycerol (w/w) ratio was 4:1. All of the investigated compositions were sonicated for 20 minutes at ca. 30°C (sonication power 180 W) to ensure a uniform composition and cooled down to room temperature prior to use.



In solutions used for fluorescence measurements, RhB was incorporated by diluting a 2.5 mM stock solution with the corresponding test solution to achieve desired fluorophore concentration.

### 2.3. Film preparation

Thin films (<250 nm) were prepared using a spin coater (Spin 150i, SPS-Europe). As a substrate, either glass slides cut to 1x1 inch<sup>2</sup> (for fluorescence recovery after photobleaching (FRAP) or CA measurements) or silicon wafers (Pi-kem, P(Boron), 0003W25) cut to 2x2 cm<sup>2</sup> (for atomic force microscopy (AFM) measurements) were used. The latter substrate provides initial control of film properties (uniform coverage) and choice of optimal spin speed as the coated substrate changes colour as a function of film thickness, enabling visual inspection of film quality.<sup>181</sup> Glass substrates, on the other hand, can be conveniently adjusted in size, are commonly used in fluorescence microscopy and are hydrophilic, hence minimising differences between substrate-polymer and bulk layers of the film.

The substrates were previously cleaned using piranha solution (mixture of 98% concentrated sulphuric acid and 30% hydrogen peroxide at a volumetric ratio of 7:3) for 1 hour to remove any organic impurities as described in reference 182. Silicon wafers were further cleaned in RCA solution (5:1:1 (v/v/v) solution of deionised water, aqueous ammonia, and 30% hydrogen peroxide solution, respectively) for 40 minutes at 80 °C. Finally, all substrates were sonicated (three times, 10 minutes each sonication) in ultrapure deionized water (Mili-q, 18.2 mΩ cm) and dried in an oven at 70 °C. Films for AFM and FRAP measurements were prepared by spin casting 200 µl of the solution on with spin speed equal to 2000 rpm for 100 s. Thin films prepared for CA measurements were prepared from 4% (w/v) solutions (both with and without glycerol) by spin coating 323 µl or 1209 µl (to account for a larger substrate) of the

solution with the spin speed equal to 2000 rpm for 100 s or 1000 rpm for 300 s, respectively, to obtain film of various thicknesses.

Solution cast films for CA measurements were prepared by dosing 400  $\mu\text{l}$  or 800  $\mu\text{l}$  of either 4% (w/v) or 10% (w/v) solutions (with or without plasticiser) onto a glass slide and placing in a vacuum oven (75°C, ca. 200 mbara) for ca. 1 hour to obtain films of micron-scale controlled thickness. Films for DVS measurements were prepared by adding 15 ml of the solution to a plastic petri dish (100  $\text{cm}^2$ ) and placing in the same conditions in the vacuum oven for ca. 4 hours.

## **2.4. Atomic force microscopy**

### **2.4.1. Operating principle**

AFM is a powerful technique that enables measurement of surface structure and topography of a sample, investigation of the nature of interactions present in the system through force-displacement curves, and manipulating the surface properties of the sample in a controlled way.<sup>183,184</sup>

In AFM, a nanoscopic probe (usually cylindrical or pyramidal) is placed at the end of a microcantilever connected to a micrometre-size chip. The choice of cantilever material depends on the application, with silicon (high spring constants, usually rectangular shape, used mostly for tapping mode) or silicon nitride (low spring constants, usually triangular shape, used mostly for contact mode) most commonly utilised. To improve signal quality, the cantilever is usually coated with thin layer of reflective material (e.g. gold, aluminium).

During an experiment, a piezoelectric actuator (the z-piezo) brings the cantilever into contact with a sample. Depending on the AFM system, it can operate in a scanned-sample (actuator moves the sample) or scanned-tip (actuator moves the chip) mode. The actuator enables movement in x, y, and z directions, thereby scanning the sample surface. While in

contact with the sample, a laser beam is emitted and concentrated near the cantilever tip, reflected by the back of the cantilever and recorded by a photodetector (Figure 2.1). As changes in surface morphology cause bending of the cantilever, the variations in the position of the beam are recorded (vertical movement and the lateral torsion of the cantilever), with signal differences corresponding to the material structure.

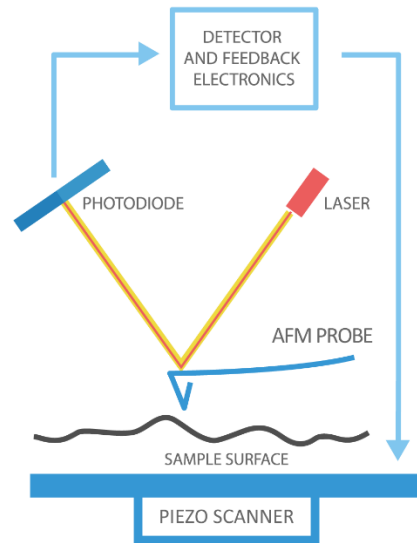


**Figure 2.1.** AFM operating principle. Reproduced from reference 185.

The principle of force microscopy is based on the Lennard-Jones model of potential energy ( $U(z)$ ) between a microscopic particle and the tip of the probe:

$$F(z) = \Delta U(z) = -\frac{dU(z)}{dz} \quad 2.1.$$

where  $F(z)$  and  $z$  are particle-tip force and distance, respectively. When the tip and the surface are separated by the distance  $z_0$  (Figure 2.2) the net tip-surface interactions force is equal to zero. For  $z > z_0$ , van der Waals forces result in attraction of the probe towards the surface, while for  $z < z_0$  overlapping of the atomic orbitals results in repulsive tip-surface interactions. Depending on the  $z$  distance, three operating modes of AFM can be distinguished: static contact mode (CM, Figure 2.2), dynamic (i.e. with the cantilever oscillating near its resonance frequency) intermittent contact mode (ICM, or tapping mode) and non-contact mode (NCM).

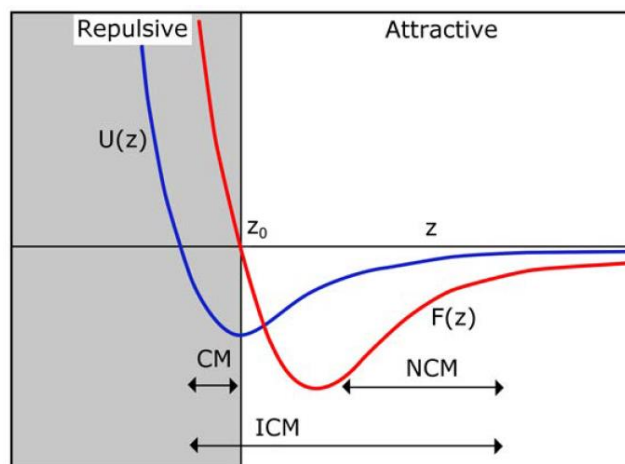


**Figure 2.2.** Lennard-Jones potential ( $U(z)$ , blue) and force ( $F(z)$ , red) distance dependence versus tip-surface separation. Reproduced from reference 186.

Because of the size of the cantilever tip, AFM has a subnanometre resolution.<sup>187</sup> Consequently, it is possible to observe single polymer molecules<sup>103</sup> or use AFM as the tool for polymer aggregate manipulation<sup>188</sup> and investigation of sample thickness within the  $z$ -scale of AFM for non-uniform samples using AFM scratch method.<sup>189</sup> Moreover, it enables the scanning of samples in variety of environments (ambient, variable RH, liquid, high vacuum). A common application of AFM is observation of changes before or after surface modification, for instance chemical contrasting<sup>190</sup> or humidity change.<sup>191</sup>

#### 2.4.2. Contact mode

In this mode, constant contact is kept between probe and the sample (brought together by the  $z$ -piezo), with short-range forces between the probe and sample enabling the scanning. Contact mode can operate in two submodes: constant force and constant height mode.

In the first case, the user defines a setpoint value. Probe-sample contact results in the cantilever bending and changes in the deflection value of the laser beam. The feedback system controls  $z$ -piezo that is extended or retracted as needed to match the deflection with the setpoint, and hence keep the force constant. The topography of the scanned sample is therefore obtained

from movement of the z-piezo that is adjusted to keep the deflection equivalent to the setpoint value. In the constant height mode, z-piezo is kept at a fixed position with no control from the feedback mechanism. The cantilever therefore flexes only according to the sample topography, and the resultant image is acquired from the photodetector signal obtained during scanning. Constant height mode is much more restrictive compared to constant force mode and is recommended to use for atomically flat surfaces only – however, if this condition is met, acquiring images is faster and they are characterised by higher resolution compared to constant force mode.

In general, contact mode is used for hard surfaces as constant contact between cantilever and the surface can lead to surface deformations.<sup>192</sup> Moreover, for surfaces with large morphological features, adjusting the parameters for scanning is difficult with the possibility of cantilever drift. However, measurement channels correlated with contact mode allow measurement of frictional information about the sample.

### **2.4.3. Dynamic modes**

Dynamic AFM modes address the problems that are encountered while imaging in contact mode. Here, the cantilever is oscillating near its resonant frequency using a bimorph that is either placed in the cantilever holder base (acoustic mode) or directly drives a cantilever coated with magnetic layer using external coils (magnetic mode). The latter in general provides measurements with less noise and better control of the process.

In tapping mode, the cantilever periodically contacts the surface and is otherwise disengaged. The user-defined amplitude of oscillation is changed during scanning as cantilever encounters morphological features, with the feedback mechanism adjusting the z-piezo to keep oscillation amplitude constant. The image is therefore obtained from the movement of the piezo. This mode can be used for soft samples (e.g. thin polymer films) as it does not create friction

during scanning. Images obtained in tapping mode are reproducible and do not change their quality after several scans.<sup>192</sup>

In non-contact mode (or frequency-modulation AFM), the cantilever also oscillates near its resonant frequency, but the amplitude is reduced such that the cantilever never touches the surface. Instead, phase shift between the driving and oscillatory frequencies is caused by long range surface-tip interactions, with the feedback system adjusting the z-piezo to obtain the initial value of phase and recording the image based on the piezo movement. This mode is mainly used in ultra-high vacuum conditions to avoid interference from capillary forces or electrostatic interactions, which significantly lower the otherwise superior resolution of this technique compared to other modes.

Dynamic modes are challenging to use in liquid environment due to the problems with identifying the peak responsible for cantilever oscillation. However, these modes can provide information about surface properties from changes in the phase shift for areas of various chemistry because phase channel signal depends on viscoelasticity, adhesion and long-range attractive forces.<sup>193</sup> For instance, it shows higher contrast for crystalline polymer regions<sup>194</sup> and makes it possible to distinguish crystalline and amorphous regions of polymers in high-resolution AFM measurements.

#### **2.4.4. Force spectroscopy**

Force spectroscopy can provide the information about the interactions between the cantilever and the surface. Besides Lennard-Jones interactions between uncharged bodies, capillary, electrostatic, and hydrophobic interactions can be detected. By chemical modification of the tip with selected chemical groups,<sup>195</sup> polymer chains<sup>191</sup> or even macromolecules it is possible to obtain information about the adhesive behaviour of the system while in contact with

different media. For systems investigated in ambient atmosphere, capillary forces are of utmost importance.

#### 2.4.4.1. Capillary forces

Every sample stored in ambient atmosphere has thin liquid layer on the surface as a result of water absorbance.<sup>196</sup> The close contact of two solid bodies covered in this thin water layer leads to the formation of a liquid bridge between those bodies – a capillary. This phenomenon happens due to spontaneous condensation of the vapour (capillary condensation) in the gaseous gap between the two surfaces, that subsequently is drawn into a meniscus to reduce the overall liquid-vapour surface area. The volume of the created meniscus depends on the RH of the environment and hydrophilicity of the surfaces involved.

Reduction of the liquid-vapour surface area between two solid surfaces minimises the surface excess energy. Consequently, the system is more stable and adhesion force between bodies increases, together with the force required to separate them. The higher the RH of the surrounding air, the higher the tip-surface adhesion force and the worse the resolution of AFM images.<sup>197,198</sup> As the contact point generally corresponds to the first force minimum, the dependence of the force at contact on RH for a spherical tip shape is given by Equation 2.2.<sup>197</sup>

$$F = \frac{2}{3} \pi^2 \varepsilon \rho_1 \rho_2 \sigma^4 r_t \left[ \frac{\sigma^8}{30D^8} - \frac{\sigma^2}{D^2} \right] - \frac{4\pi r \gamma_l \cos \theta_{tm}}{1 + \frac{D_{st}}{d(RH) - D_{st}}} = k_c z_x \quad 2.2.$$

where  $r_t$  is radius of a curvature of a tip,  $D_{st}$  is the distance between the sample and the tip,  $\rho_1$  and  $\rho_2$  are the number density of molecules in the sample and tip, respectively,  $\gamma_l$  is the liquid surface tension, RH is the relative humidity,  $\theta_m$  is the contact angle between the tip and meniscus,  $k_c$  is the spring constant of the cantilever,  $\varepsilon$  and  $\sigma$  are semi-empirical parameters, and

$z_x$  is displacement of the tip from its zero point at no loading. Parameter  $d$  is given by Equation 2.3.

$$d = -\frac{1.08 \text{ nm}}{\cos \theta \ln(RH)} \quad 2.3.$$

Generally, it is possible to reduce the adhesion force and improve the resolution and contrast of images by reducing the RH or radius of the curvature of the tip. However, for mica imaging, once RH fell below 14%, atomic resolution was abruptly lost. This occurs because at some point the oscillation of the tip-sample distance combined with decreasing humidity and, consequently, adhesion force lead to abrupt shift from the first to the second force minimum.<sup>197</sup>

Meniscus formation is mostly seen in contact mode as the cantilever tip is constantly in contact with the surface of the sample, resulting in the images in general being unaffected by capillary forces.<sup>199</sup> In tapping mode, on the other hand, the intermittent formation and rupture of capillary neck in each oscillation cycle of the AFM cantilever takes place, making the images highly influenced by the presence of capillary forces.<sup>199</sup> These changes in capillary forces can be accounted for however by modelling the cantilever movement as a simple harmonic oscillator.<sup>200</sup>

#### 2.4.4.2. Force spectroscopy measurements

Force spectroscopy measurements provide information about sample-probe interactions (including the influence of surrounding media) with piconewton sensitivity. During measurements the cantilever approaches the sample, interacts with it, and then is retracted away from the surface creating force curve. Exemplary force curves are presented in Figure 2.3.

At the beginning of the measurements, the tip is far away from the sample (point A, Figure 2.3). While approaching the sample (red line), the attractive forces overcome the



stiffness of the cantilever – the probe “jumps into contact” with the surface (point B). Figure 2.3a shows attractive interactions at point B. For lack of interactions no bending of the curve is observed, while repulsive interactions are represented by curve bended in the opposite direction compared to the one in Figure 2.3a. Then, a repulsive force resulting from the atomic shells interactions causes bending of the curve upwards. The deflection further increases until reaching point C – here, the z-piezo starts the process of withdrawing cantilever from the surface. The attraction forces (if present) result in longer contact of cantilever with the surface (point D), with the cantilever that stops reacting with the surface at point E.

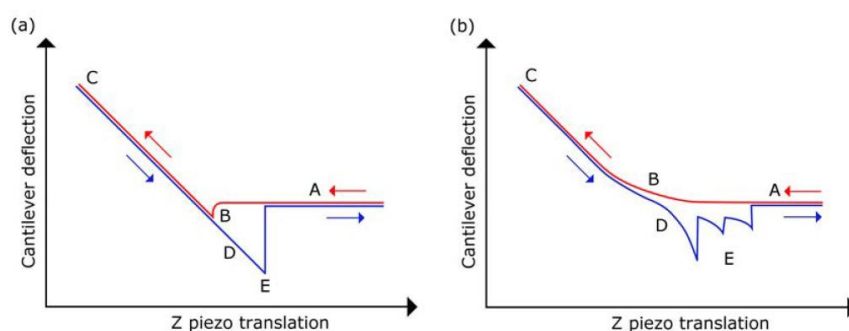


**Figure 2.3.** Exemplary force curves showing cantilever deflection as a function of z-piezo displacement, demonstrating (a) hard and (b) soft surfaces. Reproduced from reference 186.

Depending on the chemistry of the cantilever and the surface, different force curves are created. For instance, in Figure 2.3b the behaviour of the soft sample is shown. The presence of multiple peaks suggests multiple events of interaction-detachment between the cantilever and the surface that is typical for desorption and unfolding of long molecules (e.g. polymers).

Force calculations are based on the Hooke’s law, assuming that behaviour of the cantilever is similar to that of a spring:

$$F_c = -kx_c \quad 2.4.$$

where  $F_c$  is the force experienced by the cantilever, and  $x_c$  is the deflection of the cantilever. To obtain the spring constant, information from manufacturer or more accurate calibration methods (e.g. thermal tuning)<sup>201</sup> can be performed. Force curve measurements also require calibration

on a flat hard sample (e.g. mica). Here, change in the deflection coincide with the distance travelled in the z-direction, enabling to establish the deflection sensitivity of the cantilever. These calibration measurements are further used to calculate the force to account for variations between different cantilevers.

#### 2.4.4.3. Chemical force microscopy

Tip-sample interactions investigated using AFM can be expanded by chemical functionalisation of the tip or attaching particles at the end of the tipless cantilever. In this thesis, chemical force microscopy (CFM) was utilised to investigate the molecular arrangement of surfactant molecules on the film surface by preparation of self-assembled monolayers (SAMs) on the cantilever (Figure 2.4).

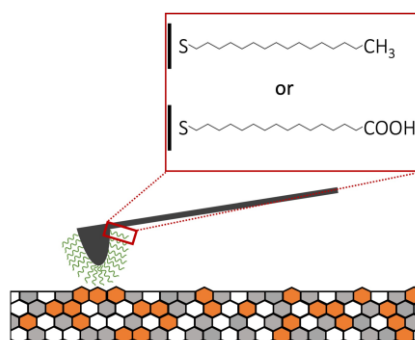


**Figure 2.4.** Schematic diagram of SAM-surfactant bloom interactions. Grey hexagons correspond to PVA, white – to glycerol, while orange – to surfactant.

SAMs are formed due to the unusually high affinity between thiol groups and gold coating on the cantilever.<sup>202</sup> By tethering thiol molecule with specific end group functionality in this way, cantilevers with different interaction strengths on surfaces with a given hydrophilicity can be created. Comparing results between hydrophilic and hydrophobic cantilevers enables detection of surface molecular orientation deconvoluted from the capillary forces present.

### 2.4.5. Experimental procedure

In this thesis, both imaging in tapping mode and CFM measurements were performed on a Dimension 3100 AFM (Veeco). Imaging in tapping mode utilised tapping mode cantilevers ( $\mu$ masch, HQ:NSC15/AL BS, aluminium coating, spring constant of ca. 40 N/m) to record changes in film morphology with changing composition (Chapter 4, 5, 6 and 7, Appendix E). Thickness variations with changes in composition or film aging were investigated using the scratch test (Chapter 4, 5, and 6). It was performed by applying potential difference equal to 14 V with scanning angle equal to  $0^\circ$ , followed by imaging at the scanning angle equal to  $90^\circ$ .<sup>189</sup> For each sample, three scratches were made and at least three profiles from each scratch were extracted. The sample thickness was taken as the average value from all analysed positions.

Prior to SAM synthesis, glassware was cleaned using piranha solution.<sup>182</sup> Then, a reported method of acid-terminated (hydrophilic) and methyl-terminated (hydrophobic) SAM preparation<sup>203</sup> was followed. 16-Mercaptohexadecanoic acid and 1-Hexadecanethiol were used due to their similar molecular structure, leading to creation of SAMs with comparable length on gold-coated contact mode cantilevers ( $\mu$ masch, HQ:NSC36/Cr-Au, spring constant ca. 0.6 N/m). The quality of the prepared SAMs was investigated prior to AFM measurements using CA goniometry on a gold-coated glass slide prepared in the same way as cantilevers. AFM force measurements were performed on regions visibly modified by surfactant presence (i.e. blooms, crystals) and background regions (no clear morphology changes due to surfactant presence) with a trig threshold equal to 5 nN.

## 2.5. Fluorescence recovery after photobleaching

### 2.5.1. Operating principle

FRAP is a fluorescence microscopy-based method used to investigate the mobility of fluorescent molecules (tracers) in the system. FRAP can be used in various systems – from

polymer films<sup>204</sup> through multilayers<sup>205</sup> to biological samples.<sup>206</sup> It is based on bleaching (irreversible conversion of a fluorescent molecule or particle into a nonfluorescent entity) the fluorescent tracer within the region of interest, therefore decreasing fluorescence intensity in this region. By continuous scanning of the image, intensity within chosen regions is monitored with time. If the tracer is mobile, an increase in intensity over time will be observed (Figure 2.5) as two motions are taking place in parallel – bleached molecules are migrating out of the bleached region, while fluorescent molecules are migrating inside. From the shape of the recovery curve it is therefore possible to calculate the fraction of both mobile and immobile tracers as well as half recovery time – an important parameter in majority of the FRAP models that describes time needed for half of the fluorescent molecules to migrate back to region of interest.

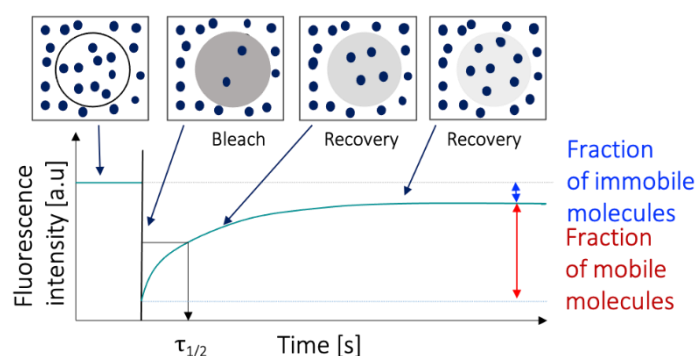


**Figure 2.5.** FRAP operating principle.

FRAP measurements utilise Fick's law with change of the sign (due to change of the migration direction) and a baseline shift (for non-complete bleaching).<sup>207</sup> Depending on the system, models can be extended to account for diffusion, intermolecular interactions or intermolecular binding. Moreover, real experiments are not characterized by an ideal intensity step change at the beginning as the laser beam has a finite width and bleaching is not an infinitely short process. This is why some corrections need to be introduced to the migration equations<sup>207</sup> as well as assumptions about 1D, 2D or 3D nature of diffusion.<sup>208</sup> When the

fluorescence recovery is higher than 50%, the system cannot be considered to be under 1D diffusion. It is a clear indication of the presence of recovery acceleration by the molecules from adjacent planes from above and below the irradiated area.<sup>209</sup> Further, the concentration of the fluorophore plays a key role in measurements. It needs to be high enough to be able to see the difference after bleaching, however, too high concentrations may lead to fluorophore aggregation and re-absorption of the fluorescence emissions and fluorophore acting as a plasticiser for the polymer.<sup>208</sup>

FRAP can be successfully applied to establish the distribution of diffusion coefficients in the system.<sup>207</sup> In inhomogeneous systems, however, measurements are often on a length scale bigger than individual mesophases, therefore the resultant diffusion coefficient will be the average diffusion coefficient over investigated length scale.<sup>210</sup> FRAP is also capable of quantifying chemical absorption as a function of position or time,<sup>208</sup> measuring the swelling process in polymer films<sup>211</sup> and proving the presence of two-photon isomerisation.<sup>212</sup>

### 2.5.2. Experimental procedure

FRAP was used to investigate changes in the diffusion coefficient with changes in sample composition (Chapter 4). Experiments were performed on a ZEISS LSM 780 confocal microscope under a 10x water immersion objective. To excite the fluorophore, the 488 nm line of an Ar laser was used with imaging at 1.5% of its maximum power and bleaching at the maximum laser power.

The radius of the bleach spot was set to 3  $\mu\text{m}$ , with the image size equal to 60.7  $\mu\text{m}^2$ . Because the resulting radius after bleaching differed from nominal radius, diffusion coefficient was calculated using the formula for 2D samples.<sup>213</sup>

$$D_{\text{FRAP}} = \frac{r_n^2 + r_e^2}{8\tau_{1/2}} \quad 2.5.$$

where  $D_{\text{FRAP}}$  is the effective diffusion coefficient of the fluorophore in the thin film,  $r_n$  is the nominal bleach radius,  $r_e$  is the actual bleach radius, and  $\tau_{1/2}$  is the half recovery time. The resulting radius was calculated using fluorescence intensity profiles following the method of Kang et al.<sup>213</sup> Intensity profiles before and after bleaching were extracted using ImageJ. Bleaching was repeated until fluorescence intensity decreased to at least 30% compared to its initial value. For some positions on the samples, diffusion was too quick and the bleaching was not possible. They were denoted as positions with no possible bleaching.

To take into consideration non-uniform distribution of the fluorophore within the film as well as possible intensity changes during imaging, background fluorescence intensity was normalised against the corners of the captured image (Figure 2.6). Normalised fluorescence intensity ( $I_N$ ) was calculated using formula:

$$I_N = \frac{I_1}{I_{2-5}} \cdot \frac{I_{2-5(b)}}{I_{1(b)}} \quad 2.6.$$

where  $I_1$  and  $I_{1(b)}$  are intensity signal in the bleached region at the given time and the average value from three measurements of the bleached region prior to bleaching. Similarly,  $I_{2-5}$  and  $I_{2(b)-5(b)}$  are the average intensity from the corners of the image at the given time and across three measurements prior to bleaching, respectively.  $I_N$  was then used to calculate  $\tau_{1/2}$ .

For each composition, three samples prepared from at least two different stock solutions were analysed. Due to the non-uniform nature of the surface for majority of the samples, 10 positions from each sample were investigated resulting in 30 total diffusion coefficient values unless stated otherwise. For samples prepared from filtered solutions, one film was prepared with 10 positions investigated.

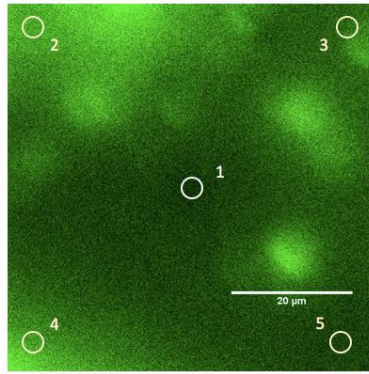


**Figure 2.6.** Positions used to calculate scaled fluorescence intensity: 1 – bleached region, 2-5 – background positions.

## 2.6. Fluorescence correlation spectroscopy

### 2.6.1. Operating principle

FCS is another fluorescence microscopy-based method that is used for investigating the mobility of the fluorescent molecules (tracer). However, in this technique the primary parameter of interest is spontaneous intensity fluctuations that are caused by a fluorescent molecule passing through the excitation volume (Figure 2.7a), represented as the deviations from the temporal average of the signal. If changes in the fluorescence are caused only by changes in the concentration, they are often represented as a function:

$$\delta F(t) = \int_{V_e} W(r) \delta(\eta C(r, t)) dV_e \quad 2.6.$$

where  $\delta F(t)$  is signal fluctuation with time,  $W(r)$  is a function describing spatial distribution of the light (usually approximated as a Gaussian distribution),  $C(r, t)$  is the function describing fluctuations in the local particle concentration at a time  $t$  (e.g. as a result of Brownian motion),  $\eta$  is a parameter describing signal-to-noise ratio (photon count rate detected per molecule per second), and  $V_e$  is the excitation volume. FCS uses an autocorrelation function ( $G(\tau)$ ) that enables extraction of characteristic time constants of the given system and measures the self-similarity of a time signal.<sup>214</sup> In normalised form it is represented as:

$$G(\tau) = \frac{\langle \delta F(t) \cdot \delta F(t + \tau) \rangle}{\langle F(t) \rangle^2} \quad 2.7.$$

The signal is therefore analysed in terms of self-similarity after the lag time  $\tau$ . As the diffusion coefficient depends on the lateral diffusion time (average diffusion time of the component through the confocal volume  $\tau_D$ , itself related to  $G(\tau)$ ), it can be estimated using Einstein's equation:<sup>215</sup>

$$\tau_D = \frac{w_{xy}^2}{4D} \quad 2.8.$$

where  $w_{xy}$  is the width of the confocal volume. It is possible to determine  $w_{xy}$  by calibrating against a fluorophore of well-known diffusion coefficient at given temperature.  $\tau_D$  for both calibration and experiments is calculated based on available models that consider Equations 2.7 and 2.8 using appropriate assumptions for the given system (e.g. 1D, 2D or 3D diffusion, possibility of triplet state excitation etc).

From the shape of the autocorrelation function it is possible to estimate the concentration of fluorophore and diffusion coefficient rate (Figure 2.7b). While discussing various diffusion processes, different timescales need to be considered (Figure 2.7c).<sup>214</sup> Further, artefacts must be accounted for in the first few datapoints regardless of model and correlation used (e.g. due to detector noise), therefore they are usually excluded from the analysis.

In FCS experiments, the concentration of fluorophore in the system is very low, typically in the 1-50 nM range, with every molecule significantly contributing to the measured signal. Moreover, the excitation volume is small (typically femtoliters), making FCS a very sensitive technique. FCS can be applied to fluorescently tagged macromolecules or common fluorophores, albeit with the requirement of colloidal stability of the measured species. This technique is also capable of providing information about chemical or photophysical reactions,



conformational changes in the molecules and intermolecular interactions due to the fluorescence fluctuations they introduce to the system.<sup>214</sup>

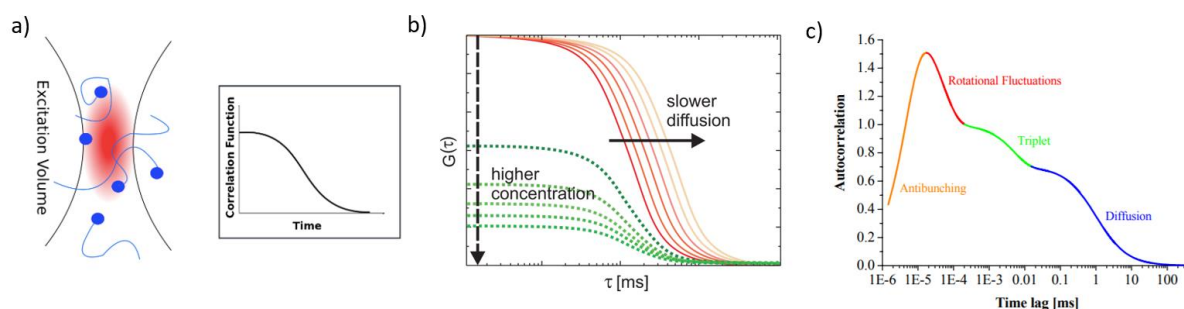


**Figure 2.7.** (a) FCS operating principle, (b) changes of the autocorrelation function shape with concentration and diffusion coefficient, and (c) characteristic fluorescence timescales. Reproduced from references 216, 217 and 214, respectively.

### 2.6.2. Experimental procedure

FCS was used to investigate changes in diffusion coefficient of the fluorescent tracer with changes in the composition of PVA-based solutions. Measurements were performed on ZEISS LSM 710 confocal microscope under 40x water immersion objective. RhB was excited using the 488 nm line of an Ar laser at 5% of its maximum power, with the 505-610 nm band-pass filter used to collect fluorescence emissions.

Calibration was performed using a 50 nM solution of RhB in HPLC water. The diffusion coefficient of the fluorescent tracer in water is known (equal to  $3.6 \cdot 10^{-10} \text{ m}^2/\text{s}$  at  $21.5^\circ\text{C}$ ),<sup>215</sup> from which the width of the confocal volume (dependent on laser power, laser calibration, environmental conditions etc.) can be established with Einstein's equation (Equation 2.8). As experiments were not performed at exactly  $T=21.5^\circ\text{C}$ , the following equation was used to obtain the value of diffusion coefficient of RhB at temperature of experiment:

$$D_{\text{RhB}} = \frac{D_{21.5} T_x \eta_{21.5}}{T \eta_x} \quad 2.9.$$

where  $D_{\text{RhB}}$  and  $D_{21.5}$  are the diffusion coefficients of RhB in water at temperature of experiment ( $T_x$ ) and  $21.5^\circ\text{C}$  ( $T_{21.5}$ ), respectively, while  $\eta_x$  and  $\eta_{21.5}$  represent the corresponding solution

viscosity. Data was analysed using the free diffusion model that accounting for triplet state excitation using ZEN 2010 software using the RhB diffusion coefficient calculated from Equation 2.8.

## 2.7. Dynamic light scattering

### 2.7.1. Operating principle

Dynamic light scattering (DLS) is used to measure the size of suspended particles both in the nano region (Nanosizer) and micron region (Mastersizer). Experiments are performed by measuring the intensity of the light scattered by molecules present in the suspension at a set angle. All variations in scattered light are a consequence of interactions with molecules other than the solvent (as solvent molecules are too small to interact with light). The rate of the changes in the scattering intensity is dependent on the size of the molecule and is described using the Stokes-Einstein equation:

$$D_{DLS} = \frac{k_B T}{6\pi\eta_x r_h} \quad 2.10.$$

where  $D_{DLS}$  is a diffusion coefficient of the particle,  $k_B$  is the Boltzmann constant,  $T$  is the temperature (given in Kelvin), and  $r_h$  is the particle hydrodynamic radius – the radius of the theoretical spherical particle that would have the same diffusion coefficient as investigating species. Using the known correlation for a given polymer it is therefore possible to calculate radius of gyration based on hydrodynamic diameter results obtained from DLS.

Similar to FCS, this technique is based on autocorrelation functions (Equation 2.7) to measure the variations of the scattered light signal with time. The diffusion coefficient is calculated using equation:

$$G(\tau) = A_{DLS} + B_{DLS} \cdot e^{-D_{DLS}q^2\tau} \quad 2.11.$$

where  $A_{DLS}$  and  $B_{DLS}$  are the function baseline and maximum (equal to 0 and 1, respectively, in the case of normalised data), and  $q$  is the light scattering vector described by equation:

$$q = \frac{4\pi n_d}{\lambda} \left( \frac{\theta_a}{2} \right) \quad 2.12.$$

where  $n_d$  is the refractive index of dispersant,  $\lambda$  is the wavelength of the laser and  $\theta_a$  is the scattering angle. The decay of the autocorrelation function is therefore dependent on the size of the particle – smaller particles move faster, which results in faster autocorrelation decay (Figure 2.8). For multicomponent solutions, however, the situation is more complicated as every particle has the ability to scatter light proportional to its diameter to the sixth power.<sup>218</sup> Therefore, even when small particles are in large excess in a system, the results will be skewed in favour of any large particles present.

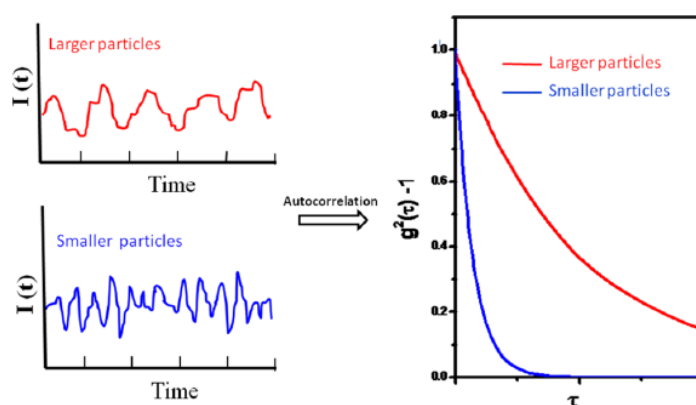


**Figure 2.8.** Changes of light intensity dependent on the size of the particle (left) and resultant autocorrelation functions (right, notated as  $g^2(t)$ ). Reproduced from reference 219.

DLS enables fast data acquisition and can provide information about diffusion coefficient of particles of a given size in any given medium (with possible particle tracking), stability of the solution, presence of intermolecular interactions as well as aggregation and chemical reaction kinetics.

### 2.7.2. Experimental procedure

In this thesis, DLS measurements were performed to investigate the intermolecular interactions between polymer and various additives. DLS measurements were performed on a Malvern Instruments Zetasizer Nano-ZS with a measurement angle of  $178^\circ$  and beam wavelength 632.8 nm at  $25^\circ\text{C}$ . Due to the presence of multiple species in some solutions, hydrodynamic diameter ( $d_H$ ) distribution was measured as a function of intensity,<sup>220,221</sup> investigated over three repeats. Data was analysed using Malvern software (particle size), with additional analysis of autocorrelation functions performed by the author to confirm observed trends.

## 2.8. Rheometry

### 2.8.1. Operating principle

Rheometry measurements can be used to investigate the behaviour of fluids under stress, enabling investigation into important rheological properties such as viscosity, shear modulus, storage modulus and loss modulus. As for the purposes of this thesis only viscosity calculations were performed, the other aspects of rheometry measurements will not be discussed.

Shear flow (as opposed to extensional flow) is the most commonly measured behaviour on rotational rheometers that enable viscosity measurements. The liquid is divided into imaginary layers (Figure 2.9), where the uppermost layer is characterised by the highest velocity in the system. The lateral force ( $F$ ) acting over a unit area ( $A$ ) is called the shear stress and causes sliding of the layer below it, which eventually results in the whole system flowing in the direction of the applied force (n.b. in rheometers, this is a rotational movement). Similarly, the velocity of the uppermost layer relative to the bottom layer, divided by the layer separation  $h$ , is defined as the shear rate.

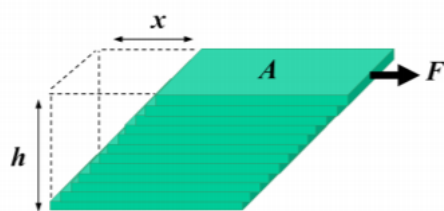


**Figure 2.9.** Graphical representation of shear flow. Reproduced from reference 222.

Fluids can be generally classified as either having Newtonian (shear stress linearly related to the shear rate) or non-Newtonian behaviour (viscosity varies as a function of the applied shear stress). Polymer-based solutions, melts and dispersions are usually non-Newtonian fluids.<sup>223</sup> Therefore, their behaviour needs to be modelled using more complicated models, usually including empirical parameters, that enable estimation of the viscosity at zero shear rate by extrapolation of solution behaviour.

An important consideration prior to measurements is the choice of rheometer geometry that will enable obtaining accurate results for given fluid. For water-based solutions, double wall geometry is recommended as it maximises the contact area (necessary due to the low viscosity of water itself).

### 2.8.2. Experimental procedure

Rheology measurements were used to investigate the viscosity of the solutions necessary for DLS measurements (Equation 2.10). The viscosity of test solutions (without RhB addition) was measured using a HR-1 Discovery Hybrid Rheometer with double wall geometry. Prior to measurements, solutions were sonicated for 20 minutes at ca. 25°C, and then allowed to cool to ambient temperature. The viscosity of each solution was examined at constant temperature equal to 25°C as a function of shear rate. The rheological data were fit to the Herschel-Bulkley model<sup>224</sup> by the TRIOS software to estimate viscosity at zero shear rate.

## 2.9. Dynamic vapour sorption

### 2.9.1. Operating principle

Dynamic vapour sorption (DVS) is a gravimetric technique that measures the rate and amount of solvent absorbed by a sample at given temperature. The solvent is present in the vapour state, in an amount regulated by changing its partial pressure in the system. Measurements are performed by changes in sample mass against a reference sample (usually an empty steel mesh basket) that is exposed to the same conditions as the examined sample (Figure 2.10). Changes in the mass are recorded by a microbalance, resulting in high precision of the results. DVS measurements can be performed using variety of solvents and enable evaluation of sample sorption behaviour (adsorption/absorption) as well as diffusion coefficient of the solvent in the system.

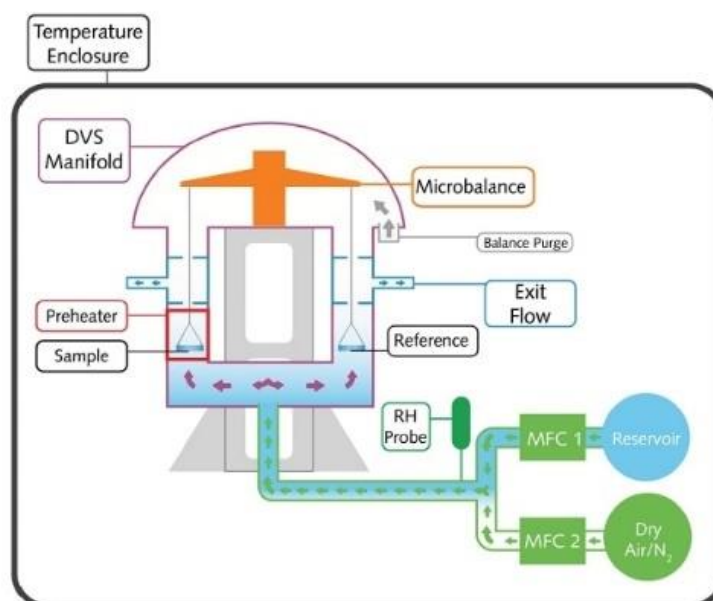


**Figure 2.10.** Graphical representation of a DVS experimental setup. Reproduced from reference 225.

Diffusion coefficient calculations are based on the mass balance equations with the appropriate boundary conditions. For the mass change of polymer films under constant partial

pressure of the solvent from completely dried material, diffusion coefficient of the solvent can be evaluated from the linear part of the sorption isotherm following the equation:

$$\frac{M_t}{M_\infty} = \frac{4}{d_s} \sqrt{\frac{Dt}{\pi}} \quad 2.13.$$

where  $M_t$  and  $M_\infty$  is the amount of solvent absorbed at the time  $t$  and at thermodynamic equilibrium, respectively, and  $d_s$  is the thickness of the sample.

### 2.9.2. Experimental procedure

In this thesis, DVS measurements were performed to evaluate changes in absorption behaviour of thick, solution cast films against changes in film composition. Measurements were performed using a DVS Advantage system. Ca. 15 mg of thick PVA-based film was placed in the weighting basket and dried for 1 hour at 75°C (ca. 1% RH) as a pre-heat step to remove moisture absorbed from the atmosphere during sample cutting. This was followed by measurements of change in mass of the sample until equilibration (change in mass less than 0.02%/min) at humidity from 5% RH to 75% with increment equal to 10% RH, followed by humidity decrease in the same manner to obtain absorption/desorption hysteresis.

## 2.10. Contact angle goniometry

### 2.10.1. Operating principle

CA measurements (or optical tensiometry) enable quantitative evaluation of liquid wetting behaviour on a given solid. They can be performed as static (i.e. a droplet placed on a surface, with CA values or their changes recorded over time) or dynamic (i.e. a liquid flowed on and withdrawn from a surface) measurements. In this thesis, static measurements were utilised. As modern CA goniometers are supplied with high-speed cameras, they enable

recording of CA values immediately after liquid/solid contact, which is especially important for solids that are soluble in the solvent of choice.

Geometrically, a CA is formed at the three-phase boundary between a solid, liquid and the surrounding atmosphere (usually air). Therefore, the description of the phenomena is based on the interactions between the three phases (Figure 2.11) and described using Young's equation:

$$\gamma_{sv} = \gamma_{ls} + \gamma_{lv} \cos\theta \quad 2.14.$$

where  $\gamma_{sv}$ ,  $\gamma_{ls}$  and  $\gamma_{lv}$  are the surface free energy of the solid, interfacial tension between liquid and solid, and surface tension of the liquid, respectively. Young's equation is empirical, and other equations have been developed to explain the wetting phenomenon in greater detail. However, Young's equation is commonly used for systems of unknown wetting behaviour.<sup>196</sup>

After rearrangement of Equation 2.14 with respect to the contact angle:

$$\cos\theta = \frac{\gamma_{sv} - \gamma_{ls}}{\gamma_{lv}} \quad 2.15.$$

it is possible to predict the system wetting behaviour for known values of parameters in Equation 2.15. For instance, in case of high surface energy solid or low surface tension liquid, the droplet is expected to wet the surface ( $CA < 90^\circ$ ). In the reverse case (low surface energy solid or high surface tension liquid), the liquid is likely to dewet the surface. Most of the time, however, this behaviour is difficult to predict as  $\gamma_{sv}$  and  $\gamma_{ls}$  are both unknown. Therefore, contact angle measurements are used to calculate surface free energy (SFE) instead of the inverse. Among the published methods are the acid-base theory, the harmonic mean method, Zisman method and equation of state approach.<sup>226</sup> All of them have significant drawbacks that make comparison of the results as absolute surface energy values difficult. However, they provide useful information while comparing results under the same experimental conditions and allow



conclusions to be drawn about the influence of varying parameters on surface free energy values.

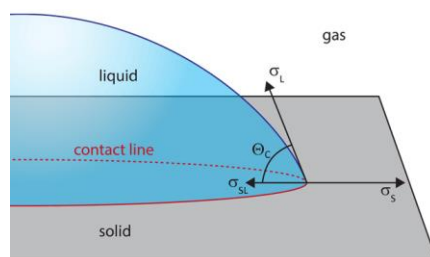


**Figure 2.11.** Forces influencing wetting behaviour of the system. Reproduced from reference 227.

### 2.10.2. Experimental procedure

CA measurements were implemented to investigate both kinetics of PVA-based films wetting and perform SFE energy calculations to determine the effect of introducing new species into the system. CA measurements were performed using a Theta Optical Tensiometer (Biolin Scientific) using an automated dispenser. As this study aims to describe initial stages of CA evolution, measurements were performed for 90 s, with image recording at 72 fps. Every measurement was preceded by camera calibration followed by placement of the syringe 0.6 cm away from the surface. Films of each kind were prepared in triplicate. Due to the proven dependence of CA evolution on the proximity of the substrate edge,<sup>228</sup> 3 measurements were performed in a triangle arrangement close to the centre of the sample, avoiding contact of any drop with other drop. Measurements were performed using water, surfactant solutions of various concentration (1% (w/v) or concentration below the appropriate CMC) and head group chemistry (anionic SDS, cationic CTAB, nonionic C<sub>12</sub>E<sub>10</sub>), or dodecane. As results may have been affected by the time difference between drop formation and drop deposition,<sup>229</sup> the drop was immediately deposited on the surface after its formation. Image analysis was performed using OneAttension software to obtain CA values, area of the liquid/surface contact, height of the droplet, and baseline length. The data was analysed using Python scripts to fit the mathematical model described in experimental Chapter 7, as well as perform geometrical

investigations into the CA evolution mechanism and validation calculations for the chosen model.<sup>230</sup> For all samples, model validation to check the assumption of the spherical droplet geometry was performed.

SFE measurements were performed by investigating contact angle (CA) between two liquids: polar water and non-polar dodecane. Then, SFE calculations were performed using the modified harmonic mean method by Wu:<sup>231</sup>

$$(1 + \cos\theta_i)\gamma_{lvi} = 4\left(\frac{\gamma_{lvi}^d - \gamma_{sv}^d}{\gamma_{lvi}^d + \gamma_{sv}^d} + \frac{\gamma_{lvi}^p - \gamma_{sv}^p}{\gamma_{lvi}^p + \gamma_{sv}^p}\right) \quad 2.16.$$

where the results are considered for two liquids ( $i = 1, 2$ ), and  $d$  and  $p$  stand for dispersion and polar components of the surface energy, respectively. Parameters  $\gamma_{vi}^d$  and  $\gamma_{vi}^p$  for used liquids were obtained from the literature.<sup>232–234</sup> In experimental Chapter 5 and 6, calculations were performed both on freshly prepared films and those aged for one week to investigate the change in SFE upon aging under various environmental conditions.

While CA and SFE measurements provide general trends of sample behaviour, due to the large droplet size measurements are averaged across the areas larger than nonuniformities resulting from changes in polymer morphology (e.g. surfactant blooming). Additionally, PVA is soluble in water, leading to possible errors while establishing initial contact angle and the necessity to perform measurements using dodecane and water on different positions. Combined, these factors can result in lower experimental errors compared to more sensitive techniques.

## 2.11. Fourier-transform infrared spectroscopy

### 2.11.1. Operating principle

Fourier-transform infrared spectroscopy (FTIR) is a vibrational spectroscopy method used for probing a wide variety of polymer materials to investigate both their chemical structure and crystallinity. In the heart of an FTIR spectroscope is a Michelson interferometer that

consists of an IR source, fixed and moving mirrors, a beamsplitter and a detector (Figure 2.12). The radiation emitted by the source is divided into two beams onto the fixed and moving mirror that recombines the beams and directs it into the sample. The moving mirror travels with a constant speed – changing the distance from the beamsplitter – which results in interference pattern change of the combined beam. The signal is further transformed from time to frequency domain using Fourier transform, which is displayed as an infrared spectrum. While performing experiments on a sample, the change in signal is observed due to sample absorbing wavelengths of relevant frequency. Spectra can be displayed with y axis as either transmission or absorbance, while x axis represents wavelength.

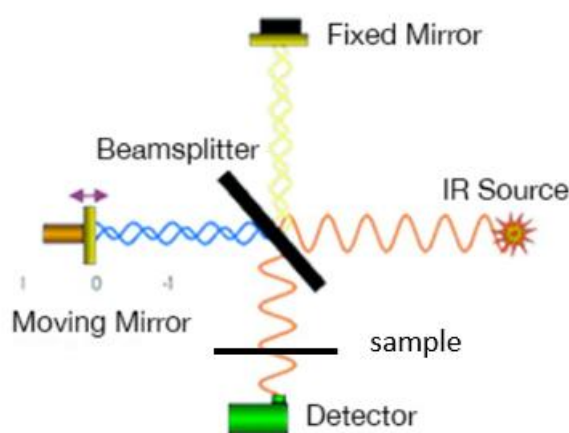


**Figure 2.12.** FTIR operating principle. Adapted from reference 235.

For each different chemical environment, absorption occurs at various characteristic frequencies. The frequency at which the absorption occurs is represented by equation:

$$f = \frac{1}{2\pi} \sqrt{\frac{k_b}{\mu}} \quad 2.17.$$

where  $f$  is the frequency of vibration,  $k_b$  is the strength of the bond, and  $\mu$  is the reduced mass. Hence, the lower the mass of the molecule or its part, the higher the frequency of absorption. Based on that, various molecular conformations can be distinguished by FTIR, such as stretching, rotation, or deformation (bending and twisting). IR absorption requires, however,

a permanent interatomic dipole and dipole alignment with the electric field. Hence, symmetric bonds such as  $N_2$  will not be visible in the IR spectra. Most of the peaks for any sample are usually localized in the fingerprint region (the region between  $400\text{ cm}^{-1}$  to  $1500\text{ cm}^{-1}$ ), so-called due to the unique spectrum for each relevant molecule.

Among FTIR techniques are transmission FTIR, Attenuated Total Reflectance (ATR) FTIR, Specular Reflection and Diffuse Reflectance. In this thesis only ATR-FTIR was used. In ATR-FTIR, the sample must contact a crystal through which the beam travels according to total internal reflection. There are many kinds of crystals used in the FTIR spectrometers, with the choice dependent on required spectral range, refractive index and depth of penetration. This method is generally non-destructive and can be paired with a stage enabling temperature control.

The measured absorbance (or transmittance) is dependent on many factors including crystal-sample contact pressure, roughness of the sample, surrounding atmosphere, the evenness of the sample, powder packing for powder samples etc. Hence, absolute values should not be compared between different samples. Instead, they are usually discussed relative to other nearby peaks in the spectrum (as the variation of the depth of penetration of evanescent waves at low and high frequencies can occur).<sup>236</sup>

Because of described ability of FTIR to probe the conformational states of polymer chains, it is possible to identify differences in vibration between chains in crystals with a unique, regular conformation and chains in non-crystalline regions with conformational irregularities, hence providing information about degree of polymer crystallinity (DC). IR gives information about short-range order or intramolecular phenomena; therefore, the DC will describe short-range crystallinity. Short-range intermolecular order is necessary for a long-range order to appear, but the reverse statement is not necessarily true, therefore DC obtained from IR will

give different results compared to e.g. XRD (long-range order crystallinity) as those two techniques give information about different kinds of crystallinity. However, IR can detect small crystalline domains that cannot be detected by long-range crystallinity techniques.<sup>237</sup>

While using IR, true crystallinity bands need to be identified which can be a challenging task due to their possible association with regularity or preferred conformations that are also likely to be present in non-crystalline phase.<sup>238</sup> Hence, IR bands should be assigned as crystalline after confirmation that the given polymer can be crystalline (by other experimental technique), and when it disappears upon sample melting. In the case of PVA, confirmed crystalline bands have been identified at  $1144\text{ cm}^{-1}$ .<sup>39,42</sup>

For bands that can be genuinely assigned to 3D crystalline order in the range of Beer-Lambert law applicability and experiment performed on FTIR, Equation 2.18 can be used to calculate DC:

$$A_{FTIR} = \log\left(\frac{I_0}{I}\right) = a_c \cdot DC_{FTIR} \cdot \rho_s \cdot d_s \quad 2.18.$$

where  $A_{FTIR}$  is the absorbance or optical density,  $I_0$  and  $I$  are the incident and transmitted intensity, respectively,  $\rho_s$  the overall sample density and  $a_c$  the absorption coefficient of the 100% crystalline material. Equation 2.18 can also be used to calculate amorphous content of the polymer if the spectrum of given polymer material contains bands that can be directly assigned to non-crystalline phases.

As fully crystalline specimens are rarely available, there is a need to estimate  $a_c$ .<sup>239</sup> Measuring crystallinity using FTIR is therefore not a direct method as the quantitative correlation between the intensity of a crystallinity band (normalized to the intensity of a reference band to exclude effect of sample thickness) as well as values of degree of crystallinity obtained by an independent method (to calculate  $a_c$ ) must be known.<sup>39,42</sup> Even though sometimes these calculations are not fully accurate as they provide the information

about various kinds of crystallinity, they can be used for monitoring changes of DC with changes in polymer matrix.

FTIR can be a very useful tool to provide complete structural information about the polymer: chain conformation, stereoregularity, characterization of polymer blends, deformation effect, inter- and intramolecular interactions, morphological units, and structural changes as a consequence of thermal annealing or mechanical stretching. FTIR has been shown to be a useful tool to investigate the effect of plasticiser (glycerol),<sup>80</sup> starch<sup>240</sup> as well as other additives (such as fillers) in the pure PVA system and their influence on polymer crystallization.<sup>241</sup> Further, the effect of polymer DH on chemical crosslinking and resultant film microstructure of PVA with glutaraldehyde has been investigated.<sup>242</sup> Moreover, FTIR was utilized for mechanical studies on PVA,<sup>243</sup> and diffusion of water and acetone into nanocomposites of PVA and clay.<sup>244</sup>

### **2.11.2. Experimental procedure**

In this work, FTIR measurements were applied to investigate the DC within solution cast PVA-based films against changes in the polymer matrix microstructure. FTIR measurements were performed on Bruker Lumos FTIR Microscope. Spectra were recorded from 4000 to 600  $\text{cm}^{-1}$  with 32 scans and resolution of 4  $\text{cm}^{-1}$  using diamond as ATR-FTIR crystal (penetration depth of ca. 2  $\mu\text{m}$ ). Baseline data correction was performed using airPLS algorithm<sup>245</sup> – an iterative algorithm that does not require any input information, hence minimising measurement error – using Python scripts. Crystallinity was determined using ratio of the intensity of the crystalline to non-crystalline peaks using three pairs of these peaks and two equations as mentioned in the literature (Chapter 7). As absorption values were too low and noise was too high for spin-coated samples, it was not possible to establish DC for thin films.

## Chapter 3. Molecular diffusion in tertiary poly(vinyl alcohol) solutions

*Accepted for publication as: Majerczak, K.; Squillace, O.; Shi, Z.; Zhang, Z.; Zhang, Z. J. Molecular Diffusion in Ternary Poly(Vinyl Alcohol) Solutions. Front. Chem. Sci. Eng. 2021.*

### 3.1. Introduction

PVA is exposed to additives and surfactants throughout the life cycle of the formulated product. Migration of additive molecules in such complex systems has a significant impact on the manufacturing process as well as on product shelf-life and performance, itself determined by the molecular interactions between PVA and the small molecules present, often in aqueous solution.

Despite advancements in models describing diffusion in polymer systems, these mechanisms still cannot fully model polymer behaviour,<sup>246,247</sup> proving the need for further investigations. Indeed, the size,<sup>248</sup> shape,<sup>93,248,249</sup> and flexibility of the molecules were proven to significantly influence the magnitude of the rotational dynamics<sup>250</sup> and translational diffusion coefficient<sup>251–254</sup> due to temporary confinement,<sup>253</sup> molecular crowding,<sup>255</sup> and reversible binding to ‘traps’ in the system.<sup>256</sup> Furthermore, intermolecular interactions between solutes and solvent are often complex, substantially influencing the anomalous character of diffusion in polymer solutions.

Investigations into the mechanisms that determine the molecular diffusion in PVA solutions are further complicated by the formation of complexes in the presence of charged molecules (e.g. surfactants).<sup>257,258</sup> For example, surfactants were shown to influence the viscosity of PVA solutions because of the changes in intermolecular interactions<sup>259,260</sup> and formation of molecular aggregates.<sup>261</sup>

For polymer solutions, extensive studies had been carried out to investigate the magnitude of the intermolecular interactions and the formation mechanisms of complexes,<sup>257,259,260,262–264</sup> with less attention paid on the effect of the additives on the molecular diffusion characteristics. Further, the majority considers only a binary system that contains the polymer and a particular guest molecule. To understand the molecular interactions in a complex, multi-component polymer solution that is relevant to industrial applications, four components are essential: solvent, polymer, plasticiser, and another additive (i.e. a surfactant of various head group chemistry).

Molecular diffusion in a polymer solution can be measured by a range of techniques, including fluorescence methods such as FCS,<sup>215</sup> DLS,<sup>265,266</sup> pulsed-field gradient spin-echo NMR,<sup>267</sup> and centrifugation (sedimentation).<sup>268,269</sup> They can be further divided into techniques measuring self-diffusion coefficient (describing the motion of the molecule due to the thermal motion that is relative to the surrounding molecules) and cooperative diffusion coefficient (transport of a number of molecules due to density gradient), both of which offer critical information about migration behaviour of molecules in a controlled environment.<sup>270</sup>

Among the techniques measuring self-diffusion coefficient, FCS enables investigation at the single-molecule level, with minimal disruption to the system being investigated. It has been used to characterise the self-diffusion of both polymer<sup>271–274</sup> and probe of various sizes, chemistry and concentration in both dilute and semi-dilute solutions,<sup>161,275–280</sup> revealing the binding,<sup>270</sup> reaction kinetics,<sup>281</sup> and crowding effects,<sup>282</sup> and offering the capability to explore an unknown microstructure.<sup>283</sup> FCS also enables investigations into diffusion mechanisms,<sup>284</sup> differentiating anomalous,<sup>160,256,285,286</sup> walking-confinement,<sup>287</sup> and time-dependent diffusion behaviours.<sup>288</sup> DLS, on the other hand, is used widely to measure the cooperative diffusion



coefficient, but is incapable of examining multicomponent systems as all solutes contribute to the scattering signal.<sup>161</sup>

In the present study, the effects of crowding and intermolecular interactions on the molecular diffusion in ternary mixtures that replicate PVA-based chemical products dissolved in water were investigated. RhB, an industrially applied,<sup>289–291</sup> well-characterised fluorophore<sup>292</sup> was selected. Initially, diffusion of RhB in PVA solutions of different polymer concentrations was measured by FCS and analysed by a hydrodynamic stretched exponential model to examine the effects of molecular crowding.<sup>293</sup> Glycerol, a plasticiser commonly used for PVA formulations,<sup>80</sup> was subsequently introduced to observe its effect on the diffusion of RhB. Finally, surfactants of various head group chemistry (cationic/nonionic/anionic) were introduced to investigate the effect of detergent on molecular diffusion. By introducing complexity in a stepwise fashion, the contribution of each newly added component was examined independently. This way, the specific interactions between each component could be characterised, revealing three primary effects: the behaviour of the polymer itself, the overall molecular crowding in the system, and specific (charged) interactions between individual species. Overall, these findings enable prediction of behaviour in complex systems.

### 3.2. Materials and methods

**Materials.** Chemical structures of the components used in this study are shown in Figure 3.1.

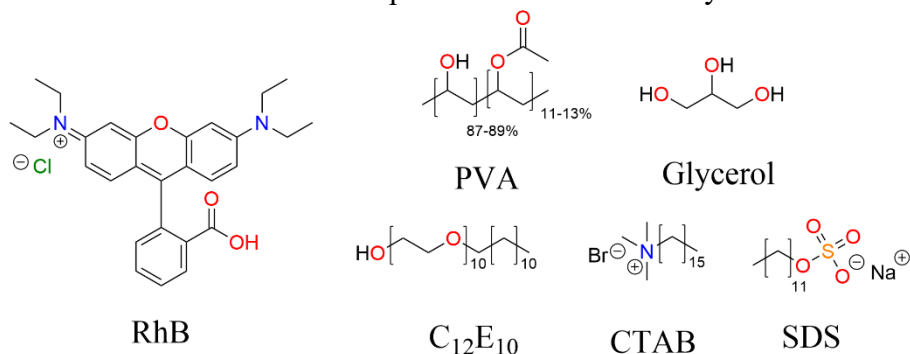


**Figure 3.1.** Chemical structure of compounds used in this study.

**Sample preparation.** Stock solutions were prepared as described in Chapter 2. Then, multiple sets of solutions were prepared by mixing PVA/glycerol/surfactant stock solutions at various volumetric ratios, as presented in Scheme 1, to examine:

- Effect of PVA concentration in the absence of other additives (Figure 3.2A)
- Effect of glycerol addition at various concentrations (Figure 3.2B, C)
- Effect of surfactant in the absence of glycerol (Figure 3.2D)
- Synergistic effect of both surfactant and glycerol at a 12:4:1 PVA/glycerol/surfactant mass ratio (Figure 3.2E, F)

Molecular probe, RhB, was introduced to the corresponding test solutions using a 2.5 mM stock solution to obtain a final concentration of 50 nM. A piranha solution cleaned cover slip<sup>182</sup> with 50  $\mu$ L of each as prepared solution was used for FCS analysis.

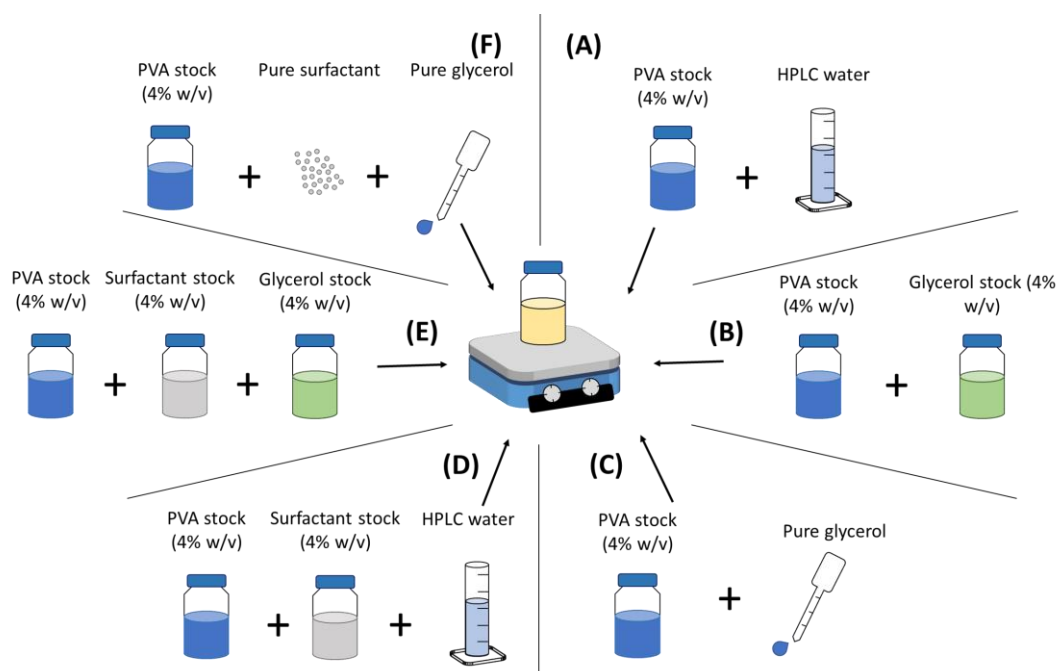


**Figure 3.2.** Preparation method for test solutions of various compositions: (A) PVA solutions of various concentrations, (B) PVA/glycerol solutions of various ratio of components (with changes in PVA concentration), (C) PVA/glycerol solutions of various ratio of components (with almost constant PVA concentration), (D) PVA/surfactant solutions, (E) PVA/glycerol/surfactant solutions and (F) concentrated PVA/glycerol/surfactant solutions.

**Methods.** FCS, DLS and rheological measurements were performed as described in Chapter 2.

### 3.3. Results and discussion

#### 3.3.1. Determining the appropriate model for PVA diffusion in solution

Dynamics of polymers in solution is determined by their concentration, with three distinguishable regimes: in the dilute regime, each polymer chain can be treated individually; in the intermediate semi-dilute regime, polymer coils overlap and their diffusion is dominated by a reptation process, with chains moving primarily parallel to their own backbones; whilst in the concentrated regime, chains are in close proximity to the others, with consequent interactions.<sup>272,294</sup> A polymer solution is in the semi-dilute regime when its concentration is greater than the overlap concentration ( $c^*$ ) that can be calculated according to Equation 3.1:<sup>272</sup>

$$c^* = \frac{3M_w}{4\pi N_A R_g^3} \quad 3.1.$$

where  $N_A$  is Avogadro's number, and  $R_g$  is the radius of gyration.  $R_g$  of the PVA molecules used in the present work is in the region of 6.7-10.3 nm, calculated with Equation 3.2.<sup>295</sup>

$$R_g = 0.0388M_w^{0.5} \quad 3.2.$$

Minimum value of  $c^*$  (1.1% (w/v)) suggests that most of the investigated solutions in the present work are in the semi-dilute regime, wherein the thermodynamic behaviour is governed by a specific correlation length ( $\xi$ ) – the average distance between the points of entanglement of different chains. While the exponent 0.5 in Equation 3.2 implies that water is a theta solvent for PVA, this form is also valid for a good solvent in the case where  $R_g$  is presented as the product of Flory expansion parameter ( $\alpha_F$ ) and radius of gyration in a theta solvent ( $R_g^0$ ).<sup>296</sup> Therefore, Equation 3.2 obtained from fitting experimental data to mathematical formula<sup>295</sup> can be used here for  $R_g$  calculations.

The difference between  $\xi$  and the size of the molecular probe introduces three sub-regimes of semi-dilute regime: for probes whose size is either far greater or smaller than  $\xi$ ,

viscosity of the solution or pure solvent, respectively, determine their diffusion rates.<sup>161,285</sup> However, for molecular size that is of the same order of magnitude as  $\xi$  (ca. 1.14 nm for RhB),<sup>297</sup> further investigation into dominating factors controlling the diffusion processes is required.<sup>161</sup> To assess  $\xi$ , Equation 3.3 was used:<sup>297</sup>

$$\frac{R_g}{\xi} = \left(\frac{c}{c^*}\right)^{0.75} \quad 3.3.$$

where  $c$  is concentration of polymer solution. The average values of  $\xi$  (Table 3.1) and its minimum in the currently investigated system (2.6 nm) are either lower or of the same magnitude as  $R_g$  of PVA, confirming the finding that all samples investigated can be treated as belonging to semi-dilute regime.<sup>298</sup> Moreover, since the value of  $\xi$  is in general of the same order of magnitude as  $d_H$  of the tracer used, it is appropriate to use the third subregime. Therein, a semi-empirical stretched exponential function (such as in Equation 3.4)<sup>293</sup> has been developed to describe its diffusion behaviour:

$$\frac{D}{D_0} = \exp(-\beta c^{n_{FCS}}) \quad 3.4.$$

where  $D_0$  is the diffusion coefficient of RhB in pure solvent;  $n_{FCS}$  is a scaling parameter related to the polymer chain excluded volume, which reflects the solubility of the polymer ( $n_{FCS}=1$  for theta solvent and  $n_{FCS}=0.75$  for good solvent); and  $\beta$  is a pre-factor related to the probe size that can be described by Equation 3.5:<sup>161</sup>

$$\beta = \frac{R_p}{r_p \cdot c^{*n_{FCS}}} \quad 3.5.$$

where  $R_p$  is the radius of the probe, and  $r_p$  is the average polymer chain size, signifying that  $\beta$  scales linearly with the size of the probe particle, which was confirmed experimentally.<sup>161</sup>

**Table 3.1.** Compositions used to investigate the dependence of RhB diffusion coefficient on PVA concentration. Average number of repeating units in PVA molecule used in the calculation is 581.

Sample	PVA concentration (%(w/v))	Average $\xi$ (nm)	Average $\eta$ (mPa·s)	Average $d_H$ (nm)
1	0.0	-	0.890 <sup>299</sup>	-
2	1.0	19.9	1.184 ± 0.016	12.6 ± 0.2
3	2.0	11.9	1.813 ± 0.032	8.2 ± 0.1
4	3.0	8.8	2.669 ± 0.024	6.1 ± 0.1
5	3.3	8.0	2.975 ± 0.024	6.0 ± 0.1
6	4.0	7.1	4.052 ± 0.081	3.8 ± 0.1

Equation 3.4 provided a satisfactory fit for changes of diffusion coefficient of particles in semi-dilute PVA solutions,<sup>161</sup> and was used in the present work to interpret diffusivity measurements as a function of PVA concentration with or without the addition of glycerol to estimate  $\beta$  and  $n_{FCS}$ .

### 3.3.2. Molecular diffusion in PVA solutions

Diffusion of the molecular probe, RhB, in PVA solutions was quantified using FCS with three sets of independent experiments on different days. Figure 3.3 shows the relationship between the measured diffusion coefficients, upon satisfactory fit of the autocorrelation function (Figure 10.1, Appendix A), and the concentrations of PVA (0-4% w/v), using Equation 3.4. It was found that there is a decrease in RhB diffusion coefficient (from 432.4  $\mu\text{m}^2/\text{s}$  to 188.4  $\mu\text{m}^2/\text{s}$  for solutions 1 and 6, respectively) with an increased PVA concentration. Using the least squares method, values of  $\beta=0.270\pm0.019$  and  $n_{FCS}=0.767\pm0.046$  were obtained, which are consistent with the values reported in literature for tracer molecules of similar chemistry and/or size,<sup>161</sup> and confirming that water is a good solvent for PVA ( $n_{FCS} \approx 0.75$ ).

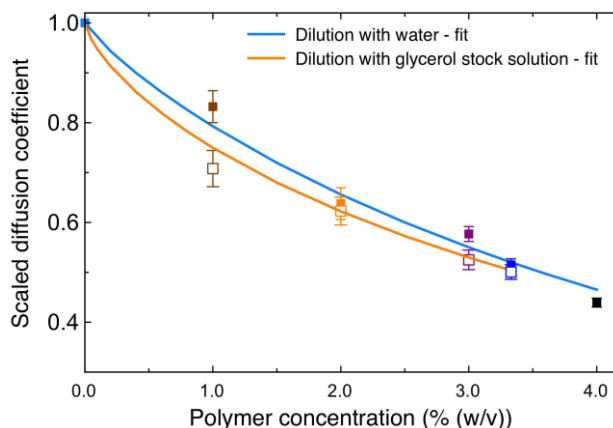


**Figure 3.3.** Normalised diffusion coefficient of RhB as a function of PVA concentration without (samples 2-6) and with glycerol (samples 1a-5a). Solid lines represent fit to Equation 3.4, with diffusion coefficient calculated using Equation 2.8. Closed symbols correspond to PVA solution diluted with water, while open symbols – PVA solution diluted with glycerol solution. Colour code for each PVA concentration corresponds to DLS data (Figure 3.4). Standard errors are based on 10 measurements.

The observed reduction in the diffusivity of RhB is likely attributed to the increased crowding density (itself a function of the polymer concentration), which can be directly correlated with the reduced  $d_H$  of PVA determined by DLS (Figure 3.4a) and the corresponding  $\xi$  (Table 3.1). For all of the investigated solutions, a polymodal size distribution was observed, which is inconsistent with a previous report for PVA of similar  $DH$ ,<sup>135</sup> but agrees with the behaviour of an almost completely hydrolysed PVA.<sup>300</sup> According to the calculated  $R_g$ , peak I in Figure 3.4 is assigned to the individual PVA chains, of which the maximum is shifted to lower  $d_H$  when there is less room available as the result of an increased number of molecules. This in turn leads to a significantly increased crowding density, impeding the migration of the probe. It is likely that peak II found in the size distribution profiles in Figure 3.4 corresponds to polymer aggregates,<sup>300</sup> whilst peak III is a sign of large clusters<sup>301</sup> in the solution. Considering that the scattered light intensity is proportional to diameter of given particle to the sixth power, the signal scattered from aggregates in intensity plot is amplified.<sup>218</sup> Majority of the scattered signal detected contributes to peak I, suggesting that the quantity of polymer aggregates and clusters is rather insignificant in the present work.

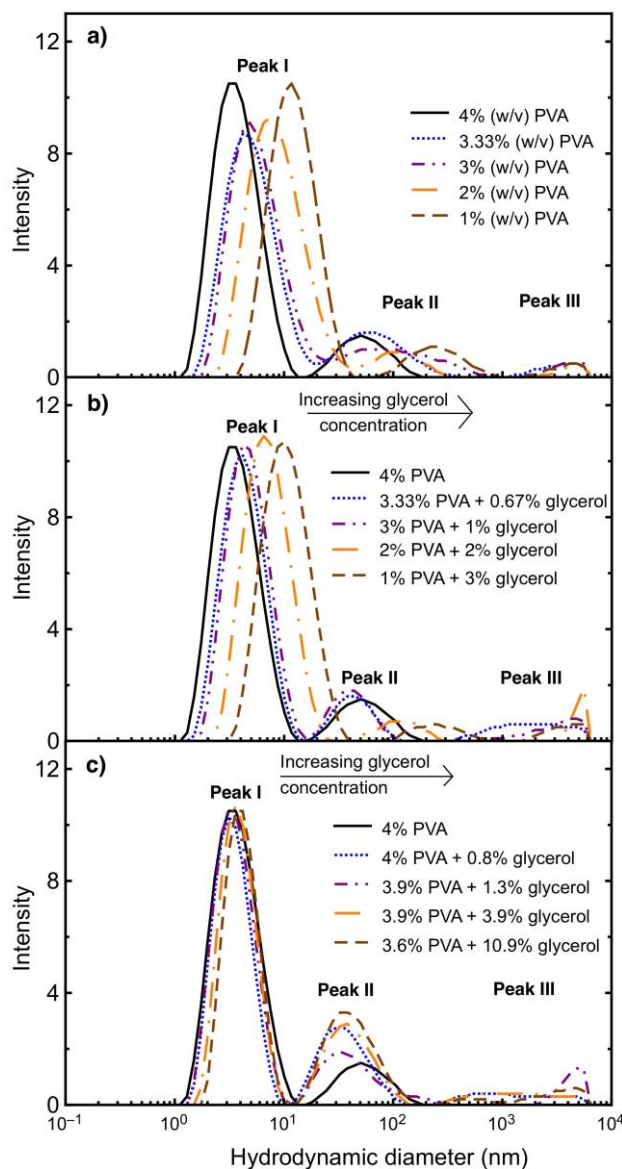


**Figure 3.4.** Distribution of hydrodynamic diameter for solutions of various PVA concentration with the addition of (a) water, (b) glycerol stock solution and (c) pure glycerol. The percentage of polymer in the graph is given in (w/v)%.

Hydrodynamic diameter of PVA was theoretically estimated to be in the range of 10.3 – 15.9 nm, following Equation 3.6.<sup>302</sup>

$$\frac{d_H}{R_g} = 1.54 \quad 3.6.$$

The value calculated from Equation 3.6 is in general smaller than the average  $d_H$  acquired from samples 2-6 (Table 3.1), which is likely due to the presence of steric obstructions in discussed

system. Since water is a good solvent for PVA, only weak excluded-volume interactions are present, with changes in viscosity directly correlated with the overlapping of the polymer chains.<sup>303</sup> The increased solution viscosity with increasing polymer concentration (Table 3.1) alongside the crowding density effects proven by DLS measurements confirm the effect of polymer-polymer interactions on molecular migration in the semi-dilute regime.

### 3.3.3. Molecular diffusion in PVA/glycerol binary solutions

Glycerol, commonly used as a plasticiser for PVA-based products such as water soluble films,<sup>17</sup> competes with PVA molecules to form PVA-glycerol hydrogen bonds at the expense of PVA-PVA hydrogen bonds. However, both types of interaction could be hampered when glycerol and PVA molecules are well solvated by an excessive amount of water. Addition of glycerol led to an increased viscosity (Table 3.2), reducing the diffusivity of the molecular probe due to the additional crowding effects.

**Table 3.2.** Composition of PVA-based solutions with the addition of glycerol. Samples of composition 1a did not provide reliable  $d_H$  results.

Sample	PVA concentration (wt%)	Glycerol concentration (wt%)	PVA:glycerol molar ratio	Average $\eta$ (mPa·s)	Average $d_H$ (nm)
Addition of glycerol solution	1a	0.0	0:1	$0.971 \pm 0.011$	-
	2a	1.0	1:1629	$1.437 \pm 0.051$	$10.4 \pm 0.1$
	3a	2.0	1:543	$2.136 \pm 0.026$	$7.5 \pm 0.1$
	4a	3.0	1:181	$3.065 \pm 0.060$	$5.2 \pm 0.1$
	5a	3.3	0.7	1:109	$3.383 \pm 0.004$
Addition of pure glycerol	2b	3.6	1:1629	$4.574 \pm 0.020$	$5.2 \pm 0.2$
	3b	3.9	1:543	$4.020 \pm 0.044$	$4.9 \pm 0.1$
	4b	4.0	1:181	$4.009 \pm 0.049$	$4.4 \pm 0.1$
	5b	4.0	0.8	1:109	$4.024 \pm 0.097$

To distinguish the effects of overall solute concentration and interactions between PVA and glycerol, two additional sets of samples (1a-5a and 2b-5b) were prepared, keeping either the total (PVA + glycerol) or PVA concentration constant, for which the molar ratio between



PVA and glycerol was equivalent (i.e. the PVA/glycerol molar ratio in sample 2a is the same as in sample 2b etc.). Compositions of the binary PVA/glycerol solutions investigated are presented in Table 3.2. As new species are introduced, it is expected that  $D$  of RhB will decrease, either due to PVA-glycerol interactions (leading to increased polymer-plasticiser aggregate size and consequent increase in RhB mean free path) or overall molecular crowding (leading to increase in macroscale viscosity).

### 3.3.3.1. Synergistic effect of water and glycerol

The diffusion coefficients of RhB in PVA/glycerol binary mixtures were found to decrease non-linearly with an increasing PVA concentration (Figure 3.3), in a similar trend to that observed for PVA solution without glycerol (samples 2-5). Both sets of FCS experiments (solutions with or without glycerol) were investigated on the same day to minimise the experimental errors due to any potential variations in environmental conditions, laser output, or calibration.

Overall, addition of glycerol solution instead of water led to an increased diffusion time for solutions of the same PVA concentration. Following a stretched exponential fit (Equation 3.4),  $\beta$  and  $n_{\text{FCS}}$  were estimated as  $0.304 \pm 0.016$  and  $0.666 \pm 0.036$  for samples 2a-5a, accordingly. In here, glycerol stock solution was treated as a new solvent, hence diffusion coefficient of RhB in this solution was used as  $D_0$  (equation 3.4). Different fitted values both of  $\beta$  and  $n_{\text{FCS}}$  may arise due to the composition of the solvent, i.e. normalisation against  $D_0$ . Statistical t-test result ( $\alpha=0.05$ ) confirms that there was no significant difference in the measured diffusion coefficients of RhB in PVA solutions with (2a-5a) or without glycerol (2-5), as presented in Table 10.1, Appendix A. It can be concluded that concentration of PVA in

the solvent plays a dominant role in determining the diffusivity of PVA at low glycerol concentration (up to 4% (w/v)).

The decreased value of  $n_{\text{FCS}}$  indicates a reduced solvent quality, whilst the increased pre-factor  $\beta$  suggests migration of molecule of larger size. These are attributed to the interactions between glycerol and the other species present. RhB-glycerol interactions will slow the tracer diffusion directly due to entrainment of larger molecules in the solvation shell, whereas in the case of PVA, larger glycerol-PVA aggregates will increase the solution molecular crowding hence indirectly slowing tracer diffusion.

The latter is responsible for the changes observed in PVA size distribution with samples 2a-5a (Figure 3.4b). Similar to samples 2-5, shift of the size distribution towards larger  $d_{\text{H}}$  with increasing dilution of the system is observed. However, increased viscosity and higher number of solute molecules present in samples 2a-5a, in comparison to samples 2-5, lead to the decrease in  $d_{\text{H}}$  of the PVA molecules (Table 3.1, Table 3.2), resulting in a decreased diffusion coefficient of the probe. Upon dilution by either pure water or glycerol solution, changes in the average  $d_{\text{H}}$  of PVA show an almost linear dependence on the viscosity of the solution, whilst the corresponding DLS autocorrelation functions show almost no change in its characteristics (Figure 10.2, Appendix A).

Although it is not possible to exclude the likelihood that the solvation shells of RhB molecules are expanded in glycerol solution, the DLS results acquired strongly imply that the additional crowding effects are responsible for the increased  $\beta$  values. PVA concentration, however, showed a dominating influence. To clarify conclusions about observed mechanisms, further experiments using higher concentrations of glycerol were carried out.

### 3.3.3.2. Effect of glycerol addition

A set of PVA/glycerol binary mixtures (samples 2b-5b, Table 3.2) were prepared by introducing pure glycerol to PVA solutions to distinguish the effects of glycerol and water on RhB diffusivity. The average diffusion coefficients (Figure 3.5) show that glycerol has no notable impact on the RhB diffusion coefficient at low concentrations (0-3.9% (w/v)), but causes it to decrease at high concentrations (> 3.9% (w/v)).

DLS results of this set of samples (Figure 3.4c) indicate that increasing glycerol concentration causes a barely noticeable increase in  $d_H$  (the minimal shift of peak I that corresponds to the individual PVA molecules), as well as an increased intensity of peak II. This suggests a formation of glycerol-PVA complexes (leading to the slight increase in  $d_H$  of peak I) and a greater number of polymer-polymer clusters (peak II). In contrast, for samples 2a-5a where the solute concentration was constant, the trend with increasing PVA concentration is similar to that of samples 2-5 (containing only PVA). It appears that chains become more compact (accelerated by the presence of other solutes) as PVA concentration increases to 4% (w/v). Conversely, when PVA concentration is constant but overall solute concentration increases, glycerol-PVA complexes form, leading to the slight increase in measured  $d_H$ .

Another factor that determines molecular diffusion is the solution viscosity, of which a constant value was observed up to 1:1 polymer to glycerol mass ratio (Table 3.2). Glycerol is therefore likely to disrupt polymer-polymer entanglements, which results in no viscosity changes. For sample 2b (containing 10.9 wt% glycerol), however, an increased solution viscosity was observed. It might be attributed to the high viscosity of glycerol itself (ca. 0.945 Pa·s for pure glycerol<sup>304</sup> cf. 0.890 mPa·s for water<sup>299</sup> at 25°C), which becomes important once 1:1 ratio of components is reached.

It is worth noting that the increased glycerol content in samples 2b and 3b resulted in a broad range of diffusion times and consequent diffusion coefficients (as can be seen by relatively large error bars in Figure 3.5 as glycerol concentration increases), with measurements of much slower diffusion time compared to samples 4b and 5b noted, and an overall decrease of RhB diffusivity. It is probable that samples 4b and 5b have a more homogeneous composition, where crowding effects is less important than for samples 2b and 3b. Samples of low glycerol content show smaller changes in  $d_H$  (Table 3.2) compared against solution 6 (4.0 wt% PVA only), which, together with the described viscosity behaviour, leads to a similar diffusion coefficient of the tracer to that in PVA stock solution. As for sample 3b, increased number of solute molecules is likely the more pronounced effect than viscosity values similar to that of PVA stock solution, despite the minor increase in the average  $d_H$ . PVA-glycerol clusters therefore influence the migration of the molecular probe: the higher glycerol concentration, the more visible change in tracer diffusion coefficient.

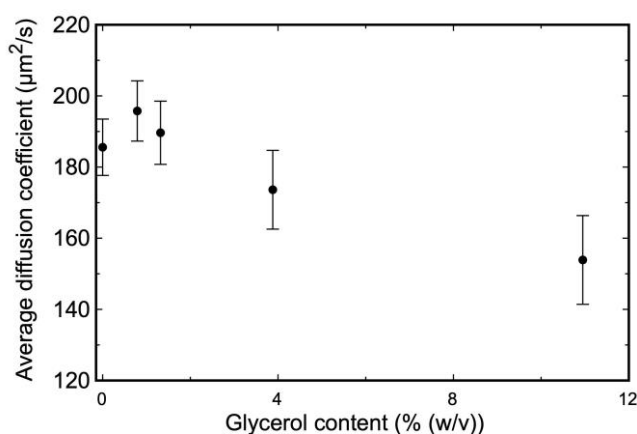


**Figure 3.5.** Diffusion coefficient of RhB in PVA solution with the addition of pure glycerol. Error bars are one standard error around the mean, number of measurements equal to 10.

Generally, adding glycerol to PVA solutions at low concentrations without adjusting the overall water concentration has a minimal effect on the diffusion characteristics of RhB or the aggregation behaviour of PVA compared to the results acquired in pure water. Addition of large quantity of pure glycerol, however, caused a reduction in the diffusivity of RhB. It is

worth noting that the size of PVA was very similar in these solutions, indicating that the hydrodynamic diameter of PVA is primarily dependent on its concentration, whilst the addition of glycerol appeared to promote the formation of PVA-glycerol complex. With this characterisation of the effects of adding glycerol on the solution behaviour, understanding the effect of introducing our model additives to the discussed system is now possible.

### 3.3.4. Molecular diffusion in PVA/glycerol/surfactant tertiary solutions

Diffusion of RhB in ternary aqueous solutions of PVA, glycerol, and surfactant were studied to quantitatively establish the effects of crowding and binding on the mobility of the probe as a function of the surfactant chemistry (cationic/nonionic/anionic). Specifically, the samples were prepared from polymer-surfactant mixtures (samples 4c-4e, Table 3.3), glycerol and surfactant solutions added to PVA solution (samples 4c-4h, Table 3.3), as well as from polymer solutions with the addition of pure glycerol and surfactant (samples 4i-4k, Table 3.3).

**Table 3.3.** Viscosity and average hydrodynamic diameter of PVA solutions with the addition of glycerol and surfactant of various head group chemistry.

Sample		Surfactant	PVA/glycerol/ surfactant molar ratio	Average $\eta$ (mPa·s)	Average $d_H$ (nm)
Addition of water	4c	SDS (-)	1:0:14.5	$2.462 \pm 0.200$	$5.6 \pm 0.2$
	4d	C <sub>12</sub> E <sub>10</sub> (0)	1:0:6.7	$2.122 \pm 0.034$	$6.9 \pm 0.1$
	4e	CTAB (+)	1:0:11.4	$2.877 \pm 0.022$	$5.1 \pm 0.1$
Addition of glycerol solution	4f	SDS (-)	1:181:14.5	$2.939 \pm 0.043$	$4.1 \pm 0.1$
	4g	C <sub>12</sub> E <sub>10</sub> (0)	1:181:6.7	$2.313 \pm 0.040$	$6.0 \pm 0.1$
	4h	CTAB (+)	1:181:11.4	$3.060 \pm 0.222$	$4.5 \pm 0.1$
Addition of pure glycerol and surfactant	4i	SDS (-)	1:181:14.5	$5.550 \pm 0.230$	$2.4 \pm 0.1$
	4j	C <sub>12</sub> E <sub>10</sub> (0)	1:181:6.7	$4.315 \pm 0.057$	$3.9 \pm 0.1$
	4k	CTAB (+)	1:181:11.4	$5.658 \pm 0.456$	$2.6 \pm 0.1$

In this case, rather than RhB diffusivity decreasing due to increased molecular crowding, it is expected that strong directional (i.e. charge-matching) interactions between the ionic surfactants and the tracer will lead to reduced diffusivity in the system. The nonionic surfactant, however, is expected to act similarly to glycerol.

### 3.3.4.1. Addition of glycerol and/or surfactant stock solutions

Average diffusion coefficients of RhB in PVA/glycerol/surfactants ternary mixtures are presented in Figure 3.6. It appears that the addition of surfactant led to a decreased diffusion coefficient of RhB: SDS has the most significant reduction (by 86%), followed by CTAB (by 70%), whilst C<sub>12</sub>E<sub>10</sub> shows the least impact (by 31%) compared with the control solution that had no surfactants. Surfactants seemed to change the nature of the molecular interactions via the formation of charge-matching complexes with RhB. Although this behaviour would likely cause the ternary mixtures to become less homogeneous,<sup>17,295</sup> diffusion coefficients measured here show a monomodal distribution with low standard error, confirming that the average values reported are representative.

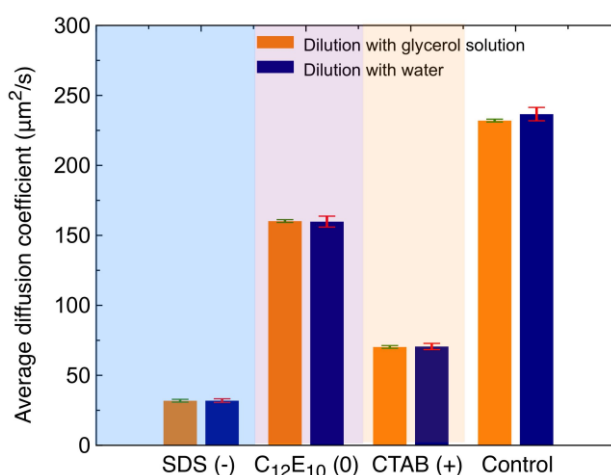


**Figure 3.6.** Average diffusion coefficient of RhB in PVA solutions with the addition of surfactant and water (samples 4c-4e) or glycerol solution (samples 4f-4h), compared against control samples with no surfactants (4, 4a). Error bars are standard error based on 10 repeats.

No notable difference in RhB diffusivity was found for system composed of PVA/surfactant solutions with the addition of glycerol stock solution (samples 4f-4h, orange bars in Figure 3.6), in comparison to the ones diluted by water (samples 4c-4e, blue bars in Figure 3.6). Indeed, experiments performed on the same day resulted in the average diffusion times and distributions of very similar range with no statistically significant difference ( $\alpha=0.05$ ). It is clear that the addition of glycerol at low concentration does not influence the diffusion coefficient of RhB in the polymer solutions with the presence of surfactant and therefore that the surfactants are primarily responsible for such a significant change in probe diffusivity. This is consistent with the findings acquired from the PVA/glycerol binary mixtures (solutions 2a-2e, Table 3.2), where addition of glycerol solution has minimal effects on RhB diffusivity and PVA particle size.

Strong interactions between RhB and charged surfactants have been identified elsewhere as controlling their behaviour both below and above the critical micelle concentration (CMC) due surfactant-dye aggregation or entrapment within micelles.<sup>305</sup> In this study, surfactants were above their respective CMC for all formulations studied with the exception of samples 4c and 4f (however, the CMC is expected to be decreased in the presence of PVA).<sup>125</sup> Indeed, the aggregation between RhB (in its zwitterionic form following dissociation)<sup>306</sup> and surfactants hinders its diffusion rate. The findings presented here agree with a previous study which showed that the diffusion coefficient of RhB was significantly reduced due to the SDS-RhB interactions that is dependent on the pH of the solution.<sup>307</sup> In addition, there is a possible polymer-surfactant attraction, whose magnitude is determined by the counterion effect of surfactant on water<sup>308</sup> and the chemical characteristics of the compounds involved.<sup>309</sup>

Similarly to SDS, CTAB is likely to form charged aggregates with RhB, leading to a substantial change in the diffusion coefficient of RhB, with a similar magnitude for SDS and

CTAB.<sup>305</sup> Even though the number of possible interaction sites for cationic and anionic surfactant is the same, accessibility is probably sterically hindered to the anionic moiety of RhB, which explains the differences of RhB diffusivity in ternary PVA solutions with cationic and anionic surfactant (Figure 3.7a).

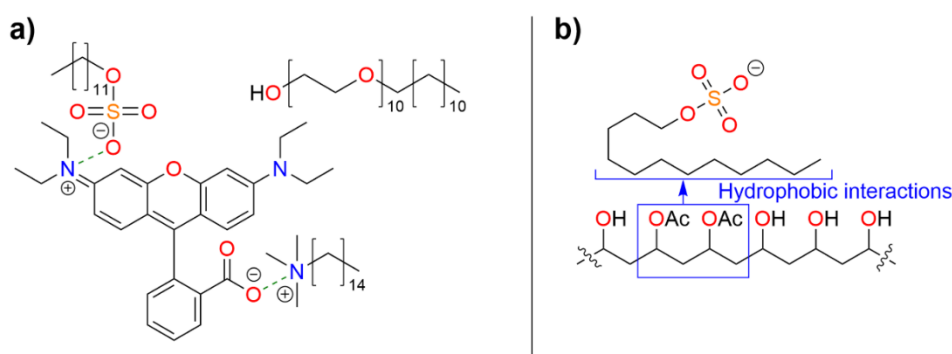


**Figure 3.7.** Possible interactions between (a) RhB and both cationic and anionic surfactants; (b) PVA-surfactant tail group interactions, using SDS molecule as an example.

### 3.3.4.2. Specific effects of ionic surfactants (SDS and CTAB)

Upon the introduction of charged surfactants, DLS shows a reduction in average  $d_H$  of the PVA molecules (Figure 3.8, Table 3.2 and Table 3.3). This effect is consistent in both PVA-surfactant mixtures diluted by water (Figure 3.8a) and by glycerol (Figure 3.8b).

The polymer-surfactant interactions via their hydrophobic parts are believed to be a major driving force in the system (Figure 3.7).<sup>134,310</sup> SDS was shown to disrupt polymer aggregates in aqueous solution<sup>259</sup> – such effect was more pronounced for PVA of low degree of hydrolysis (i.e. 70% DH) due to an increased fraction of acetate groups in the polymer chains.<sup>135</sup> Moreover, SDS is capable of shifting PVA-glycerol interaction to glycerol-SDS interactions in PVA films.<sup>17</sup> Even though presented measurements are in liquid state, those interactions are also plausible. The combined effect of increased molecular crowding due to the presence of surfactant micelles as well as polymer-surfactant interactions led to more compact molecular packing, hence decreasing  $d_H$  of the PVA.



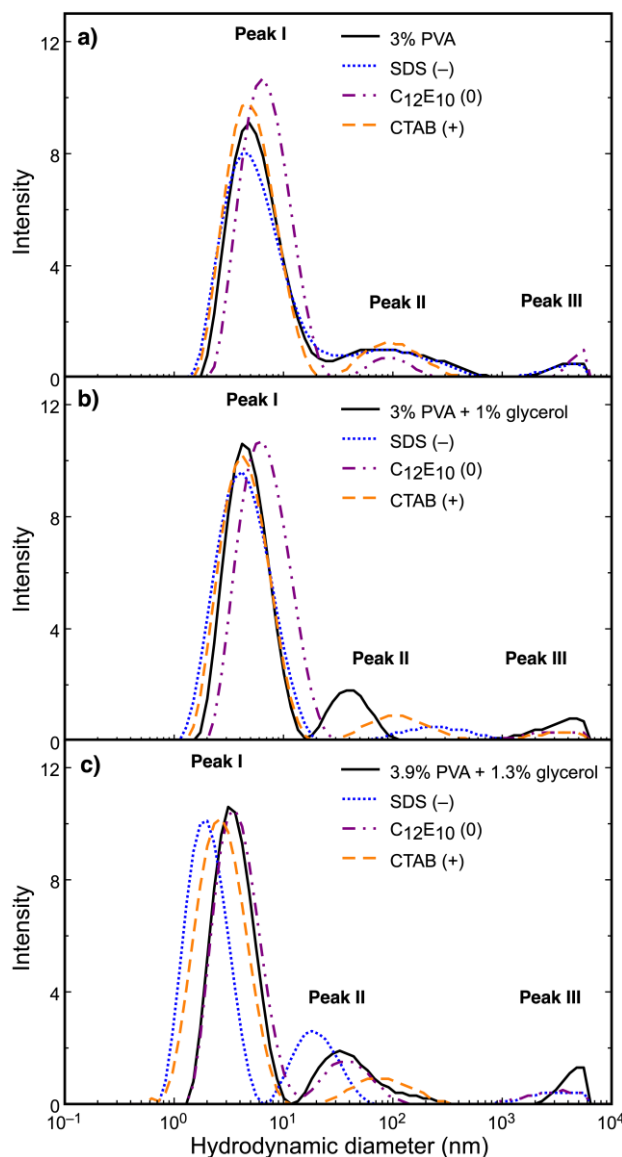


**Figure 3.8.** Particle size distribution for (a) PVA/water/surfactant (compositions 4c-4e), (b) PVA/glycerol/surfactant solutions (compositions 4f-4h) and (c) PVA/pure glycerol/pure surfactant solutions (compositions 4i-4k). The percentages of polymer and glycerol in the graphs are given in (w/v)%.

In addition to the polymer-surfactant interaction, it is likely that the dilution itself could play an important role in the ternary PVA solutions by reducing solution viscosity. In PVA-SDS mixtures, hydrophobic interactions between species result in a preferential adsorption of the surfactants on polymer chains,<sup>311</sup> and change viscosity depending on the degree of hydrolysis of PVA<sup>134</sup> and amount of surfactant added.<sup>311</sup> Accordingly, both decreased<sup>134,311</sup> and increased<sup>312</sup> viscosity values of PVA solutions containing SDS have been reported. In this study

the viscosity decreased, primarily due to the reduced PVA concentration in all solutions discussed in this section after the introduction of surfactant solutions.

Previous studies suggest that CTAB would interact with PVA chain in a similar fashion to SDS, and form a polymer-surfactant complex.<sup>130,134,312</sup> Even though the PVA solution was diluted by the surfactant stock solution in the present work, the average  $d_H$  of PVA decreased (Table 3.2, Table 3.3), while viscosity either increased or remained unchanged compared to samples 4 and 4a (without addition of surfactant). It is therefore likely that CTAB interacts with PVA via hydrophobic interactions, disrupting the PVA-PVA interactions.

To conclude, two main factors hinder the diffusion of the molecular probe in the PVA-based ternary solutions: firstly, crowding effect that is caused by the increased polymer size and the presence of surfactants; secondly, interaction between RhB and surfactants that slow down the diffusion of the probe<sup>305</sup> (Figure 3.7a).

#### 3.3.4.3. Effects of nonionic surfactant solutions

Although adding surfactant solutions resulted in only a slight dilution of PVA-glycerol mixture compared to sample 4a, the presence of nonionic surfactants appeared to have a noticeable effect on the diffusion of the fluorescent probe (Figure 3.6). While charge-matching aggregation between C<sub>12</sub>E<sub>10</sub> and RhB cannot occur due to its nonionic nature, it remains possible for C<sub>12</sub>E<sub>10</sub> to interact with PVA via hydrophobic interactions between surfactant tail and acetate groups on the polymer. However, such effect appears to be less pronounced in comparison to CTAB and SDS addition as the ionic strength of the solution remains constant.

Unlike that of SDS and CTAB, stock solution of C<sub>12</sub>E<sub>10</sub> showed a monomodal size distribution (Figure 10.3, Appendix A), with a  $d_H$  very similar to peak I of the PVA particle-

size distribution. Indeed, overall  $d_H$  of solutions 4d and 4g increased compared their corresponding surfactant-free solutions (4 and 4a). The increased intensity of peak I in sample 4d (Figure 3.8a, b) can be related to both individual PVA molecules and micelles of  $C_{12}E_{10}$ . Therefore, the nonionic surfactant acts in a similar way to glycerol in the system, however with a larger effect due to the much larger molecular weight of  $C_{12}E_{10}$ .

Building upon the findings of surfactant-PVA and surfactant-RhB interactions at low concentrations, systems with the addition of pure glycerol and surfactant to PVA stock solution were investigated to study their influence in the absence of dilution (additional water being introduced) in the system.

#### **3.3.4.4. Crowding and binding effects**

Adding pure surfactant and glycerol to PVA solutions showed the same trend to that observed with adding their stock solutions. Their effects on the diffusion of RhB were pronounced in PVA solutions with the addition of anionic surfactant, which decreased by 67% for composition 4i compared to composition 4c (90% compared to 4b). For cationic and nonionic surfactants, the diffusion coefficients decreased by 44% and 46% respectively compared to compositions 4d and 4e (Figure 3.9), and by 75% and 41%, respectively compared to composition 4b. It is likely that the increased concentration of surfactants led to an additional crowding effect (as seen in the decrease in hydrodynamic diameter in Figure 3.8c). This is amplified due to the strong interactions between the RhB and surfactant in the now more concentrated solutions. The variation with different head group chemistry provides further evidence for preferential probe-surfactant interactions for charged surfactants, while the relatively weak response of  $C_{12}E_{10}$  compared to solution 4b again demonstrates its similar behaviour to glycerol.

Addition of surfactant to PVA solutions therefore has a significant retarding effect on the diffusivity of RhB, with the driving force for these changes being largely dependent on head group chemistry:

- For nonionic surfactant ( $C_{12}E_{10}$ ), a minimal interaction with the fluorescence probe is suspected, with the diffusivity of RhB being determined by the enhanced crowding effects the surfactant places on the PVA molecules.
- For anionic surfactant (SDS), there are strong surfactant-PVA and surfactant-probe interactions, leading to a significantly reduced diffusivity compared to  $C_{12}E_{10}$ .
- For cationic surfactant (CTAB), although the same type of interactions is present as in the system with SDS (i.e. hydrophobic interactions between tail group and PVA, and charge-matching interactions between head group and RhB), steric barriers reducing the surfactant-tracer interaction strength cause a less pronounced decrease in RhB diffusivity.

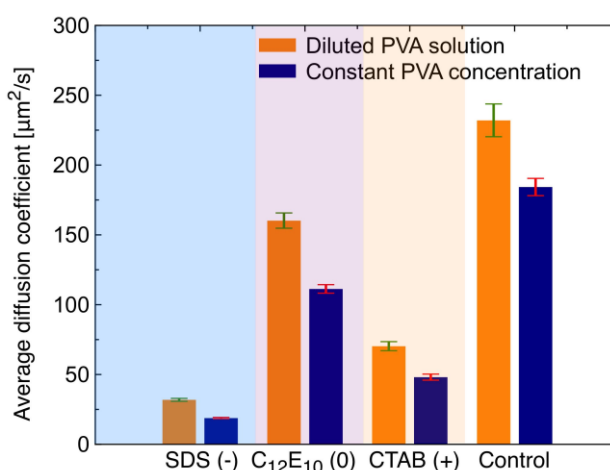


**Figure 3.9.** Average diffusion coefficients of RhB in PVA solutions with the addition of pure glycerol and surfactant (samples 4i-4k, blue columns) compared against equivalent samples with the addition of glycerol and surfactant solutions (4f-h, orange columns) and corresponding control solutions containing no surfactant (4a and 4b). Error bars are standard error based on 10 repeats.

The explanations above are supported by the viscosity data presented Table 3.3. The changes in the viscosity of PVA ternary solutions is negligible when nonionic surfactant was

used, but significant when ionic surfactants were interacting with the PVA molecules, in agreement with previous findings.<sup>312</sup> For all investigated solutions, no phase separation was observed (which is in line with results published for PVA-water-SDS system).<sup>17</sup>

### 3.4. Conclusions

Diffusion behaviour of a molecular probe (RhB) in a series of aqueous PVA solutions, representing complex formulations involved in industrial processes, was examined in the present work as a function of polymer and plasticiser concentration, as well as presence of surfactants of various head group chemistry. For the PVA solutions, our results present a good agreement with the scaling theory of anomalous diffusion in semi-dilute polymer systems, showing a non-linear increase of diffusion coefficient of the probe with decreasing polymer concentration. PVA solutions diluted by glycerol solutions instead of pure water do not exhibit significant changes in the mobility of RhB, proving the dominant nature of polymer concentration in the system. For PVA solutions with increased glycerol concentration, crowding effects play an important role in the system, leading to a decreased diffusivity of the probe due to the increased diffusion path length.

Crowding effects also provided a plausible explanation for the diffusion kinetics in the PVA solutions with the addition of nonionic surfactant. However, for solutions with the addition of cationic and anionic surfactant, surfactant-PVA and surfactant-RhB interactions play a dominant role, slowing down the migration of the tracer. These interactions are strengthened in the more concentrated PVA solutions with additional pure glycerol and surfactant (rather than their respective solutions), indicating that the concentration of each individual chemical compound (polymer and additives) present in the PVA ternary solutions has a profound influence on the diffusivity of the molecular probe.

## Chapter 4. Kinetics of molecular migration in thin poly(vinyl alcohol)-based films

### 4.1. Introduction

Notwithstanding recent advances in polymer science, it is currently impossible to fully predict the main mechanism of migration for any multicomponent polymer composite either theoretically or computationally due to their complexity. Theoretical investigation (e.g. through statistical thermodynamics methods such as Flory-Huggins compatibility theory)<sup>313,314</sup> of such systems is quite intricate because even though models can be used to describe bulk mixing between two chemically different species, they cannot be applied to the systems where local segregation close to the polymer/atmosphere interface takes place.<sup>315</sup> Therefore, they are inappropriate for modelling many real-world industrial formulations (e.g. polymer films doped with a surfactant) that exhibit the tendency for non-uniform distribution of the additive e.g. the creation of a surfactant wetting layer, both at the air-film<sup>316,317</sup> and air-water interface<sup>128,129</sup> due to incompatibility between the species.<sup>17,295,316</sup> Moreover, the character of mesostructures created in these products is dependent on specific intermolecular interactions<sup>128</sup> – ionic, polar, and nonpolar. Therefore, phenomena arising as the consequence of these interactions need to be considered to provide a possible set of design criteria which minimise guest molecule migration in the polymer matrix while ensuring optimum distribution of additives.<sup>295,318</sup>

A common approach to make these complex systems experimentally manageable is by using individual additive simulants rather than several additives, as are used in real-life polymer formulations.<sup>319</sup> Consequently, current research focuses on two-component<sup>246</sup> or three-component systems.<sup>251</sup> While there is in-depth understanding of interfacial phenomena in polymer blends<sup>320</sup> (including wetting layer formation),<sup>321</sup> the character of guest molecule migration is highly dependent on the chemical interactions between the migrant and polymer

matrix<sup>244</sup> and its overall rigidity (as increasing rigidity results in lower amount of the migrant molecule on the polymer surface).<sup>315</sup> Therefore, there is a need to extend experimental studies of molecular migration to multi-component systems as opposed to simpler formulations.

Furthermore, while many studies have been carried out to explain the diffusion of molecules from plastic films to surrounding media,<sup>94,322–325</sup> fewer describe migration in the opposite direction.<sup>326</sup> By mimicking migration towards the packaging film – e.g. by studying three component polymer/plasticiser/surfactant, rather than two component polymer/plasticiser or polymer/surfactant systems – prediction of more complex migration behaviour will become possible.

Techniques used for migration measurements can establish rapid diffusion coefficients (i.e.  $10^{-8}$ - $10^{-5}$  cm<sup>2</sup>/s, corresponding to the movement of single molecules or submicron-sized particles in low viscosity liquids),<sup>208</sup> as well as slow diffusion processes (i.e.  $10^{-12}$ - $10^{-8}$  cm<sup>2</sup>/s, corresponding to the movement of particles in solids).<sup>208</sup> Raman correlation spectroscopy,<sup>327</sup> photon correlation spectroscopy,<sup>328</sup> FCS<sup>215</sup> or capillary flow<sup>329</sup> are exemplary techniques from the first group, while NMR spectroscopy,<sup>330</sup> holographic relaxation spectroscopy<sup>331</sup> and FRAP<sup>332</sup> – the latter. Among these, FRAP is one of the most well-established methods<sup>333</sup> that additionally allows to control the time scales of the measurements by varying the size of the bleached region.<sup>208</sup> FRAP has been successfully applied to various systems – from polymer films (also below their  $T_g$ )<sup>204</sup> through multilayer systems<sup>205</sup> to biological samples<sup>206</sup> – enabling direct detection of fluorophore diffusion within the film, calculation of fraction of immobile molecules, and investigation into the dominant diffusion mechanisms present.

Therefore, this chapter uses FRAP and AFM to probe the migration of RhB through PVA-based films. Changes in migration kinetics and mechanisms were recorded as a function of additive concentration (plasticiser) and guest molecule presence (surfactants of various head

group chemistry) in the polymer matrix. To gain more systematic understanding of the behaviour of the system, investigations were performed on thin (ca. 100 nm) PVA films. It was proven that properties of thin polymer films show significant difference compared to their micron-thick counterparts<sup>334–336</sup> due to the necessity to consider interface-polymer interactions. However, as the presence of a surface layer of several nanometres thickness was proven for thick films,<sup>337</sup> it is concluded that a thin film may be a representative of this surface layer alone. Using thin films together with relatively low numerical aperture of the objective leads to bleaching without noticeable gradient in z-direction, hence enabling investigation of lateral migration only.<sup>210</sup> Investigating migration in thin films enables identification of key factors that influence tracer movement in formulations with surfactants that were proven to display preferential segregation at the interface.<sup>295</sup> Explaining migration phenomena on the smaller scale should therefore help with providing answers for problems faced in multicomponent formulations, and provide natural translation of results from Chapter 3 to solid films.

## **4.2. Materials and methods**

**PVA film preparation.** Thin, spin-coated PVA-based films were prepared as described in Chapter 2. The compositions of the resultant films are presented in Table 4.1. Following spin coating, films on substrates were placed facing down on cover slips cleaned with piranha solution, with silicone elastomer (Merck, GF74606283, thickness 0.45 mm) used as a spacer (Figure 10.4, Appendix B).

**Experimental techniques.** FRAP (migration kinetics) and AFM (imaging and investigation into sample thickness) were used following the protocols described in Chapter 2.



### 4.3. Results and discussion

#### 4.3.1. Effect of glycerol concentration

Glycerol present in PVA matrix acts as a plasticiser, replacing PVA-PVA hydrogen bonds with PVA-glycerol bonds. As a consequence, the elasticity of the PVA chain increases due to increase in free volume<sup>51</sup> and mechanical properties of the polymer film improve.<sup>80</sup> This in turn is expected to lead to increase in migration rate of the guest molecules in the system. To study the influence of glycerol on migration of the tracer, samples of different plasticiser content in thin films were prepared (Table 4.1).

**Table 4.1.** Compositions and thickness of investigated thin films. Calculations of the glycerol content in the films do not include water present in the films. Due to high non-uniformity and poor film-forming properties of glycerol, scratch test was not performed on these samples. P in the table stands for PVA, G – for glycerol, and S – for surfactant.

Sample	S used	P:G:S solution volume ratio	P:G:S molar ratio	G concentration (wt%)	Film thickness (nm)
A	-	1:0:0	1:0:0	0	140 ± 3
B	-	1:0.25:0	1:109:0	16.5	136 ± 5
C	-	1:0.33:0	1:181:0	24.8	116 ± 4
D	-	1:1:0	1:543:0	49.5	102 ± 3
E	-	1:3:0	1:1629:0	74.3	79 ± 3
F	-	0:1:0	0:1:0	99	-
G	SDS (-)	1:0.33:0.33	1:181:14.5	23.3	29 ± 4
H	C <sub>12</sub> E <sub>10</sub> (0)	1:0.33:0.33	1:181:6.7	23.3	99 ± 1
I	CTAB (+)	1:0.33:0.33	1:181:11.4	23.3	84 ± 17

Compositions A-E all produced films of uniform thickness (Table 4.1). Increased glycerol concentration led to decreased film preparation solution viscosity (Chapter 3, Table 3.2), leading to formation of thinner films. Despite changes in glycerol content, no substantial change in PVA film morphology was visible – characteristic roughness of ca. 0.4 nm was present for all investigated glycerol concentrations (Figure 4.1) – indicating that the plasticiser was uniformly distributed in the polymer matrix.<sup>295</sup> In the absence of a polymer matrix to structure the film, it was impossible to reliably determine the thickness of films with

composition F. Addition of RhB does not change polymer morphology – no variations in polymer structure were observed compared to samples without presence of the fluorescent probe.

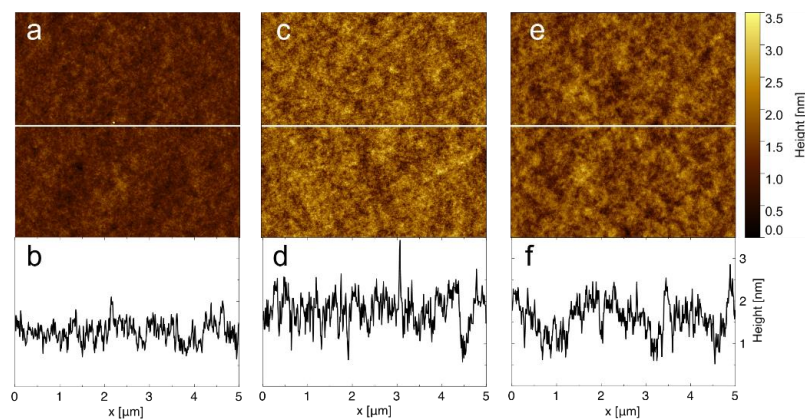


**Figure 4.1.** Morphology and height profile of compositions (a,b) A, (c,d) C and (e,f) D investigated using AFM.

Not only film thickness, but also RhB diffusion through the film showed significant dependence on plasticiser content (Figure 4.2). In composition A (pure PVA films), a diffusion rate of  $0.231 \mu\text{m}^2/\text{s}$  was observed, which increased to  $0.589 \mu\text{m}^2/\text{s}$  and  $0.712 \mu\text{m}^2/\text{s}$  for compositions B and C, respectively. This signifies that glycerol addition leads to an increase in RhB diffusivity until reaching the threshold of 49.5 wt% glycerol content. At this concentration, diffusion decreased to a plateau at  $0.090 \mu\text{m}^2/\text{s}$  and  $0.082 \mu\text{m}^2/\text{s}$  for samples D and E, followed by slight increase in tracer diffusion coefficient in films prepared from pure plasticiser solution ( $0.215 \mu\text{m}^2/\text{s}$ , Figure 4.2).

The thin films examined here showed a similar trend to that previously reported for thick PVA-glycerol films of 30-50  $\mu\text{m}$  thickness (cf. 80-140 nm).<sup>208</sup> Therein, significant increase in RhB diffusion coefficient was observed upon addition of glycerol, increasing from  $10^{-5} \mu\text{m}^2/\text{s}$  at 0 wt% glycerol to  $10^{-1} \mu\text{m}^2/\text{s}$  at 40 wt% glycerol. The significantly faster diffusion coefficients reported here may be a consequence of the different method of preparation and

thickness of the films – in thin films, due to vicinity of the surfaces and interfaces, polymer-interface interactions need to be considered, while in bulk films, they are negligible compared to bulk polymer interactions.<sup>334,338</sup> As a consequence, properties of thin films vary compared to their thicker equivalents. While the methodology applied here can model migration as a 2D process, similar assumptions are not valid for thick films where bleaching and diffusion take place not only at the surface, but also at the layers below the surface. Moreover, thick films are more prone to water absorption due to the higher weight of glycerol present in the matrix compared to thin counterpart. Due to its hydrophilic nature, glycerol increases the water sorption in hydrophilic polymer films, leading to increase in diffusion coefficient up to 2 orders of magnitude compared to pure polymer matrices.<sup>339</sup>

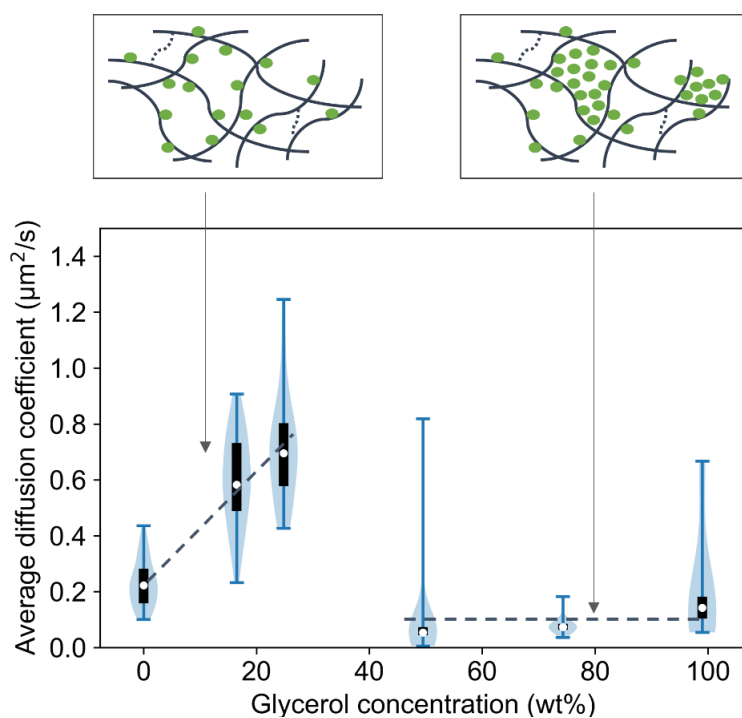


**Figure 4.2.** Recorded diffusion coefficients of RhB in samples A-F. White circle represents median value, black rectangle – interquartile range (25-75%), while blue lines represent the whole range of recorded values. The shape of the violin (shaded area on both sides) is the estimated distribution, according to the kernel density estimation algorithm. In schemes above the graph, lines represent PVA single chains, dashed lines – PVA-PVA bonding, while green circles – glycerol. Dashed lines on the graph represent approximate trend of RhB diffusion coefficient changes with increasing glycerol concentration.

RhB had a non-uniform distribution in investigated thin films, evidenced by variation in the background intensity (Table 10.2, Appendix B) also visible for other fluorophores (Figure 10.5, Appendix B). With increasing glycerol concentration, the number of regions of higher intensity increased while the average background intensity decreased. This in turn led to dependence of RhB diffusion coefficient on position in the sample and higher standard error for samples E and F (Figure 4.2). Therefore, increased glycerol content creates inhomogeneous molecular arrangement, with RhB aggregation expected to occur in regions high in glycerol. The observed drop in diffusivity is a consequence of reaching PVA-glycerol compatibility limit<sup>51,82</sup> – in partially hydrolysed PVA used in measurements, glycerol and polymer are compatible up to 39 wt% plasticiser content,<sup>51</sup> which is in good agreement with presented results (Figure 4.2). Before reaching compatibility limit, addition of glycerol leads to increase in free volume of the film and mobility of the fluorescent tracer therein. However, further addition of plasticiser results in increased impact on chain separation leading to phase separation<sup>82</sup> in the films and creation of regions rich in glycerol or polymer. Consequently, the diffusion coefficient of RhB decreases as it separates into one of the two phases.

The influence of plasticisation can also be confirmed by looking at number of positions with immobile molecules during FRAP analysis, signified by a lower equilibrium fluorescence signal after bleaching than before. For pure PVA films, nearly all investigated positions had some proportion of immobile molecules. However, fewer positions had immobile molecules after addition of glycerol (Table 4.2) including for systems above the PVA-glycerol compatibility limit, even though the average fraction of immobile molecules increased once the PVA-glycerol compatibility limit was reached.

The value of the diffusion coefficient depends on both nominal and actual bleach radii in addition to  $\tau_{1/2}$  values (Equation 2.5). Therefore, recovery  $\tau_{1/2}$  and diffusion coefficient do

not necessarily depend equally on glycerol content. Indeed, while for formulations A-D this trend was identical – initial increase and then decrease of average  $\tau_{1/2}$  with increasing glycerol concentration, Table 4.3 (*vide infra*) – for sample E a small decrease of  $\tau_{1/2}$  values was noted. For formulation E, the actual bleach radius decreased compared to formulation D (Table 10.3, Appendix B), which explains the difference in  $\tau_{1/2}$  values for these two samples (less time required for recovery due to decreased bleach size) despite the similar values of diffusion coefficient for compositions D and E.

**Table 4.2.** Immobile molecules data and bleaching data for samples A-F.

Composition	Positions with immobile molecules	Average fraction of immobile molecules	Positions with required secondary bleaching	Positions with no possible bleaching
A	28	0.055	0	0
B	4	0.033	0	0
C	3	0.013	0	1
D	8	0.166	8	0
E	5	0.053	2	1
F	6	0.358	3	24
G	5	0.1173	6	4
H	0	0.1705	0	0
I	9	0.1260	2	5

Sample F (pure glycerol) showed a particularly high dependence on analysis position, with many positions recording no possible bleaching due to too fast migration of RhB (values not included in average diffusion coefficient calculations, Table 4.2). A different characteristic recovery profile compared to the polymer-based films was observed in regions where measurements were possible – after initial increase of normalised intensity and reaching more than 50% of the recovery, decreased fluorescence was observed (Figure 4.3a). Non-uniform morphology and poor film-forming properties of glycerol may be responsible for this unexpected behaviour observed after reaching half recovery. The fluorophore is located in glycerol aggregates that create characteristic pattern on the surface on a similar length scale to

the bleached spot size (Figure 4.3b and Figure 10.6, Appendix B), indicating that the measured migration takes place within a single aggregate or a few small ones. Experiments on pure glycerol films are therefore useful for interpreting the behaviour of other films which exhibited strong non-uniformity. Hence, positions in which RhB showed a slow diffusion coefficient is a consequence of migration in regions between the aggregates, while very fast diffusion or not possible bleaching may indicate fast diffusion within aggregates. Similarly, single positions with no possible bleaching for samples of composition C and E suggest creation of nano-domains rich in glycerol in otherwise uniform polymer films.

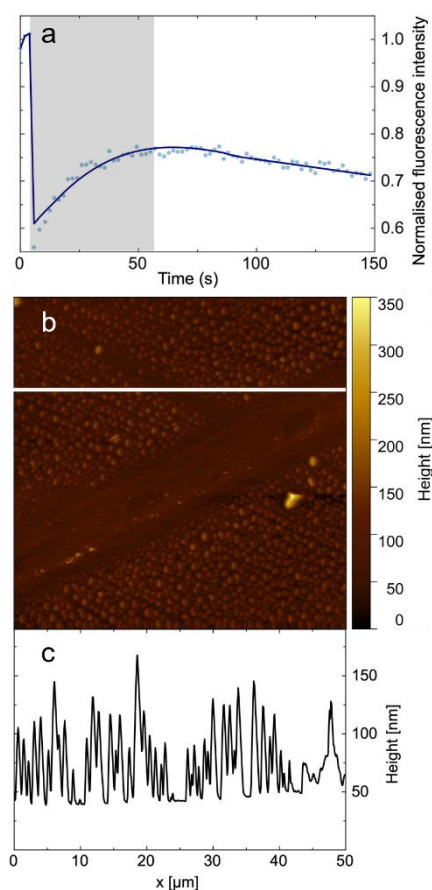


**Figure 4.3.** (a) FRAP recovery curve for representative position for pure glycerol sample, (b,c) AFM image and surface profile of pure glycerol sample (scratch region). Shaded area represents half recovery time.

Overall, as presented in Chapter 3, the plasticiser has a complex impact on tracer diffusion within the system. At low glycerol concentration further plasticiser addition promotes

faster RhB diffusion, however, diffusion is significantly reduced once the compatibility limit of glycerol and PVA is reached. At the extreme of diffusion through pure plasticiser, precise diffusion measurement is hampered by the poor film-forming behaviour of glycerol. These characteristic behaviours for different film compositions can be further investigated by analysing not just the measured rate of RhB diffusion, but also the shape of the curve to determine the recovery mechanism.

### 4.3.2. Investigations into migration mechanisms in thin polymer films

The decrease in the diffusion coefficient above the glycerol-PVA compatibility limit occurred simultaneously to a change of the diffusion character compared to films B and C, doped with 16.5 wt% and 24.8 wt% of glycerol, respectively. This can be seen in Figure 4.4a and 4.4b, which show the normalised recovery curves for sample B and D, respectively.

When glycerol concentration was below 49.5 wt%, fluorescence recovery occurred in two distinct stages. The initial bleach was followed first by a sharp increase in fluorescence intensity, after which the sample slowly reached equilibrium (Figure 4.4a). For samples with glycerol concentration higher than 49.5 wt%, the recovery behaved differently – without the initial fast recovery, the sample reached equilibrium at a constant rate (Figure 4.4b). Consequently,  $\tau_{1/2}$  became longer and resulted in lower calculated diffusion coefficient of the fluorophore.

The changes in the recovery curves suggest that different mechanisms of migration are responsible for the observed differences in diffusivity. Two fundamental processes occur during fluorescence recovery: tracer molecules diffuse through the film (unbleached tracers into the analysis region and bleached tracers out) and bind, replacing bleached tracer molecules with fluorescent ones within the bleach region, typically at a slower rate than pure diffusion. How

these processes relate to one another results in differences in the measured recovery mechanism (Figure 4.5). The processes of diffusion and binding can either occur separately (diffusion-uncoupled mechanism, Figure 4.5a), or at the same time (diffusion-coupled mechanism, Figure 4.5b). By determining the mechanism of migration it can be concluded whether the detected diffusion coefficient applies only to pure diffusion or to effective diffusion of the tracer within the sample.

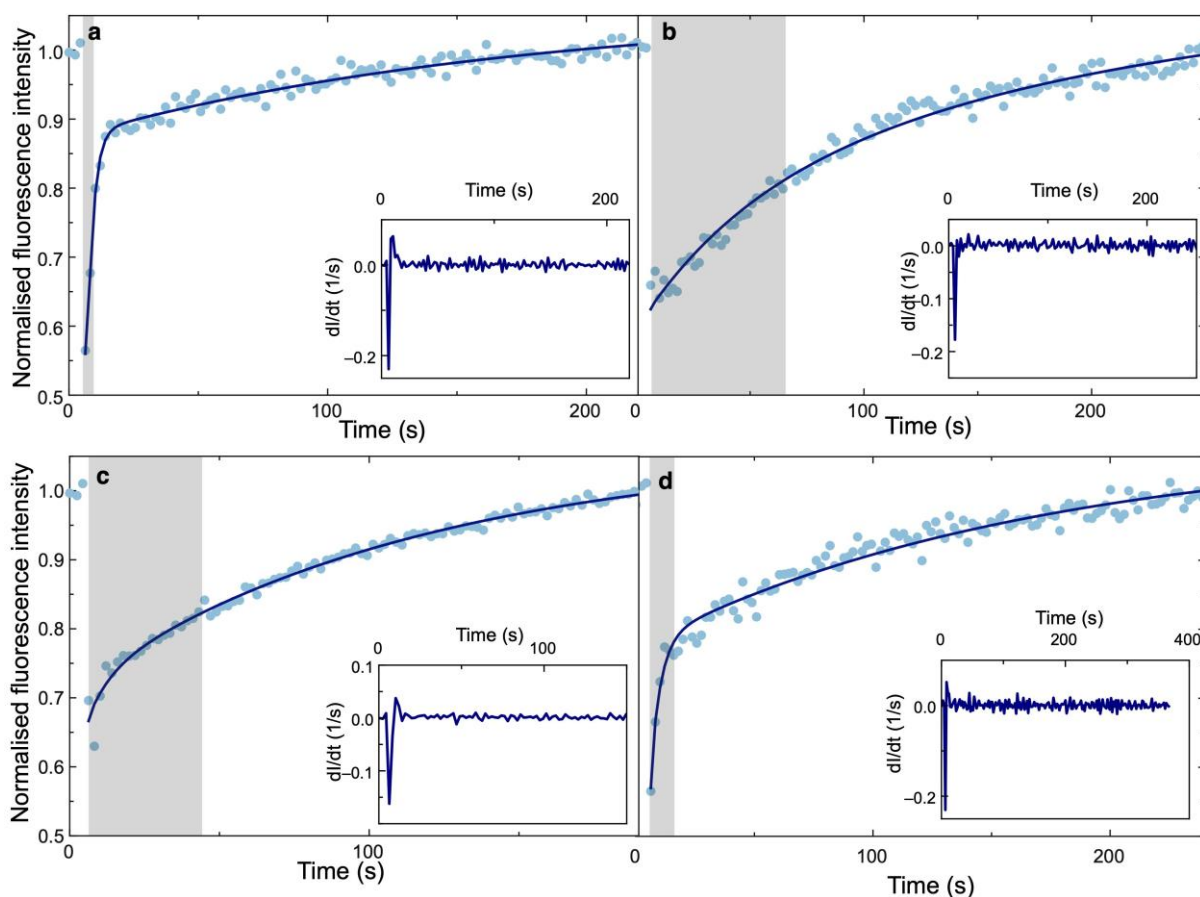


**Figure 4.4.** Fluorescence recovery curve for samples of compositions (a) C, (b) D, (c) C with increased bleach size, and (d) C prepared from filtered solutions (dots) and fits to Equation 4.1 (lines). The insets present the derivative of fluorescence intensity over time, while shadowed regions represent half recovery time for given formulation.

In the diffusion-uncoupled mechanism, the recovery curve is divided into two sections (Figure 4.5a). At the beginning, tracer molecules rapidly diffuse into the bleached region due to the concentration gradient and occupy available positions. Binding only occurs once the



diffusion is complete. The rate of recovery for this part of the curve corresponds to the strength of binding – the slower the recovery, the tighter the binding state.<sup>340</sup> In diffusion-coupled recovery, no distinction between diffusion and binding is possible due to similar time scales of these mechanisms.<sup>340</sup> They occur together – individual particles migrate then replace bleached molecules with fluorescent molecules – until the equilibrium is reached (Figure 4.5b).

**Table 4.3.** Half recovery times for different bleach radii as a function of film composition.

Composition	Average $\tau_{1/2}$ for bleach size 3 $\mu\text{m}$ (s)	Range of $\tau_{1/2}$ for bleach size 3 $\mu\text{m}$ (s)	$\tau_{1/2}$ for bleach size 5.1 $\mu\text{m}$ (s)	Expected diffusion mechanism
A	19.71±0.86	12.43-33.75	24.43; 26.11	Diffusion-uncoupled
B	6.26±0.19	4.28-8.48	6.10; 11.24	Diffusion-coupled
C	5.31±0.17	3.89-7.83	7.56; 17.8	Diffusion-coupled
D	57.15± 3.18	5.54-85.48	24.35; 102.34	Diffusion-coupled
E	34.03± 1.67	19.87-62.22	47.40; 88.3	Diffusion-coupled

Because diffusion is dependent on the bleach radius, while binding kinetics are not, the mechanism of diffusion can be determined by performing measurements on two different bleach sizes. Diffusion-coupled recovery shows different  $\tau_{1/2}$  values for samples of different bleach radius (as diffusion in these samples is gradual), while for diffusion-uncoupled recovery they remain the same within experimental error. As full recovery did not take place in all investigated samples and second bleaching at the same position was proven to have different kinetics compared to the first,<sup>341</sup> the measurements of recovery within increased bleach size were performed at different positions. Given the large range of absolute  $\tau_{1/2}$  values recorded during initial 3  $\mu\text{m}$  bleaching experiments, experiments on a larger (5.1  $\mu\text{m}$  size) spot size were compared against the absolute values of RhB recovery  $\tau_{1/2}$  rather than the average value (Table 4.3). Regardless, conclusions about the recovery mechanism could be made for all compositions except pure glycerol F, due to the aforementioned non-uniformity of these samples.

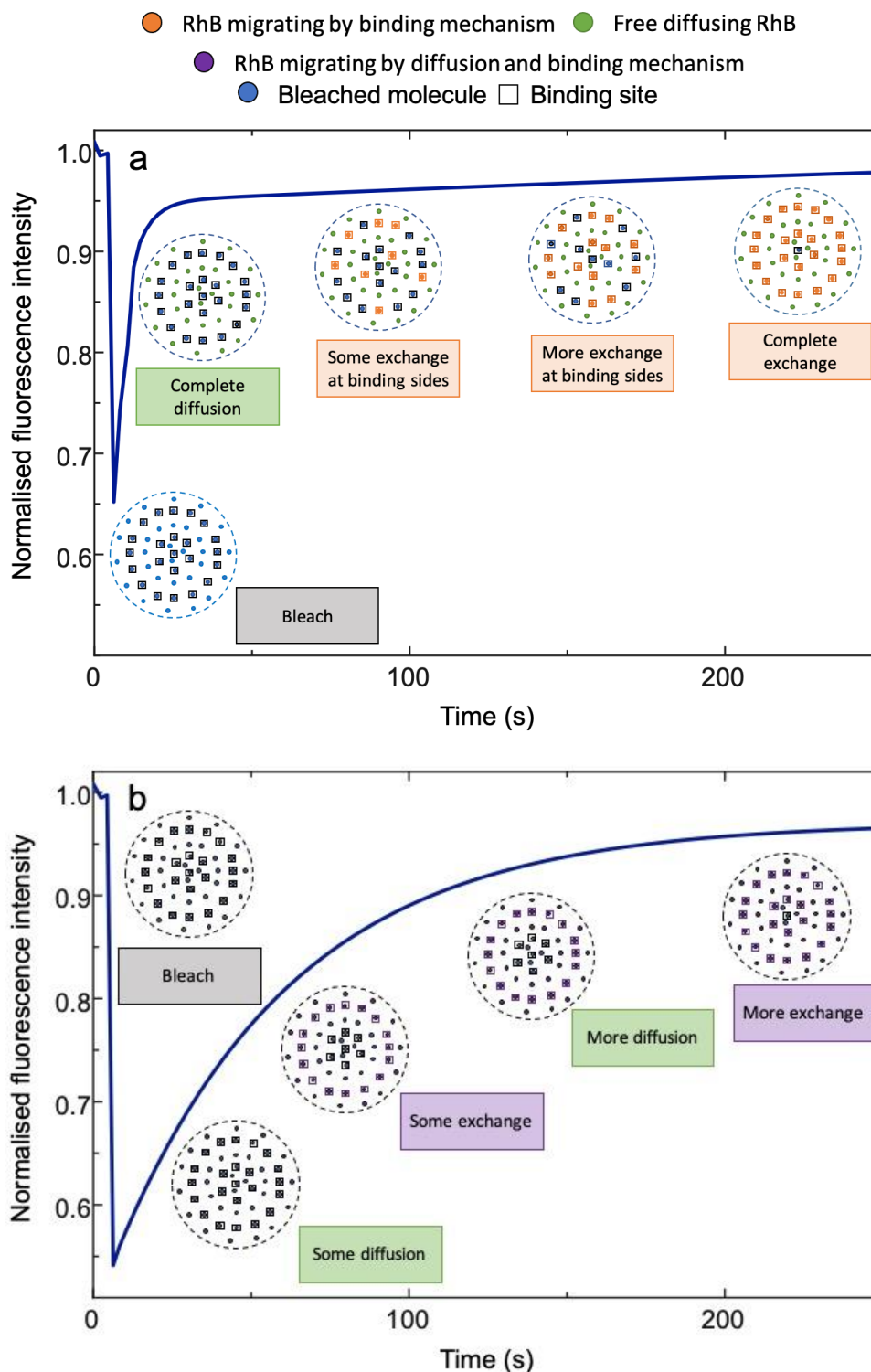


**Figure 4.5.** Graphic representation of: (a) diffusion-uncoupled mechanism and (b) diffusion-coupled mechanism. Adapted from reference 340.

Even though recovery curves for samples B and C initially suggest a diffusion-uncoupled mechanism, at least one measurement at the increased bleach size was outside the

range of the 3  $\mu\text{m}$  spot size, suggesting a shift of the distribution to the higher  $\tau_{1/2}$  values. Moreover, the shape of the recovery curve for increased bleach size changed, with initial fast recovery less pronounced compared to the 3  $\mu\text{m}$  bleach size (Figure 4.4c cf. Figure 4.4a), suggesting a diffusion-coupled mechanism. The exception to this pattern was composition A, where  $\tau_{1/2}$  values overlapped completely between both bleach sizes, indicating diffusion-uncoupled mechanism. However, due to the wide distribution of absolute  $\tau_{1/2}$  values there is a distinct possibility that the diffusion kinetics are diffusion-coupled and recorded values are in the lower end of the shifted  $\tau_{1/2}$  distribution. Therefore, all compositions were analysed using diffusion-coupled mechanism, with calculated diffusion coefficient representing the effective diffusivity (i.e. describing all mechanisms that influence diffusion in these systems).

The diffusion-coupled mechanism in the investigated system can further be interpreted on a physical basis. At low glycerol content, the PVA chain is expected to become more flexible with an increase in free volume in the system, leading to faster diffusion of the tracer compared to pure PVA film. With further increase of glycerol concentration, the overall diffusion value is a result of two antagonistic factors: plasticisation of PVA molecules, and increasing glycerol aggregation (i.e. plasticiser-plasticiser hydrogen bonding)<sup>4,80,84</sup> in films of decreasing thickness (Table 4.1). Given that there is no substantial change in film morphology for formulations A-E, the steric effects due to glycerol aggregation are the most likely explanation for changes in the diffusion mechanism after reaching threshold of PVA-glycerol compatibility.

### 4.3.3. Modelling fluorophore migration

To further establish phenomena behind observed changes in migration kinetics with film composition despite all exhibiting the diffusion-coupled mechanism, the FRAP recovery curves can be represented as sum of two exponentials representing fast and slow migrating species

present in the system. The parameters for effective diffusion of each component in the system can be modelled using equation:<sup>342</sup>

$$I_N = I_{N(b)} - I_{N,fast} \cdot \exp\left(-\frac{t}{T_{fast}}\right) - I_{N,slow} \cdot \exp\left(-\frac{t}{T_{slow}}\right) \quad 4.1$$

where  $I_N$  and  $I_{N(b)}$  are the normalised (following Equation 2.6) intensities of the recovery curve at given time  $t$  and at the beginning of experiment, respectively,  $I_{N,fast}$  and  $I_{N,slow}$  are normalised amplitudes of fluorescence after photobleaching of the fast and slow migrating molecule fractions (correlated with their fractional concentration). Using fitted parameters  $T_{fast}$  and  $T_{slow}$ , the values of  $\tau_{1/2}$  for given kind of molecules can be calculated.<sup>343</sup>

$$\tau_{1/2x} = \ln(0.5) \cdot T_x \quad 4.2$$

where  $T_x$  is either  $T_{fast}$  or  $T_{slow}$ , and  $\tau_{1/2x}$  is the half recovery time for the respective molecules. While Equation 4.2 cannot accurately calculate strength and number of binding interactions for diffusion-coupled recovery,<sup>340</sup> here it is only used to evaluate the diffusion kinetics of the two species (Table 4.4).

The satisfactory fit of FRAP recovery data to Equation 4.1 (Figure 4.4a, Figure 4.4b) suggests that there are three kind of species present in discussed system:<sup>339</sup>

- Fast migrating molecules, with low value of  $\tau_{1/2}$  likely exhibiting weak physicochemical interactions between the tracer and PVA/glycerol matrix.
- Slow migrating molecules that can not only interact in a similar way to fast population, but also are more prone to binding effects and steric hindrance effects.
- Entirely immobile molecules over the time scale of experiment.

The trend in average values of  $\tau_{1/2}$  for fast and slow migrating molecules is clearly dependent on the glycerol content in the films and follows the changes in average diffusion coefficient calculated assuming only one kind of migrating species (Figure 4.2) – initial increase

below the compatibility limit, followed by a decrease. The ratio of normalised amplitude for faster and slower molecules does, however, change. For example, a higher fraction of faster molecules and lower fraction of slow migrating molecules were detected in composition B compared to composition C. Nevertheless, effective diffusion is faster for sample C than sample B due to the lower  $\tau_{1/2}$  of both material types in the former material (Figure 4.2). Similarly, for samples D and E, variations in amplitude and  $\tau_{1/2}$  balance out, leading to similar effective diffusion times after accounting for variations in the bleached spot size (Table 10.3, Appendix B).

**Table 4.4.** Average  $\tau_{1/2}$  and normalised amplitude for fast and slow migrating molecules for investigated samples.

Composition	$I_{N,fast}$	$\tau_{1/2,fast}$ (s)	$I_{N,slow}$	$\tau_{1/2,slow}$ (s)
A	$0.31 \pm 0.0053$	$15.05 \pm 0.68$	$0.20 \pm 0.0073$	$166.88 \pm 14.62$
B	$0.41 \pm 0.011$	$5.47 \pm 0.24$	$0.14 \pm 0.0067$	$151.90 \pm 11.73$
C	$0.30 \pm 0.0087$	$3.67 \pm 0.11$	$0.19 \pm 0.0040$	$115.04 \pm 5.58$
D	$0.15 \pm 0.018$	$42.00 \pm 4.11$	$0.26 \pm 0.020$	$201.15 \pm 19.86$
E	$0.23 \pm 0.014$	$23.96 \pm 2.1$	$0.19 \pm 0.016$	$288.29 \pm 48.13$
G (SDS)	$0.13 \pm 0.016$	$8.18 \pm 1.43$	$0.25 \pm 0.019$	$157.15 \pm 15.33$
H (C <sub>12</sub> E <sub>10</sub> )	$0.14 \pm 0.012$	$2.16 \pm 0.34$	$0.31 \pm 0.0085$	$51.24 \pm 4.17$
I (CTAB)	$0.23 \pm 0.017$	$4.15 \pm 0.99$	$0.23 \pm 0.017$	$101.00 \pm 14.13$

#### 4.3.4. RhB migration in thin films prepared from filtered solutions

Prior to spin coating, molecular interactions and plasticisation lead to creation of aggregates that change the molecular arrangement in the resultant film and thereby influence tracer diffusion coefficient. To exclude this effect, thin polymer films were prepared from solutions filtered through syringe filter (0.22  $\mu\text{m}$  pore size) and investigated as described above.

In most cases, filtration of solutions prior to spin coating (and sonication, Table 10.4 and Section B1, Appendix B) does not lead to substantial changes in RhB diffusion coefficient (Figure 4.6). This may be a consequence of two factors: firstly, PVA-glycerol aggregates larger than 0.22  $\mu\text{m}$  do not play significant role in influencing the polymer matrix structure and, consequently, in changing diffusion coefficient of the tracer; secondly, filtration blocks

aggregates from entering the solution, but further aggregates form after filtration and prior to spin coating. Composition C is the only formulation that shows substantial differences in diffusion coefficient of the tracer compared to film prepared from non-filtered solution. The  $\tau_{1/2}$  value is dependent on investigated position, which was not observed for all three samples prepared from non-filtered formulations (as can be seen by a standard error of 0.099 cf. 0.037 for the unfiltered equivalent). In terms of diffusion kinetics, regions exhibiting fast diffusion show similar behaviour to non-filtered samples (Figure 4.4d). However, initial trend of the fast recovery in filtered samples is shorter compared to the unfiltered formulations (Figure 4.4a) and results in slower diffusion coefficient of fluorescent tracer, similar to FRAP recovery curve for bleach of increased size (Figure 4.4c). The dependence of diffusion coefficient on the position is probably a consequence of non-uniform composition of the sample: it is likely that removal of PVA-glycerol aggregates leads to overall decrease of PVA concentration and increase of glycerol concentration, leading to diffusivity behaviour closer to that of formulation D and E.

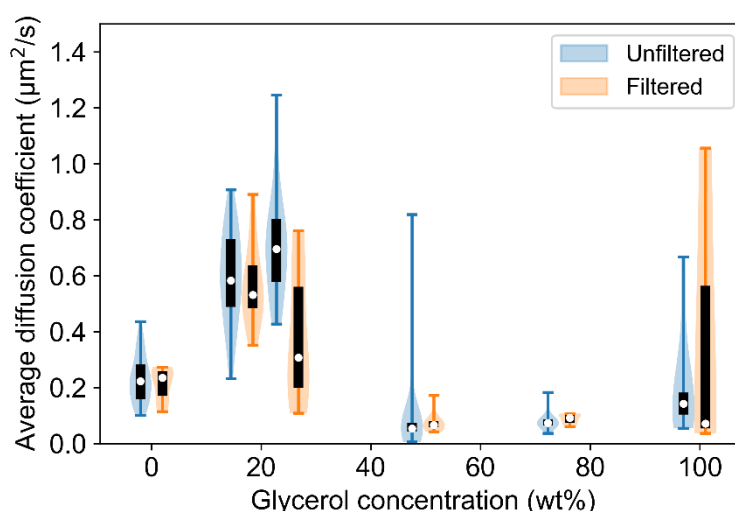


**Figure 4.6.** Comparison of average diffusion coefficient for filtered and non-filtered solutions A-F.

Overall, for filtered samples the trend in average  $\tau_{1/2}$  values for fast migrating molecules remains unchanged compared to their unfiltered counterparts, while there is an increase in

mobility for slow migrating molecules in pure PVA films (Table 10.5, Appendix B). The decreasing ratio of amplitudes between fast and slow migrating species for sample C results in decrease of overall diffusion coefficient measured for the whole of migrating species compared to non-filtered samples.

Generally, pre-spinning filtration of the solution appears to promote formation of inhomogeneous regions in plasticised glycerol films, although kinetics of recovery only differs significantly compared to unfiltered counterparts when the glycerol content is close to the PVA-glycerol compatibility limit. To confirm this finding further model additives, in the form of surfactants with various head group chemistry, were introduced into the film.

### **4.3.5. Effect of surfactant of various head group chemistry addition**

Surfactants of various head group chemistry (cationic, nonionic and anionic) present at high concentrations in plasticised PVA matrix have been proven to change its morphology and molecular arrangement, with the magnitude of changes dependent on compatibility of the surfactant with the matrix and surfactant surface energy.<sup>17,295</sup> These factors are also expected to dominate formulations of plasticised PVA with lower surfactant content. As size of the migrating tracer remains unchanged, by introducing molecules with various head group chemistry and consequent charge one can make a conclusion about role of intermolecular interactions in influencing diffusion coefficient of the fluorescent tracer. Compositions of films prepared from the same polymer/plasticiser/surfactant weight ratios are presented in Table 4.1.

Addition of surfactant at 5.8 wt% to glycerol-plasticised PVA films results in overall slower diffusivity of the tracer by 30%, 61% and 88% for cationic, nonionic and anionic surfactant compared to composition C (the equivalent composition when not doped with surfactants, Figure 4.7), respectively. However, the diffusion rate is highly dependent on the position on the sample, suggesting surfactant blooming or phase separation in the films. This

mirrors previous reports that have shown phase separation in surfactant-doped films, despite the substantially lower surfactant concentrations used here than in those studies.<sup>17,295</sup> As a result, the average value of tracer diffusion coefficient does not give full information about the properties of the surfactant-doped compositions; instead, they are represented by the distribution of the absolute recorded values of diffusion coefficient.

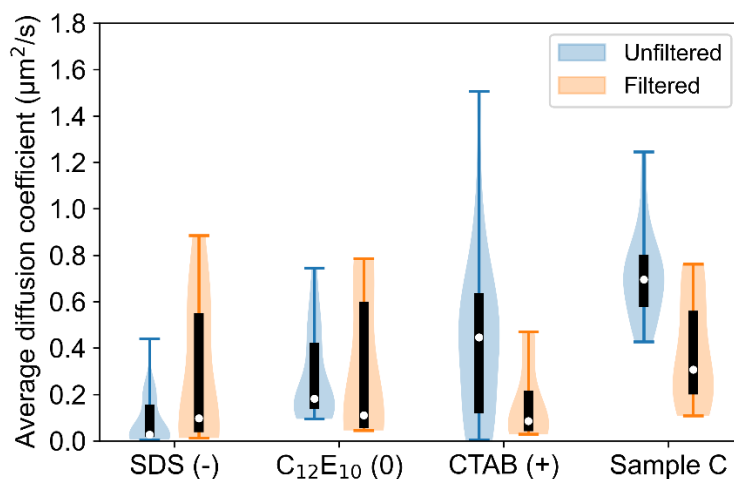


**Figure 4.7.** Average diffusion coefficient and its distribution for surfactant-doped films prepared from filtered and non-filtered solutions.

The largest changes in diffusivity were observed for systems with cationic and anionic surfactants, with both positions of substantially lower RhB diffusion coefficient compared to control composition C and positions where bleaching was not possible. The latter appeared as the fluorescence recovery rate became faster than bleaching or the fluorophore re-absorbed,<sup>344</sup> and in most cases was connected with regions of higher fluorescence intensity prior to bleaching. Distribution of the fluorophore does not substantially vary compared to sample C (Table 10.2, Appendix B). As number of positions where bleaching was not possible was the highest for pure glycerol films, it is expected that in samples containing SDS and CTAB, these regions correspond to high local concentration of the plasticiser.



Regions with slow diffusion coefficient of the tracer, on the other hand, are expected to be connected with excess of surfactants. RhB was proven to interact with SDS<sup>292,307</sup> and CTAB on the same level of magnitude<sup>305</sup> due to ion-ion interactions. However, SDS-RhB interactions are expected to be more favourable than CTAB-RhB interactions due to steric hindrance effects (Chapter 3). These interactions are clearly visible while comparing morphology of the films with and without addition of RhB. For PVA/glycerol/SDS films, surfactant blooms are incorporated into the film structure (Figure 4.8a,b). In the presence of RhB, the film morphology is similar to that of plasticised PVA films (Figure 4.1, Figure 4.8c,d). Moreover, prior to spinning, small green crystals were observed when fluorophore was added into the solution used for film preparation. The amount of crystals increased with increasing concentration of fluorophore. It is likely that due to favourable electrostatic interactions, the anionic surfactant head groups interact with cationic functional groups of the fluorophore and form an active centre to accelerate nucleation of RhB crystals.<sup>345</sup> However, a lower average diffusion coefficient compared to sample C was still recorded in the regions without crystals (Figure 4.7), suggesting that SDS and RhB are also present in PVA-glycerol matrix. AFM measurements on samples of different SDS content indicate that SDS concentration above 2 wt% changes the PVA film morphology on the preparation day (Chapter 5, Figure 5.3). In addition to morphology, SDS also changes PVA-glycerol interactions into SDS-glycerol interactions, resulting in creation of lamellae at higher surfactant concentrations.<sup>17</sup> This in turn results in lower degree of PVA plasticisation and consequent possible reduction of tracer diffusion coefficient. The sum of these factors – decelerated diffusion of RhB due to interactions with SDS present in the matrix and non-uniform morphology of sample G – can explain the strongest decrease in tracer diffusion coefficient observed upon introducing SDS into the system.

These findings can be further confirmed by analysing scratch test results (Table 4.1). For samples doped with SDS, scratches were performed at positions without visible surface features and showed a decrease in film thickness equal to 75% compared to film C. The thickness of films containing C<sub>12</sub>E<sub>10</sub> and CTAB also showed decreased thickness compared to PVA/glycerol films of the corresponding plasticiser concentration. For films with C<sub>12</sub>E<sub>10</sub>, this can be correlated with decrease in viscosity of the solutions used for film preparation (Chapter 3, Table 3.3). For samples with CTAB, however, the decrease in film thickness is observed despite similar viscosity of the solution used for preparation of sample I compared to sample C (Chapter 3, Table 3.3). These trends indicate more dense molecular packing for systems doped with ionic surfactants as a result of glycerol-surfactant, PVA-surfactant and RhB-surfactant interactions, with overriding importance in SDS-doped films.

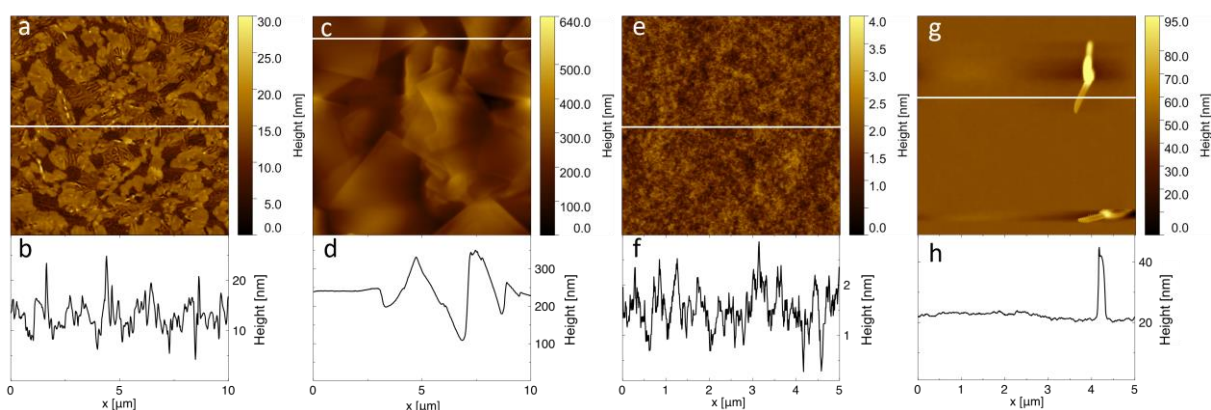


**Figure 4.8.** Morphology and surface profiles of sample G (a,b) in the absence of RhB and (c,d) containing RhB; sample H doped with RhB: (e,f) background morphology and (g,h) surface features.

Incorporation of cationic surfactants into the plasticised polymer matrix shows the largest standard error in sample thickness. CTAB is expected to create wetting layers at both the film-air and substrate-film interfaces,<sup>295</sup> with its excess in the system leading to creation of surfactant crystals at film-air interface (Chapter 5, Figure 5.2). Compared to formulation C, there are no visible morphology changes in the films after addition of CTAB at the investigated concentration, although when both CTAB and RhB were included in the formulation, rod-

shaped features appear. These features are also visible for samples containing  $C_{12}E_{10}$  however, hence likely indicate the presence of the tracer (Figure 4.8g,h).

It is expected that positions with similar diffusivity to the control sample are indicative of similar local composition – i.e. PVA plasticised with glycerol with little to no surfactant present – while areas of high local surfactant concentration will slow down migration of the tracer with resultant slower diffusion coefficient. While migrating through regions with high local concentration of CTAB within the matrix, intermolecular interactions will change migration kinetics and hence tracer diffusivity. For these compositions, similar to solutions doped with SDS, visible phase separation can be observed prior to spin coating, with crystals observed in the solution. While in samples containing SDS, they were visible on the preparation day, such crystals could only be observed after ca. 3 days of storage for solutions doped with CTAB, proving weaker CTAB-RhB interactions compared to SDS-RhB interactions.

The average diffusion coefficient of the tracer shows the least significant change for the addition of cationic surfactant compared to blank sample C. However, bleaching was possible in all tested positions in samples with  $C_{12}E_{10}$ , contrasting with both SDS and CTAB; furthermore, compositions containing  $C_{12}E_{10}$  exhibited morphology that was most similar blank sample C (Figure 4.8e,f). Due to its nonionic nature,  $C_{12}E_{10}$  is unlikely to interact with fluorescent tracer. The higher  $M_w$  of  $C_{12}E_{10}$  results in overall fewer moles of this substance being present in the system (Table 4.1) as well as higher entropy penalty connected with its presence on the surface compared to the shorter ionic surfactants.<sup>295</sup> Together with additional factor of glycerol action that is expected to increase compatibility between this surfactant and PVA,<sup>295</sup>  $C_{12}E_{10}$  is likely the most uniformly-distributed surfactant in the polymer among three investigated. Slower diffusivity of RhB in this system is hence mainly a consequence of steric effects – additional molecules decrease room available for plasticised PVA chain, decreasing its

elasticity and decreasing a diffusion coefficient of fluorescent tracer. Crowding and binding effects for samples doped with surfactants are further indicated by the increase in average fraction of immobile molecules compared to blank sample (Table 4.2).

#### 4.3.6. Modelling fluorophore migration in surfactant-doped films

Due to a very strong dependence of RhB diffusion coefficient on bleaching position, investigation into mechanism of migration would not give reliable results. Therefore, it is assumed that expected intermolecular interactions and crowding effects would result in diffusion-coupled mechanism and calculated diffusion coefficient is effective diffusion coefficient of RhB in given matrix, presenting results for both one (Figure 4.7) and two types of migrating species (Table 4.4). In the double exponential model, intermolecular interactions influence fast and slow migrating species, with  $\tau_{1/2}$  decreasing according to the affinity of RhB molecule to each surfactant ( $\tau_{1/2\text{SDS}} > \tau_{1/2\text{CTAB}} > \tau_{1/2\text{C}_{12}\text{E}_{10}}$ ). The faster species likely only interacts with the polymer backbone rather than glycerol aggregates and surfactants. Less mobile molecules, however, are likely to be dependent on both additional steric effects due to presence of molecules of higher molar mass (nonionic surfactant) or due to ion-ion bonding with migrating tracer (ionic surfactants). Similarly, the more uniform distribution of C<sub>12</sub>E<sub>10</sub> introduces the smallest changes in the matrix, while the energetically preferential surface excess of the ionic surfactants leads to lowered uniformity of the film. Interestingly,  $\tau_{1/2}$  values for films doped with nonionic or cationic surfactants are lower or very similar to composition C, indicating that the relative abundance of fast- and slow-moving species changes between formulations, rather than the intrinsic diffusivity of RhB.

#### 4.3.7. RhB migration in surfactant-doped films prepared from filtered solutions

As presence of the crystals and surface features may influence the effective diffusion coefficient of the fluorophore in thin films, the absolute diffusion coefficient values of RhB for films prepared from filtered solutions were compared with their non-filtered equivalents.

The trend of average RhB diffusion coefficient in thin films obtained from filtered solutions (Figure 4.7) is similar to that obtained from FCS experiments in solutions of the same compositions (Chapter 3, Figure 3.6). However, due to the position-dependence of the diffusion coefficient and lower number of samples investigated, no strong conclusions can be made about the change in the average diffusion coefficient in these films. By analysing the range of absolute diffusion coefficient values, no significant difference between samples prepared from filtered and non-filtered solutions appears, except for CTAB-doped films where the diffusivity reduces compared to its unfiltered counterpart, similar to composition C. This change is correlated with PVA-CTAB-glycerol competitive interactions, leading to decreasing concentration of PVA upon removal of aggregates during filtration and consequently amplified steric effects as well as intermolecular interactions. For samples containing SDS, however, crystal formation does not lead to substantial differences in diffusion coefficient of RhB, as diffusion coefficient before and after filtration has similar average values and range.

Filtration drastically hinders the recovery rate (i.e.  $\tau_{1/2}$  values) for both fast and slow migrating molecules in nonionic surfactant formulations, while only small changes were observed for anionic surfactant formulations (Table 10.5, Appendix B), indicating that filtration changes the solution composition in the former case (Figure 4.7). Moreover, the absolute values of RhB diffusion coefficient in filtered samples containing CTAB fit better to a single rather than double exponential equation, resulting in non-physical values when fitting to double exponential model for some investigated positions. This suggests only one kind of migrating

species for these compositions, therefore, the fit values to Equation 4.1 (Table 10.5, Appendix B) should not be directly compared with samples prepared from non-filtered solutions.

#### 4.4. Conclusions

Investigations of molecular migration in complex industrial formulations were performed on thin films, where diffusion can be approximated as lateral. Diffusion characteristics of RhB were found to be dependent on the presence of glycerol (plasticiser) and chemistry of any added surfactant (cationic/anionic/nonionic). Different migration kinetics were observed in thin films of various PVA/glycerol ratio – tracer diffusion coefficient increased with increasing glycerol concentration up to the compatibility limit of ca. 50 wt%, whereupon it decreased below the diffusion rate even of unplasticized PVA. Above the PVA/glycerol compatibility limit, further increase in plasticiser concentration resulted in glycerol aggregation and consequent phase separation on microscale which inhibited the probe molecule from migrating freely.

Addition of any surfactant (at ca. 6 wt%) hindered the diffusion coefficient of RhB (by 30%, 61% and 88% for cationic, nonionic and anionic surfactant compared to control sample, respectively). Steric effects due to the presence of guest molecules of higher  $M_w$  in the system seem to explain those phenomena in compositions containing the nonionic surfactant. However, for films with cationic or anionic surfactant, it is likely that surfactant-fluorophore interactions play a main role, slowing down the migration of the RhB and leading to RhB crystallisation.

Following the assessment of how internal contamination influences migration behaviour in PVA-based films presented in this chapter, the influence of environmental conditions on diffusive behaviour within films can be characterised. Specifically, the z-migration of contaminants such as surfactants during contact with humid atmosphere is of great interest, being a strong mimic of real-world storage conditions.

## **Chapter 5. Humidity- and surfactant-accelerated aging of thin polymer films**

### **5.1. Introduction**

Most packaging materials are polymers whose affinity to water is determined by their chemistry. High affinity to water can widely affect the shelf life of packaging materials<sup>98</sup> by changing the product properties as a consequence of water infiltration, both during and after production (e.g. because of swelling, changes in elasticity, impact strength or tensile strength).<sup>10</sup> Understanding how RH affects the properties of polymers (especially water-soluble ones, susceptible to degradation upon water infiltration) is therefore vital for improving their shelf-life.

PVA films structurally consist of amorphous, crystalline, and interfacial regions which display distinct behaviour and properties (Chapter 1, Sections 1.2.1-1.2.3). Water infiltration disrupts crystalline regions, increasing the size of amorphous regions while leaving remaining crystallites water-free.<sup>101</sup> Overall water content is therefore equal to the water content in amorphous regions only. Water in the amorphous region promotes chain mobility due to lubrication, interacts with macromolecules via hydrogen bonds and removes further barriers for bonds to move.<sup>4</sup> As stated in free volume theory, diffusion in polymer systems can be described as a series of movements of migrant molecules that jump from one hole available to the other, following a concentration gradient.<sup>167,346</sup> Plasticisers (e.g. water or glycerol) occupying these holes contribute to the total free volume, swelling the film<sup>346</sup> and facilitating the segmental motion of PVA chains. Ambient water has therefore two important roles in PVA systems: it controls the crystal structure in the films, but also acts like a plasticiser.

As with water, guest molecule migration only occurs in the amorphous region. Guest molecule, shape, polarity,<sup>346</sup> and compatibility with single elements of the system<sup>17,295</sup> have

crucial importance in this process. Furthermore, by swelling the film, water has an indirect effect on the migration of other guest molecules, in turn resulting in increased diffusion rates.<sup>347</sup> This effect is of great industrial importance as it leads to faster aging of the product due to the non-uniform distribution of guest molecules present in the system or migration from adjacent media.

Water infiltration itself is a complex phenomenon, with multiple studies investigating the nature of water migration within PVA, proving both Fickian<sup>348,349</sup> (independent of water content) and anomalous non-Fickian<sup>2,350</sup> (relaxation-controlled) character of water diffusion in this polymer matrix. These inconsistent reports highlight a need to fully establish this mechanism especially for industrial (multicomponent) PVA packaging materials. Indeed, polymer chain-chain interactions, crystallinity, and presence of additives demonstrate that even small changes in PVA matrix composition influence this mechanism.

Even though there are reports about changes of the material properties prepared at various RH,<sup>351</sup> little has been done to understand the influence of environmental conditions on aging of complex polymer materials. This is especially important while considering packaging materials that are in close contact with concentrated media e.g. detergent liquids – in those systems, migration of small molecules from adjacent media to polymer systems can lead to further undesired changes in properties of the materials. In higher RH conditions, increased migration is expected. Consequently, the time scales required to observe changes in systems properties are likely to be decreased.

Here, an exemplar system mimicking single unit laundry pods – plasticised PVA films in contact with concentrated detergent – is aged under various environmental conditions to investigate the effect of RH on molecular migration. Measurements were performed on thin (ca. 100 nm), spin-coated PVA-based films doped with surfactant molecules of different head



group chemistry and concentration that imitate the polymer layer adjacent to the concentrated detergent medium at various migration stages. These samples were investigated using *in-situ* AFM, CFM (i.e. under controlled RH environments)<sup>352,353</sup> and DVS, giving insight into dependence of chemistry on the amount of absorbed water.<sup>348</sup> Combined, these methods can provide the kinetics of guest molecule migration as a function of RH of the environment and system chemistry. As a result, the impact of surfactant concentration, head group chemistry and RH on surfactant migration kinetics in simulated single use detergent packaging materials will be characterised.

## 5.2. Materials and methods

**PVA film preparation.** In this chapter, compositions doped with cationic, anionic or nonionic surfactants in the range of 1-5 wt% were used alongside control samples of plasticised and unplasticised PVA with no surfactant. Thin, spin-coated films (ca. 100 nm thickness) were used for AFM and CA measurements, and solution cast films (ca. 40  $\mu\text{m}$  thickness) were used for DVS measurements. Films were prepared as described in Chapter 2.

**Humidity control.** AFM measurements on each sample on day 0 were performed in ambient conditions. Samples were then aged in a desiccator with saturated salt solutions to maintain constant RH. Lithium chloride, potassium acetate, magnesium chloride, potassium carbonate, and magnesium nitrate were purchased and used as received to prepare saturated salt solutions, providing a humidity range between 15% and 55% RH (as higher RH would likely cause microscope damage).

AFM measurements were performed using a custom-built humidity chamber<sup>107</sup> modified by the author wherein RH was regulated by the ratio of dry and wet nitrogen streams. The wet stream flowed through 3 Duran bottles: the first 2 filled with water, and the third with glass

beads to prevent condensation on the microscope. The dry stream flowed directly into a mixing chamber and then the humidity chamber surrounding the AFM. Humidity and temperature were monitored using a thermo-hygrometer (ATP HTD-625). Between measurements, samples were stored in desiccator with controlled RH for a total of 6 weeks.

**Measurement techniques.** AFM (imaging, thickness measurements and CFM), DVS, as well as CA measurements for SFE calculations were used following the protocol described in Chapter 2. At least 3 samples were investigated for each composition and environmental condition studied. To ensure that AFM images were taken at approximately the same position, a cross scratch was made on every sample using a scalpel prior to investigation. Two further nearby scratches were made using AFM, following the experimental procedure described in Chapter 2. Samples were imaged following a set pattern around the scratches, with at least five images of different sizes taken from every sample. Afterwards, the sample was scanned using the optical microscope connected to the AFM, with further imaging performed in the region of observed morphological changes.

### 5.3. Results and discussion

Spin coating leads to creation of thin films with molecules kinetically trapped in the polymer matrix due to rapid solvent evaporation during preparation.<sup>354-356</sup> Therefore, molecular migration would be easily visible as the film equilibrates over time. When surfactants are present in the film, two main factors influence the system behaviour over time: concentration of the surfactant and compatibility with other additive species present. As compatibility (i.e. similarity of Flory-Huggins interaction parameter) decreases, surface segregation is promoted which in turn results in wetting layer formation (surfactant excess at the film surface).<sup>357</sup> Therefore, by

spin coating thin films, the effect of incompatibility (i.e. surfactant concentration) and water infiltration (i.e. RH conditions) on segregation rates (i.e. additive diffusion) can be investigated.

These phenomena were probed in two different ways: first, changes in morphology due to aging of thin films of various composition and surfactant concentration were probed. For these experiments, samples were stored in ambient conditions for the whole period of aging (~35% RH, 21°C, 2 weeks storage). Afterwards, the influence of RH conditions on sample morphology at fixed surfactant concentration was investigated.

### 5.3.1. Films aged at ambient RH

Initially, pure PVA films and glycerol plasticised PVA films were prepared to provide a benchmark before introduction of surfactants. Pure PVA films had a very typical flat, uniform morphology characterised with low root mean square roughness ( $R_q=0.3$  nm, Figure 5.1a,b). Introduction of glycerol led to no substantial change in morphology ( $R_q=0.4$  nm, Figure 5.1c,d), in agreement with previous findings that show glycerol is uniformly distributed within thin PVA films.<sup>295</sup> Equally, aging for two weeks showed no visible effect on sample morphology, with roughness staying approximately constant. These findings prove that either rapid equilibration occurs in ambient RH conditions, films are already in equilibrium as-cast, or changes in glycerol and distribution during aging do not lead to significant changes in film surface morphology.

Next, surfactant molecules were introduced into the formulation. To mimic initial stages of the real-world phenomenon of surfactant migration into the film from adjacent media, plasticised PVA films were prepared doped with relatively low concentrations (1-5 wt%) of surfactants with various head group chemistry (cationic, nonionic or anionic). Aging was performed as before (two weeks in ambient conditions), with AFM measurements performed on days 0, 7, and 14.

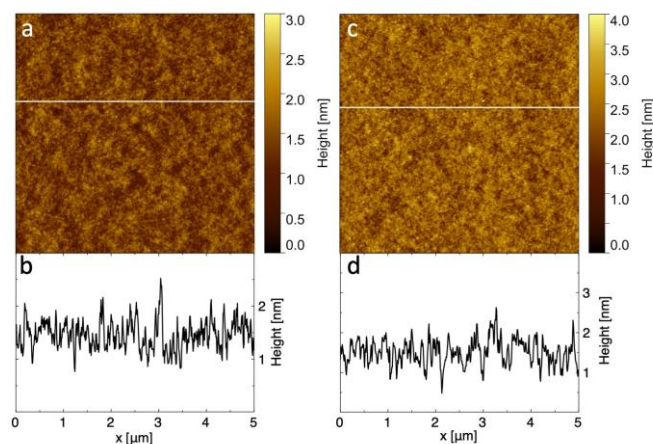


**Figure 5.1.** Morphology and height profile of: **(a,b)** PVA film and **(c,d)** glycerol-plasticised PVA film on day 0.

### 5.3.1.1. Effect of CTAB addition on morphology of the PVA-based films

Ionic surfactants are known to associate with polymers.<sup>125</sup> Indeed, in aqueous solutions CTAB was previously reported to interact with PVA chains via hydrophobic interactions, with hydrophobic surfactant tail creating a complex with acetate groups on the polymer.<sup>130,134,312</sup> In the systems investigated herein, no changes in polymer morphology were observed throughout the two weeks aging period when CTAB concentration was below 4 wt% (appearing similar in morphology to Figure 5.1). Therefore, additional measurements were taken after a total aging time of 2 months, showing changed morphology in the 3 wt% formulation, with some limited depressions forming at the film surface (Figure 5.2a,b, Figure 10.7, Appendix C). These changes are ascribed to the CTAB as no such features were observed for control samples over 2 months. Conversely, these features were observed in films with 4 wt% and 5 wt% CTAB concentration after only one week (Figure 5.2c,d, Figure 10.8, Appendix C). They are likely to consist of hydrophilic mesophases arising from intermolecular interactions in the system, leading to surfactant being pushed away from the polymer/glycerol matrix (although at insufficiently high concentration to form crystals).<sup>358</sup>

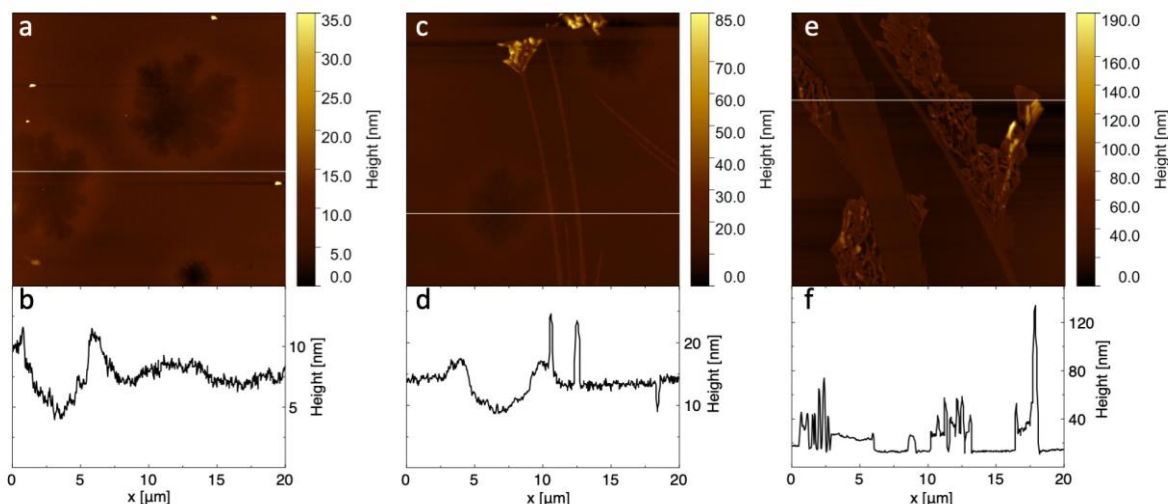


**Figure 5.2.** AFM image and height profile of: (a,b) depressions visible on the surface of plasticised PVA film with 3 wt% CTAB concentration after 2 months of aging; (c,d) crystallites and depressions correlated with presence of 5 wt% CTAB and (e,f) large crystals visible on the surface of the film with 5 wt% CTAB on day 7. Optical microscope images of the bloom regions on day 0 and day 7 are presented as Figure 10.9, Appendix C.

The sample with the highest CTAB concentration (5 wt%) was characterised by both depressions and crystallites on the surface visible from day 0 (Figure 5.2c,d). After one week of aging, crystal size increased, creating large dendritic structures across the whole film (Figure 5.2e,f, Figure 10.9, Appendix C).

In thin, unplasticised PVA-CTAB films, surfactant was proven to be uniformly distributed in the polymer matrix, even at high concentration (ca. 20 wt%).<sup>295</sup> It was inferred that the even distribution of CTAB in PVA was caused by similarities in component surface energy, contrasting with the much higher value for glycerol.<sup>295</sup> As a result, upon introducing plasticiser to the system, regions of surfactant excess in substrate-film and film-air interface form. Glycerol is therefore likely to create more favourable interactions with amorphous PVA regions compared to cationic surfactant, outcompeting PVA-CTAB interactions and decreasing compatibility between the three components.<sup>295</sup> Consequently, at CTAB concentrations above 3 wt%, spin-coated films display segregation after aging in ambient conditions. At CTAB concentrations of 5 wt% and above the crystal formation is likely driven by the system being below  $T_k$  for CTAB (25 °C).<sup>359,360</sup> Although the cationic surfactant is expected to be uniformly

distributed in as-cast films, after storage in ambient conditions the driving force of increasing non-compatibility between the components (especially for films with 4-5 wt% CTAB) causes surfactant excess at the interface, aided by ambient humidity.

### 5.3.1.2. Effect of C<sub>12</sub>E<sub>10</sub> addition on morphology of the PVA-based film

Upon addition of relatively low quantities of C<sub>12</sub>E<sub>10</sub> (1-5 wt%) no blooming was observed throughout the investigation period (as presented in Figure 5.3o,p). Both on day 0 and 14, characteristic polymer morphology is visible ( $R_q=0.4$  nm), similar to the control formulations. Combined, these results suggest the film structure is either equilibrated as-cast or not sensitive to changes in molecular arrangement within the film.

Indeed, nonionic surfactants are known not to form strong interactions with homopolymers<sup>361</sup> – indicating higher compatibility. For C<sub>12</sub>E<sub>5</sub> (a structurally similar surfactant to C<sub>12</sub>E<sub>10</sub>) however, different behaviour was observed. This surfactant, when mixed with pure PVA, segregates to the surface due to its much lower surface energy compared to PVA, with decreasing surface excess upon glycerol addition.<sup>295</sup> Due to higher  $M_w$  of C<sub>12</sub>E<sub>10</sub> and consequent higher entropy penalty connected with its surface segregation, the surface excess will be lower for the surfactant studied here. Furthermore, as suggested by Flory-Huggins theory, increasing  $M_w$  of the surfactant will decrease compatibility in the PVA-C<sub>12</sub>E<sub>10</sub> system compared to PVA-C<sub>12</sub>E<sub>5</sub>. Therefore, the incompatibility between elements is expected to be the main driving force leading to C<sub>12</sub>E<sub>10</sub> segregation in pure PVA films. However, at the relatively low concentrations used here, and given the presence of glycerol which acts to increase compatibility,<sup>295</sup> no substantial morphology changes compared to blank sample were observed.

### 5.3.1.3. Effect of SDS addition on morphology of the PVA-based films

As seen in systems with CTAB and C<sub>12</sub>E<sub>10</sub>, morphology changes are very much dependent on the chemistry of the surfactant added. This is further shown upon addition of SDS to the film. For this system, lower concentrations and shorter aging times were required to observe surface morphology changes compared to either of the other surfactants. Further, unlike the depressions or crystals characteristic of CTAB, SDS created blooms on the surface of the film.

For films with 1 wt% SDS, addition of surfactant did not lead to substantial changes in polymer morphology on day 0 ( $R_q=0.5$  nm), however, individual blooms were occasionally visible (with a similar morphology to the film presented in Figure 5.3a,b). Nevertheless, after one week of aging, surfactant blooms were uniformly distributed on the surface of the sample (Figure 5.3a,b) with no further changes observed after the second week of aging.

Surfactant blooms increased in size when increasing concentration from 1 wt% to 2 wt% SDS (Figure 5.3e,f), with visible uniform distribution of blooms on the surface of the film from day 0 (Figure 10.10, Appendix C). For these samples, characteristic polymer morphology was still visible between the SDS blooms, however with some positions where changes were observed indicating surfactant incorporation into the polymer morphology (Figure 5.3c,d,  $R_q=0.6$  nm). Blooms had the same height in both formulations – ca. 4 nm (Figure 5.3b, Figure 5.3f). This value corresponds very well to that reported by Coiro et al.<sup>362</sup> for individual SDS lamellae in highly concentrated aqueous solutions, highlighting similarities in surfactant behaviour between solid and liquid systems. Therefore, it is surmised that the surfactants in films investigated here also create single lamellae.

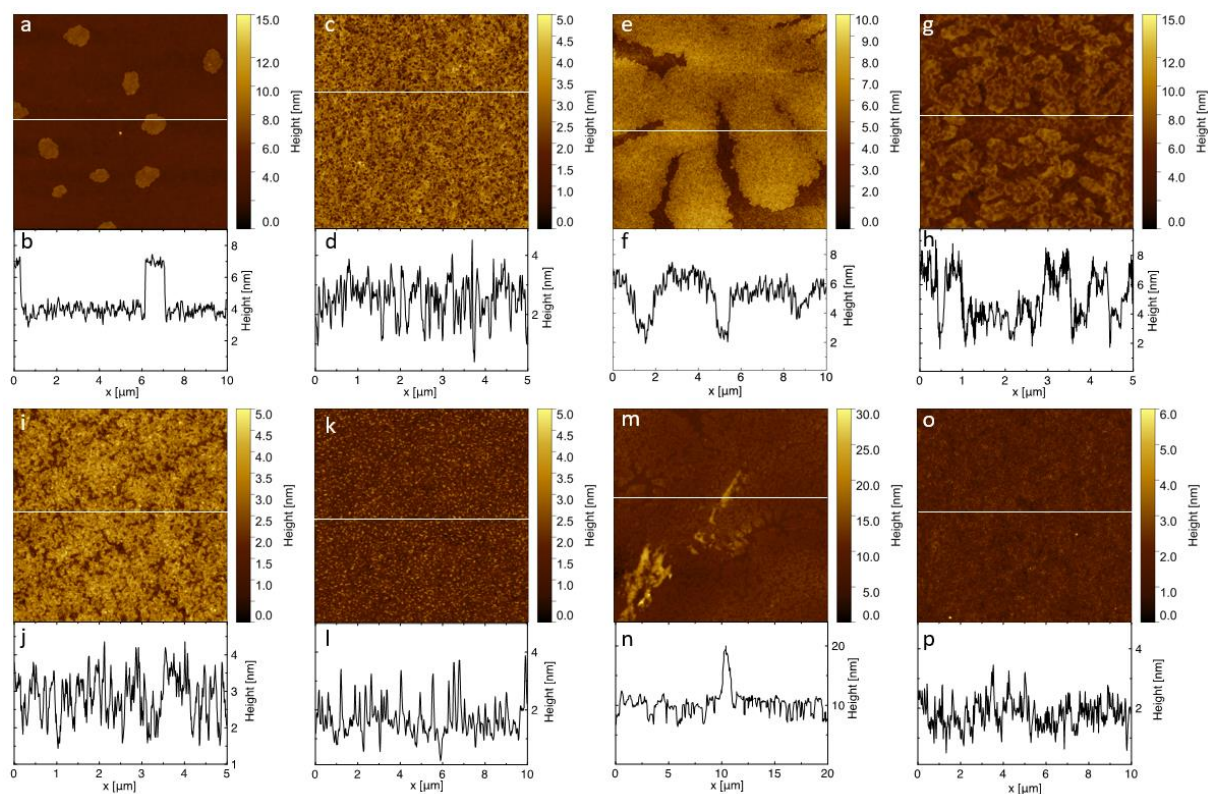


**Figure 5.3.** AFM image and height profile of: (a,b) plasticised PVA containing 1 wt% SDS on day 7; (c,d) modified background polymer morphology due to surfactant addition and (e,f) surfactant blooms on the surface of plasticised PVA film with 2 wt% SDS on day 0; (g,h) modified polymer morphology for plasticised PVA film with 3 wt% and (i,j) 4 wt% SDS on day 0; (k,l) modified polymer morphology and (m,n) blooms on the surface of plasticised PVA film with 5 wt% SDS on day 0; (o,p) polymer morphology of sample with 5% C<sub>12</sub>E<sub>10</sub> addition on day 14.

Surfactant content equal to 3 wt% led to further morphology changes, with both SDS blooms throughout the film and increased roughness in the background polymer morphology (Figure 5.3g,h). Even further concentration increase resulted in phase separation in films, greater changes to polymer morphology (Figure 5.3i,j, Figure 5.3k,l) and creation of large surfactant blooms on the sample surface (Figure 5.3m,n, Figure 10.11, Appendix C).

Throughout these experiments, SDS was shown to be the least compatible surfactant in plasticised PVA films among those studied. Blooming of SDS in plasticised PVA systems at high surfactant concentrations (20 wt%) has been shown to be thermodynamically-driven due to interactions between SDS head groups and glycerol, enhancing the formation of smectic layers.<sup>17</sup> The total free energy of the system is likely minimised in two ways: firstly, as SDS has



lower surface energy than PVA, it is present at the surface in multilammellar structures with glycerol; secondly, by segregating in this way SDS does not disrupt arrangement of the PVA chain below the smectic layers.<sup>17</sup>

Although the systems investigated here have much lower SDS concentrations, this scenario seems to explain the tendency of SDS to create a wetting layer at the surface of the film. Even at 1 wt% SDS, changes in PVA-based film morphology are observed (blooms at the film-air interface), with further changes appearing while increasing concentration of the anionic surfactant. For samples of between 2 wt% and 5 wt% SDS, however, no morphology changes during two weeks of sample aging were observed. This implies that the equilibrium molecular arrangement is likely to be achieved either during spin coating or immediately after. For the lowest investigated concentration of 1 wt% SDS, aging up to 1 week was required for the equilibrium to be reached.

Regardless of head group chemistry or surfactant concentration, scratch test measurements showed that thickness of all samples equilibrates after 1 week of sample storage (Table 10.6 and

Table **10.7**, Appendix C). Increasing surfactant concentration in general led to decreased film thickness due to decreasing viscosity of the solution used for film preparation. However, formulations with 1 wt% C<sub>12</sub>E<sub>10</sub> were ca. 6% thicker compared to plasticised PVA film despite decreasing viscosity (Chapter 3, Table 3.2, Table 3.3). Higher C<sub>12</sub>E<sub>10</sub> concentrations showed a decrease in film thickness with increasing surfactant concentration. As expected, thickness decrease was noted from 1 wt% CTAB and SDS surfactant addition (ca. 29.6% and 14.3% compared to plasticised PVA for SDS and CTAB doped PVA-based films on day 1, respectively), being the most pronounced for SDS samples despite similar viscosity of both solutions used for film preparation. Further deviations were only noted for SDS, where no clear

trend in film thickness with increasing surfactant content was observed on day 0, however the trend of decreased film thickness with increasing surfactant concentration was observed after 1 week of sample storage. These results suggest that at low concentrations, the higher  $M_w$  of C<sub>12</sub>E<sub>10</sub> compared to ionic surfactant studied here leads to increase in PVA-based film thickness. However, ionic surfactants change arrangement and packing in the system (likely correlated with glycerol distribution in the system),<sup>17,295</sup> with SDS causing the most significant thickness variations.

#### 5.3.1.4. Effect of glycerol evaporation on thickness of the PVA-based films

Generally, the thickness decreased ca. 20% for all plasticised films (with or without the addition of surfactant) – approximately equal to the initial glycerol concentration. The two notable exceptions from this behaviour were unplasticised PVA films and plasticised formulations containing 5 wt% SDS. For the former, no significant changes in thickness were observed throughout the 2 weeks aging time, with slight thickness variations correlated with changes in humidity and temperature of ambient conditions. For the latter, conversely, a drastic thickness decrease was found after 1 week of aging (decrease of ca. 40%). This can be explained by the fact that scratches were taken in regions with no large surfactant blooms (i.e. morphology consistent with Figure 5.3k, not Figure 5.3m), where glycerol local concentration may be higher.

It is suggested that decreasing film thickness upon storage is a consequence of glycerol evaporation from PVA films.<sup>181</sup> While this phenomenon may appear counter-intuitive at ambient conditions due to the high glycerol boiling point (290 °C),<sup>97</sup> the rate of pure component evaporation at 25 °C was reported to be equal or higher than 0.016 g/(m<sup>2</sup>·h),<sup>363,364</sup> corresponding to an approximate value of 2.1 mg for 2 weeks storage time. The mass of thin films studied here was calculated to be ca. 0.05 mg. Considering that surface area is much greater than thickness

of the film and diffusion rates values that were reported to be 10 to 100 times larger than evaporation rates,<sup>93</sup> glycerol evaporation appears to be a relevant explanation for observed changes in the systems studied here.

These conclusions are consistent with the previous findings for PVA films doped with glycerol only, where it was found that for an equivalent PVA polymer (i.e. identical  $M_w$  and DH as used here) equilibrium was reached after ca. 5 days of sample storage at ambient temperature and RH, with constant rate of glycerol evaporation.<sup>181</sup> However, the changes in film thickness with aging might also result from changes in surfactant assembly in the presence of glycerol. This phenomenon was observed for SDS assembly in glycerol,<sup>365–367</sup> with significant variation in surfactant behaviour compared to water systems, correlated with changes in solvent polarity. In the systems discussed here, these interactions might result in changes in system packing, hence thickness variations. Moreover, as plasticised films without glycerol addition also showed decreased film thickness, these changes might be additionally influenced by physical aging – a process of reaching equilibrium and minimising system energy by reducing free volume in polymer matrix below  $T_g$ ,<sup>368</sup> accelerated by glycerol plasticisation.

Overall, spin-coated plasticised PVA films doped with surfactants reach equilibrium upon aging due to both glycerol evaporation and surfactant migration. Inter-component compatibility and atmospheric water sorption are the main driving factors for this equilibration. This is evidenced by the different concentrations of each surfactant required for blooming in spin-coated films – 3% wt for CTAB, 1% wt for SDS, but ca. 20 wt% required to consistently observe changes in C<sub>12</sub>E<sub>10</sub> doped films (Figure 5.4a,b and Figure 5.4c,d). The time-dependency of bloom formation seems to be unique for thin, spin-coated films. When films were prepared using solution casting method (thickness ca. 40  $\mu\text{m}$ ), they exhibited phase separation immediately after film preparation for films doped with 1 wt% of SDS (Figure 5.4g,h) and

$C_{12}E_{10}$  surfactant (Figure 5.4e,f). This behaviour is linked to the longer evaporation time and increased temperature during solution casting, hence longer time available to reach equilibrium via surfactant migration, rather than being directly related to the increased thickness of the films.

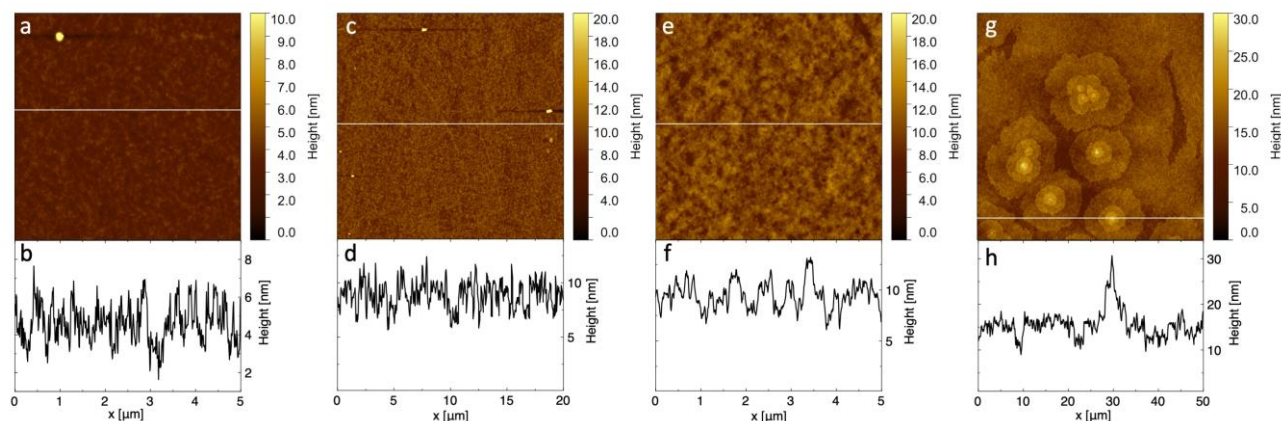


**Figure 5.4.** AFM images and height profiles of (a,b) spin-coated, glycerol-plasticised film with 20 wt%  $C_{12}E_{10}$  on day 0 and (c,d) day 7 (exhibiting chequerboard pattern of surfactant blooms); (e,f) solution cast thick film with 1 wt%  $C_{12}E_{10}$ , and (g,h) SDS blooms on the surface of plasticised PVA thick film with 1 wt% SDS.

### 5.3.1.5. Chemical character of surfactant doped films

To further understand the arrangement of surfactants within the blooms, CFM was implemented using two chemically modified cantilevers – acid-terminated (hydrophilic) and methyl-terminated (hydrophobic). Their different chemistries result in different capillary forces in the ambient environment,<sup>369</sup> highlighting the relative degree of hydrophilicity<sup>353,370</sup> and enabling differentiation between hydrophilic and hydrophobic surface groups (i.e. the orientation of the surfactants – tail-up or head-up) via force measurements. They were performed on a plasticised PVA film control sample and samples containing SDS (1 wt% and 2 wt% for measurements of the positions without blooms and positions with and without large blooms, respectively, to ensure cantilever-bloom interactions), CTAB (5 wt%) and  $C_{12}E_{10}$  (20 wt%). Concentrations used for all surfactant chemistries allow for surfactant blooms or crystals to be created within 1 week – following scratch test results, samples in general equilibrate within this timescale, hence comparison between freshly prepared (day 0) and

equilibrated (day 7) PVA films is possible. Complementary contact mode imaging (friction channel) was performed on areas with surfactant blooms to confirm adhesion results (i.e. the relative difference between adhesion for background and bloom regions). In all cases, conclusions from imaging were consistent with those obtained from force measurements.

The control sample on day 0 showed on average stronger adhesion for acid cantilever than methyl cantilever which is expected due to stronger capillary force for this chemistry (Figure 5.5). This was visible also from the shape of the force curve which recorded longer rupture distances for acid-terminated cantilever (Figure 5.6). While the acid-terminated cantilever interacts with PVA hydroxyl groups and glycerol uniformly distributed in the film,<sup>181</sup> the methyl-terminated cantilever is attracted to acetate groups of unhydrolysed PVAc and glycerol methylene groups. For both chemistries, the adhesion force between cantilever and the surface decreases after one week of sample aging (Figure 5.5b).

Conversely, SFE values (Table 5.1) increased after one week of sample aging by ca. 6 mN/m independent of sample formulation, suggesting increase in films hydrophilicity and highlighting the complex nature of investigated systems. It is hypothesised that glycerol evaporation or changes in its surface concentration are responsible for this phenomenon. Glycerol was observed to significantly enhance water sorption in polymer films<sup>339</sup> (also in Section 5.3.2.1, *vide infra*), hence its presence will result in overall higher capillary force and higher adhesion values and consequent decrease in adhesion values upon its loss. Further, as SFE measurements are based on CA goniometry, and CA was shown to significantly change over time due to PVA dissolution (Chapter 7), it is possible that plasticised samples require longer time for droplet stabilisation compared to unplasticised samples. Alternatively, free volume previously occupied by glycerol is likely replaced by water once equilibrating, with possible faster droplet infiltration for matrices where some free volumes remain unoccupied,

hence lower initial CA hence SFE. Regardless, it is unclear why hydrophilicity increases for unplasticised formulations.

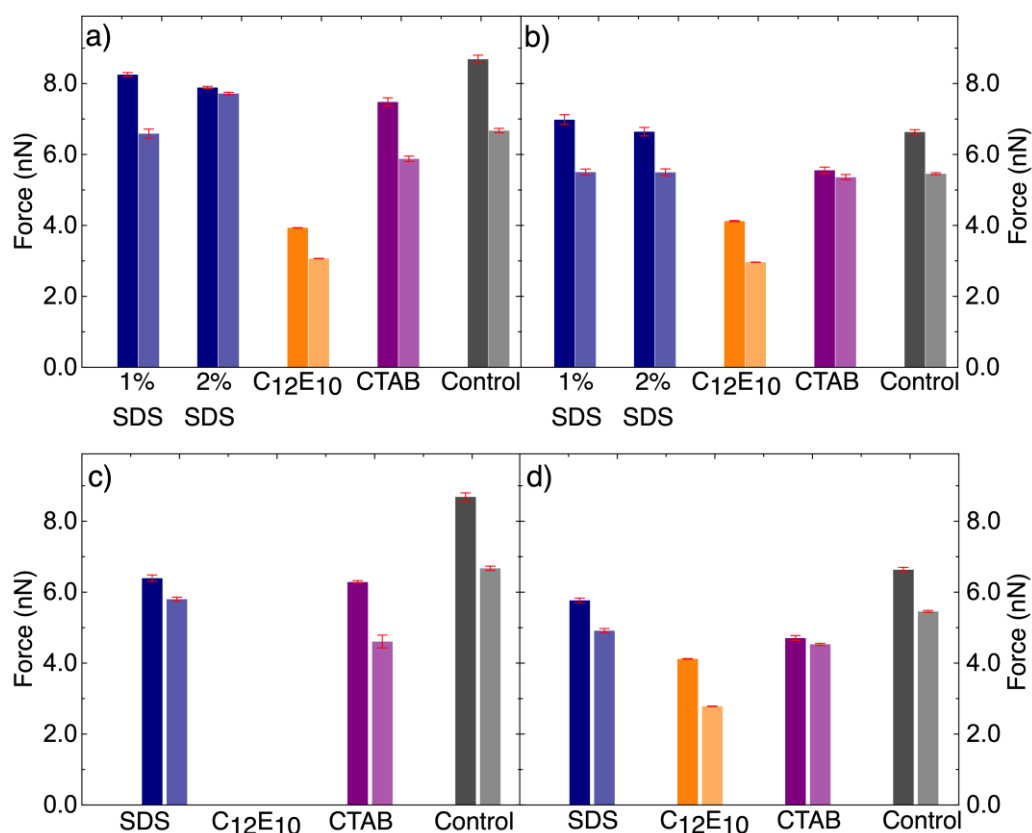


**Figure 5.5.** CFM measurements on areas without surfactant blooms: (a) day 0, and (b) day 7; surfactant blooms/crystals on: (c) day 0, and (d) day 7. Darker colours correspond to measurements with acid-terminated cantilever, while lighter – methyl-terminated cantilever.

Comparing between different formulations, the SFE of the PVA film with 1 wt% SDS was lower than plasticised PVA (Table 5.1). Addition of CTAB at 5 wt% and C<sub>12</sub>E<sub>10</sub> at 20 wt% concentrations led to increased surface energy values, however it is unclear whether this is due to increasing surfactant concentration or the change in surfactant head group chemistry. Conclusions about relative hydrophilicity between control and formulations doped with surfactant are in general inconsistent with adhesion results (Figure 5.5, Table 5.1), suggesting that surfactant might enhance wetting on the latter formulations (Chapter 7).

**Table 5.1.** Average SFE values for freshly prepared formulations and those aged for one week. Error bars are one standard deviation around the mean (n=6, mean  $\pm$  SD).

Sample	SFE for day 0 (mN/m)	SFE for day 7 (mN/m)
PVA + glycerol	46.56 $\pm$ 0.30	51.31 $\pm$ 0.43
PVA + glycerol +1% SDS	43.70 $\pm$ 0.87	48.55 $\pm$ 0.16
PVA + glycerol +20% C <sub>12</sub> E <sub>10</sub>	50.39 $\pm$ 0.56	57.48 $\pm$ 3.93
PVA + glycerol +5% CTAB	48.76 $\pm$ 0.02	54.61 $\pm$ 0.04

For measurements on the sample containing 1 wt% SDS, lower average adhesion forces were recorded for both hydrophobic and hydrophilic cantilevers compared to plasticised PVA samples. These values for the acid-terminated cantilever further decreased at higher SDS concentration in the system (Figure 5.5) and were likely connected with the preferable interactions between glycerol and surfactant in the film (hence lower glycerol concentration on the surface) as well as with the presence of surfactant tail group on the surface, lowering the hydrophilic nature of these areas. For SDS blooms (Figure 5.5c and Figure 5.5d), lower adhesion was consistently recorded compared to the non-bloomed regions. Changes after aging were smaller for blooms than for the remainder of the film, indicating no impact of the glycerol evaporation (or changes in its surface concentration) as little to no glycerol was incorporated in surfactant blooms. Specific to SDS, hydrophobic tails are believed to be exposed to ambient atmosphere as the films age, creating single surfactant lamellae in agreement with the findings of Briddick et al.<sup>17</sup>

The high concentration of C<sub>12</sub>E<sub>10</sub> led to the most significant changes in surface chemistry, both on the preparation day and upon aging, characterised by much longer rupture distance compared to formulations with other surfactants (Figure 5.6). These findings suggest that there is surfactant excess at the surface, similar to that suggested in the literature<sup>295</sup> and by AFM imaging (showing increased  $R_q$ , Figure 5.4a,b), with hydrocarbon tail of C<sub>12</sub>E<sub>10</sub> exposed. This concentration of surfactant was also sufficient for formation of characteristic, chequerboard patterns of blooms after one week of aging (Figure 5.4c,d, Figure 10.12, Appendix C). Unlike

other surfactant chemistries, no significant difference in adhesion was observed for these bloom regions compared to regions without visible blooms, which may suggest that at such a high surfactant concentration a significant amount of surfactant molecules remain within the film even after blooming. This would also explain the similarity of adhesion measurements before and after aging for this sample as the composition of films with 20 wt%  $C_{12}E_{10}$  is changed less compared to formulations with other surfactants (or plasticised PVA).

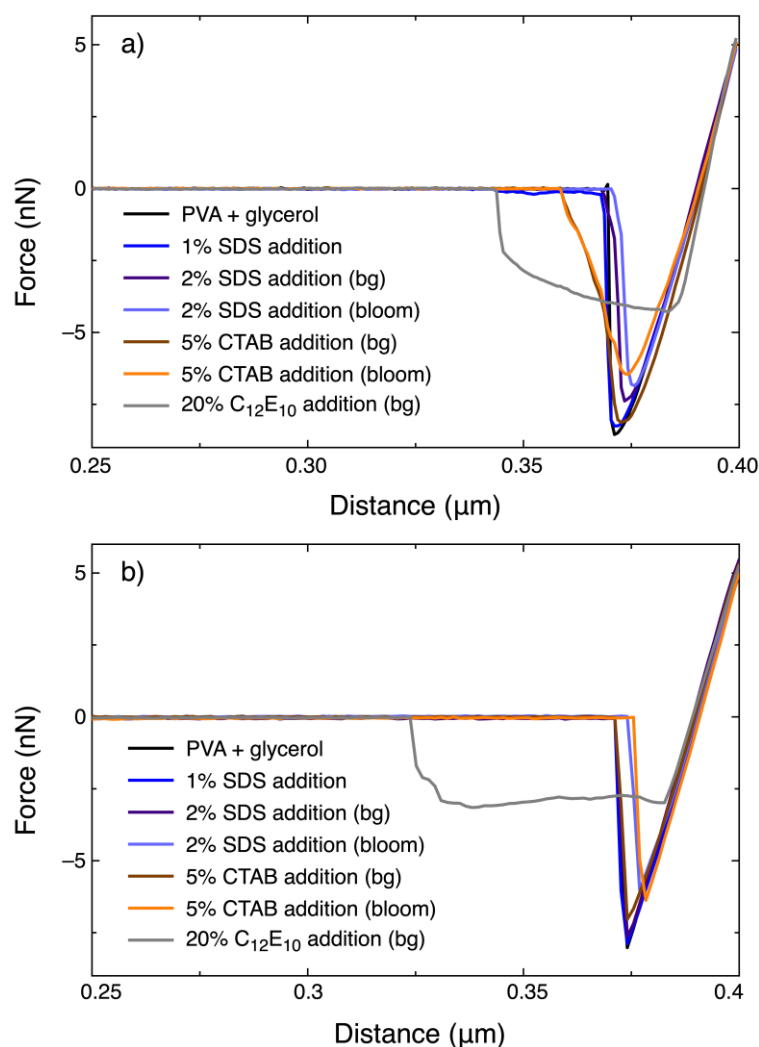


**Figure 5.6.** Exemplary force curves obtained on day 0 using (a) acid- and (b) methyl-terminated cantilevers. Bg stands for background – regions without surfactant blooms.

Lastly, background areas on the sample doped with CTAB showed similar behaviour to the control sample (Figure 5.5a,b). As for CTAB crystals, lower values of adhesion for both



cantilever chemistries compared to control formulation suggest arrangement with hydrophobic tail exposed. Formulations with both cationic and anionic surfactants therefore present a similar arrangement, with force curve shape and rupture distance alike that of plasticised PVA films (Figure 5.6). Adhesion in these systems is primarily driven by capillary forces. In formulations with nonionic surfactant, however, the surfactant wetting layer uniformly distributed on the film surface results in dominant viscous force,<sup>371</sup> increasing rupture distance of the force curve.

### **5.3.2. Films aged at various RH conditions**

#### **5.3.2.1. Effect of RH on water sorption in solution cast films**

To establish how changes in film chemistry at different stages of guest molecule migration influence water sorption, thick films (characterised in Table 10.10, Appendix C) containing surfactants of various chemistry and concentration were prepared and investigated using DVS.

As PVA films have a hydrophilic nature, they contain certain amount of water in ambient conditions (ca. 6.5 wt%).<sup>101</sup> Water in the PVA system can be divided into three groups: nonfreezing water, freezable bound water, and free water<sup>100,101,372,373</sup> (Chapter 1, Section 1.4.1.4). For almost fully hydrolysed PVA (DH=99.8% cf. 87-89% used here), when total water content in the film is below ca. 22 wt%, it acts as nonfreezing water.<sup>101</sup> This water disrupts the interfacial hydrogen bonding between PVA crystallites and amorphous regions by changing configuration of the polymer chain – from zigzag crystalline planar configuration to random, amorphous configuration. In this way, greater motion of the alcohol sidechain is allowed upon water adsorption, and effective crystallinity in the system decreases. Simultaneously, water molecules swell the amorphous polymer matrix, increasing overall mobility of the PVA matrix and its free volume. For thick PVA films (ca. 40  $\mu\text{m}$ ) moisture is readily absorbed after reaching

ca. 50% RH,<sup>374</sup> therefore significant changes in film behaviour are expected above this humidity level.

In this study, for pure PVA films these changes were seen only above 65% RH. Figure 5.7 presents the equilibrium amount of absorbed water at a given RH for the various compositions studied in this chapter. Addition of glycerol to PVA films led to substantial increase in water absorption compared to pure PVA formulation, leading to double amount of water adsorbed compared to unplasticised polymer sample (12 wt% and 5.9 wt% uptake at 75% RH, respectively). This echoes previous results of water absorption into plasticised PVA,<sup>339</sup> which showed that glycerol increases water absorption.

As previously stated, in solution cast films (such as were used for DVS), there is more time for the system to reach equilibrium during water evaporation. Investigated compositions exhibited surfactant blooms at the surface (visible white regions on the otherwise-transparent films). As only freshly made films were used for DVS analysis, significant structural changes are not expected to occur before the sorption measurements. However, if the equilibrium was not reached during film preparation, migration is likely to take place during the measurements, causing rearrangement in the film structure.

In these systems, calculation of diffusion coefficient at given RH would be inaccurate not only because film thickness changed during the measurement (performed continuously without knowledge of the thickness at each starting RH), but also because of non-uniform thickness of the original film segment used (Table 10.10, Appendix C). For instance, films with SDS did not create uniform structure either in thickness or in surfactant distribution (evidenced by visible white blooms) above 2 wt% surfactant concentration. Therefore, it was not possible to measure equivalent film segments for these formulations compared to other surfactant-doped films.

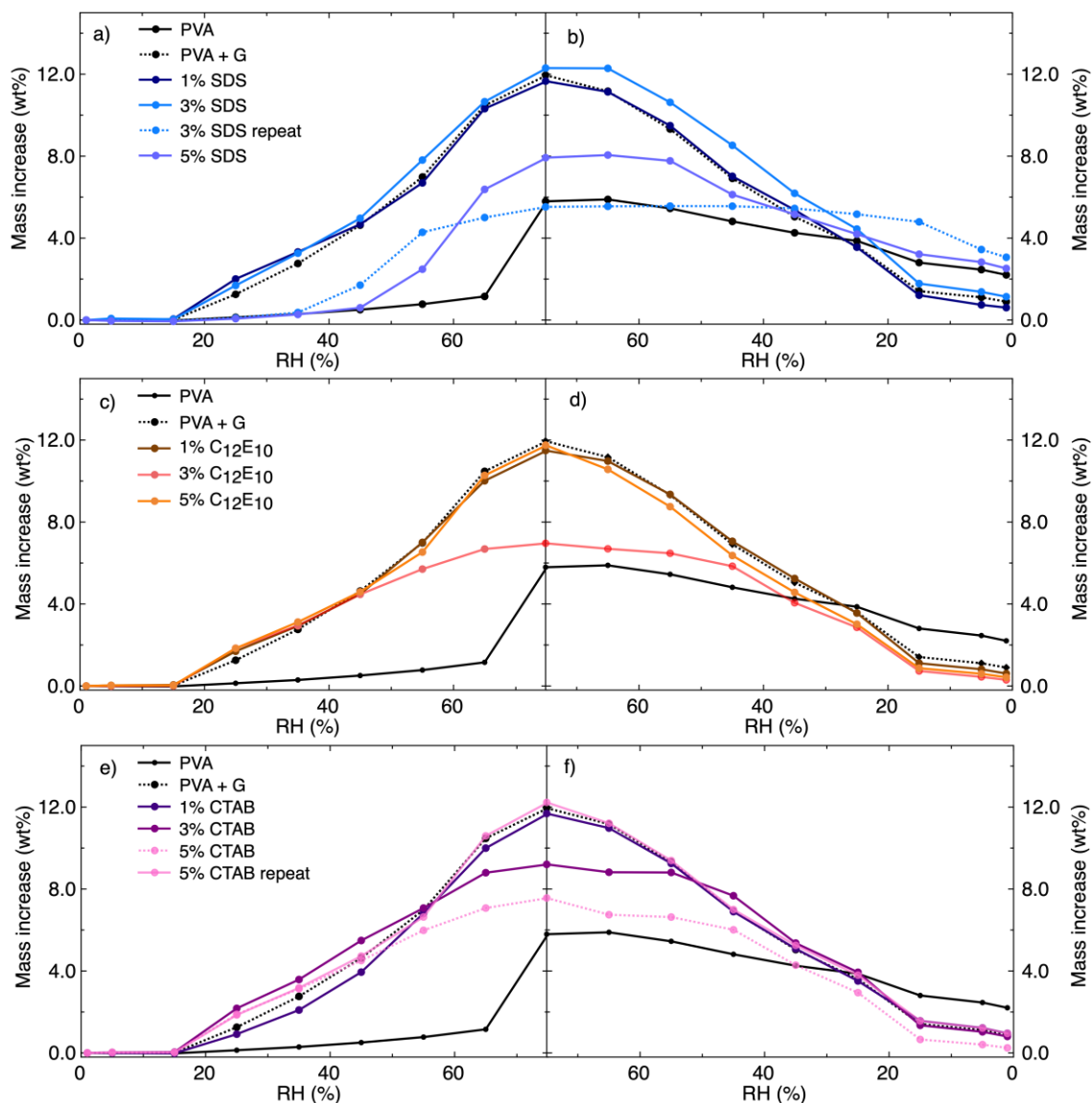


**Figure 5.7.** Equilibrium water sorption versus RH for (a,c,e) absorption and (b,d,f) desorption processes. Samples were doped with (a,b) SDS, (c,d) C<sub>12</sub>E<sub>10</sub>, and (e,f) CTAB.

Generally, plasticised PVA films doped with surfactants did not show greater water absorption than plasticised PVA sample (around 12 wt% absorbed water at 75% RH, Figure 5.7). This conclusion is valid for all investigated head group chemistries of the surfactants and all concentrations used. However, phase separation and variations in thickness of the film also led to inter-sample variation in sorption behaviour for samples of the same composition. For these samples it is assumed that due to the phase separation, the composition of the film

segments being analysed may resemble pure PVA or plasticised PVA, dependent on exhibited sorption behaviour.

Surfactant impact on water sorption is not explicit. Generally, these additives are expected to affect the film water sorption capability due to their hydrophilic properties<sup>358</sup> – both because of presence of surfactant aggregates within the film (leading to hydrophilic pathways) and creation of hydrophilic pockets/aggregates. Such hydrophilic pockets were proven to lead to prolonged water absorption due to creation of a strong osmotic driving force for water diffusion.<sup>358</sup>

In terms of uptake kinetics, at low RH conditions (i.e. 1-15% RH), all investigated samples (pure PVA films, plasticised PVA, plasticised PVA doped with surfactants) reached equilibrium after ca. 10 minutes (Table 10.11, Appendix C). As humidity increased to between 25% and 65% RH, time to equilibrate did not change for pure PVA films, however, all plasticised samples (with or without the addition of surfactants) showed significant increase in sorption time – to ca. 50 minutes. The only exceptions were some investigated films with 3 wt% SDS (Figure 5.7a, sample labelled 3 wt% SDS repeat) and 5 wt% SDS – a further indication of phase separation in the system. Accordingly, these compositions showed sorption behaviour like that of unplasticised PVA. Significant increase in sorption time for these samples was only observed from 35% RH and 45% RH, respectively. It is worth noting that, at 75% RH, sorption time for pure PVA increased to be at least twice as long as for all other samples, while other compositions mostly showed reduced sorption time at this RH value. For desorption times, values for plasticised PVA were again longer with overall lower changes in mass of the film after the whole hysteresis cycle compared to pure PVA films (Table 10.11, Appendix C).

Despite having the same compositions, repeated DVS measurements on different samples tended not to give the same results, showing that a variety of factors influence the

sorption process (film thickness, surfactant chemistry and concentration, and molecular arrangement of the structure). Despite this variability, glycerol clearly influences water sorption the most, both when it comes to sorption times and amount of absorbed water. Introducing surfactants into the system causes variations in sorption time and amount of absorbed water even within the films of the same composition, suggesting phase separation taking place in these formulations.

### **5.3.2.2. Effect of various RH conditions on molecular migration in thin PVA-based films**

Having shown that water absorption is quantitatively similar in all plasticised PVA films (with the caveat that surfactant-doped films show significantly higher variability), this section focuses again on thin films. On films with 1 wt% SDS (Figure 5.3a,b), surfactant blooms only appeared after aging in ambient atmosphere for one week. It is hypothesised that this behaviour (and equivalent behaviour with other surfactants) is dependent on RH conditions due to the hydrophilic nature of the plasticised PVA – with increasing RH the amount of water in the film also increases (additionally enhanced by glycerol presence), further plasticising PVA-based matrix and enabling quicker equilibration.

In this section, the influence of non-compatibility in the system as a driving force is minimised by only using a low concentration of surfactant (i.e. 1 wt%). To compare the morphology changes with blank samples, both pure PVA films and films plasticised with glycerol were prepared and investigated. After preliminary tests, it was shown that at low humidity (below 35% RH), no significant changes in morphology take place. Moreover, in the investigated humidity range differences were noticed only for samples containing SDS. Therefore, based on the described behaviour, a detailed experimental plan was created (Table 5.2).

**Table 5.2.** Experimental plan for investigation into effect of RH conditions on morphology of the thin films. Symbols stand for: x – all samples analysed given day, (-) – only samples containing SDS were analysed.

Time (day)→ RH (%) ↓	0	3	7	14	21	28	35	42
11	x	(-)	(-)	x	(-)	x	(-)	x
23	x	(-)	x	x	x	x	x	x
35	x	x	x	x	x	x	x	x
43	x	x	x	x	x	x	x	x
53	x	x	x	x	x	x	x	x

### 5.3.2.3. Specific observations on SDS-doped thin films

On day 0, samples doped with SDS had uniform polymer morphology characteristic for pure PVA films. Surfactant blooms are only visible in limited places (as presented in Figure 5.3a,b). For samples stored at 11% RH, no additional blooms appeared on the surface over the whole aging period. At 23% RH, changes started to appear after three weeks in the form of individual blooms (in the regions where they were previously absent). After 5 weeks, the number of blooms on the surface increased, however, they still appeared only in some irregularly distributed regions on the sample surface. For samples stored at ambient conditions (ca. 35% RH), small blooms were uniformly distributed on the whole surface after 3 days of storage. The most significant morphology changes were visible for samples stored at higher humidity (45% RH or 55% RH), with large blooms (Figure 5.8) uniformly distributed on the surface after 3 days. The size of these blooms increased with increasing humidity.

As was seen in the DVS experiments (Figure 5.7), placing a film in a controlled RH environment leads to a water concentration gradient between film and surrounding air. At low RH, no significant water uptake was recorded; for higher RH, however, water uptake became important. Increased water content accelerates molecular migration of surfactants, leading to equilibrium molecular distribution (i.e. blooming). In bulk SDS-containing systems, water stimulates formation of surfactant lamellae by forming hydrogen bonds between the sulfate groups of opposing monolayers.<sup>17</sup> Given the different behaviour at lower RH, it is clear that

plasticisation solely by glycerol is not sufficient to reach this equilibrium, especially considering changes in glycerol concentration and distribution in the investigated formulations. As a result, kinetically trapped surfactant molecules are able to migrate to the surface of the film at higher RH conditions, which is thermodynamically preferable and driven by inter-species compatibility as well as reduction of SDS surface tension by glycerol.<sup>17</sup> For low RH this additional plasticisation with water is less significant, hence no morphology changes due to surfactant migration were observed.

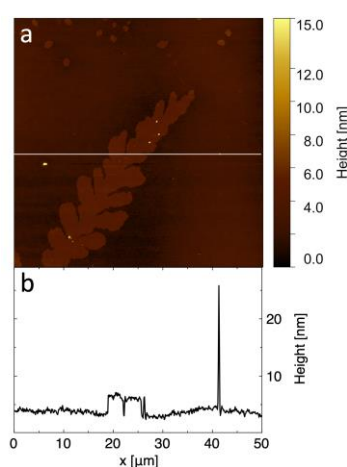


**Figure 5.8.** AFM image and height profile of a bloom on the surface of plasticised PVA film containing 1 wt% SDS stored at 55% RH for 3 days.

#### 5.3.2.4. General observations for all film compositions

Samples with 1 wt% CTAB and C<sub>12</sub>E<sub>10</sub> aged in the same way as control samples showed no substantial morphology changes at humidity below ambient (15% RH, 25% RH) within the investigated time scale. However, samples stored at RH conditions between 35% and 55% led to PVA crystallite formation for all investigated compositions including PVA and plasticized PVA (Figure 5.9).

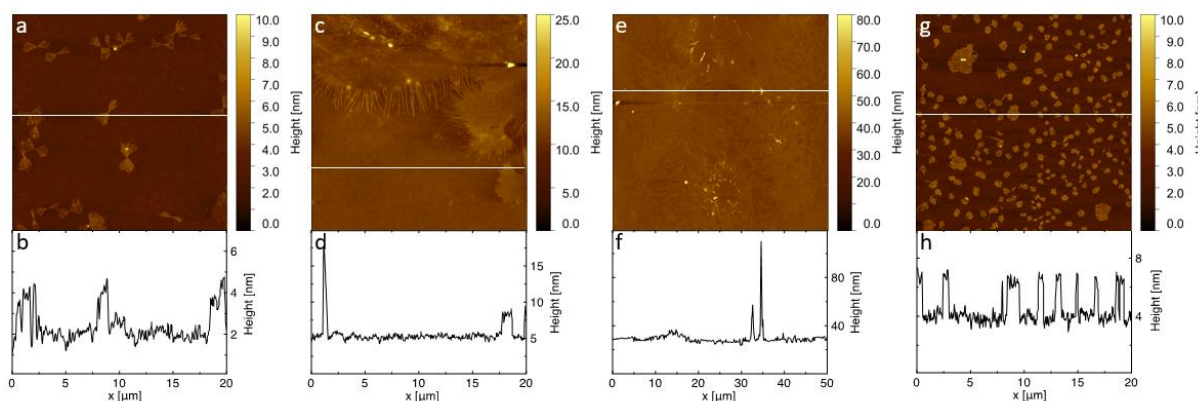


**Figure 5.9.** AFM image and height profile of (a,b) crystal features visible on pure PVA sample stored at 45% RH for 4 weeks, (c,d) large crystals created at the surface of pure PVA films after storage at 55% RH for 5 weeks, (e,f) and (g,h): SDS blooms on which PVA crystals are created at the surface of plasticised PVA sample with 1 wt% SDS imaged after 1 month at 45% RH.

During PVA film casting, evaporation at any temperature does not lead to creation of crystal nuclei when below the sol-gel transition point. Above this point, nucleation with simultaneous crystal growth takes place until reaching composition for gel-glass transition.<sup>375</sup> A significant crystallinity starts to develop at polymer content below ca. 70 wt%,<sup>76,375</sup> continues more rapidly between 80 wt% and 95 wt%, and becomes very slow near the glass transition composition (ca. 97.5 wt%), aided by the ambient humidity.<sup>194</sup> For high RH conditions, however, significant crystallinity is already developed at 65-75 wt% PVA.<sup>76</sup> In case of low RH conditions, crystal growth is constricted before crystallites are fully developed, leading to glassy film morphologies.

Despite that  $T_g$  of PVA is above the aging temperature of films in this study, crystals were observed above 35% RH conditions due to the hydrophilic nature of the polymer. Ambient humidity acts therefore as a plasticiser and facilitates slow, cold crystallization at these temperature conditions. This behaviour results in creation of dendritic or hedritic PVA crystals (stacks of crystals viewed along the chain axis)<sup>376</sup> at the surface, also observed for thick films (ca. 10  $\mu\text{m}$  thick).<sup>194</sup> In this study, due to the rapid evaporation of the solvent during spin coating, these large crystals were unlikely to have enough time to develop and grow. At low RH



conditions, the amount of atmospheric water is not enough for slow, cold crystallization to happen. At higher RH, this behaviour is indeed observed (Figure 5.9a,b and Figure 5.9c,d), showing similarities between spin-coated, thin PVA films and solution cast thick films. Ambient humidity in PVA films has therefore a double role; after entering the system, it increases free volume and disrupts crystals within the polymer matrix, but also helps to facilitate creation of the large crystallites on the surface of the film.

Large PVA crystal structures are also created on the sample upon introduction of SDS. However, in this situation surfactant blooms act as a heteronucleation site, with PVA crystals changing the morphology of surfactant blooms. This leads to the formation either of large crystal areas (Figure 5.9e,f) or crystals incorporated into single surfactant blooms (Figure 5.9g,h).

For the investigated humidity range, and across all compositions, film thickness decreased by 20% during the first week of storage, remaining at a constant thickness thereafter (Table 10.8, Table 10.9, Appendix C). Hence, RH conditions do not significantly influence the final thickness of investigated formulations, with changes in glycerol concentration being similar across investigated range of RH conditions and the most notable changes within first week of sample aging.

### **5.4. Conclusions**

In this work, the aging of PVA-based films under various environmental conditions was studied. The effect of introducing SDS, C<sub>12</sub>E<sub>10</sub>, and CTAB (i.e. common industrial anionic, nonionic, and cationic surfactants) to the polymer matrix was investigated, and the impact of film thickness (i.e. preparation by spin coating and solution casting) was assessed.

It was found that thin PVA-based films undergo aging to reach equilibrium after preparation, and that behaviour of the sample is dependent on the following parameters:

1. Chemical nature of the surfactant – changes in film morphology are the most significant for samples with the addition of SDS, followed by CTAB and C<sub>12</sub>E<sub>10</sub> (with changes observed upon 1 wt%, 5 wt% and ca. 20 wt% addition, respectively). The importance of surfactant concentration in investigated systems highlights different levels of compatibility between guest molecule and plasticised polymer matrix as a function of head group chemistry. Choice of surfactant for industrial formulation should be therefore understood as fine balance between its action and compatibility with other molecules present in the system.

2. RH conditions and aging time – glycerol evaporation/changes in glycerol surface concentration and water infiltration are both time-dependent processes, with water infiltration also dependent on local RH. Low RH was proven to inhibit the surfactant migration process, highlighting the plasticising behaviour of water. Above a threshold RH (ca. 35% RH), surfactants bloom on the surface as a function of time, eventually reaching an equilibrium molecular arrangement within the film. Variations in surface glycerol concentration lead to decreased surface adhesion, with the rate of changes independent of RH conditions.

3. Sample preparation method – film changes upon aging are due to relaxation towards thermodynamic equilibrium. Consequently, if film formation occurs over a longer time period (i.e. by solution casting rather than spin coating), the materials are equilibrated immediately after preparation, resulting in surfactant blooms being visible on day 0.

For formulations with cationic and anionic surfactant, the hydrophobic tail was found to be exposed to the atmosphere, evidenced by decreased adhesion from an acid-terminated cantilever compared to a control formulation. For nonionic surfactant, however, different

behaviour was observed, with surfactant wetting layer and hydrocarbon tail exposed to gaseous phase.

The complex relationship between polymer, plasticisers (such as glycerol and water), and other guest molecules can have a defining impact on formulation behaviour even at low concentrations. The effect initial composition and storage conditions have upon polymer film chemistry is highly relevant to many of their industrial applications due to the impact of film aging on product shelf-life. Therefore, to ensure prolonged shelf life of any given packaging material one should consider action of additives, compatibility between all species present, and storage conditions that are especially important for materials with high affinity to water.

## Chapter 6. Aging of surfactant-doped poly(vinyl alcohol) films at elevated temperatures

### 6.1. Introduction

Investigating diffusion and segregation in polymer films presents significant challenges due to the crowded nature of these systems, causing substantial behavioural modifications compared to the uncrowded state.<sup>377</sup> As stated in Chapter 1, properties of the semicrystalline polymer matrix change with its characteristics (for PVA:  $M_w$ , DH), which influence entanglement, free volume cavity radius,<sup>51</sup> and DC.<sup>242</sup> Moreover, the size and shape of a migrating guest molecule,<sup>378</sup> its concentration,<sup>379–381</sup> compatibility towards the other components in the system,<sup>122,382</sup> presence of charge, and environmental conditions (i.e. RH<sup>181</sup> or temperature<sup>383</sup>) all need to be accounted for while investigating these phenomena.

Among these factors, presence of a second chemical species of the same type (i.e. presence of two surfactants, as found in common industrial formulations) and the convoluted influences of temperature and guest migration on film morphology have received relatively little attention in the literature – not only when it comes to changes within the polymer matrix, but also while discussing release kinetics of substances from the polymer.<sup>384</sup> Within temperature ranges that do not involve any thermal transitions of the polymer, the Arrhenius and van't Hoff expressions can be used to describe changes of diffusion ( $D$ ), solubility ( $S$ ), and permeability coefficients ( $P$ ) of the additive:<sup>385</sup>

$$D = D_b \exp\left(-\frac{E_d}{RT}\right) \quad 6.1$$

$$S = S_b \exp\left(-\frac{H_a}{RT}\right) \quad 6.2$$

$$P = P_b \exp\left(-\frac{E_p}{RT}\right) \quad 6.3$$

where  $D_b$ ,  $S_b$ , and  $P_b$  are pre-exponential factors,  $E_d$  is activation energy for diffusion,  $H_a$  is the

heat of absorption, and  $E_p$  is the activation energy for permeation.

In PVA-based systems, the release of migrating agents was proven to follow the Arrhenius dependence for elevated temperatures (up to ca. 40 °C).<sup>384,386</sup> This simplistic model of an exponential increase in diffusivity with temperature cannot be used for complex polymer formulations containing multiple additives, however.<sup>387</sup> Specific to plasticised matrices, glycerol significantly increases flexibility of the PVA polymer chains, hence leading to a decrease in  $T_g$  dependent on its concentration.<sup>122</sup> Even slight increases in temperature are therefore likely to result in a transition from glassy to rubbery state, in which migration of molecules is more easily accommodated in the system. Upon introducing more additives into the system, intermolecular interactions and compatibility lead to emergent trends of particle arrangement (e.g. segregation).

In addition to being sensitive to RH variations, PVA-based formulations are sensitive to temperature.<sup>388</sup> This is because the mechanism of water infiltration and temperature in such systems is generally similar: plasticisation and increase in free volume due to lubrication induced by disruption of polymer-polymer hydrogen bonding. For atmospheric water this is due to water-polymer interactions, while for increased temperature conditions – thermal energy.<sup>11</sup> Accordingly, many properties correlated with migration in PVA systems are dependent on temperature (e.g. conductivity<sup>389</sup> and storage modulus<sup>240,390</sup>), with polymer relaxation and overall aging accelerated by increased temperature and humidity.<sup>391</sup> Moreover, increased temperature not only influences the diffusion coefficient of already mobile molecules, but also increases the amount of mobile molecules in the system.<sup>335</sup> Therefore, in parallel with RH, storage at elevated temperatures may reduce shelf-life of PVA-based formulations of consumer goods.

In this chapter, the question of how temperature and presence of a second surfactant influences molecular arrangement and aging in plasticised PVA systems was addressed. The influence of temperature was investigated by aging samples under three distinct environmental conditions: elevated temperature and low RH; ambient temperature and ambient RH; and ambient temperature and low RH. First, single surfactant formulations were investigated in PVA of various DH (partially- and fully hydrolysed). Then, 87PVA formulations with two surfactants were investigated. AFM imaging was used to assess systems that present the most significant changes upon aging, while CFM was applied to study the molecular arrangement of additives within these formulations. As demonstrated previously (Chapter 5), visible morphological differences in PVA films occur as a result of surfactant migration, with concentration at which these changes appear dependent on its head group chemistry. Accordingly, films containing 1 wt% SDS, 5 wt% CTAB, and either 10 wt% or 20 wt% C<sub>12</sub>E<sub>10</sub> were studied to investigate how temperature influences surfactant migration. Samples of plasticised PVA with no surfactant were studied in parallel as a control.

## **6.2. Materials and methods**

Thin films of various surfactant concentration were prepared as described in Chapter 2. AFM measurements were performed on each sample on day 0 in ambient conditions before aging. Samples were then aged in one of 3 conditions: in the oven (60 °C, ca. 4% RH), in a desiccator with silica gel (ca. 21 °C, 4% RH), or at ambient conditions (ca. 21 °C, 40% RH) for 2 weeks to investigate the effect of temperature on film morphology. As water vapour pressure is dependent on temperature, the amount present in the surrounding air (and, as a consequence, creating equilibrium with polymer film) at 60 °C will be ca. 10 times greater compared to that of ambient temperature (7.08 vs 0.70 g/kg of water vapour for 4% RH at 60 °C

and 23 °C, respectively).<sup>392</sup> Similar absolute humidity to 60 °C conditions is achieved at 23 °C using higher RH (45% RH, 7.93 g/kg). Accordingly, aging under these 3 conditions enabled RH influence to be decoupled from the temperature influence.

AFM imaging was performed in a controlled RH environment using a modified custom-built humidity chamber (Chapter 5), with a minimum of 6 images taken from each investigated formulation and 3 repeats of each formulation and aging conditions.

## 6.3. Results

### 6.3.1. Effect of temperature and humidity on surfactant migration

Plasticised PVA formulations (20 wt% glycerol addition) were examined as a control to investigate the effect of various aging conditions on polymer morphology. Both 87PVA and 99PVA created thin films of similar morphology and low roughness that did not change at any investigated condition (Figure 6.1), with specific  $R_q$  consistently below 1 nm independent of aging time. As 99PVA has a higher  $M_w$ , it created thicker films compared to its 87PVA counterpart (increase of 20% in average film thickness, Table 6.1). With increasing DH, the SFE increased due to an increased number of hydrophilic groups in the system (Table 6.1). These changes in the structure are expected to result in different interactions when surfactant molecules introduced to the polymer matrix.

Accordingly, 99PVA showed overall lower compatibility with any surfactant studied compared to lower DH counterpart, exhibiting visible morphological changes from day 0 onwards (*vide infra*). SFE values were, moreover, consistently higher for 99PVA samples both on day 0 and day 7 for all surfactant chemistries studied, except for the sample with 20 wt% nonionic  $C_{12}E_{10}$ . For 87PVA-based samples, SFE increased in order: anionic surfactant < no surfactant < cationic surfactant < nonionic surfactant – both on day 0 and day 7 – indicating that

no major change in matrix molecular arrangement took place given that SFE increased by ca. 5 mN/m for each composition as a result of changes in glycerol surface concentration (Chapter 5). Behaviour for 99PVA-based samples was different, however. Here, values of SFE increased in order: cationic surfactant < no surfactant < nonionic surfactant < anionic surfactant on day 0 and nonionic surfactant < no surfactant < cationic surfactant < anionic surfactant on day 7. This indicates more dynamic interactions within 99PVA matrices doped with surfactants, suggesting non-equilibrated structures which will be discussed below.

**Table 6.1.** Average SFE values for freshly prepared formulations on day 0 and day 7, and thickness for freshly prepared investigated samples. Error bars are one standard deviation around the mean (n=6, mean±SD).

Sample	SFE for day 0 (mN/m)	SFE for day 7 (mN/m)	Thickness (nm)
87PVA + glycerol	46.56±0.30	51.31 ± 0.43	116.6±0.1
87PVA + glycerol + 1% SDS	43.70±0.87	48.55 ± 0.16	82.0±0.5
87PVA + glycerol + 10% C <sub>12</sub> E <sub>10</sub>	-	-	65.0±4.7
87PVA + glycerol + 20% C <sub>12</sub> E <sub>10</sub>	50.39±0.56	57.48 ± 3.93	44.9±1.6
87PVA + glycerol + 5% CTAB	48.76±0.02	54.61 ± 0.04	87.1±1.4
87PVA + glycerol + 1% SDS + 5% CTAB	53.98±0.53	60.58 ± 0.05	67.2±1.7
87PVA + glycerol + 1% SDS + 10% C <sub>12</sub> E <sub>10</sub>	59.12±1.56	58.62 ± 0.91	59.0±3.0
87PVA + glycerol + 5% CTAB + 10% C <sub>12</sub> E <sub>10</sub>	62.84±0.87	58.00 ± 0.37	44.2±1.5
99PVA + glycerol	57.10±0.26	59.03 ± 0.37	140.3±1.1
99PVA + glycerol + 1% SDS	63.73±0.29	61.05 ± 2.56	89.6±5.3
99PVA + glycerol + 10% C <sub>12</sub> E <sub>10</sub>	-	-	52.3±1.9
99PVA + glycerol + 20% C <sub>12</sub> E <sub>10</sub>	57.30±3.35	52.62 ± 2.92	40.3±3.4
99PVA + glycerol + 3% CTAB	-	-	79.0±5.2
99PVA + glycerol + 5% CTAB	54.40±2.15	60.10 ± 1.69	73.1±1.0

While films were prepared from the same volume of solution, their thickness decreased with increasing surfactant concentration; this happened because addition of a higher volume of master surfactant solution led to dilution of the final mixture and consequently decreased viscosity of solutions used for film preparation, with parallel changes in molecular arrangement within the matrix due to the surfactant addition and changes in system compatibility.



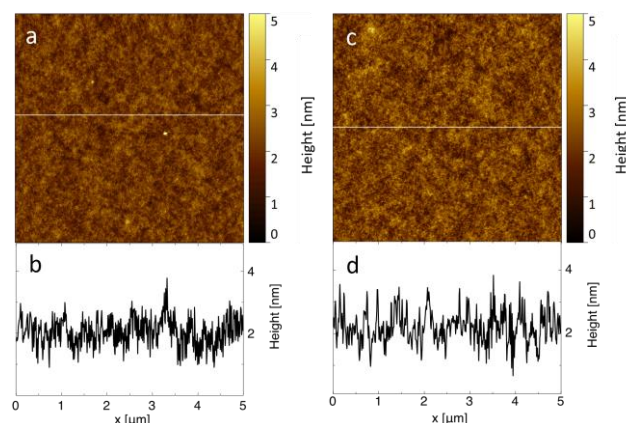


**Figure 6.1.** Morphology and height profile of: **(a,b)** 87PVA film plasticised with glycerol and **(c,d)** 99PVA film plasticised with glycerol on day 0.

### 6.3.2. Anionic surfactant formulations

The general morphology of 87 PVA samples doped with anionic surfactant was similar to that of plasticised 87PVA samples (Figure 6.1a, Figure 6.2a), with similar roughness ( $R_q=0.5$  nm for samples investigated on day 0). As reported in Chapter 5, aging at ambient temperature and RH led to creation of surfactant blooms uniformly distributed on the surface, with size increasing with increasing RH. For some samples aged at ambient temperature and low RH, single surfactant blooms were visible on the surface from day 0 (Figure 6.2c) – however, no further blooming was observed as the sample aged. After aging at elevated temperatures, SDS blooms were visible in limited places with smaller sizes compared to those reported during ambient aging – ca. 1  $\mu\text{m}$  during ambient aging (Chapter 5, Figure 5.3a,b) and ca. 500 nm here (Figure 6.2g,h). Therefore, aging at elevated temperature with low RH did not lead to uniform bloom distribution as was observed for aging at elevated RH conditions. For one investigated sample, after aging at elevated temperature conditions, PVA crystals were observed (Figure 6.2e,f). This unique behaviour may be a consequence of crystallization similar to the slow, cold crystallization observed for RH conditions of ca. 35% RH and above (Chapter 5, Figure 5.9). Here, however, it is likely that the surfactant acts as a heterogeneous nucleation

centre in parallel with polymer plasticisation by glycerol (enabling rearrangement within the matrix accelerated by elevated temperature).

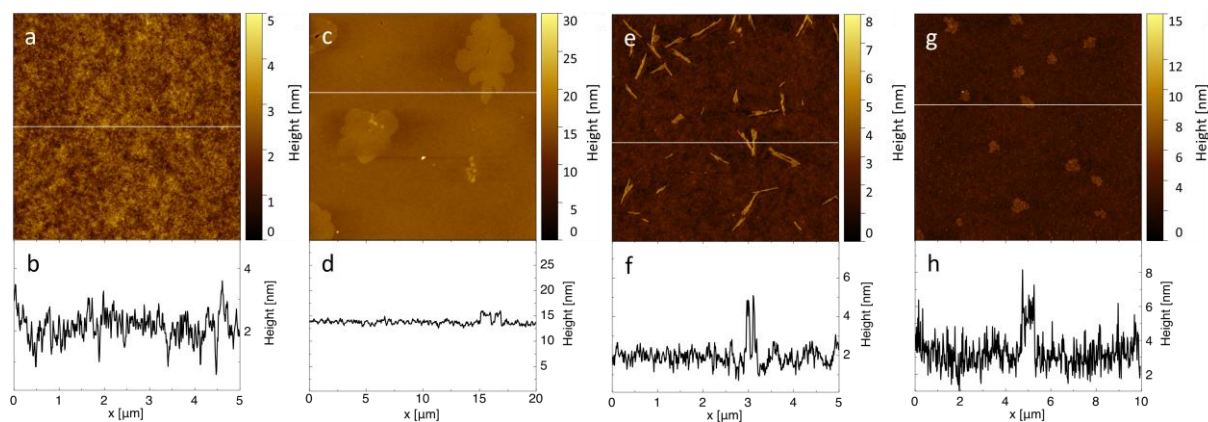


**Figure 6.2.** Morphology and height profile of plasticised 87PVA film containing 1 wt% SDS: (a,b) background morphology on day 0, (c,d) SDS blooms visible on day 1 during storage at low RH conditions, (e,f) PVA crystals visible on day 1, (g,h) SDS blooms visible in limited positions on day 2 at elevated temperature conditions.

SDS in plasticised 99PVA matrices created structures with a range of morphologies (Figure 6.3), with background regions between SDS blooms exhibiting similar morphology to the plasticised control composition from day 0 ( $R_q=0.4$  nm). Micron-scale pictures collected using the microscope connected with AFM (not shown here, for brevity) indicated that the size of SDS blooms did not change during aging for either the elevated temperature or low RH conditions.

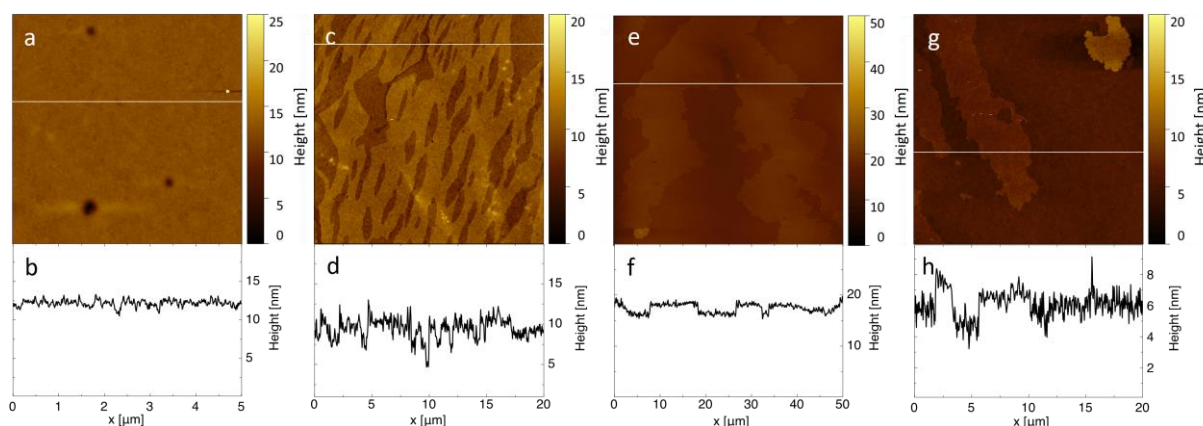


**Figure 6.3.** Morphology and height profile of plasticised 99PVA film containing 1 wt% SDS stored at elevated temperature on day 0: (a,b) background film morphology, (c,d,e,f) SDS blooms, (g,h) large SDS blooms.

### 6.3.3. Cationic surfactant formulations

Similar to compositions with SDS, 87PVA-based formulations doped with CTAB did not exhibit morphological differences in background polymer structure nor changes in  $R_q$  (0.5 nm and 0.6 nm for day 0 and day 14, respectively) compared to control samples (Figure 6.1a,b, Figure 6.4a,b). However, single small crystals were formed (Figure 6.4e,f), with similar morphology to those reported after aging at ambient conditions (Figure 6.4c,d and Figure 5.2e,f) and increasing size with increasing RH at ambient temperature. No crystals were observed for elevated temperature aging as system is above  $T_k$  of CTAB.

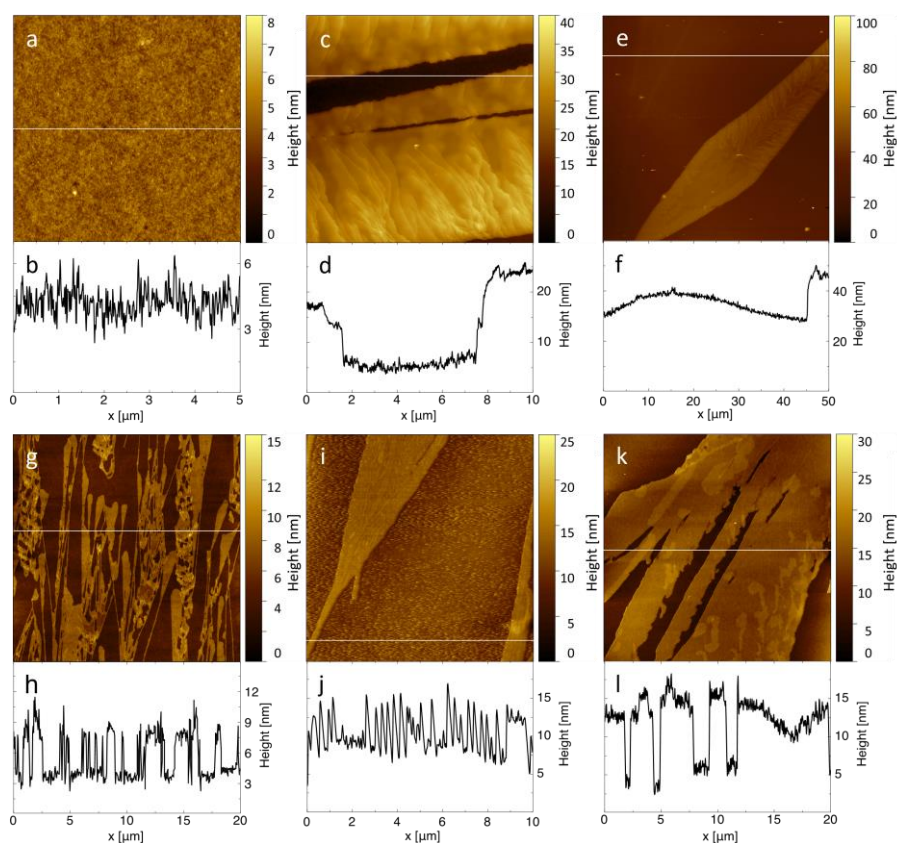


**Figure 6.4.** Morphology and height profile of plasticised 87PVA films containing 5 wt% CTAB: **(a,b)** film morphology on day 0, **(c,d)** CTAB blooms after storage at ambient temperature and RH on day 7, **(e,f)** small CTAB blooms for sample stored at low RH on day 7; plasticised 99PVA films stored at elevated temperature on day 0: **(g,h)** typical large crystal structures on a sample containing 3 wt% CTAB, **(i,j)** glycerol structures visible for a sample containing 3 wt% CTAB, **(k,l)** crystals on a sample containing 5 wt% CTAB.

Compositions based on 99PVA showed large crystals uniformly covering the sample surface on day 0 (Figure 6.4k,l). These large blooms remained visible when formulations with

only 3 wt% CTAB were prepared (Figure 6.4g,h), proving the lower surfactant compatibility with 99PVA compared to 87PVA. Furthermore, imaging was challenging for 99PVA formulations because of glycerol presence on the film surface (Figure 6.4i,j), with imaging only becoming possible after 3 days of sample storage. It is therefore hypothesised that cationic CTAB changes the intermolecular interactions present in the system, leading to an increased glycerol surface concentration, which is likely to further evolve during aging (Chapter 5).<sup>363</sup> After equilibration, regions without blooms exhibited similar morphology to plasticised PVA:  $R_q=0.6$  nm to 0.9 nm for 5 wt% CTAB addition on day 0 and 14, respectively; and  $R_q=0.6$  nm to 0.7 nm for 3 wt% CTAB addition on day 0 and 14, respectively.

#### 6.3.4. Nonionic surfactant formulations

The addition of  $C_{12}E_{10}$  at high concentrations (10 or 20 wt%) led to morphology changes in both 87PVA and 99PVA-based formulations. For 87PVA, background polymer morphology became less uniform compared to samples with no surfactant:  $R_q$  was between 0.4 nm and 0.9 nm on day 0, and larger surface features were observed (Figure 6.5a-d). At 10 wt% surfactant concentration, no morphology changes were observed upon aging at any investigated conditions. Conversely, surfactant blooms with a characteristic chequerboard pattern (Figure 6.5i-n) appeared in 20 wt%  $C_{12}E_{10}$  samples after 2 weeks of aging. These structures did not appear at elevated temperature conditions (Figure 6.5e-h) but were observed for samples aged at ambient conditions after 3 to 7 days. Generally, spin-coated films containing  $C_{12}E_{10}$  were less uniform compared to other surfactants – likely due to the higher concentration of nonionic surfactant in the film, lower viscosity of the solution and possible inhomogeneity in the solution prior to spin coating.

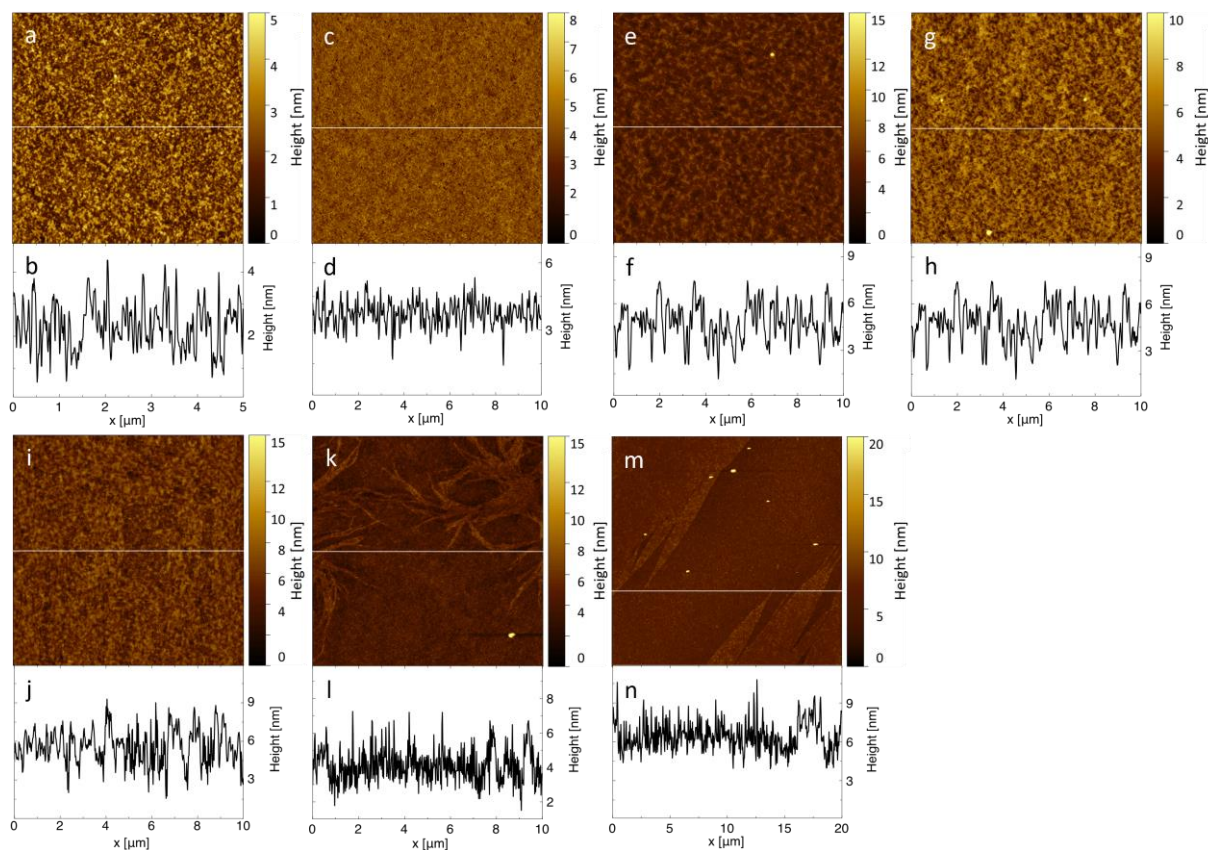


**Figure 6.5.** Morphology and height profile of plasticised 87PVA films containing  $C_{12}E_{10}$ : (a,b,c,d) film morphology on day 0 at 10 wt% surfactant, (e,f) film morphology on day 0 and (g,h) day 14 at 20 wt% surfactant, aged at elevated temperature; (i,j,k,l,m,n)  $C_{12}E_{10}$  blooms created in films at 20 wt% surfactant stored at ambient conditions on day 14.

As expected from the discussed morphology changes upon addition of ionic surfactants, more surface nonuniformities were visible for  $C_{12}E_{10}$ -doped samples of 99PVA compared to 87PVA. Glycerol was observed either in the form of a uniformly distributed surface excess or as concentrated glycerol mesophases (Figure 6.6c-f), in line with behaviour observed for systems doped with cationic surfactant. As glycerol surface concentration changed during sample aging, the size and amount of regions rich in glycerol blooms observed under optical microscope decreased over time. While glycerol-associated morphological features were visible in optical microscope images, no blooms of surfactant were observed while aging films at elevated temperature, showing lack of  $C_{12}E_{10}$  surface excess. Depressions (characteristic of glycerol or surfactant phase separation, Figure 6.6a,b) were also noted, both in AFM images



and optical microscope images for freshly prepared samples containing 10 wt% surfactant ( $R_q=1.2$  nm).

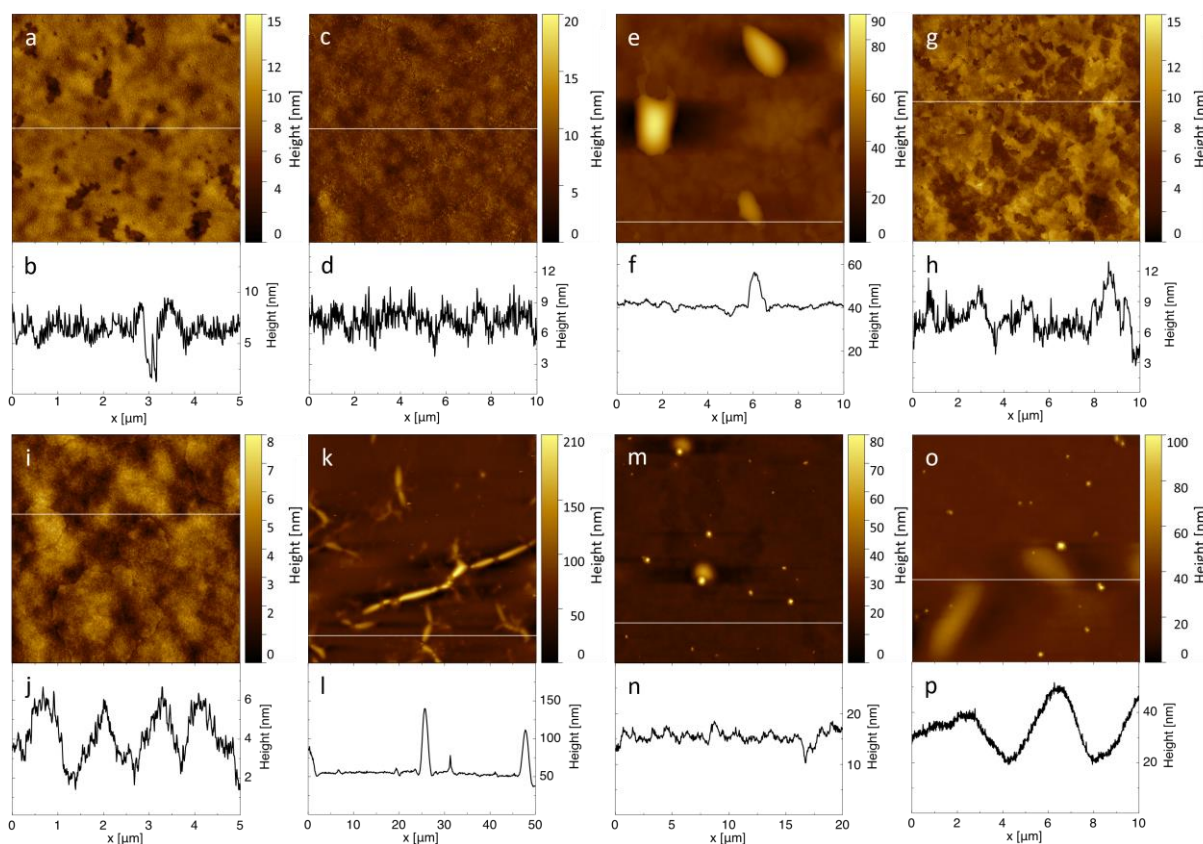


**Figure 6.6.** Morphology and height profile of plasticised 99PVA films containing 10 wt%  $C_{12}E_{10}$ : (a,b,c,d) surface nonuniformities visible on day 0, (e,f) glycerol aggregates observed on day 3 aged at elevated temperature. Samples containing 20 wt%  $C_{12}E_{10}$ : (g,h,i,j) surface morphology on day 0, (k,l,m,n) surface irregularities on day 3 and 9, respectively, and (o,p) surfactant blooms on day 14 aged at elevated temperature.

For 99PVA samples, changes in morphology upon addition of 20 wt%  $C_{12}E_{10}$  were observed from day 0 onwards (Figure 6.6g,h and Figure 6.6i,j,  $R_q=1.8$  nm and 1.0 nm, respectively). Similar to samples with 10 wt%  $C_{12}E_{10}$ , glycerol was visible on the surface both in the background polymer morphology and in aggregates due to phase separation in the system (surface profile lines in Figure 6.7e-h). At ambient temperatures and low RH, glycerol was also detected on the surface after 2 weeks of aging (indicated by difficulties in imaging because of glycerol viscosity). Among all investigated compositions doped with surfactants, 99PVA with 20 wt%  $C_{12}E_{10}$  showed the highest variation in morphology immediately after spin coating (e.g.

Figure 6.6m,n). This is presumed to be a result of phase separation either before or during the spin coating process, as the concentration of surfactant was so high that each aliquot of stock solution was unlikely to be homogeneous.

99PVA samples were the only investigated compositions to show dependence on temperature conditions during storage. With increased temperature, no blooming – either chequerboard pattern regions or crystal-like structures as in Figure 6.5k,l or Figure 6.7a-d – were visible. Instead, lamella-like structures of elevated height were observed (Figure 6.6k,l and Figure 6.6o,p), covering a significant portion of the film as confirmed by optical microscopy. Meanwhile, storage at ambient temperatures and low RH resulted in creation of crystal-like, chequerboard pattern structures with (Figure 6.7o,p) or without (Figure 6.7i-m) concurrent glycerol blooms.

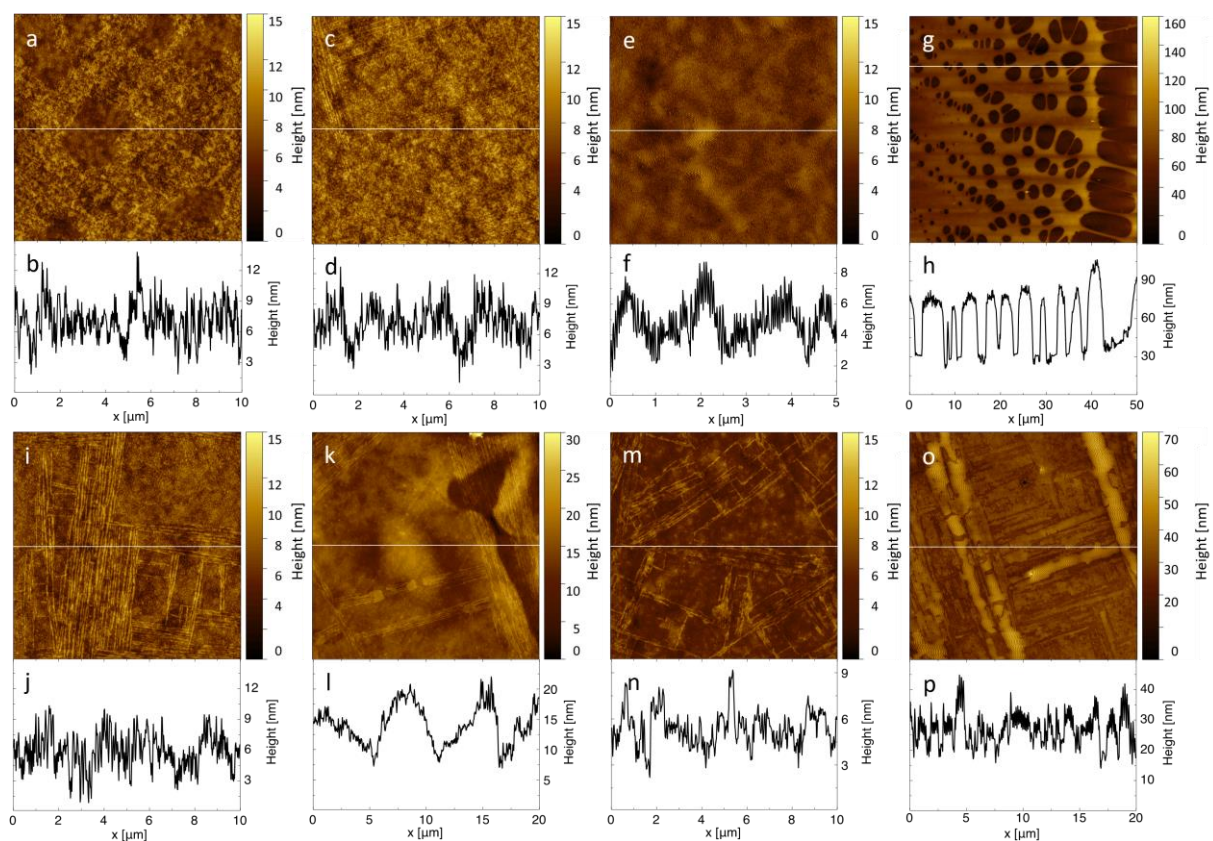


**Figure 6.7.** Morphology and height profile of plasticised 99PVA films containing 10 wt%  $C_{12}E_{10}$  stored at low RH conditions: (a,b,c,d) surfactant blooms visible on the surface on day 3. Samples containing 20 wt%  $C_{12}E_{10}$ : (e,f,g,h) film morphology with surface glycerol blooms on day 7, (i,j,k,l,m,n,o,p),  $C_{12}E_{10}$  blooms on day 7.

## 6.4. Binary surfactant mixtures

As has been demonstrated with glycerol and individual surfactants, interactions between additives in PVA-based formulations have a significant impact on film behaviour upon aging. As real-world industrial formulations commonly contain multiple surfactants, films containing binary surfactant mixtures were synthesised and aged to investigate how surfactant-surfactant interactions affect aging and morphology. Given that 99PVA films showed little aging effect regardless of the head group chemistry of the added surfactant, only 87PVA formulations were investigated, with the added benefit of being more broadly used in industry. Formulations were prepared by mixing surfactants in the aforementioned concentrations (i.e. 1 wt%, 5 wt% and 10 wt% for anionic, cationic, and nonionic surfactants, respectively), leading to three surfactant combinations, which were tested in turn.

### 6.4.1. CTAB + C<sub>12</sub>E<sub>10</sub> system

Presence of both cationic and nonionic surfactant did not lead to changes in background polymer morphology (regions between the surface features in Figure 6.8). While single crystals characteristic to the cationic surfactant formulations were visible, they appeared only in the neighbourhood of scratches made for thickness measurement. It is hypothesised that the act of scratching creates a heterogeneous nucleation centre for CTAB crystals, indicating that the system is in a metastable state, with nonionic surfactant preventing spontaneous CTAB crystallisation. For some compositions, small depressions like blisters<sup>393</sup> were observed (Figure 6.8a,b) that were also seen in formulations with the addition of only cationic surfactant at 5 wt% (not shown here, for brevity).

No changes were observed upon aging at ambient temperature and low RH. However, for samples stored at elevated temperatures small features appeared on the surface (Figure



6.8e,f), that were visibly similar to nonionic surfactant structures created at elevated temperature (Figure 6.6k-p) as creation of smaller CTAB crystals is unlikely for a system significantly above its  $T_k$ .

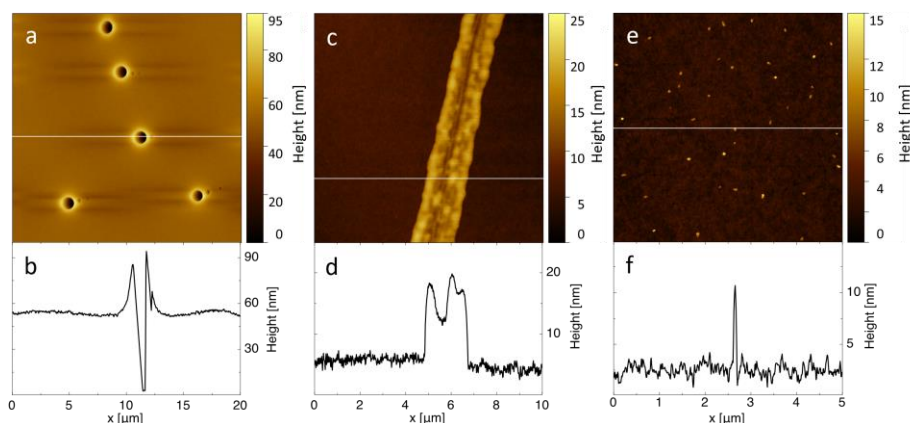


**Figure 6.8.** Morphology and height profile of plasticised 87PVA films containing 5 wt% CTAB and 10 wt%  $C_{12}E_{10}$ : (a,b) depressions on sample stored at ambient conditions on day 3, (c,d) CTAB crystal created around the scratch on day 3, (e,f) surface features for sample stored at elevated temperature on day 7.

#### 6.4.2. SDS + $C_{12}E_{10}$ system

Samples with SDS and  $C_{12}E_{10}$  showed greater changes with environmental conditions compared to the cationic/nonionic surfactant composition. Film morphology was very variable for these samples: large SDS blooms were visible on day 0 in one sample (out of three prepared, Figure 6.9a,b), indicating inhomogeneities in the stock solutions, similar to the 99PVA with  $C_{12}E_{10}$  system. As with CTAB/ $C_{12}E_{10}$  samples, this formulation seemed to be sensitive to heterogeneous nucleation, as blooms (likely corresponding to  $C_{12}E_{10}$ ) appeared only on one investigated film close to a scratch made by tweezers (Figure 6.9c,d).

SDS blooming upon aging was visible in all investigated conditions, however, with the bloom morphology dependent on the storage temperature and RH. At low RH and ambient temperature, SDS blooms were uniformly distributed on the whole sample (Figure 6.9i,j), with significantly smaller size than those reported on day 7 in samples doped with SDS only (ca. 100 nm vs 500 nm, respectively). For aging at ambient temperature and RH, these blooms were

larger (ca. 200 nm, Figure 6.9e,f) but scattered unevenly on the surface. Blooms observed at elevated temperature conditions were distributed evenly across the surface, with similar morphology to these observed for aging in ambient RH (Figure 6.9g,h), however, their size (ca. 100 nm) seemed to be diminished by elevated temperature conditions.

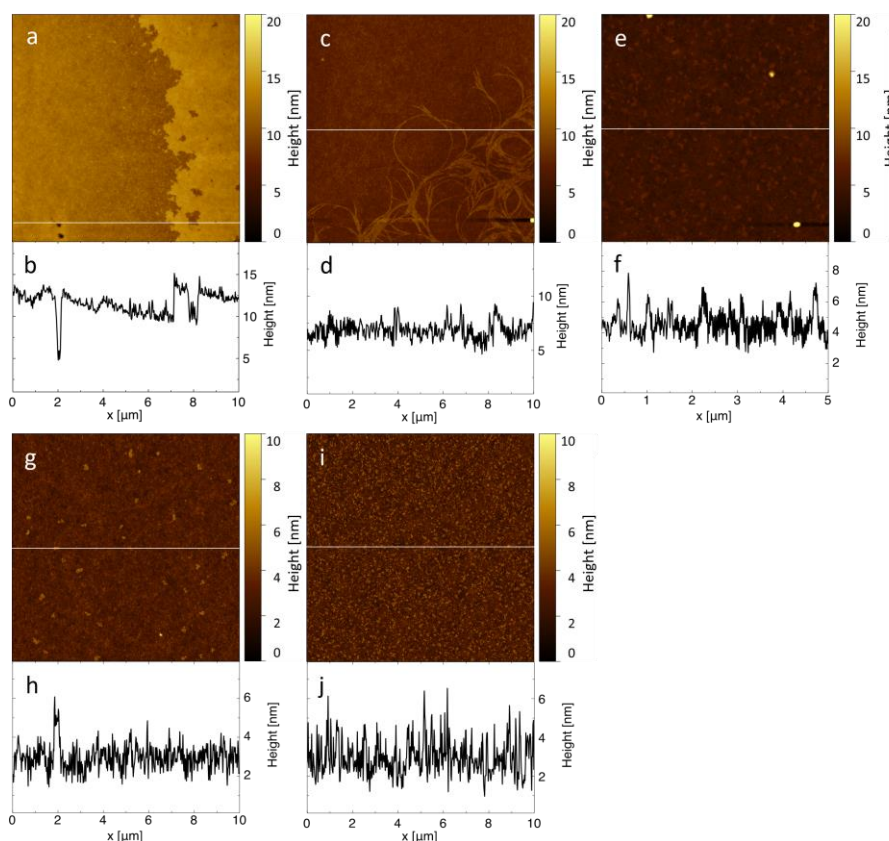


**Figure 6.9.** Morphology and height profile of plasticised 87PVA films containing 1 wt% SDS and 10 wt%  $C_{12}E_{10}$ : (a,b) SDS blooms on day 0, (c,d) blooms created on day 3; SDS blooms on the sample stored at: (e,f) ambient conditions, day 7; (g,h) elevated temperature, day 7; (i,j) low RH conditions, day 7.

### 6.4.3. SDS + CTAB system

Despite having the highest thickness among samples containing two surfactants (Table 6.1), the composition containing cationic/anionic surfactant showed strong intermolecular interactions even prior to film preparation (turbid stock solution compared to transparent for all other formulations). After spin coating, these films showed the most significant variations compared to both other mixed surfactant formulations and even single surfactant formulations

(Figure 6.10). From day 0 onwards, characteristic depressions and blooms were visible (Figure 6.10a-d), with depressions likely connected with CTAB presence and blooms related to SDS presence (Chapter 5, Figure 5.2 and Figure 5.3). In these samples, depressions exhibited different morphology compared to plasticised PVA sample doped with only CTAB at concentrations higher or equal to 3 wt% (flower-like compared to round shape reported here), likely due to additional interactions with SDS that altered the self-assembly behaviour of both surfactants. These interactions also led to creation of intermediate morphologies (blooms within the depressions, Figure 6.10c,d).

The morphology of cationic samples showed dependence on the aging conditions. Crystal creation, correlated with CTAB due to the similar morphology to the single surfactant system, was observed for samples stored at ambient temperature (Figure 6.10e,f). Moreover, small crystals (Figure 6.10g,h) were created in low RH conditions as opposed to samples aged in elevated temperature, where no crystallisation was observed.

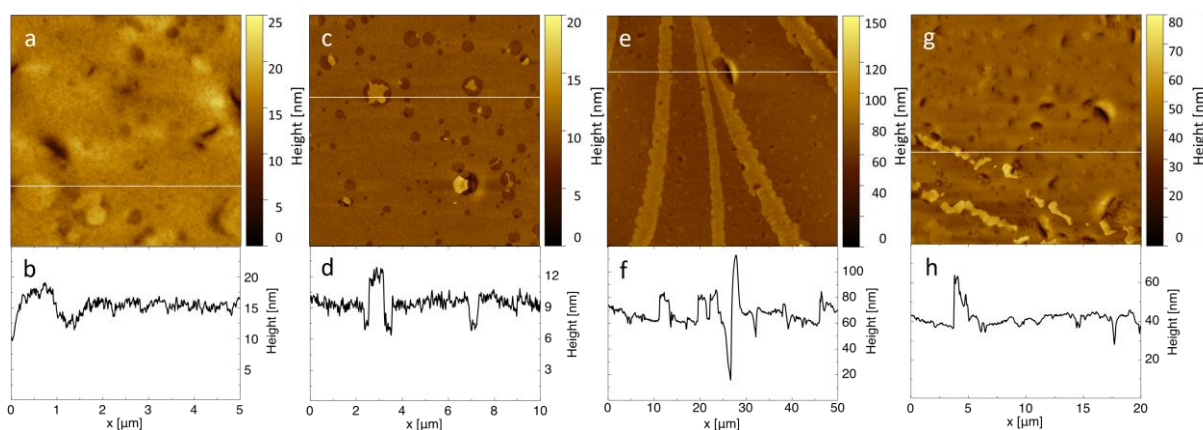


**Figure 6.10.** Morphology and height profile of plasticised 87PVA films containing 5 wt% CTAB and 1 wt% SDS: (a,b,c,d) film morphology on day 0, (e,f) CTAB crystal structures on day 3 for sample stored at ambient conditions and (g,h) low RH conditions.

## 6.5. Chemical characteristics of the films

CFM measurements were taken using two types of chemically modified cantilevers (a hydrophilic acid-terminated and hydrophobic methyl-terminated cantilever, as in Chapter 5)

to quantitatively compare the chemical character of the films and establish surfactant arrangement within the polymer matrix. Like AFM measurements, CFM was performed on plasticised PVA samples as a control, as well as on the background region and blooms/crystals (if present) for formulations with one or two surfactants. Measurements were taken on day 0 and day 7 for samples aged in ambient conditions, as these conditions caused the most substantial morphology differences during AFM imaging. Complementary contact mode imaging (friction channel) was carried out on the areas with surfactant blooms to confirm adhesion results. In all cases, conclusions from imaging were consistent with those obtained from adhesion measurements.

On day 0, the plasticised 99PVA control sample showed on average weaker adhesion for acid-terminated cantilevers compared to the 87PVA control, with no significant differences between values of adhesion for methyl-terminated cantilevers –  $7.0 \pm 0.3$  and  $6.4 \pm 0.4$  nN, respectively for 99PVA, (Figure 6.11), and  $8.7 \pm 1.2$  and  $6.7 \pm 0.6$  nN for 87PVA (Figure 5.5). These results are unexpected as plasticised 99PVA had a higher SFE compared to 87PVA (Table 6.1) correlated with higher hydrophilicity. However, for all control samples, adhesion became weaker after 1 week of aging – dropping to  $6.4 \pm 0.7$  and  $4.6 \pm 0.8$  nN for 99PVA, as well as  $6.6 \pm 0.7$  and  $5.5 \pm 0.3$  nN for 87PVA (acid- and methyl-terminated cantilevers, respectively).

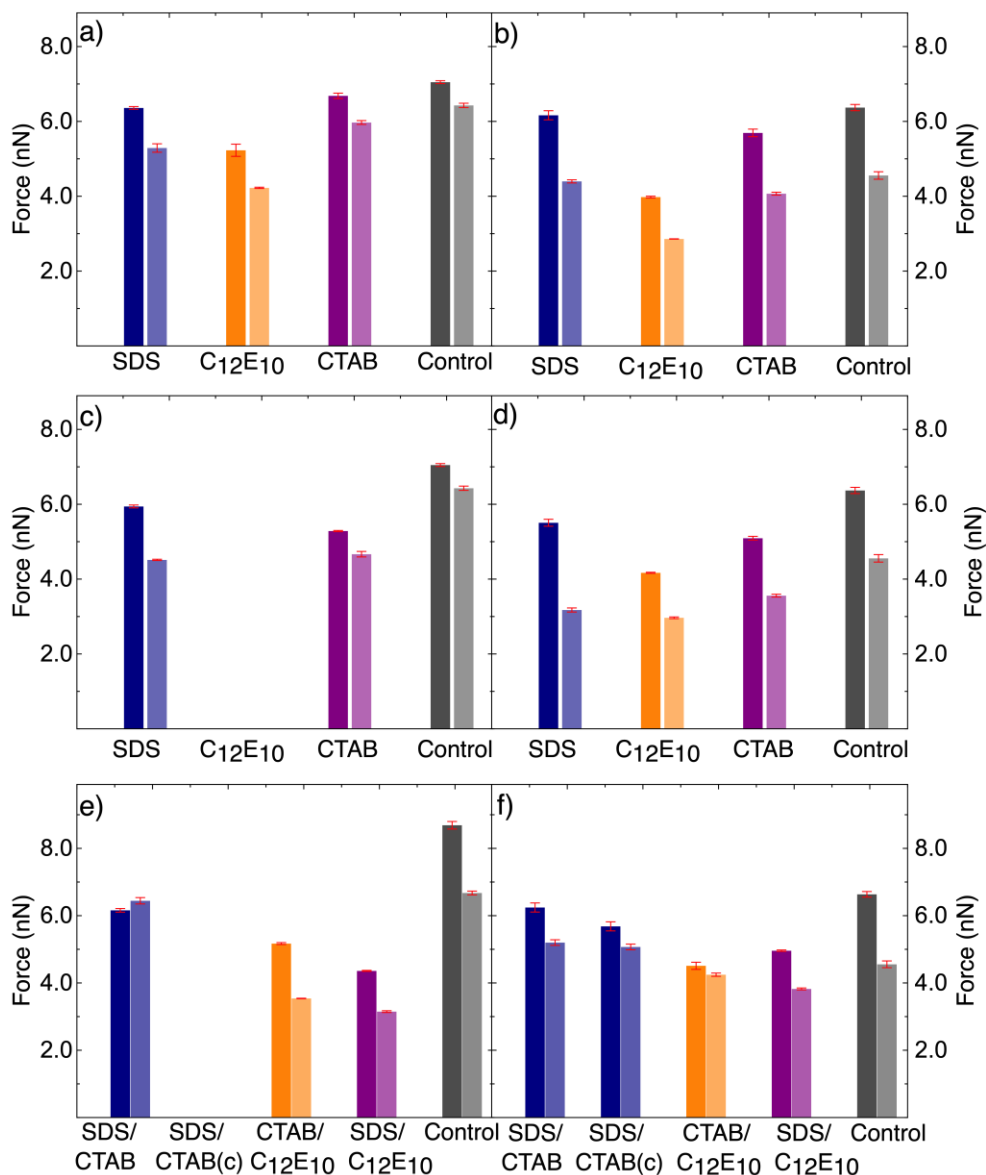


**Figure 6.11.** AFM force curve measurements on samples prepared with 99PVA: **(a)** areas without surfactant blooms, day 0; **(b)** areas without surfactant blooms, day 7; **(c)** surfactant blooms/crystals, day 0; **(d)** surfactant blooms/crystals, day 7; 87PVA with two surfactants: **(e)** day 0, **(f)** day 7.

The overall lower adhesion values for acid-terminated cantilever on 99PVA compared to its lower DH counterpart on day 0 are suggested to be a consequence of different surface glycerol concentration for these formulations – as 87PVA has a lower  $M_w$ , the free volume associated with the polymer chain ends will be higher, therefore creating more free volume to be occupied by glycerol. The almost identical values of adhesion for acid-terminated cantilever for both PVA types after 1 week of sample storage suggests that decrease in glycerol surface

concentration is responsible for this discrepancy in aging behaviour. The smaller change in adhesion over the aging period for samples of 99PVA compared to 87PVA is speculated to be a consequence of higher number of -OH groups on the former, hence changes in glycerol concentration on the surface will have less significant influence on adhesion value. Alternatively, there may be a different evaporation mechanism of the plasticiser from the film – higher chain entanglement in the 99PVA compared to lower  $M_w$  87PVA films may lead to diffusion-controlled glycerol evaporation behaviour and consequent smaller changes in adhesion values, while plasticiser loss would be expected to be evaporation-controlled in the 87PVA films.

Lower adhesion values with the methyl-terminated cantilever are expected for the 99PVA compared to 87PVA due to the lower amount of acetate groups in the polymer chain. However, values were the same for freshly prepared samples and only different after 1 week of aging (adhesion reducing on average 1.8 nN for 99PVA and 1.1 nN for 87PVA), highlighting the role of glycerol in capillary formation.

### **6.5.1. Single surfactant systems**

Upon addition of surfactants of various head group chemistry to the system, the overall trend of adhesion changes for 99PVA-based system compared to 87PVA-based system was very similar: lower values of adhesion were recorded both on background regions and crystallites/bloom regions compared to control samples (Chapter 5). Background regions of samples doped with CTAB showed the least significant changes compared to plasticised 99PVA films (from 7.05 and 6.37 nN on day 0 to 6.68 and 5.69 nN on day 7 for acid- and methyl-terminated cantilevers, respectively, Figure 6.11). The most substantial changes, as with changes in film morphology, were noted for  $C_{12}E_{10}$ -doped samples, likely due to the overall

high surfactant concentration within the system. Because of this similarity in changes seen for both PVA-based systems, it is suggested that molecular arrangement of the surfactant in the system is as follows:

- SDS: lamellar blooms with hydrophobic tails exposed to ambient atmosphere.
- CTAB: crystal structures with hydrophobic tail exposed to the ambient atmosphere.
- $C_{12}E_{10}$ : surfactant wetting layer with hydrocarbon tail exposed to the atmosphere.

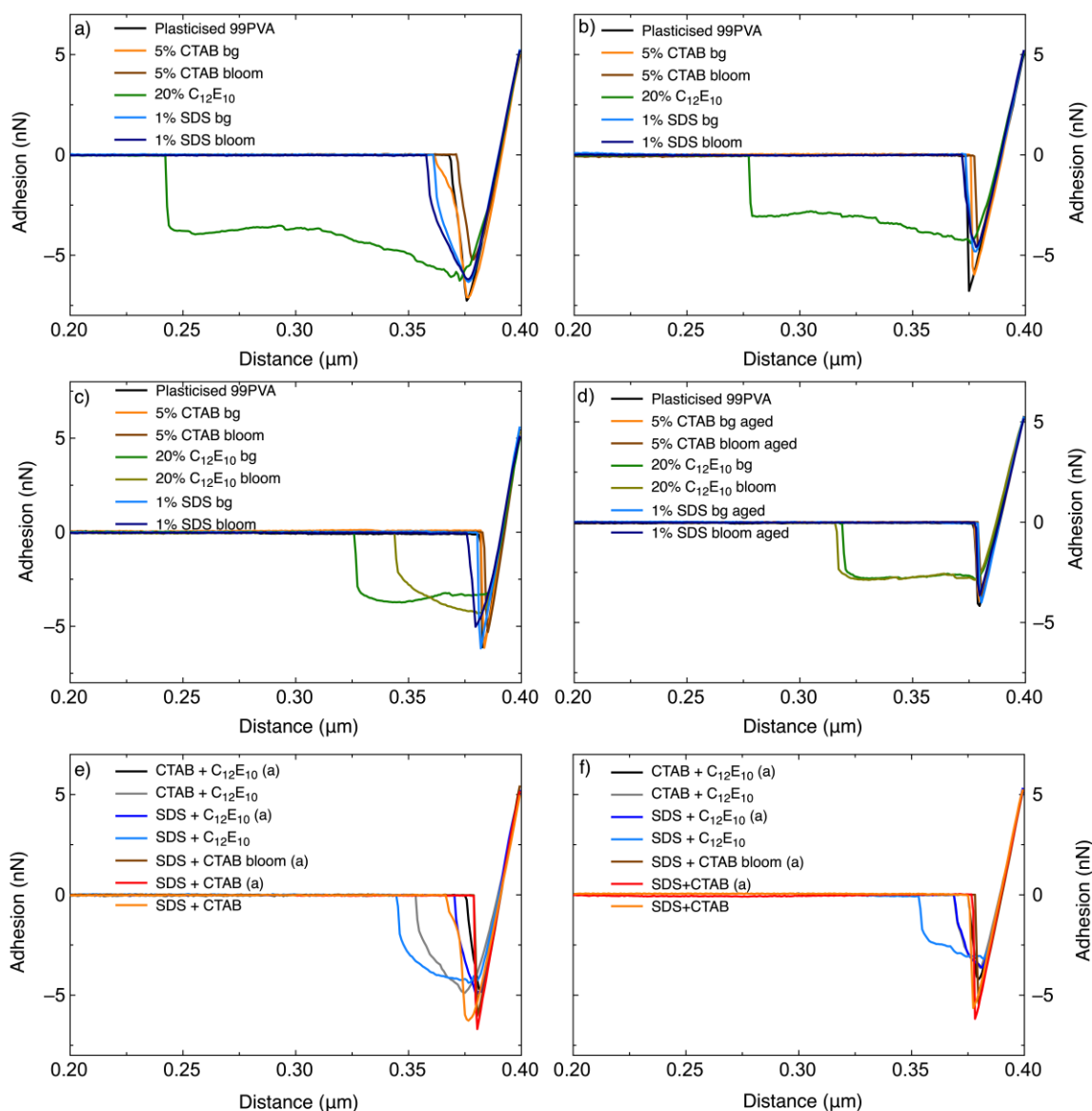


**Figure 6.12.** Representative force curves for: **(a,c)** acid-terminated cantilever, measurements on plasticised 99PVA samples on day 0 and day 7, respectively; **(b,d)** methyl-terminated cantilever, measurements on plasticised 99PVA samples on day 0 and day 7, respectively; **(e,f)** acid- and methyl-terminated cantilever 87PVA on samples doped with two surfactants.

Increased rupture distance was visible in all surfactant-doped compositions for acid-terminated cantilevers on day 0 and on SDS blooms for methyl-terminated cantilever, also on day 0 (Figure 6.12). However, these differences appeared only slight when compared against the changes introduced by nonionic surfactants. The rupture distance has been shown to decrease with sample aging, possibly due changes in glycerol and C<sub>12</sub>E<sub>10</sub> concentration on the film surface. Surfactant evaporation was previously demonstrated in the literature for C<sub>12</sub>E<sub>5</sub><sup>122,181</sup> and other additives<sup>394</sup> and while C<sub>12</sub>E<sub>10</sub> is a longer molecule, this behaviour is still likely to occur.

### 6.5.2. Binary surfactant systems

The behaviour of 87PVA-based formulations doped with two surfactants was significantly different depending on the specific surfactant pair used. Nonionic surfactant presence on the surface could not be directly concluded from sample morphologies as the background polymer morphology was similar to that of plasticised polymer sample in regions without blooming. However, the adhesion values for both acid- and methyl-terminated cantilevers (Figure 6.11) confirm C<sub>12</sub>E<sub>10</sub> presence on the surface. Accordingly, similar adhesion values to samples doped only with nonionic surfactant were measured, especially after 7 days aging: with an acid-terminated cantilever adhesion increased from 4.12 to 4.51 and 4.95 nN for sample doped with C<sub>12</sub>E<sub>10</sub> only, CTAB+C<sub>12</sub>E<sub>10</sub> and SDS+C<sub>12</sub>E<sub>10</sub> sample, respectively; while for a methyl-terminated cantilever, values rose from 2.96 to 4.24 and 3.83 nN in the corresponding samples.

Comparison of only adhesion values does not fully describe changes in the system, however; all formulations containing nonionic surfactant showed increased rupture distance in the force curves confirming its presence (Figure 6.12e,f). After one week of aging this distance was vastly decreased, with the shape of the force curves closer to those seen in films with anionic



or cationic surfactant only. These changes can be explained by two possible scenarios. Firstly, presence of a second surfactant results in nonionic surfactant excess immediately after spin coating, resulting in nonionic surfactants being kinetically trapped on the surface; with aging, C<sub>12</sub>E<sub>10</sub> migrates into the bulk of the film to minimise surface energy of the system. Alternatively, C<sub>12</sub>E<sub>10</sub> evaporates from the surfaces as a consequence of ambient aging, similarly to glycerol in the control films.<sup>181</sup>

The dynamic character of changes in binary surfactant systems can be also confirmed by looking at the changes in the SFE values in these formulations (Table 6.1). On day 0, SFE decreased in order: no surfactant < SDS+CTAB < C<sub>12</sub>E<sub>10</sub>+SDS < C<sub>12</sub>E<sub>10</sub>+CTAB. After 1 week of aging, however, the order became no surfactant < CTAB+C<sub>12</sub>E<sub>10</sub> < C<sub>12</sub>E<sub>10</sub>+SDS < SDS+CTAB, with absolute SFE values significantly increasing only for the SDS+CTAB formulations. Unique adhesion behaviour was also visible in SDS+CTAB sample as acid-terminated cantilever measurements recorded constant values between days 0 and 7 (6.16 vs 6.24 nN on average, respectively). In contrast, a decrease was noted for methyl-terminated cantilever (6.44 vs 5.20 nN on average, respectively) – similar to that of control samples and formulations doped with only one surfactant. These changes indicate equilibration upon aging and were not as heavily influenced by changes in glycerol concentration on the film surface as the previously discussed formulations.

### 6.5.2.1. SDS + CTAB system

In Section 6.4.3, three different characteristic surface features were identified: crystals, depressions, and intermediate morphologies (blooms within the depressions). Similar adhesion values were recorded on crystals compared to samples doped with CTAB only (Figure 5.5, Chapter 5), suggesting that these surface features were created by CTAB molecules with little

to no contribution from the SDS. By contrast, formation of depressions is connected with increased hydrophilic character of these areas compared to the background structures, evidenced by insubstantial changes for methyl-terminated cantilever compared to the background and increased friction for the acid-terminated cantilever (Figure 6.13).

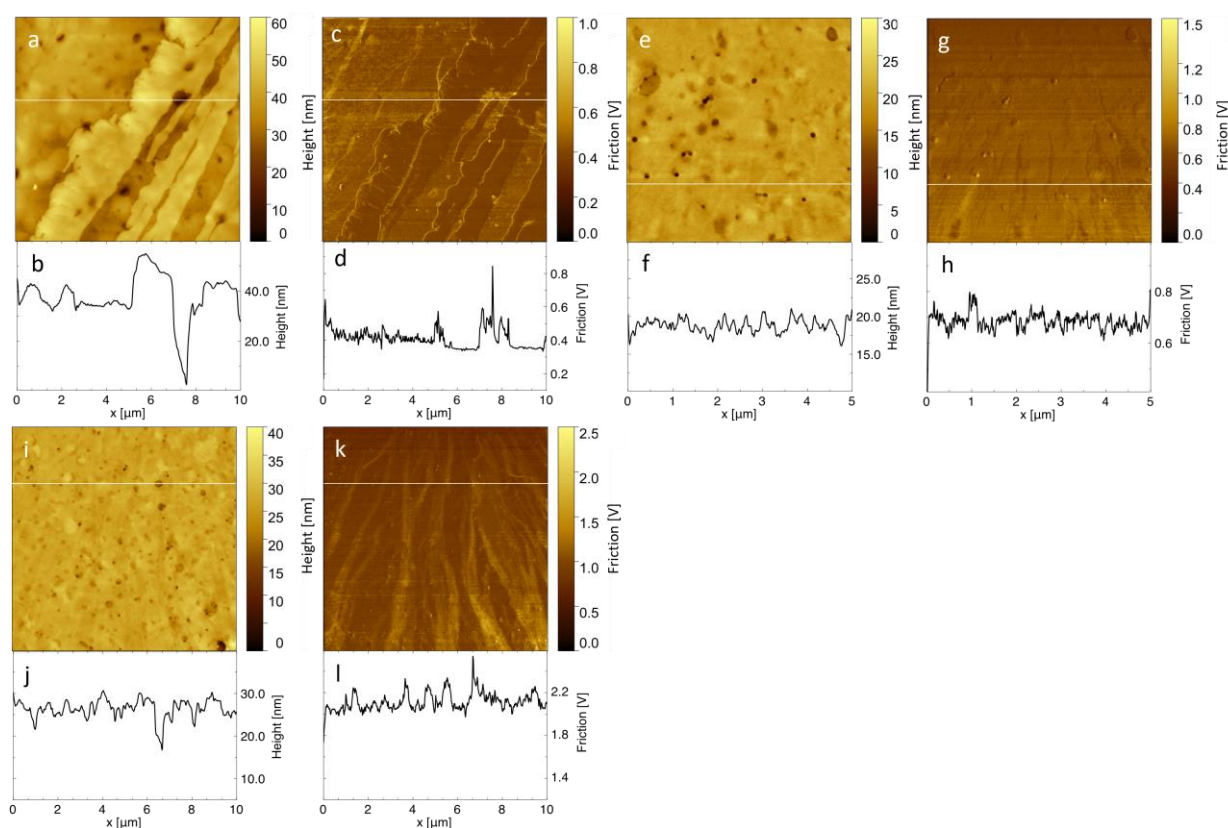


**Figure 6.13.** (a,e) Height and (c,g) friction channels for SDS+CTAB samples for acid-terminated cantilever with corresponding profiles; (i,k) height and friction channels, respectively, for SDS+CTAB samples for methyl-terminated cantilever with corresponding profiles.

While depressions were previously observed in pure CTAB systems, these were very rare within the films and exhibited a pronounced flower-like morphology (Figure 5.2a,b, Chapter 5). In this mixed-surfactant system, these depressions were both significantly more common and with a smaller, circular shape. It is posited that these differences are due to catanionic mesophase formation as described by Tah et al.,<sup>395</sup> with head groups exposed to the thin layer of water covering the film.<sup>196</sup> Finally, CTAB creates crystal-like structures that could

not be directly recognised from height channel analysis only but were clearly distinguished in the friction channel (Figure 6.13). These dendritic structures seemed to have molecular arrangement like CTAB crystals (tail-up), however did not form crystals. Because of the solution behaviour of this sample – becoming turbid after mixing the two surfactants – and creation of crystals on limited areas for SDS+CTAB formulations, SDS does not seem to reduce  $T_k$  of CTAB significantly. Instead, SDS seems to promote CTAB surface segregation, while CTAB discourages surface segregation – i.e. blooming – of SDS.<sup>122</sup>

#### **6.5.2.2. SDS + C<sub>12</sub>E<sub>10</sub> system**

Insignificant SFE differences were recorded for aged SDS+C<sub>12</sub>E<sub>10</sub> samples compared to their freshly prepared counterparts. Increased adhesion with aging was recorded with both acid- and methyl-terminated cantilevers: from 4.4±0.1 to 5.0±0.2 nN for the acid-terminated cantilever; and 3.1±0.2 to 3.8±0.2 nN for the methyl-terminated cantilever, respectively. These results are likely to be a consequence of SDS diffusion to the surface upon aging and concurrent C<sub>12</sub>E<sub>10</sub> migration into the bulk or evaporation<sup>122</sup> (as can be seen from the changed force curve shape, Figure 6.12). Similar to the samples doped with SDS only, adhesion values and morphology changes suggest a tail-up conformation of SDS, while the C<sub>12</sub>E<sub>10</sub> backbone is exposed to the atmosphere (i.e. a surfactant wetting layer). It was proven that in mixed surfactant systems, distribution of glycerol tends to be connected with distribution of SDS in the system due to interaction of these two additives.<sup>181</sup> Combined, the effects of surfactant migration, preferential distribution of glycerol, and possible evaporation of both plasticiser and nonionic surfactant led to the observed differences in adhesion values for both acid- and methyl-terminated cantilever.

### 6.5.2.3. CTAB + C<sub>12</sub>E<sub>10</sub> system

Formulations of CTAB and C<sub>12</sub>E<sub>10</sub> are the only binary-surfactant formulations that showed a substantial decrease in SFE while aged in ambient conditions (Table 6.1). Background adhesion for acid-terminated cantilevers also decreased over time (from 5.2±0.03 to 4.5±0.1 nN), which may again be connected with expected changes in glycerol (and possibly C<sub>12</sub>E<sub>10</sub>) concentration on the film surface. However, increasing hydrophobic interactions over time (from 3.5±0.02 to 4.2±0.05 nN) indicated that, despite lack of morphological changes (i.e. CTAB crystals) on the surface, CTAB migrates to the surface with crystal formation only induced by creation of heterogeneous nucleation centres (i.e. film scratching).

## 6.6. Discussion

### 6.6.1. General remarks

Steric effects (e.g. increasing concentration of guest molecules) are crucial when considering changes in the polymer formulations discussed here; it has previously been observed that changes in system packing are more impactful on additive diffusion than changes in  $T_g$ <sup>377</sup> (though these parameters are interconnected). This stands to reason, as strong forces correlated with crowding (i.e. more hydrogen bonding within the PVA matrix) can significantly reduce the motion of guest molecules in the system. Steric effects can be observed by comparing diffusion coefficient of water vapour in the 10-40 °C range between polar and nonpolar polymers.<sup>98</sup> However, the polymer matrix is itself influenced by the increase in temperature: for both plasticised and unplasticised formulations, the cavity radius has been shown to increase up to 110°C, with a small step increase around  $T_g$  (45-65 °C for compositions with up to 10 wt% glycerol). No equivalent transition was observed for samples plasticised with glycerol level

comparable to this study (24 wt%), however. Changes in the cavity radius between plasticised and unplasticised samples with temperature were not visible up to threshold of 65 °C.<sup>51</sup>

For systems investigated here, it is therefore expected that the high glycerol concentrations – like those used in real-world industrial formulations – will increase the flexibility and cavity radius of the PVA. Similar effects are expected upon film aging at elevated temperature<sup>51</sup> as thermal energy disrupts the hydrogen bonding and enlarges the matrix free volume cavities.<sup>11</sup> Despite the similar lubrication effect provided by water ingress and increased temperature, these two phenomena have a very different influence on crystallinity in the system. Water dissolves the crystalline regions leading to overall decreased DC, however introducing thermal energy is expected to increase the film crystallinity.<sup>11</sup>

Considering the influence of crystallinity and intermolecular interactions is important because polar interactions and hydrogen bonding are the dominant forces in PVA-based systems.<sup>98</sup> PVA of higher DH and  $M_w$  creates a matrix of lower cavity radius and higher  $T_g$ <sup>51,181,396</sup> because chain entanglement increases for fully hydrolysed PVA, thus hindering additive migration. As fully hydrolysed polymer chains contain fewer acetate groups, the frequency of hydrogen bonding increases enabling stronger interactions and increased DC.<sup>63,181</sup> PVA of lower DH therefore exhibits higher flexibility in general, as the chain itself and created matrices have more steric obstacles that prevent creation of perfect structures. Accordingly, these differences in polymer behaviour are likely responsible for changes in the behaviour between partially- and fully hydrolysed PVA matrices.

Increased temperature results in overall higher energy of the system, however, it does not necessarily increase additive mobility (measured as the time at which noncompatible surfactant molecules reach the surface) as other factors – e.g. exceeding  $T_g$ , changes in solubility and compatibility – change the dynamics of the system. Although the increased

prominence of entropic effects with increasing temperature may also contribute to the segregation observed in this study,<sup>377</sup> only migration of smaller additives instead of long polymer chains is considered here, therefore compatibility and specific intermolecular interactions seem to be a far more likely explanation for this phenomenon.

## **6.6.2. Effect of aging conditions on migration in single surfactant systems**

### **6.6.2.1. General remarks**

As absolute humidity was similar at the elevated temperature and ambient conditions used, overall differences in water vapour content are not expected to be the main reason for differences in behaviour between these systems. Aging the films at 60 °C instead of ca. 20 °C leads to higher system energy that does not seem to cause morphological changes in most of the systems investigated here. This can be explained by the fact that increased temperature increases the solubility and compatibility of the surfactant in the system, while morphological changes are driven by incompatibility in the system.

Morphological variability between repeated samples was visible in some formulations on day 0, independent from the DH of the PVA (higher/lower number of regions rich in surfactant or glycerol), suggesting that inhomogeneity existed within the stock solutions. After (or during) spin coating, surfactant either quickly achieved equilibrium structure or was kinetically trapped in energetically unfavourable arrangement. Increased temperature of the system and overall higher mobility of the matrix above  $T_g$  allows that equilibrium to be reached more quickly. SDS and C<sub>12</sub>E<sub>5</sub> are known to be very incompatible with PVA,<sup>17,122,295</sup> while CTAB is compatible with unplasticised PVA at the concentrations used in this study. Introducing glycerol to the system, however, changes the overall compatibility of the system,

resulting in higher compatibility of PVA-glycerol- $C_{12}E_5$  system while lowering compatibility for PVA-glycerol-CTAB system.<sup>295</sup>

### 6.6.2.2. Nonionic surfactant formulations

It is expected that due to the higher  $M_w$  of  $C_{12}E_{10}$  compared to  $C_{12}E_5$  it will be less compatible with the polymer matrix and also less energetically favourable to occupy the surface (due to the entropy penalty for higher  $M_w$  molecules to occupy the surface). However, the behaviour of the two  $C_{12}E_x$  surfactants at elevated temperatures is likely to be similar – evaporation from the system in parallel with migration into the bulk of the film due to increased solubility of surfactant in the polymer film.<sup>122</sup> This phenomenon is very different to that of the  $C_{12}E_x$  surfactants in solutions as their solubility decreases with increasing temperature (until reaching  $T_{cp}$ ).<sup>122,126</sup>

For films doped with nonionic surfactant, its presence is visible also in characteristic surfactant structures (Figure 6.6, Figure 6.7) indicating interactions between glycerol and  $C_{12}E_{10}$ . Due to the similarities in the structure of these two components, they may compete for occupation of the available free volume in the matrix. Therefore, as glycerol evaporates and ceases to occupy the matrix free volume, increased migration of surfactant into the bulk will be possible. Although rather unexpected, similar behaviour was previously reported for the slip additive erucamide in linear low-density polyethylene and polyolefin elastomer.<sup>397</sup>

This behaviour is more pronounced at elevated temperature due to the increased volatility of glycerol and any adsorbed water, with a more significant change expected for the latter molecule (due to its lower boiling temperature).<sup>122,181</sup> Accordingly, for systems where glycerol occupies more free volume cavities compared to water, increased thermal stability is observed.<sup>122</sup> Moreover, glycerol has overall higher affinity to PVA with higher DH as acetate

groups do not form hydrogen bonds with glycerol, hence overall migration/evaporation is slower. As a result, changes in the matrix properties are diminished for plasticised 99PVA compared to 87PVA.

### 6.6.2.3. Ionic surfactant formulations

Distribution of SDS at low concentrations for both fully- and partially hydrolysed PVA shows little change with temperature increase, in line with results for significantly higher surfactant concentrations (albeit for much shorter aging times and 87PVA only).<sup>122</sup> As glycerol does not substantially change compatibility in PVA-based films doped with anionic surfactant, changes in its concentration are not expected to lead to significant changes in the arrangement of the system. Instead, temperature increases system compatibility, preventing SDS blooming in partially hydrolysed PVA (as seen in Chapter 5). It should be noted further that these blooms are unlikely to be correlated with  $T_k$  for SDS as it is below any experimental conditions investigated herein (ca. 14 °C).<sup>359,398</sup>

At elevated temperatures, no CTAB crystals are observed on the surface of 87PVA samples, which is expected as temperature of the system is far above  $T_k$  for CTAB (25 °C).<sup>359,360</sup> Presence of cationic surfactant on the surface is not indicated by changes in morphological structure, evidenced by the similar  $R_q$  in control samples. It is therefore suggested that at elevated temperature where crystal formation is not energetically favourable, changes in glycerol concentration restore the equilibrium structure of CTAB uniformly distributed in the polymer matrix for partially hydrolysed PVA.<sup>295</sup> For fully hydrolysed PVA, CTAB and glycerol excess is visible in the form of crystals and nonuniformities that prevent AFM imaging, respectively. Elevated temperature does not decrease CTAB crystal size suggesting that once



nucleation has occurred, increasing film temperature above  $T_k$  does not reverse this process despite increased thermal kinetic energy of the system.

#### **6.6.2.4. Effect of aging conditions on migration in binary surfactant systems**

Formulations doped with two surfactants are more strongly influenced by aging conditions compared to single surfactant formulations. Properties of these systems are dependent on the pair of surfactants used, with the most significantly modified behaviour noted for the anionic-cationic surfactant combination. This is expected to be a result of charge-matching head group interactions – as both of these surfactants have linear hydrophobic tails and similar head group size, the interactions are not reduced by steric effects associated with branching or bulkiness.<sup>399</sup>

#### **SDS + CTAB system**

For the CTAB+SDS formulation, strong interactions are evident prior to film preparation in the form of turbid stock solutions.  $T_k$  generally decreases for binary surfactant solutions compared to single surfactant mixtures as mixed micelle formation is energetically favourable,<sup>400</sup> also leading to lower CMC and reduced concentration required for crystallisation.<sup>401</sup> Here, aggregation was clearly observed, as the stock solution became turbid, however it was impossible to visually determine if the aggregates formed were crystals or micelles. It is possible that, similar to systems where salt is introduced to surfactant solutions,<sup>402,403</sup>  $T_k$  is elevated by the increased ionic strength of the solution (arising from the  $\text{Br}^-$  and  $\text{Na}^+$  counterions).

These favourable interactions are also highlighted on the film surface where depressions, blooms and crystals associated with surfactant were all present, but distinct from features in the

single surfactant systems. In binary surfactant systems, segregation of only one component is usually entropically unfavourable. However, when two components form a surface excess, the entropy of mixing increases while free energy of the system decreases.<sup>122</sup> For the SDS+CTAB system, the surface excess of cationic surfactant is clearly increased, while concentration of SDS probably decreases as fewer surface features correlated with this surfactant are observed. It is likely that surface features consist of mixed micelles stabilised by electrostatic interactions as confirmed by their morphology that varies compared to single surfactant systems.<sup>399</sup>

While some CTAB crystals are visible on the surface during aging at ambient temperature, they are not visible for elevated temperature conditions (again, due to its  $T_k$  value). Friction measurements on these formulations have shown presence of regions rich in surfactant – likely corresponding to CTAB excess – that were not observed for single surfactant formulations, either at ambient temperature or at elevated temperature conditions. Therefore, SDS seems to have a great influence in the CTAB segregation in the system. CTAB, on the other hand, is likely to inhibit segregation of SDS, similar to reports of SDS/zwitterionic DDAO systems.<sup>122</sup> This behaviour may be also connected with glycerol distribution in the system – as plasticiser is likely to be associated to the distribution of anionic surfactant.<sup>122</sup> However, further investigations would be required to confirm if the interactions between SDS and glycerol are suppressed by the presence of CTAB.

### **SDS + C<sub>12</sub>E<sub>10</sub> system**

In systems with nonionic surfactants these strong interactions are not observed, with compatibility appearing as the main driving force for surfactant distribution within the PVA matrix. Changes in SFE and adhesion for acid- and methyl- terminated cantilevers indicate that the tail-up configurations of either SDS or CTAB seen in single-surfactant 87PVA systems is

not affected by the presence of C<sub>12</sub>E<sub>10</sub>. Moreover, changes in surface morphology suggest that segregation of either surfactant is reduced compared to single surfactant formulations – evolution of SDS blooms upon aging is significantly reduced and no chequerboard patterns associated with C<sub>12</sub>E<sub>10</sub> are observed. While glycerol in the system in general increases the compatibility of individual surfactants with PVA, presence of two surfactants seem to make the formulation as a whole more compatible as this conformation is more energetically favourable. For systems with SDS+C<sub>12</sub>E<sub>5</sub>, short storage at elevated temperature conditions lead to C<sub>12</sub>E<sub>5</sub> segregation at both air-film and substrate film interfaces.<sup>17,122,295</sup> Therefore in the systems studied here, glycerol may be outcompeting SDS-C<sub>12</sub>E<sub>10</sub> interactions, and SDS-glycerol stacked micelles are being formed – albeit of a smaller size – as a result of these interactions. This hypothesis is supported by the distribution of SDS blooms with temperature: small, although uniformly distributed blooms are observed for ambient temperature and low RH conditions. Blooms created at ambient temperature and RH are less uniformly distributed but larger compared to elevated temperature conditions – as higher mobility of the molecules in system above  $T_g$  allows faster equilibration, with possible migration of C<sub>12</sub>E<sub>10</sub> into the bulk, similar to behaviour observed in the single surfactant system.

### **CTAB + C<sub>12</sub>E<sub>10</sub> system**

CTAB, as a compatible surfactant with PVA, can promote the compatibility of any other surfactant in the polymer matrix.<sup>122</sup> That is likely the case in the CTAB+C<sub>12</sub>E<sub>10</sub> system studied here. Mixed ionic-nonionic surfactants systems usually exhibit  $T_{cp}$  higher than these of pure nonionic surfactants.<sup>404</sup> Solutions investigated here were transparent, with hydrophobic interactions between surfactants (rather than electrostatic as observed for SDS/CTAB system) playing a main role. Limited segregation of ionic surfactant is observed when present alongside

a nonionic surfactant (CTAB crystals only formed when heterogeneous nucleation centres were present), cf. spontaneous crystallisation in the systems doped with CTAB only. Moreover, no morphology changes are visible in the background polymer morphology on day 0, suggesting improved compatibility between the components and lack of air-film excess of nonionic surfactant or glycerol which leads to substantial morphology changes in the single-surfactant systems. Small structures observed on the film surface correlated with an excess of  $C_{12}E_{10}$  are highlighted after decrease in glycerol concentration on the surface, consequently decreasing system SFE. While entropy penalty for larger molecules (here,  $C_{12}E_{10}$  rather than CTAB or SDS) occupying the surface is higher, compatibility appears to be the most important factor here, leading to surface excess for  $C_{12}E_{10}$ .

At elevated temperatures migration in the CTAB+ $C_{12}E_{10}$  formulation is faster because of higher energy of the system, while at ambient conditions steric effects slow down or prevent this process. Changes in glycerol distribution are expected to significantly influence the dynamics of migration – leading to more pronounced  $C_{12}E_{10}$  surface excess and less pronounced CTAB excess. Therefore,  $C_{12}E_{10}$  migrates towards the surface and CTAB migrates to achieve uniform distribution in the bulk film (Figure 6.11, Figure 6.12). These phenomena highlight the complex and time-dependent nature of interactions in the system, further changed by possible  $C_{12}E_{10}$  evaporation.

To sum up, 3 parameters influence the behaviour of mixed-surfactant systems: surface energy, entropy of mixing, and compatibility of the 4-component system. Surface energies should be considered for the system as a whole, as surface energies of individual components are not additive (although they are capable of suggesting the tendency of given component to segregate).<sup>122</sup> To predict the system behaviour over time, changes of the three identified

parameters should be considered as a function of environmental conditions and changes in film composition.

### 6.7. Conclusions

In PVA-based plasticised films doped with surfactants, system behaviour is influenced by the system chemistry and environmental conditions experienced during aging; accordingly, system non-specific conclusions can be made.

While increased RH facilitates the changes in the polymer matrix and leads to surfactant blooms visible on the surface, elevated temperature for all investigated formulations seems to have the opposite effect, with increased compatibility observed between the elements of the system and decreased surfactant excess present at air-film interface. These changes are correlated with increased flexibility of the system, improved compatibility as a result of increased energy in the system as well as possible changes in crystallinity.

Fully hydrolysed PVA is less compatible with any of the surfactants studied (SDS, C<sub>12</sub>E<sub>10</sub>, and CTAB) compared to 87PVA. Phase separation and surface features connected with surfactant presence were visible from day 0 for 99PVA, caused by more pronounced chain entanglement and hydrogen bonding density compared to 87PVA. For these samples, aging at elevated temperatures did not change the morphology of already formed surfactant blooms/crystals, while the molecular arrangement of the blooms was proven to be the same as for previously investigated formulations of partially hydrolysed PVA.

In films doped with binary surfactant mixtures, for any formulation containing nonionic surfactant, the presence of an ionic surfactant seems to increase the compatibility in the system. In the SDS+CTAB system strong interactions are visible, leading to creation of characteristic surface structures that do not change under any environmental conditions applied. Generally,

CTAB segregation seems to be increased in mixed-surfactant systems, while SDS segregation seems to decrease. For nonionic/ionic surfactant systems, changes upon aging are dependent on environmental conditions, suggesting that temperature minimises the energy of the system and leads to increase in system compatibility.

## Chapter 7. Kinetics of water migration in PVA-based formulations

### 7.1. Introduction

In the manufacturing process of single-dose detergents, a thin water layer is distributed on two PVA-based films followed by pressing together. Due to the hydrophilic nature of PVA, the wetting process leads to partial film dissolution, enabling interdiffusion of polymer chains hence sealing the pouch. Despite the overall simplicity of this procedure, an array of problems can occur due to complicated polymer matrix-water interactions, changes in DC and crystallite size, and possible segregation of additives within the matrix. All these factors can cause product failure either during storage or use (e.g. leading to incomplete dissolution of a capsule), consequently consumer dissatisfaction.

The short time scales associated with the sealing process generate a need to understand polymer wetting mechanism immediately upon contact with a liquid medium, as well as to establish the influence of system chemistry on this phenomenon. The latter has been a significant scientific interest of late. For example, interactions have been probed in humid air to investigate water sorption in the presence<sup>348,405,406</sup> and absence<sup>350</sup> of additives. Moreover, changes in the structure of PVA formulations (i.e. swelling) upon contact with various liquids<sup>349,407–409</sup> as well as solvent (i.e. water<sup>2,7,244</sup> and acetone<sup>244</sup>) migration in pure<sup>2</sup> and modified polymer matrices with fillers<sup>244</sup> and plasticisers<sup>7</sup> was tackled. These studies highlight the importance of the system chemistry on its overall behaviour, albeit providing inconsistent conclusions for the same system.<sup>2,244</sup> Moreover, despite the diversity of systems studied, no information pertaining to the initial polymer/solvent contact can be concluded due to the limitations of the experimental techniques used (e.g. FTIR, Raman spectroscopy, or swelling tests).

By contrast, CA goniometry combined with high speed cameras is an excellent technique to measure initial wetting kinetics on polymer films. Generally understood as a constant value, contact angle for materials soluble in the medium (here – hydrophilic PVA soluble in water) naturally changes over time until an equilibrium is achieved. CA measurements provide information about evolution of contact angle, allowing study of the wetting mechanism – droplet formation, spreading (liquid movement in x,y-direction) and absorption (liquid movement in z-direction) into the system<sup>410,411</sup> as well as changes in wetting upon aging at various RH conditions<sup>412</sup> and enabling calculation of system SFE.

To accelerate the CA evolution of the liquid medium, surfactants can be dissolved in the water. This category of molecules exhibits interesting behaviour in contact with hydrophobic surfaces, showing surfactant-enhanced spreading<sup>229</sup> or even superspreading,<sup>229,413,414</sup> making these molecules desirable additives in cosmetics, detergents, or even during enhanced oil recovery.<sup>414</sup> Surfactants also decrease the surface tension of water (ca. 70 mN/m for pure water by up to 50 mN/m upon surfactant addition)<sup>415</sup> consequently changing the molecular interactions, thermodynamic driving forces,<sup>416</sup> and surface molecular arrangement in the system.<sup>417</sup> Indeed, the complexity of surfactant solution-polymer film interactions are additionally compounded by the fact that there is not always a clear relationship between spreading rate and spreading coefficient.<sup>418</sup> Therefore, theoretical models for spreading usually require many assumptions, making them inappropriate for predicting system behaviour.<sup>415</sup> Moreover, past studies were mainly focused on surfactant enhanced spreading phenomena for hydrophobic films only,<sup>196,413,419</sup> as opposed to the hydrophilic films discussed here.

Findings from lower energy (hydrophobic) substrates cannot be directly translated to higher energy (hydrophilic) substrates due to the additional phenomena present in the system.<sup>415</sup> While investigating wetting of PVA by water, one needs to consider the amount of solvent



already present in the system due to the hydrophilic nature of this polymer. Even before any processing, PVA powder contains ca. 6.5 wt% water at ambient temperature,<sup>11</sup> with water content increasing with increasing RH (Chapter 5). At low concentrations (below ca. 22 wt%),<sup>101</sup> water in polymer films is present in a nonfreezing state. This amount can be further increased in the presence of additives with high affinity to the polymer chain.<sup>100</sup> After exceeding this threshold, water becomes mobile within the matrix and begins to disrupt the intermolecular hydrogen bond network between amorphous and crystalline PVA regions.<sup>101</sup> As water is not present in the region of intact crystallites, the total amount of water in the system is equal to water content in the polymer amorphous region.<sup>101</sup> As a result, overall DC is an important factor when considering dissolution of PVA by water.

Understanding wetting phenomena for various liquid media (water, water with detergent, and non-polar control media) can therefore enable tuning of both the PVA-based films and composition of the solution inside single-dose detergents, improving control over detergent release kinetics and film aging behaviour. This chapter aims to understand how changes in the film composition ( $M_w$  and DH of PVA, addition of plasticiser, change in the storage RH) as well as liquid medium (aqueous solution of surfactants with different head group chemistry above and below CMC, use of non-polar solvent) influence the wetting mechanism of PVA-based films of various thickness (spin-coated films of thickness below 250 nm and solution cast films of thickness above 10  $\mu\text{m}$ ). Changes in thickness, together with mathematical modelling, will help to gain insight into the main mechanism of CA evolution – spreading or absorption. First, established models used to determine wetting mechanism from CA measurements are presented. Then, the influence of system chemistry on wetting behaviour is discussed for both thin and thick films, alongside evaluation of changes in film morphology through AFM measurements. As changes in the film composition are expected to change overall

DC, FTIR measurements were undertaken to study the influence of crystallinity on the polymer wetting behaviour.

## **7.2. Materials and methods**

Solutions of 87PVA and 99PVA (plasticised and unplasticised) as described in Chapter 2 were used to prepare both spin-coated and solution cast films. Investigation into wetting kinetics was performed using a CA goniometer with the following liquid media: water, dodecane, 1% (w/v) solutions of cationic, anionic and nonionic surfactant, and surfactant solutions further diluted below their respective CMCs. The effect of RH was examined by storing freshly prepared films in a desiccator with silica gel (ca. 4% RH), saturated solution of potassium carbonate (ca. 45% RH) or water (100% RH) for one week prior to CA measurements (as described in Chapter 2). CA goniometry was additionally utilised to calculate SFE of investigated formulations.

FTIR was utilised to investigate the DC in PVA-based films, while AFM was used to observe changes to surface morphology with composition, and to measure film thickness (for spin-coated films) following experimental procedure described in Chapter 2. Thickness of solution cast films was determined using a digital micrometer.

## **7.3. Results and discussion**

### **7.3.1. Wetting models**

CA evolution over time is a consequence of the liquid/solid/air interactions which can be deconvoluted into two key phenomena – spreading and absorption. Spreading arises due to variations in energy states of the solid surface, its adsorption behaviour and wetting kinetics, which can be correlated to the droplet shape and structure of the surface. Conversely, absorption

is mainly connected with the surface structure of the solid,<sup>410</sup> its porosity, and free volume. In the case of PVA-based formulations, the hydrophilic nature of the polymer, its dissolution in water and changes in free volume of the material all contribute to absorption.

To account for the concurrent absorption and spreading observed in water-soluble polymers,<sup>230</sup> Farris et al. developed a model using semi-empirical exponential decay akin to the Avrami mechanism of crystallisation kinetics,<sup>420</sup> or equations used to establish the length of a capillary.<sup>421,422</sup> The equation takes the following form:

$$\theta(t) = \theta(0)\exp(kt^n) \quad 7.1$$

where  $\theta(t)$  and  $\theta(0)$  are the contact angles at given time  $t$  and time 0, respectively,  $k$  is the rate of contact angle evolution, and  $n$  is linked to physicochemical phenomena underlying the overall process, describing the fractional values normally attributed to the presence of two or more phenomena that occur simultaneously. Theoretically,  $n=0$  in the case of pure absorption (a constant CA value) and  $n=1$  in the case of pure spreading (exponential decrease in CA). To corroborate the mechanism implied by the value of  $n$ , geometrical analysis of the solvent droplet should be performed:

$$\Delta S_B = (\Delta S_B)_{\text{absorption}} + (\Delta S_B)_{\text{spreading}} \quad 7.2$$

$$(\Delta S_B)_{\text{absorption}} = 3\left[\frac{(V - V_0)}{h} \cdot \left(\frac{1 + \cos\theta}{2 + \cos\theta}\right)\right] \quad 7.3$$

$$(\Delta S_B)_{\text{spreading}} = 3V_0\left[\frac{1}{h} \left(\frac{1 + \cos\theta}{2 + \cos\theta}\right) - \frac{1}{h_0} \cdot \left(\frac{1 + \cos\theta}{2 + \cos\theta}\right)\right] \quad 7.4$$

where  $V$ ,  $V_0$ ,  $h$ , and  $h_0$  are the volume and height of the droplet at time  $t$  and 0, respectively.  $\Delta S_B$  is the area of liquid-solid contact (the basal area). To conclude which phenomenon is predominant, all  $\Delta S_B$  values should be normalised by the initial area,  $S_{B0}$ .

Several further models of CA evolution have been developed, however each contains a set of assumptions making it inappropriate to address the presented research problem. Models

based around first order kinetics<sup>410,411</sup> do not distinguish between the spreading and absorption phenomena, while these using molecular kinetic theory<sup>423</sup> require knowledge of further parameters including the number of adsorption sites per unit area and the frequency of solvent molecular displacement which cannot be determined for the current system. Moreover, while these models can predict CA, they do not explain the mechanism of wetting.

Models have also been developed considering spreading only as a function of time,<sup>424</sup> however these models convolute CA with droplet surface area over time, necessitating numerical solutions only. Further models of CA evolution frequently approximate the rate of spreading according to a power law<sup>416,425,426</sup> or flow processes,<sup>427</sup> which require chemical-specific constants that are unknown in the systems described herein.

In summary, no existing model accurately describes both the physics and hydrodynamics behind the wetting phenomenon<sup>228</sup> – as spreading, absorption, change in the surface structure, slip mechanism, dissolution, and properties of the surface on multiple length-scales (chemical structure, roughness etc.) may all need to be included. Accordingly, assumptions around the spreading rate and contact angle are made even for more detailed models applied for surfactant solution superspreading<sup>417</sup> rather than being based purely on physical description of the phenomenon.

Because of the additional geometrical check of the dominating wetting mechanism in the system, the model by Farris et al. seems to be the most appropriate for the current investigation – it includes both absorption and spreading, the phenomena that are certain to take place in PVA-based system. Further, from preliminary testing of the models (not shown here), only the model by Farris et al. could adequately describe all the films prepared in this study. Hence, in this chapter the empirical Avrami equation with spreading/absorption and rate of CA evolution together with geometrical corroboration is implemented. Although this model

assumes a perfect spherical droplet shape, the combined approach enables validation of this assumption.

To confirm the other assumptions of the Farris model are appropriate for this study, i.e. that the effects of gravity and evaporation are negligible, the following equation can be used:<sup>428</sup>

$$l_0 < \left( \frac{2\gamma_{lv}}{\rho g} \right)^{0.5} \quad 7.5$$

where  $l_0$  is lineal dimension of the droplet,  $\rho$  is the density of the liquid, and  $g$  the gravitational acceleration. Given  $l_0$  was smaller than the right hand side of Equation 7.5 (here found to be ca. 3.5 mm and 3.8 mm respectively, at  $t=0$ ), it was determined that gravity can be neglected. Similarly, to confirm that evaporation does not play a significant role, preliminary measurements on pure glass substrates were performed finding no significant change to droplet volume over the length of the experiment. These result together with the short measurement duration (<90 s cf. several minutes for experiments where evaporation plays an important role)<sup>412</sup> confirm that evaporation is negligible.

### 7.3.2. General remarks on film structure

As stated in Chapter 5, spin coating is based on rapid solvent evaporation, leading to creation of thin films with non-equilibrium structure. For solution-casting, however, elevated temperature and prolonged evaporation time allow the sample to reach an energetically favourable structure. Despite the differences in method used, films prepared using the two described techniques were both characterised by uniform morphology (Figure 7.1) and low roughness (maximum of ca. 1 nm, Table 10.12, Appendix D). In general, 99PVA films had higher roughness, however the difference was not substantial. Therefore, for further investigations these films were treated as flat and uniform (within investigated AFM image

size), hence any differences in characteristics between the two preparation methods arose due to phenomena other than film roughness.

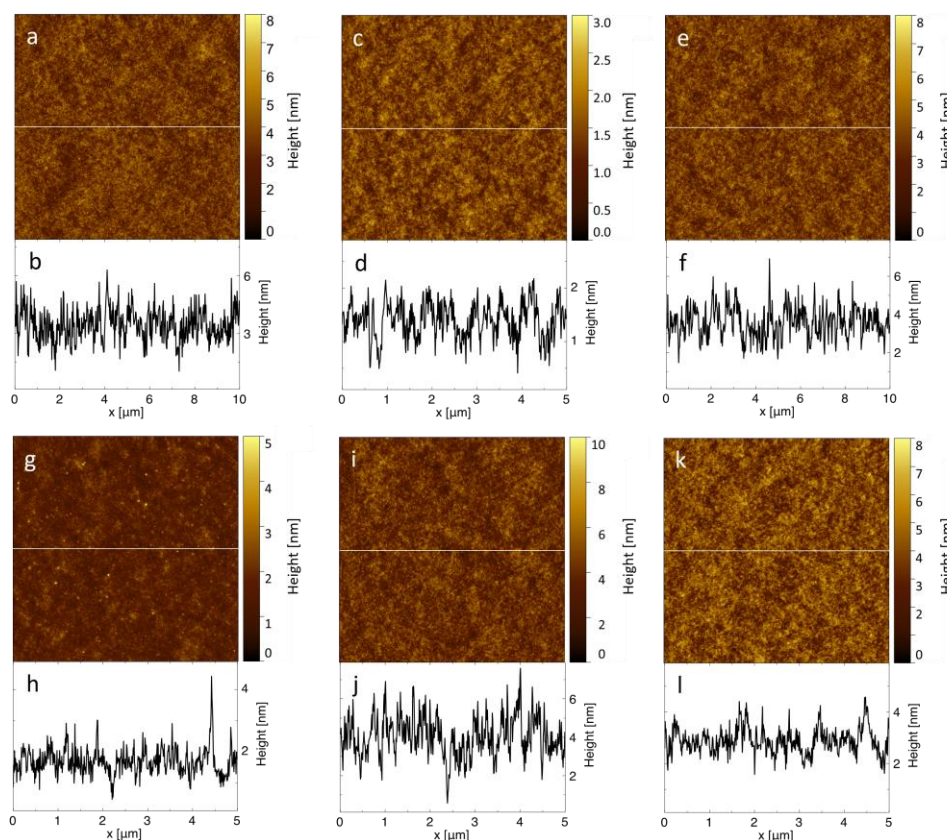


**Figure 7.1.** Morphology and height profile of: (a,b) spin-coated plasticised 87PVA film, (c,d) solution cast 87PVA film, (e,f) solution cast plasticised 87PVA film, (g,h) spin-coated 99PVA film, (i,j) solution cast 99PVA film, and (k,l) solution cast plasticised 99PVA film.

Due to the higher  $M_w$  of 99PVA, films of these polymer were ca. 38% thicker than these of 87PVA. Glycerol was introduced to the system in either pure form or as glycerol solution to create films containing 20 wt% plasticiser. This was proven to lead to sufficiently flexible films without causing significant changes in thickness.<sup>7</sup> Indeed, the addition of glycerol did not typically decrease the film thickness by more than 20%. The most significant differences were observed for solution cast films prepared from mixed 4 wt% polymer and surfactant solutions, while a difference of only max. 6% was observed for thin films prepared using lower spin speed (Table 10.12, Appendix D).

### 7.3.3. Effect of composition change on water spreading behaviour for thin films

While the nonequilibrium structure of spin-coated PVA-based films cannot be disregarded, thin films can be treated as a 2-dimensional rather than 3-dimensional matrix, therefore approximating a segment of the thick film. Formulations prepared from PVA of various DH exhibited distinct changes in the CA evolution (Figure 7.2a). For unplasticised 87PVA (Figure 7.2a, black and grey lines), an initial exponential decrease was observed. For 99PVA the trend appears almost as a linear decrease (Figure 7.2a, red and orange lines). In fact, 99PVA exhibited similar CA behaviour to that of hydrophobic materials for which CA changes are caused by evaporation (in prolonged experiments).<sup>429</sup> Generally, the thinner the film, the quicker the CA evolved. However, because the character of CA evolution did not change with the film thickness for any of the investigated DH, the differences in CA evolution between 87PVA and 99PVA cannot be attributed to differences in film thickness alone; they result from the intrinsic properties of the matrix.

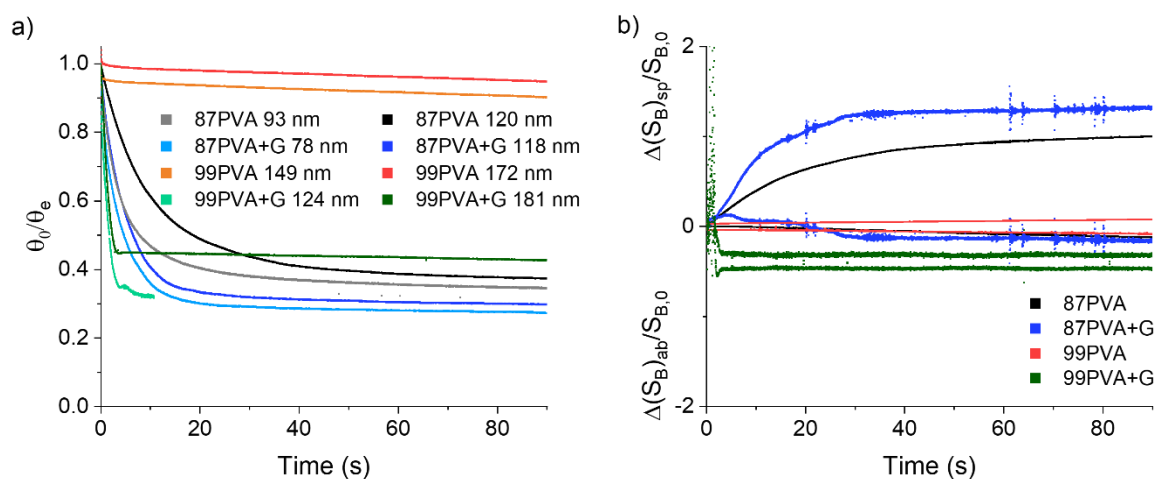


**Figure 7.2.** (a) CA evolution for spin-coated PVA films of various composition. (b) Corresponding geometrical investigations for spin-coated samples prepared using 1000 rpm spin speed. Positive values correspond to spreading behaviour, while negative – to absorption.

To explain these differences in CA evolution behaviours, it is imperative to consider the underlying spreading and absorption mechanisms. In general, spreading is a much faster process

compared to absorption due to the necessity of solvating polymer chains of the latter.<sup>244</sup> Therefore, the initial fast CA evolution is likely correlated with spreading, followed by infiltration. From geometrical analysis of water droplets (Equation 7.2-7.4) on 87PVA samples (Figure 7.2b, black), spreading evidently had a larger effect than absorption as expected from thin films. For 99PVA, however, contributions from spreading and absorption were similar in magnitude (Figure 7.2b, red).

99PVA is more hydrophilic compared to 87PVA (increased presence of -OH groups), which resulted in a lower initial CA (Table 10.13, Appendix D) and higher SFE (ca. 49 and 58 mN/m for 87PVA and 99PVA, respectively, Table 10.12, Appendix D). This greater population of hydroxyl groups can also explain the slower CA evolution – assuming that a single water molecule will attach itself to every hydroxyl group in the polymer chain<sup>101</sup> before acting as a freezable water, the amount of water molecules needed for 99PVA saturation would be 2.09 times higher than that required for 87PVA. Although reality is more complex, with plasticisation and solvation occurring before this limit is reached,<sup>101</sup> the changes in PVA hydrogen bonding behaviour with DH can explain the distinct change in the system behaviour. Moreover, despite the fast solvent evaporation kinetics during spin coating, the overall degree of crystallinity (DC) is expected to be higher for 99PVA; these crystallites are additional obstructions for migrating water. Indeed, crystallinity was proven to change the dissolution mechanism of PVA thin films by controlling the polymer relaxation rate and swelling behaviour.<sup>409</sup> Hence, higher amount of crystallites would result in decelerated CA evolution behaviour.

An alternative explanation can be found based upon the difference in  $M_w$  of the two PVA types studied – 87PVA had a lower  $M_w$  than 99PVA – which could affect the physical properties of the film.<sup>51,181</sup> The high  $M_w$  and DH of 99PVA result in interchain interactions which creates a matrix of higher tortuosity. This behaviour is similar to PVA behaviour in solutions as



decreased solubility is observed for polymers with higher DH or  $M_w$ , where more energy is required to disrupt the hydrogen bonding and cause dissolution.

Plasticisation of the PVA films with glycerol markedly accelerated the CA evolution of both PVA types used. For 87PVA, an exponential decrease in CA was observed (Figure 7.2a, blue lines), however for 99PVA an immediate step change in contact angle was noted, followed by linear decay similar to the unplasticised counterpart (Figure 7.2a, green lines). This rapid change in droplet CA prevented meaningful image analysis for plasticised 99PVA films, as after the initial CA decrease the droplet edges could not be reliably detected.

For all other samples (both plasticised and unplasticised), a simple geometric check was performed to confirm that the droplet shape can be approximated as spherical. The trigonometric relationship between CA and droplet volume, height and contact area was derived<sup>230</sup> (summarised in Table 10.13, Appendix D), and instantaneous values were plotted against each other (not shown here, for brevity). For unplasticised samples, little deviation from this theoretical behaviour was found (as expected due to nano-thickness of the film), however larger deviations were observed upon introduction of glycerol, likely for the same reasons as described for 99PVA.

These findings are in good agreement with fits to the model of Farris et al. (Equation 7.1). The average values of  $n$  were 0.26-0.37 for 87PVA (with or without the presence of glycerol, Figure 7.3b, Table 10.12, Appendix D), suggesting that spreading contributes substantially to the wetting mechanism in these samples. By contrast, samples of unplasticised 99PVA showed  $n$  values of only 0.15-0.21, implying a predominance of absorption rather than spreading. Plasticised 99PVA samples showed the inverse behaviour, however, with  $n$  values of 0.37-0.54, indicating even more spreading than any 87PVA sample (Figure 7.3b and Table 10.12, Appendix D for a complete list of model fittings). Fitted values for time constant  $k$  (Figure

7.3a, Table 10.12, Appendix D) naturally mirrored the overall change in CA across the duration of the experiment (Figure 7.2a, Table 10.13, Appendix D).

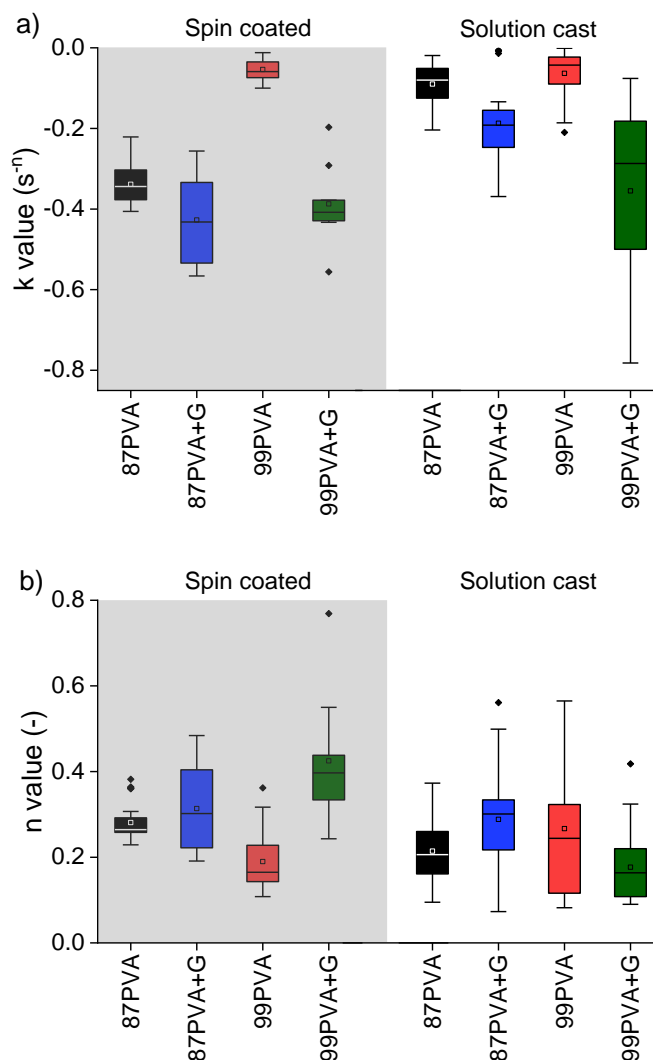


**Figure 7.3.** Fitted values to the model by Farris et al for parameters (a)  $k$  and (b)  $n$  for spin-coated and solution cast films.

As a final characterisation of the thin films, SFE was measured by comparing dodecane CA against water CA. In general, the value of SFE decreased when introducing glycerol to the system (e.g. from ca. 50 to ca. 45 mN/m in the case of 87PVA, Table 10.12, Appendix D) – in agreement with increase in SFE values upon glycerol loss observed in Chapter 5 and 6. Initial CA values for these samples were, rather surprisingly, also higher (ca. 54 and 61° for unplasticised and plasticised 87PVA, respectively, Table 10.13, Appendix D). Lower SFE is

correlated with weaker bulk interactions within the film compared with pure PVA films – glycerol replaces PVA-PVA interactions with PVA-glycerol interactions, increasing flexibility of the chains as well as hydrophilicity; however, increasing values of CA suggest more hydrophobic character of the surface. For PVA of both DHs, inclusion of glycerol within the formulation also increased  $\Delta CA$  over the entire duration of the experiment (Table 10.13, Appendix D). Glycerol introduced to the system forms hydrogen bonds with available -OH groups of PVA, therefore lowering water content required to reach limit of nonfreezing state and accelerating disruption of hydrogen bond network – hence faster spreading and absorption.

#### **7.3.4. Effect of composition change on water spreading behaviour for thick films**

For 99PVA samples, an initial period of quick CA change was followed by a linear decrease, while prolonged exponential CA decrease was observed for 87PVA samples, i.e. very similar behaviour to thin, spin-coated films (Figure 7.4a, summarised in Figure 7.3). Therefore, the mechanisms of water infiltration are similar regardless of film preparation method due to the similar changes in the amount of free hydroxyl sites for water binding, DC, and physical structure of the polymer matrix. Indeed, for vacuum-dried films of 99PVA, the cavity radius was found to be smaller than that of equivalent 87PVA (2.45 Å compared to 2.64 Å, respectively<sup>51</sup> cf. van der Waals radius of water, 1.7 Å<sup>430</sup>). Several thicknesses of films were cast, all exhibiting similar CA evolution mechanisms regardless of film thickness (Table 10.12, Appendix D).

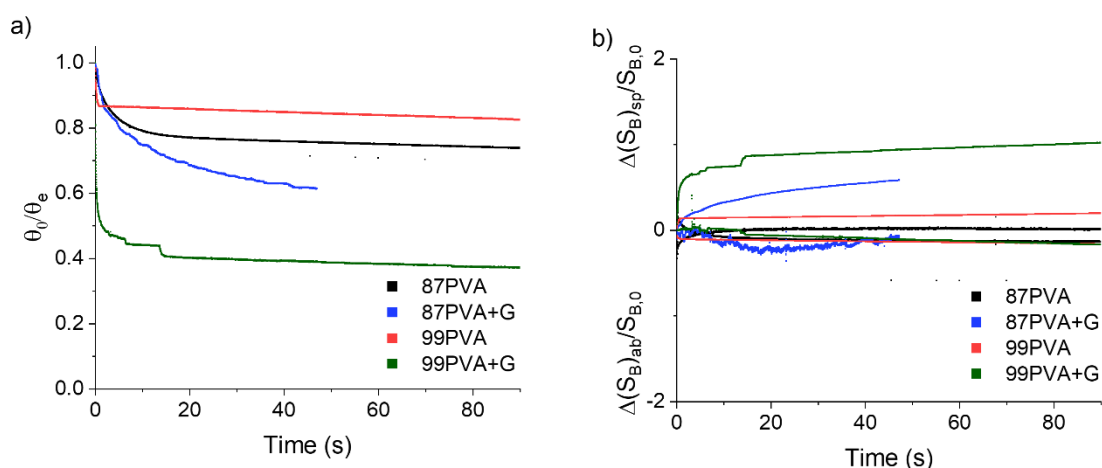


**Figure 7.4.** (a) CA evolution for solution cast PVA-based films of various composition prepared from solutions of 10% (w/v) concentration (400  $\mu$ l). (b) Corresponding geometrical investigations for these samples.

Plasticised 87PVA formulations exhibited quicker CA reductions than their unplasticised counterparts, albeit with overall similar character of CA evolution (Figure 7.4a, Table 10.13, Appendix D). Using the model proposed by Farris et al. the fitted time constant  $k$  changed from -0.1 and -0.2, and exponent  $n$  increased from ca. 0.2 to 0.275 for unplasticised and plasticised samples, respectively.

Glycerol-plasticised 99PVA films exhibited additional step-change phenomena in their CA evolutions (Figure 7.4a, green), which appeared on the goniometer video capture as sudden spreading events. This unusual observation could be attributed to two possibilities: first, dissolution of glycerol and PVA into the droplet changed the liquid surface tension and viscosity hence CA evolution behaviour, which was supported by visible marks appearing in thick films after the experiment was complete and film dried; in thin films fewer molecules were available to dissolve, therefore, changes in adjacent to film water-based solution were insignificant. The second possible mechanism is glycerol incorporation into PVA crystallites as inclusion defects, decreasing the overall DC without changing the crystallite size distribution for 87PVA (although

broadening the distribution for 99PVA),<sup>82</sup> in turn leading to accelerated dissolution of crystallites.<sup>429,431</sup>

Following the geometrical analysis of the water droplet one can deduce that spreading and absorption play similar roles to one another for unplasticised polymer films (Figure 7.4b), with fast initial changes leading to steady linear increase in both factors (black and red, Figure 7.4b). Addition of glycerol to the 87PVA formulation changed this behaviour to an exponential-like trend while step-change behaviour was still observed for plasticised 99PVA (blue and green, respectively, Figure 7.4b). Despite the fact that the values of  $n$  overall increased for plasticised 87PVA (cf. unplasticised 87PVA), no equivalent increase in  $n$  was observed for 99PVA, presumably as the increased number of -OH groups on the polymer backbone reduces the impact of plasticisation (Table 10.12, Appendix D).

In general,  $n$  values for thin films were greater compared to their thick counterparts with the exception of plasticised 99PVA, where this trend is not as clear (Figure 7.3, Table 10.12, Appendix D). In thick films absorption and spreading both involve PVA dissolution after reaching the nonfreezing water threshold value in a given location. Aside from plasticised 99PVA, overall initial CA values for thick films were higher with lower SFE values compared to their thinner counterparts (Table 10.12, Appendix D). This can arise due to two reasons: first, despite the fact that spin-coated films are ca. 100 nm thick, polymer-substrate and polymer-air interactions can play an important part in the film behaviour; second, differences in preparation method for the two film types will result in different molecular arrangement, including more perfect crystals in solution cast polymer matrices compared to spin-coated ones.

The presence of more molecular layers in thick films also led to smaller  $\Delta CA$  than in thin films with the notable exception of unplasticised 99PVA which exhibited the same  $\Delta CA$  in both film types (Table 10.13, Appendix D). As higher amount of water migrates inside the thick films

compared to thin formulations, less is available for spreading at the surface, in general slowing down x,y-migration of water (on the surface) in favour of z-migration. Accordingly,  $k$  values were smaller for thick films than in thin films, while  $\Delta A$  (change in drop surface area) decreased (again, aside from 99PVA which remains unchanged, Table 10.12, Table 10.13, Appendix D). While it is expected that  $\Delta V$  would become more pronounced in thick films compared to thin films, no significant difference was observed between the film preparation methods. These similar  $\Delta V$  values imply a limitation in the goniometry technique itself: the strict geometrical assumptions used by the software to calculate droplet volume may lead to inaccuracies as the droplet becomes non-ideal upon absorption into the film. To account for this limitation and attempt to estimate  $\Delta V$  indirectly, the discrepancy between measured droplet height and calculated droplet height assuming  $\Delta V=0$  was determined following Farris et al.<sup>230</sup> (not shown here, for brevity). This further analysis was inconclusive, therefore further study is required to determine if absorption phenomena are more prominent in thick films than thin films.

To summarise, CA evolution of water on PVA shows a clear distinction between PVA samples of different DH, as well as presence of plasticiser. Two possible underpinning mechanisms may cause this behaviour – polymer crystallinity and matrix tortuosity – and affect the rate of water ingress into the matrix. To discern between these two possible mechanisms, FTIR can be used to quantitatively evaluate the degree of crystallinity, which requires PVA films of micrometre thickness.

### **7.3.5. FTIR characterisation of crystallinity in PVA-based formulations**

FTIR is an established method for characterising the behaviour of PVA film formulations by analysing the nature of hydroxyl and acetate groups within the film as well as interactions with any additives present. In this section, characterisation of crystallinity in PVA films systems

is discussed. Detailed analysis of the spectra presented in Figure 7.5 can be found in Section D1, Appendix D.

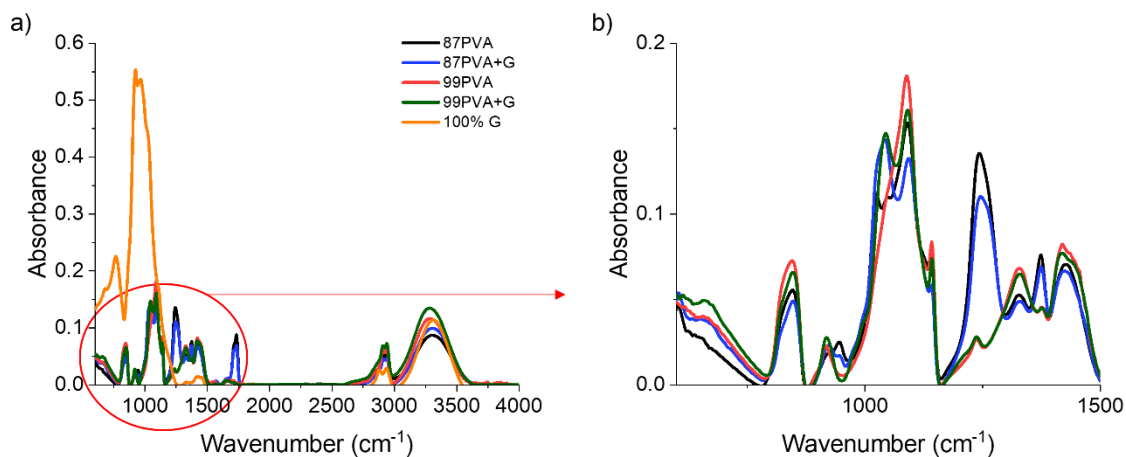


**Figure 7.5.** FTIR spectra of PVA-based films of various composition prepared from solutions of 10% (w/v) concentration (400  $\mu$ l).

At its simplest, crystallinity can be estimated as the intensity ratio between peaks corresponding to crystalline phase and a reference band.<sup>37,58,241,242</sup> In PVA, crystalline peak was assigned at 1140  $\text{cm}^{-1}$  (C-C stretching mode or C-O stretching),<sup>242</sup> while the reference peaks – to 850  $\text{cm}^{-1}$  ( $\text{CH}_2$  rocking),<sup>241</sup> 1425  $\text{cm}^{-1}$  ( $\text{CH}_2$  bending),<sup>37,58</sup> or 1094  $\text{cm}^{-1}$  (C-O stretching).<sup>39,242</sup> This method can, however, result in estimation of nonphysical values (i.e. a DC above 100%). Hence, the calculated values need to be calibrated by supplementary techniques to establish an empirical formula for crystallinity in the polymer films.<sup>39,432</sup> However, this approach leads to errors due to different approaches of identifying crystals (i.e. through spectroscopic or diffraction-based phenomena). Therefore, all peak ratio methods mentioned above were compared as well as those calibrated against XRD<sup>39</sup> or bulk density<sup>432</sup> measurements (Table 10.15, Appendix D), with the term DC referring to the degree of crystallinity estimated by these methods.

It is worth noting that FTIR peaks corresponding to glycerol overlap with the 850, 1094, and 1141  $\text{cm}^{-1}$  peaks used in DC calculations (Figure 7.5). By comparing equivalent methods for plasticised and unplasticised PVA, it becomes clear that the calculated DC is relatively higher in methods using these overlapping peaks (i.e. DC is reduced by ca. 20% for the 1140/1425 peak ratio, but only by ca. 10% for the 1140/850 and 1140/1094 peak ratio methods).

Regardless, DC was approximately constant for all unplasticised PVA and all plasticised PVA formulations, irrespective of film thickness or DH (Table 10.15, Appendix D). This indicates that changes in CA evolution behaviour is not correlated with the overall film crystallinity. Small crystals, or those with low packing density, can more easily dissolve however,<sup>409</sup> potentially accelerating spreading and absorption. It is hypothesised that crystallites are larger, with more regular packing at higher DH PVA due to the greater amount of hydroxyl groups and overall longer polymer chains. It takes therefore longer time to dissolve these structures, resulting in a slow, linear decay seen in Figure 7.4a. Introducing glycerol to the system caused significant decrease in system crystallinity; replacement of intra- and intermolecular PVA-PVA hydrogen bonds with glycerol-PVA bonds appears to explain this phenomenon. Even within crystallites, the presence of glycerol results in more defective structure and smaller sizes<sup>7</sup> that is more easily disrupted by migrating water hence leading to faster CA evolution. More direct studies of crystallinity (e.g. using XRD) would be required to prove this hypothesis and provide a more robust assessment of DC.

### **7.3.6. Effect of liquid medium change on water spreading behaviour**

To investigate the effect of solution composition on CA evolution, further wetting experiments were performed using surfactant solutions and dodecane as the liquid medium, rather than water. As with other surfactant-based studies in this thesis, cationic, anionic, and



nonionic surfactants (CTAB, SDS, and C<sub>12</sub>E<sub>10</sub>, respectively) were tested to account for the effect of head group chemistry. Further, pure dodecane was also used to enable analysis of initial SFE and infiltration of a nonpolar, nonaqueous medium into the polymer films.

The excess free energy of the droplet  $\Phi$  can be described by equation:<sup>196</sup>

$$\phi = \gamma_{lv}S + P_e V + \pi R_s^2(\gamma_{sl} - \gamma_{sv}) \quad 7.6$$

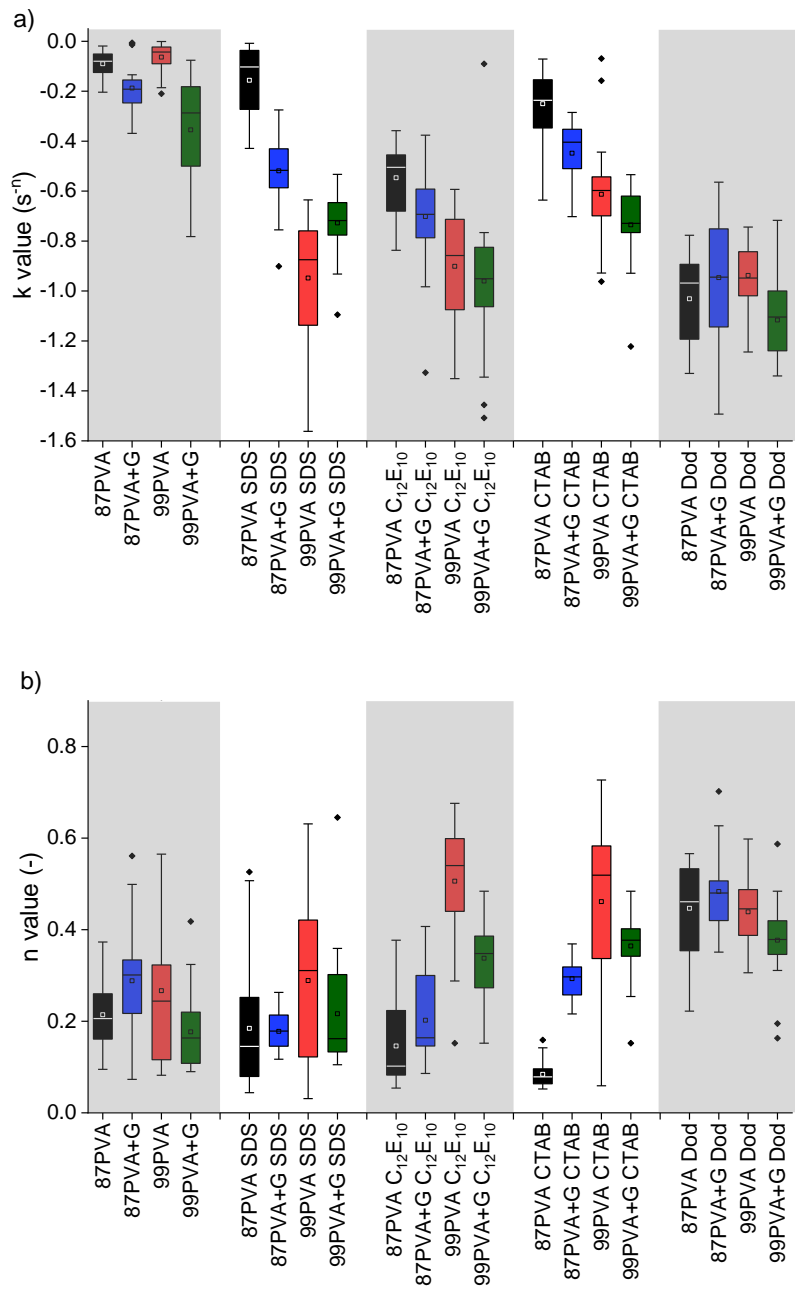
where  $R_s$  is the radius of the solid-liquid interface,  $V$  is droplet volume,  $S$  is the solid-liquid interface area, and  $P_e$  is the excess pressure inside the liquid. The last term in Equation 7.6 represents the energy difference of the surface covered by liquid droplet and the one without the droplet. The excess free energy can therefore decrease when  $\gamma_{lv}$  or  $\gamma_{sl}$  decrease, or when  $\gamma_{sv}$  increases. Surfactants reduce both  $\gamma_{lv}$  and  $\gamma_{sl}$ , while surfactant migration into the film overall leads to expansion of liquid-vapour interface and further reduction of excess free energy,<sup>229</sup> leading to lower CA values. Furthermore, while the main mechanisms responsible for spreading of pure solvents are disjoining pressure, capillary forces, gravity (for large droplets), viscous resistance to the motion and inertia,<sup>416</sup> additional intermolecular interactions need to be considered for spreading of surfactant solutions.

Some groups of surfactants (i.e. trisiloxanes)<sup>416</sup> have been widely reported to improve the spreading significantly, leading to a phenomenon called superspreading. Among many discussed mechanisms that cause this unusual behaviour are “caterpillar motion” of the surfactant molecule that reduces viscous resistance, formation of bilayers on the leading edge of spreading,<sup>433</sup> or Marangoni flow.<sup>416</sup> Superspreading is therefore a consequence of diffusion, Marangoni stresses, chemistry of the surfactant, surface, and environmental conditions.<sup>413</sup> Advances of the flow front as a consequence of a Marangoni effect was described by a power law (i.e. proportional to  $t^a$ , where  $a$  equals 0.5 for hydrophobic surfaces).<sup>417</sup> However, in other studies, an  $a$  value of 0.2 for surfactant spreading was reported,<sup>196</sup> showing that additional

effects such as high surfactant-surface affinity, transport efficiency of the superspreaders to the surface, or direct adsorption of the micelles at the air-liquid and solid-liquid interface are the reason for the observed deviation from perfect Marangoni behaviour.<sup>417</sup>

In the investigated hydrophilic, water-soluble systems, addition of surfactants did not follow the behaviour described for hydrophobic systems. The surface area followed a power law dependence with  $a < 0.2$ , which is indicative of a different spreading mechanism compared to hydrophobic films. The most significant differences were observed for nonionic surfactant which may, at first glance, be correlated with different  $M_w$  and CMC values compared to investigated ionic surfactants (Table 7.1). To determine whether surfactants below CMC will accelerate CA evolution, further tests were performed with sub-CMC surfactant solutions on some representative compositions. No significant deviation from the behaviour of pure water was observed for these sub-CMC solutions. This behaviour agrees with previous studies on hydrophobic surfaces, where sub-CMC solutions were only partially capable of wetting the surface, with complete spreading<sup>434</sup> and the lowest CA<sup>411</sup> observed for concentrations above CMC. This phenomenon can be explained by considering the CMC itself (Table 7.1) – for C<sub>12</sub>E<sub>10</sub>, sub-CMC concentration can be at most 135  $\mu\text{M}$  which may easily be fully depleted as surfactant molecules adsorb onto the surface, leading to overestimation of the CA for these solutions.<sup>229</sup> Furthermore, for the higher 1% (w/v) surfactant concentrations used for measurements presented in Figure 7.7 and Figure 7.8, the molar concentration of C<sub>12</sub>E<sub>10</sub> was still significantly lower than that of CTAB or SDS, meaning that the number of micelles present in the system will also be lower (given a similar micellar aggregation number,  $N_{\text{agg}}$ , Table 7.1). Should the number of micelles become too high however, the viscosity of the solutions will increase (proven to slow down the polymer dissolution rate<sup>413</sup> hence spreading and absorption). In the systems investigated here, the solution viscosity was similar to that of pure water (Chapter

3), therefore it can be assumed that any effects of viscosity and solution crowding were negligible.



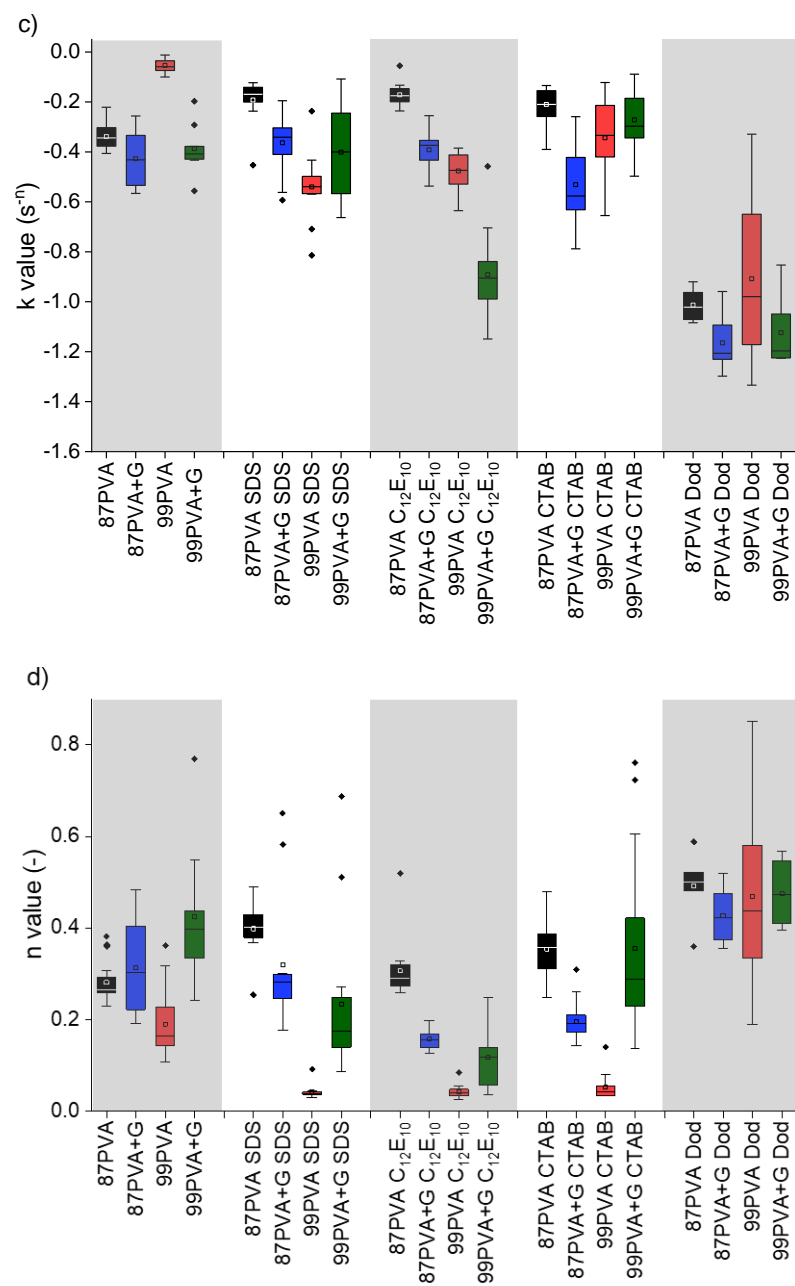


**Figure 7.6.** Fitted values to the model by Farris et al for parameters (a,c)  $k$  and (b,d)  $n$  for solution cast and spin-coated formulations, respectively, during spreading of surfactant solutions and dodecane compared against water.

Independent of the chemistry of the surfactant, their addition to water above the CMC within the investigated timescale (ca. 90 s) resulted in similar CA evolution on thin films compared to spreading of pure water. However, more substantial changes in CA were visible for thick films. Spreading of surfactant solutions resulted in an exponential decrease of CA over

time for plasticised thick films, but step changes followed by slow, linear CA evolution for their non-plasticised counterparts (Figure 7.7). At the end of the experiment, CA was much closer to an equilibrium value in thin films compared to thick films, where constant decrease was reported, unless full infiltration took place. From the model of Farris et al.<sup>230</sup> it is clear that spreading is the predominant wetting mechanism for thick films (Figure 7.6b, Figure 7.7), which is expected due to the associated decrease in liquid surface tension. Thin films showed a relatively small influence of absorption compared to spreading, however for thick films, the influence of absorption could not be overlooked (Figure 7.7b,d,f,h and Figure 7.8b,d,f,h). The CA evolution behaviour of surfactant solutions follows models presented in the literature, where droplet behaviour is divided into two regimes: fast spreading (until ca. 1 s), followed by slow spreading.<sup>229</sup> Timescales presented in investigations herein (Figure 7.7, Figure 7.8) correlate well to the values reported in literature.

**Table 7.1.** CMC and  $N_{agg}$  values for surfactants used in this study.

Surfactant	CMC (mM)	$N_{agg}$ (-)
SDS (-)	8.3 <sup>434</sup>	65 <sup>435</sup>
C <sub>12</sub> E <sub>10</sub> (0)	0.136 <sup>436</sup>	59 <sup>437</sup>
CTAB (+)	1.0 <sup>434</sup>	64 <sup>438</sup>

For some positions on the investigated films, the measured CA started to increase rather than decrease over time (Figure 7.7c,e) or otherwise evolve in a disjointed fashion (Figure 7.7e,g, Figure 7.8g). This was due to deformation of surfactant droplets (termed the fingering effect)<sup>196,228</sup> leading to data artefacts during fitting. The instability resulted in spreading of the liquid in a dendrite-like manner, with exact shape dependent on the chemistry of the surfactant and film. Asymmetric droplet structure has previously been correlated with arrangement of the surfactant molecules at a hydrophobic film surface: for negatively charged surfaces, CTAB adsorbs vertically with the hydrophobic tail upwards, while SDS and C<sub>12</sub>E<sub>10</sub> adsorb

horizontally.<sup>228</sup> In this way, some of the regions on the surface are hydrophilised, leading to faster local spreading behaviour.

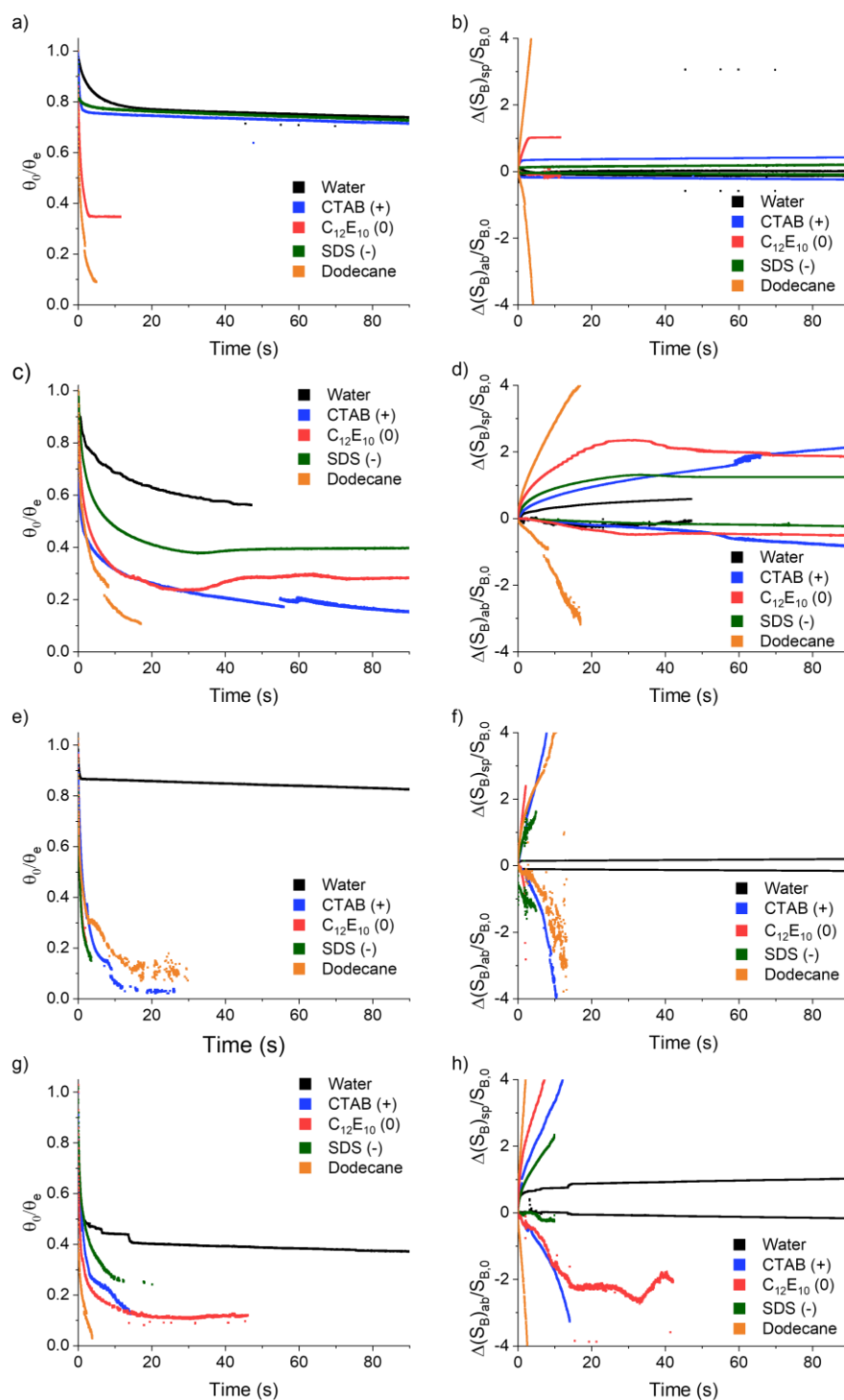


**Figure 7.7.** CA evolution with time and corresponding geometrical investigations for solution cast films prepared from solutions of 10% (w/v) concentration (400  $\mu$ l): (a,b) 87PVA, (c,d) plasticised 87PVA, (e,f) 99PVA, (g,h) plasticised 99PVA.

As the surface investigated here is hydrophilic, and covered with thin water film from the atmosphere,<sup>196</sup> it is hypothesised that surfactant heads are in contact with polymer surface<sup>411</sup> and a surfactant bilayer is formed. This bilayer enables faster local spreading on the surface, with further expansion and surfactant arrangement as the droplet spreads, leading to asymmetric CA evolution. Uneven droplet spreading may also be a result of nonuniform liquid absorption into the film: on hydrophobic films, the rate of water advancement has been shown to depend on the rate of surfactant molecule migration from solution into the bare polymer surface.<sup>229</sup> Similarly, surfactants were shown to aid water infiltration into pharmaceutical tablets by “sandwiching” between primary particles, creating channels through which water could advance into the matrix.<sup>411</sup> In this way, one could speculate that surfactant-accelerated absorption in PVA proceeds by a similar mechanism by lubricating the polymer-water interface.

Comparing plasticised and unplasticised formulations of various DHs, solution-cast polymer films of 99PVA showed both higher spreading and infiltration rate upon addition of surfactant (Figure 7.7b,d,f,h), as well as higher overall  $\Delta CA$  (Table 10.20 – Table 10.22, Appendix D). While slow and steady spreading of pure water was observed in the 99PVA formulations, this process was much faster after introducing any surfactant regardless of surfactant chemistry. Despite the similarity in SFE between 87PVA and 99PVA, the presence of hydrophobic acetate groups at the 87PVA film surface will retard surfactant surface layer formation. This in turn leads to quicker and uniform surfactant arrangement on the surface of 99PVA, allowing abrupt spreading and infiltration. Plasticisation of the polymer matrix is therefore less important here, as surfactants themselves change intermolecular interaction and infiltrate into the system.

Below, specific effects of spreading observed for ionic and nonionic surfactants are discussed.

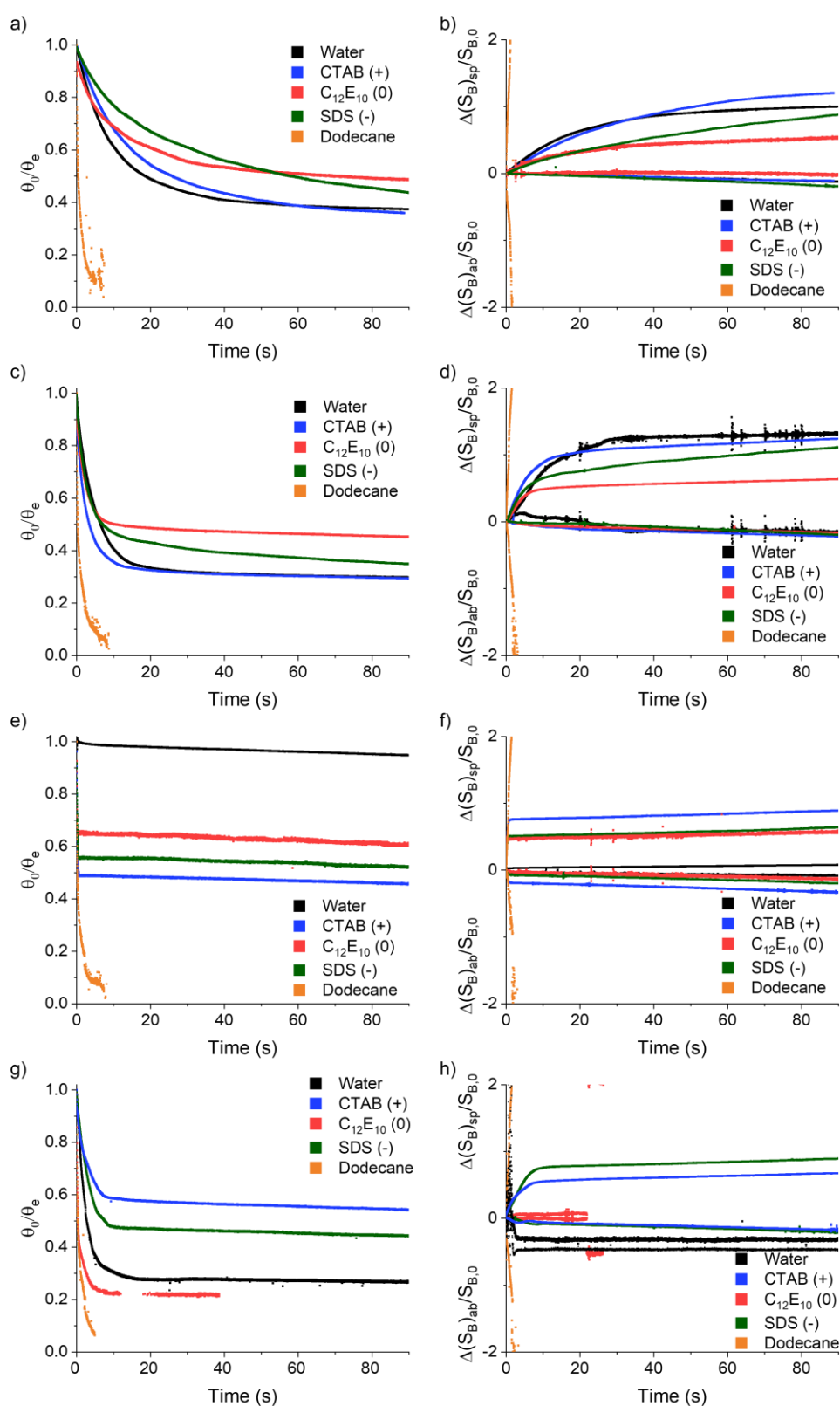


**Figure 7.8.** CA evolution with time and corresponding geometrical investigations for spin-coated films prepared from solutions of 4% (w/v) concentration (1209  $\mu$ l): (a,b) 87PVA, (c,d) plasticised 87PVA, (e,f) 99PVA, (g,h) plasticised 99PVA.



### 7.3.6.1. Specific behaviour of surface wetting by ionic surfactants

In terms of film formulation, the lower surface tension of surfactant solutions resulted in lower initial CA, with values following the same trend as with pure water: 87PVA > plasticised 87PVA > 99PVA > plasticised 99PVA. As with pure water wetting, no clear trends could be drawn between solution-cast film thickness and CA evolution (Table 10.16 – Table 10.17, Appendix D).

Parameter  $k$  had a larger magnitude in solution cast films when wetted with ionic surfactants compared to spreading of water in terms of the model by Farris et al.<sup>230</sup> For example, in the case of 87PVA  $k$  increased from ca. -0.10 during water spreading to ca. -0.20 and -0.25 in the case of SDS and CTAB solution spreading, respectively (Figure 7.6a). However, for this formulation both ionic surfactants exhibited overall similar wetting behaviour when compared against water, with similar initial CA values and  $\Delta$ CA (Table 10.20 -Table 10.21, Appendix D).

For spreading parameter  $n$  (Figure 7.6b), surfactant wetting was similar in solution cast films compared to water wetting. The notable exception to this is for CTAB infiltration into 99PVA, where  $n$  was higher for both plasticised and unplasticised films, indicating a greater predominance of spreading instead of absorption for this surfactant.

Similar behaviour was not seen for thin films, however (Figure 7.6c,d). In the 87PVA films, fitting parameter  $k$  had a smaller magnitude for SDS and CTAB compared to water, indicating slower CA evolution. 99PVA had a larger magnitude of  $k$  for surfactant solution spreading, while CA evolution was not significantly altered in plasticised films of either DH value. Spreading parameter  $n$  also substantially changed in unplasticised films: 87PVA showed a larger  $n$  value (hence greater effect of spreading), while 99PVA had an  $n$  value of almost 0 (almost no spreading). No overall change in average  $n$  value was recorded for plasticised films in contact with SDS and CTAB solutions, mirroring the pattern in parameter  $k$ .

The trend in Farris parameter  $n$  can be confirmed by inspecting  $\Delta A$  and  $\Delta V$  directly (discussed in detail in Table 10.20, Table 10.21, Appendix D). Higher values were recorded for both parameters during surfactant spreading in thick films compared against the corresponding findings for water. These contrasts demonstrate a change in absorption behaviour for the surfactant solutions into these formulations, indicative of a change in the absorption mechanism. As would be expected, almost no change in  $\Delta V$  was recorded for thin films upon change in liquid medium; given the ca. 100 nm height of these films, any large  $\Delta V$  values recorded were considered to be data artefacts. Detailed discussion of trends in  $\Delta A$  and  $\Delta V$  during surfactant solution wetting can be found in Section D2, Appendix D.

The substantial difference in film behaviour, exemplified by accelerated CA evolution for thick films and retardation for thin films, highlights the importance of surfactant solution infiltration into PVA matrix compared to spreading at the surface. For thin films, the negligible  $z$  dimension means that  $x,y$ -spreading is the only possible mechanism of wetting behaviour, instead of absorption or infiltration-based spreading (i.e. spreading of the liquid medium after absorption rather than spreading on the surface only). Based on the contrast between the two film types, it is probable that infiltration-based spreading is the dominant mechanism of surfactant solution wetting on PVA-based films. One could therefore postulate that thin films represent the intended layer-like approach – with infiltration responsible for the changes in the second part of the measurements that cannot be present in thin films as obstruction in the form of substrate is met.

Similar to a previous study on hydrophobic surfaces,<sup>416</sup> common ionic surfactants used in this study improved wetting of the surface. The importance of infiltration rather than pure surface spreading was concluded in studies of hydrophobic surfaces,<sup>411</sup> which was also established here for hydrophilic films. Small differences between the behaviour of SDS and

CTAB in the films imply that specific interactions between surfactants and the film can modify the spreading behaviour observed in agreement with previous findings for PVA-surfactant solutions (Chapter 3). To confirm this hypothesis, further experiments on the films were performed with the nonionic surfactant C<sub>12</sub>E<sub>10</sub> and nonpolar molecule dodecane.

### **7.3.6.2. Specific wetting behaviour of nonionic surfactant and nonpolar dodecane**

Of all the surfactants studied, including C<sub>12</sub>E<sub>10</sub> led to the most significant changes in CA evolution behaviour. The mechanism of CA evolution (i.e. the shape of the curves in Figure 7.7 and Figure 7.8 and changes in model parameters in Figure 7.6) remained similar to that of ionic surfactants – accelerated when compared to water for thick films whereas only 99PVA showed a different behaviour compared to water for thin films. Moreover, C<sub>12</sub>E<sub>10</sub> was the only surfactant that showed a substantial acceleration in CA evolution rate compared to water for thin, plasticised 99PVA films (Figure 7.2c, Figure 7.8g). As with all investigated liquid media, no clear relationship between wetting with nonionic surfactant and film thickness was observed.

With the exception of 99PVA films, values of parameter  $k$  for C<sub>12</sub>E<sub>10</sub> on all solution cast formulations had a higher magnitude compared to water and ionic surfactant spreading (change in median value by ca. 0.2 and 0.7 compared to ionic surfactant and water, respectively – Figure 7.6a). Values of  $k$  for CA evolution of C<sub>12</sub>E<sub>10</sub> solution were much larger for thick films compared to thin films (generally about 2 times higher, Figure 7.6). These differences reinforce the aforementioned observations: spreading plays a significant role during the initial stages of wetting, while no further changes appear for thin films as there are no more layers of polymer to enable infiltration (i.e. considerable spreading with a  $z$ -component). For 87PVA formulations, C<sub>12</sub>E<sub>10</sub> solutions showed a 5-10° decrease in initial CA however no significant difference in final CA compared to ionic surfactant solutions, hence overall smaller  $\Delta CA$  (Table

10.20, Table 10.22, Appendix D), without clear changes for other investigated polymer formulations. These fittings can be confirmed by analysing droplet geometry of the  $C_{12}E_{10}$  solutions, discussion of which can be found in Section D3, Appendix D.

Comparing between thin and thick films, changes in parameter  $k$  were more pronounced than changes in parameter  $n$ . For the latter quantity, no clear differences were found – average values of parameter  $n$  were between ca. 0.1 and 0.55 for all thicknesses investigated (Figure 7.6b,d and Table 10.16, Table 10.18, Appendix D). The discrepancy in behaviour both in fitted  $k$  and  $n$  values and droplet geometry of various surfactant solutions indicates that chemical structure of surfactant plays an important role in facilitating the spreading within the polymer matrix. Even though the behaviour of nonionic surfactant spreading on PVA films did not show clear, significant changes in wetting parameters compared to ionic surfactants, overall increase in parameter  $k$  magnitude suggests more marked changes in system behaviour. This trend is in line with those observed in hydrophobic films, where linear  $C_{12}E_x$  surfactants were reported to be capable of showing similar superspreading behaviour to trisiloxanes,<sup>229</sup> proving that a T-shaped surfactant structure able to form bilayers<sup>413</sup> is not necessary for this phenomenon to occur. Instead, the similar superspreading behaviour of  $C_mE_x$  and trisiloxane surfactants was correlated with the similarities of their phase diagram and chemical nature of hydrophilic portion of the surfactant.<sup>415</sup> However, as  $C_{12}E_x$  head groups have smaller cross sections compared to that of trisiloxane surfactants, shorter chain lengths ( $x=3,4,5$ ) were expected exhibit superspreading effect and therefore only these shorter chains were investigated previously.<sup>415</sup> Hence, the behaviour of  $C_{12}E_{10}$  is predicted to have slower spreading rates compared to  $C_{12}E_5$ .<sup>415</sup> At the same time, for  $C_mE_x$  surfactants on hydrophobic substrates, spreading rates increased in samples with lower hydrophobicity and greater  $x$ , in a similar way

to trisiloxane-based counterparts.<sup>415</sup> Further, on hydrophobic surfaces superspreading was not observed for common ionic surfactants.

These differences in surface bilayer formation as a function of surfactant and film chemistry provide a tentative explanation for the significant differences in CA evolution for surfactant solutions on 99PVA compared to less hydrophilic 87PVA. Ionic molecules were unable to quickly replenish the interface with bulk-solvated surfactant molecules, preventing complete surface coverage and creation of an advancing bilayer.<sup>413</sup> Absorption was also identified as more important for nonionic C<sub>12</sub>E<sub>5</sub> than for CTAB and SDS.<sup>229</sup> While there is no clear trend in the changes of  $\Delta V$  in the system, the liquid absorbed by the polymer matrix is likely to spread quicker for nonionic surfactant solutions compared to ionic surfactant solutions in the vicinity of the surface (both in the x, y- and z directions) due to its linear hydrophilic section, resulting in one molecule creating longer hydrophilic pathways. C<sub>12</sub>E<sub>10</sub> is therefore capable of ‘sandwiching’ the matrix molecules quicker compared to ionic surfactants despite its higher molar mass. Therefore, from the present study it is speculated that the lack of head group charge for nonionic surfactant (hence no charge screening effect during infiltration), linear structure of the molecule, and overall changes in compatibility with the matrix<sup>295</sup> are responsible for the distinction in behaviour between investigated surfactant species.

Introducing dodecane to the system led to more striking and consistent contrasts in CA evolution behaviour (Figure 7.7 and Figure 7.8). Values of both  $k$  and  $n$  parameters were within the same range regardless of film composition (both for thick and thin films), with median  $k$  values equal to ca. -1, and median  $n$  values equal to ca. 0.5 (Figure 7.6 and Table 10.19, Appendix D). In the same vein, values of initial CA were very similar (below 20 degrees, Table 10.23, Appendix D), with rapid infiltration and spreading (< 15 s) following droplet deposition. It is suggested that the mechanism for this superspreading is a result of plasticisation of the PVA

film by dodecane. The linear structure of the molecule (similar to  $C_{12}E_{10}$ ), low  $M_w$  and surface tension, as well as structure similar to that of PVA are all indicative of their high compatibility.

### 7.3.7. Effect of aging RH conditions on the water spreading behaviour of thick films

In Chapter 5, it was established that PVA-based films could change their overall properties by absorbing atmospheric water over time. Here, solution-cast thick films were used to investigate the effect of RH on water CA evolution after 1 week of aging. As PVA absorbs more water with increased RH, changes in crystallinity and molecular packing within the matrix are likely. It is expected that aging in ambient atmosphere would plasticise the PVA matrix – water present in the atmosphere migrates into the polymer film, decreasing DC and increasing free volume in the system. As a consequence, acceleration of CA change for formulations stored at ambient RH compared to 4% RH is likely to increase.

In general, no notable changes in CA evolution on thick PVA-based films were observed after one week of storage at 4% RH compared to simulated ambient conditions (45% RH) or measurements performed on preparation day, as concluded from the spreading and absorption components (Figure 7.10b,d). Despite some changes in wetting kinetics (Figure 7.9), both previously identified CA evolution mechanisms – linear (e.g. Figure 7.10c, blue, red) or exponential CA decrease (e.g. Figure 7.10c, black, maroon, and green) – were observed in 87PVA films. Both behaviours were occasionally observed for these samples on day 0 (not shown here, for brevity) therefore this observation was correlated with the intrinsic properties of the films themselves rather than as an effect of aging. The lack of changes observed with variable RH conditions were attributed to insufficient aging of the samples, leading to only the surface layers of the matrix changing their molecular arrangement.

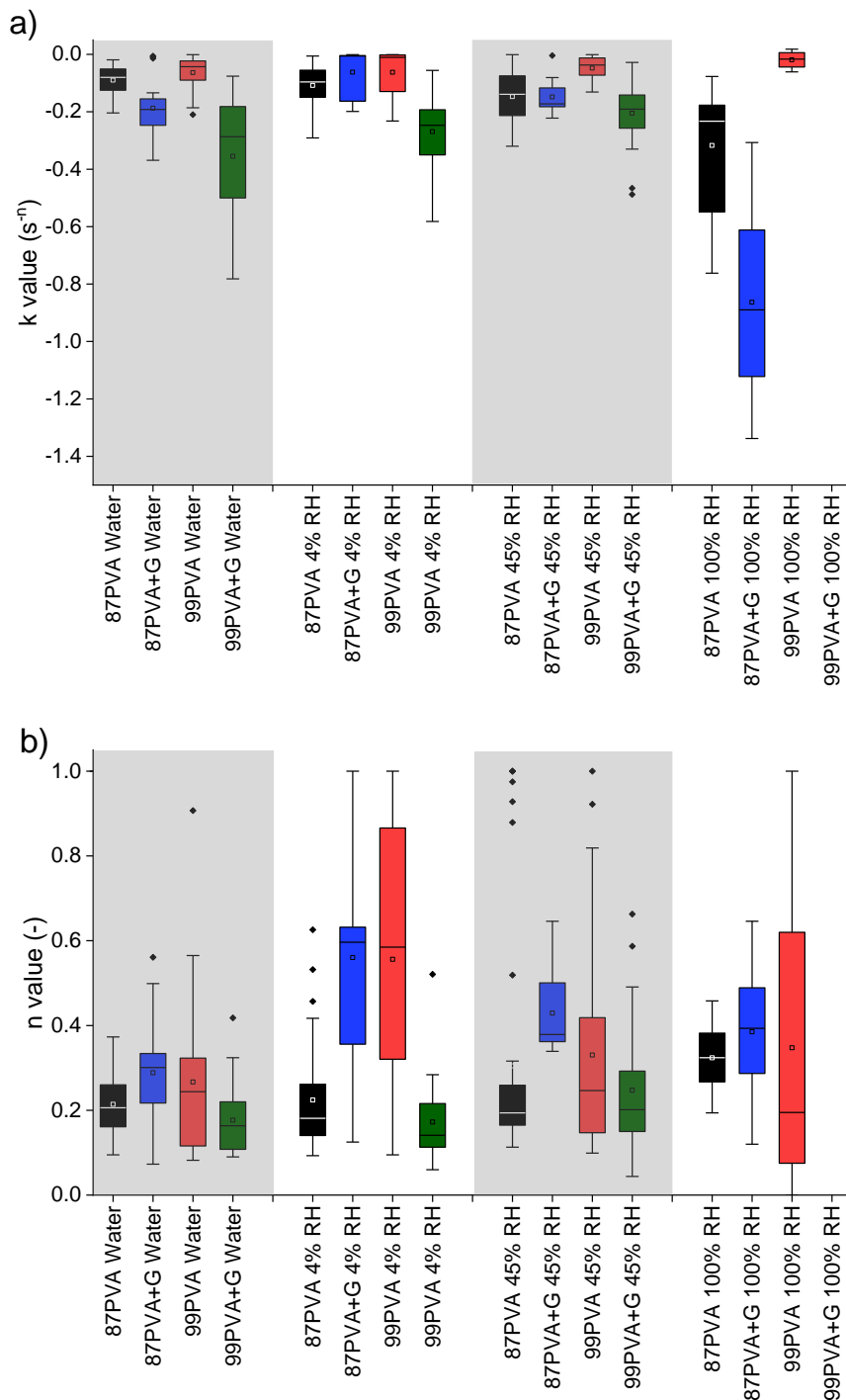


**Figure 7.9.** Box and whisker graphs of Farris model fits for parameter (a)  $k$  and (b)  $n$  for spreading of water on samples stored at various RH conditions.

This supposition is supported in Figure 7.10 (a,c,e, and g), where the initial part of the curve shows oscillations in CA independent of the formulation (not observed for films investigated on day 0). For 99PVA films (both plasticised and unplasticised) one can conclude

that aging at both 45% RH and 4% RH causes lower CA evolution rates compared to formulations investigated on day 0. However, as the presented curves are representative of different behaviours, once all repeated measurements had been taken into account (i.e. Figure 7.9) no clear changes were observed. Moreover, the influence of spreading and absorption (shown in Figure 7.10f,h) indicates that the mechanism is largely unchanged due to similar shapes of the curves and spreading/absorption ratio.

These findings were corroborated by the model parameters of CA evolution (Figure 7.9). Parameters  $k$  and  $n$  showed no significant difference between freshly prepared samples and those aged for one week at 4% RH and 45% RH (Figure 7.9). The only notable difference in average model fit values were recorded for plasticised 87PVA films aged at 4% RH. For these formulations (Table 10.25, Appendix D), average  $k$  parameter values changed from -0.187 and -0.225 to -0.06 and -0.04 for measurements on freshly prepared samples and stored for one week at 4% RH, respectively, while  $n$  parameter values changed from 0.274 and 0.257 to 0.589 and 0.619, respectively. This anomalous behaviour was confirmed by geometric analysis of  $\Delta A$  – the changes were insignificant and comparable to 99PVA films and can be attributed to more positions on the film exhibiting linear CA evolution than exponential (i.e. as in Figure 7.10c, blue cf. black curves), lowering the average  $\Delta A$ . It is suggested that this phenomenon is a result of changes in molecular arrangement due to water and glycerol evaporation from the surface. 87PVA is again more sensitive to these changes due to overall lower amount of -OH groups compared to 99PVA films. Changes in other parameters ( $\Delta CA$ , initial CA values,  $\Delta A$ ,  $\Delta V$ ) do not indicate a consistent trend.



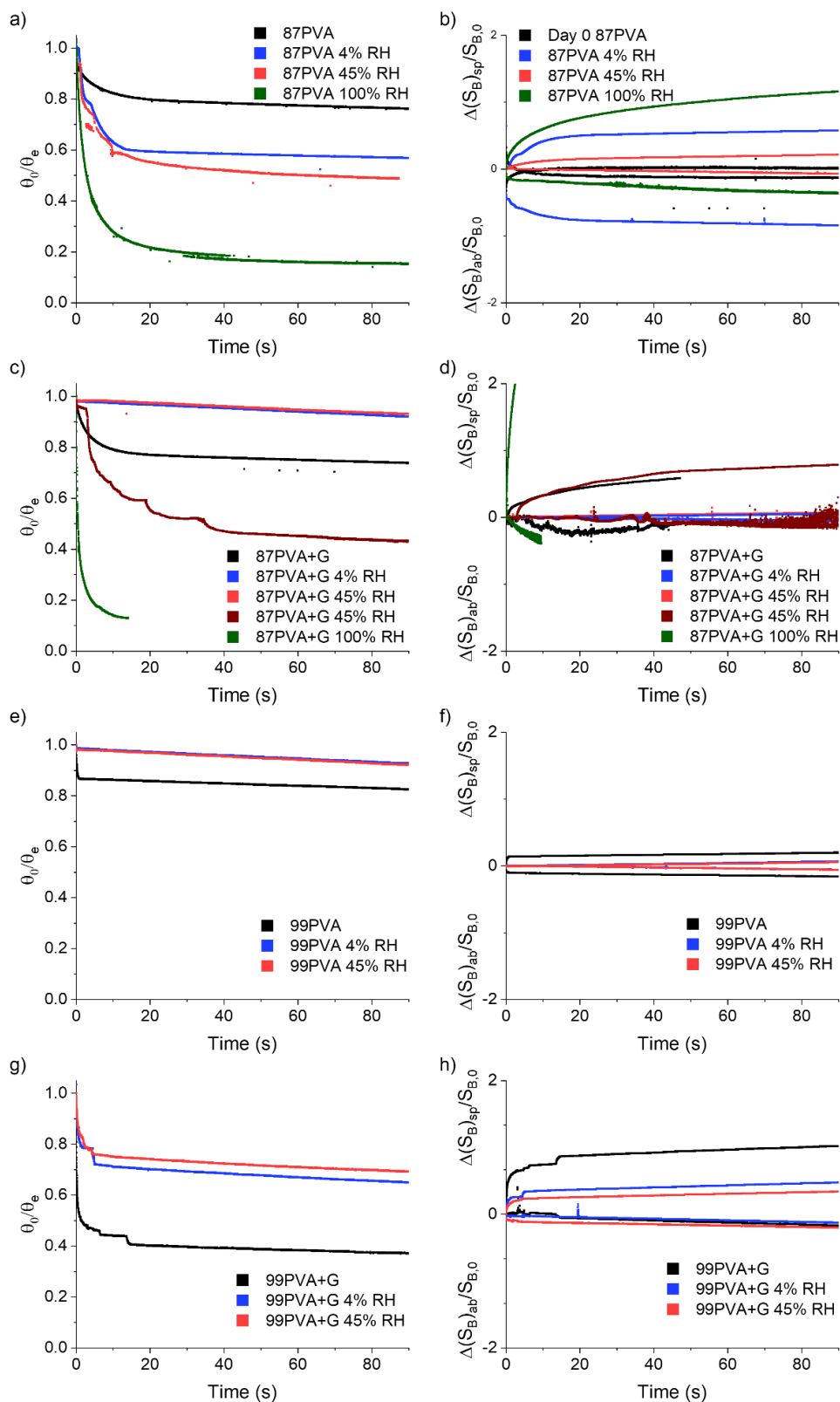


**Figure 7.10.** CA evolution with time and corresponding geometrical investigations for solution cast films: (a,b) 87PVA, (c,d) plasticised 87PVA, (e,f) 99PVA, (g,h) plasticised 99PVA.

The most significant changes, as expected, were noted for formulations stored at 100% RH. In this case, films clearly absorbed water from the atmosphere, resulting in characteristic morphological changes for formulations of different DHs. 87PVA samples created a gel-like structure that sticks to the substrate. 99PVA, on the other hand, retained a swollen film that no longer adhered to the substrate. Because of these problems, measurements were not possible on majority of plasticised and unplasticised 99PVA formulations (uneven surfaces rendering image analysis impossible), while for 87PVA these measurements were no longer reliable due to nonuniform structure of the film after atmospheric water infiltration. Regardless, aging at 100% RH resulted in almost immediate infiltration of the water droplet into the film (ca. 2 times and 4 times decrease of parameter  $k$  for unplasticised and plasticised 87PVA, respectively). Insignificant changes in  $n$  parameter (ca. 30% increase for 87PVA compared to freshly prepared samples, no clear trend for plasticised 87PVA) confirmed problems of precise measurements with non-uniform surface. For samples of 99PVA where measurements were possible, no changes compared to behaviour of freshly prepared samples were reported. Interestingly, increase in initial CA was noted for 87PVA formulations (but not for 99PVA) compared to formulations on day 0, with consequent increase in overall  $\Delta CA$  (i.e. complete infiltration into the film).

These observations were further confirmed by crystallinity measurements. No clear trend or substantial changes in FTIR spectra was observed for samples stored at 4% RH and 45% RH compared to freshly prepared samples (Figure 7.11). From this, it is concluded that no variations in intermolecular interactions or DC are present as aging only affects the surface layer of the film (while ATR-FTIR crystal penetration depth of ca. 2  $\mu\text{m}$  does not only give information about the film surface, but also layers below). Among the few notable observations, one can mention a higher ratio of 3300/2900 peak (OH stretching correlated with hydrogen bonds/ $\text{CH}_2$

stretching and bending)<sup>37,38,242,439</sup> for 99PVA samples stored at 4% RH, with peaks shifted slightly to lower wavenumbers, which indicate small variations in character of hydrogen bonding in the system. Changes in samples aged at uncontrolled ambient conditions were more pronounced (Figure 7.11d). However, from insubstantial increases in the 1140/850 peak ratios (Table 10.24, Appendix D), one can conclude that there is not an overall tendency of crystallite C-O stretching (at 1140  $\text{cm}^{-1}$ ) becoming dominant over C-C stretching (at 850  $\text{cm}^{-1}$ ) for these samples. Combined, these results indicate that DC is not significantly changed over time at ambient RH – neither in terms of further crystallisation nor crystallite dissolution.

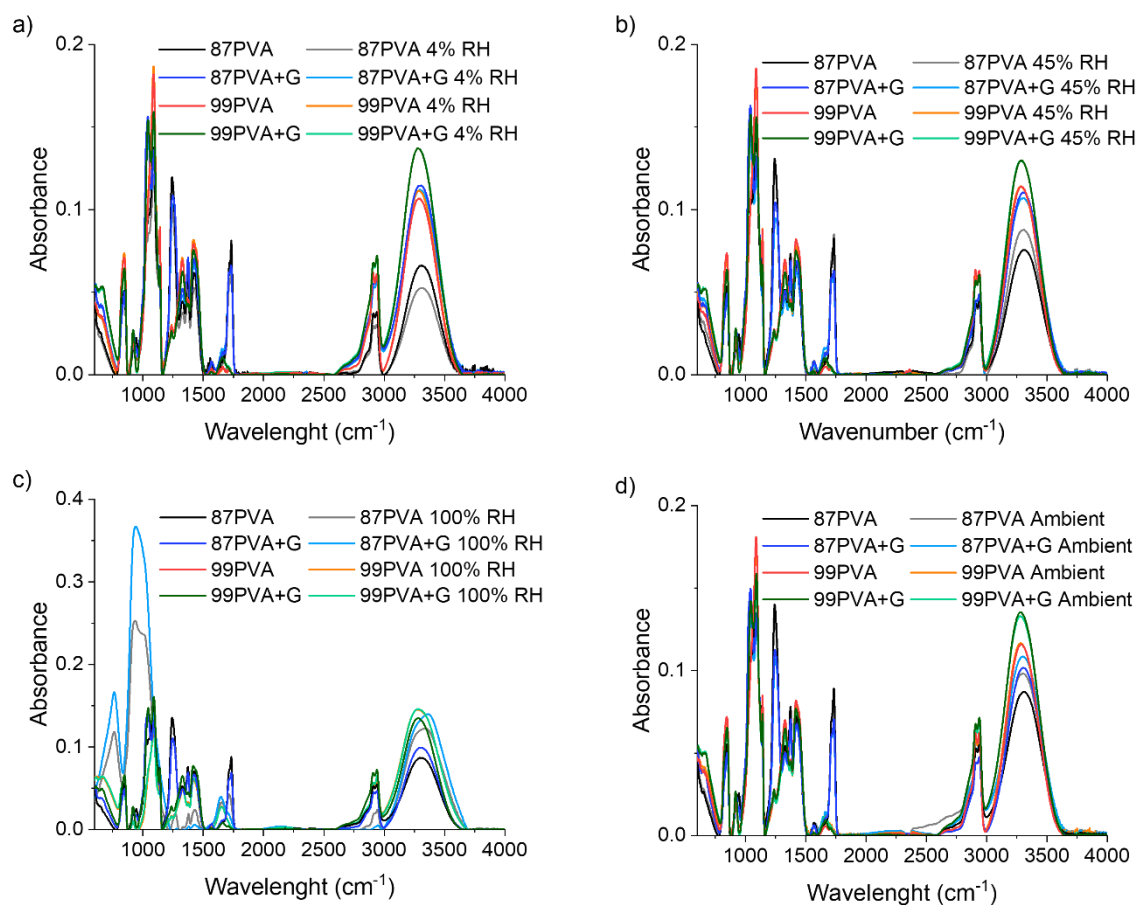


**Figure 7.11.** FTIR spectra of solution cast PVA-based films stored at various RH conditions, compared against freshly prepared samples. (a) 4% RH (ambient RH), (b) 45% RH, (c) 100% RH, and (d) samples aged in ambient atmosphere.

For samples stored at 100% RH, no conclusions about crystallinity changes can be drawn for 87PVA-based samples due to clear changes in the matrix structure, dissolution of the matrix and consequent non-physical results obtained. For these formulations, characteristic PVA peaks were no longer visible, being replaced by peaks at 900 and 1000  $\text{cm}^{-1}$  with increased absorbance of the hydrogen bond peak at 3300  $\text{cm}^{-1}$ . Hence, a modified water spectrum was observed rather than polymer spectrum. For 99PVA-based films, however, measurements were possible (as swollen films were still one entity) and indicated clear decrease in DC with storage at 100% RH. Plasticised films showed more significant decrease in DC calculated according to the Peppas model<sup>432</sup> based on 1140/1425 peak ratio (41% and 57% decrease for unplasticised and plasticised films, respectively), compared to other two methods: a 10% and 21% decrease for unplasticised and plasticised films, respectively, for crystallinity defined as ratio of 1140/850  $\text{cm}^{-1}$  peaks; and 17% and 31% decrease for unplasticised and plasticised films, respectively, for crystallinity defined according to the Trettinikov model (based on 1150/1094 peaks).<sup>39</sup> While water content increased in the polymer matrix, the most significant changes in the structure were associated with hydrogen bonding and C-OH group interactions (950  $\text{cm}^{-1}$ ). Accordingly, an individual peak at 1050  $\text{cm}^{-1}$  was no longer visible for 99PVA-based composition, indicating overall weaker C-O stretching interactions, with increased importance of hydrogen bonding again observed as water ingress replaced PVA-PVA hydrogen bonds with PVA-water hydrogen bonds.<sup>407</sup> This resulted in creation of liquid-like clusters for samples stored at 100% RH that further changed the character of intermolecular interactions in polymer systems.<sup>407</sup>

To interpret these findings, one must consider the thermodynamics of polymer dissolution. This phenomenon is always associated with a very small positive entropy change, therefore the sign of the Gibbs free energy change is determined by the enthalpy term (Equation

1.16).<sup>440</sup> Water uptake in polymer films is controlled by solvation of the polymer chains,<sup>244</sup> as dissolution involves two processes: solvent diffusion and chain disentanglement resulting in changes from glassy structures into rubbery structures.<sup>440</sup> Dissolution occurs in layers: first by solvent filling the matrix free volume; then the amorphous, glassy polymer matrix will undergo transition into gel-like swollen layer due to diffusion of the solvent into the film (as can be observed in samples aged at 100% RH). As a consequence, two separate interfaces are created: between glassy polymer and gel layer, and between gel layer and the solvent. After an induction time, polymer dissolution takes place.<sup>440</sup>

According to Uerberreiter,<sup>440</sup> dissolution of polymer films results in creation of yet more layers: pure polymer, infiltration layer, solid swollen layer, gel layer, liquid layer and pure solvent. The polymer dissolves into surrounding solvent, while solvent migrates into polymer matrix creating more rubber-like polymer structure. The water concentration gradient within the matrix is the driving force for further changes in the layers below those in direct contact with the solvent. Therefore, solvent penetration into the polymer results in the increase of swollen surface thickness until this process becomes polymer diffusion controlled.<sup>440</sup> In the presented study, the water in contact with the film is found in a surface adsorbed layer, caused by the vapour-liquid equilibrium at the film surface. Despite this lack of pure solvent phase, the difference in aging behaviour as a function of polymer DH (which follows trends in bulk solubility of the corresponding polymer) proves that this model is at least partially valid for describing the aging of polymer films at 100% RH.

The nature of the polymer chain itself determines much of the internal film structure and hence its ease of dissolution when in contact with water. For uncrosslinked, amorphous polymers, differences in free volume and segmental stiffness, along with the tacticity of the polymer<sup>440</sup> all influence the dissolution rate of the polymer material. As stressed before, despite

its overall atactic configuration, PVA has high preference to create crystallites because of relatively small size of the hydroxyl group and strength of hydrogen bonding.<sup>407</sup> Water can be bonded to the polymer on one side (weak bonding), two sides (strong bonding) and be placed in the interface region between crystallites and amorphous region of the polymer.<sup>407</sup> Changes in polymer dissolution behaviour are therefore a direct consequence of physical crosslinks (crystallites) present in the system as a prolonged amount of time is required for dissolution of these crystals compared to migration in completely amorphous matrices. Moreover, the dissolution rate was proven to be inversely proportional to the polymer  $M_w$  up to a certain limit characteristic for a given polymer.<sup>440</sup> This is connected with the chain disentanglement (also function of a polymer  $M_w$ , generally the higher the  $M_w$ , the higher the level of disentanglement). For higher degrees of disentanglement, higher degree of swelling is noted before dissolution.<sup>440</sup>

These findings are all in line with results presented here. The higher  $M_w$  and number of -OH groups (available sites to create hydrogen bond with infiltrating water molecules) in the 99PVA polymer results in overall tighter molecular packing, less influenced by infiltrating water than 87PVA samples. From the similar behaviour of plasticised versus unplasticised formulations after swelling, one can conclude that higher chain entanglement is the main reason for these contrasts between different DH values. Moreover, changes in the morphology of the crystallites are believed to be the consequence of differences between 87PVA and 99PVA formulations. While addition of glycerol influences the degree of crystal perfection, overall DC, and increases free volume and chain flexibility, it does not change the continuity of 99PVA film upon water infiltration. According to the description by Uerberreiter, the 99PVA film as a whole behaves like a swollen polymer layer, while the 87PVA film behaves as a gel.

The interfacial character of water exchange between the atmosphere and film is also confirmed by investigations at low RH. While no significant changes in geometrical parameters

of wetting kinetics, fit parameters and FTIR spectra are observed, more variability in CA evolution for a droplet is noted. This indicates that while transport and water infiltration at 4% and 45% RH is unlikely to cause as significant of the changes as for 100% RH, they influence the wetting behaviour of the surface. As below ca. 30 wt%, water is only present in the formulations in the nonfreezing state, the absolute humidity is not enough to cause significant changes in matrix properties for investigated thickness of the film. While 45% and lower RH values were enough to cause molecular migration of the surfactant for thin films (Chapter 5), thickness of the films (and ratio of the surface water layer to the film thickness) likely determines the minimum absolute humidity for these effects to be observed. Not reaching threshold of maximum nonfreezing water content therefore provides a good explanation for the similar behaviour of 4 wt% and 45% RH in this chapter.

### 7.4. Conclusions

The dissolution behaviour of water-soluble PVA films was investigated using CA goniometry. It was proven that the kinetics of CA evolution is determined by film composition – primarily DH and  $M_w$  of the polymer, presence of glycerol in the system, and the film preparation method (spin coating vs solution casting). Both thin and thick films prepared with partially hydrolysed PVA showed a longer initial period of CA evolution with overall higher change (exponential trend), followed by slower, linear change of CA when compared against fully hydrolysed PVA. For formulations of unplasticised 99PVA films, this initial period of more significant changes was much shorter and was followed by linear decrease in CA, resulting in significantly slower overall CA changes compared to 87PVA counterparts. It is suggested that size and morphology of the crystallites (despite non-significant changes in overall DC between these samples), higher  $M_w$  for 99PVA film compared to 87PVA film (resulting in

higher degree of chain entanglement), changes in polymer structure (amount of -OH groups), and differences in free volume within the matrix are all responsible for these changes. They cannot be, however, correlated with film thickness as no substantial changes with changing thickness for the same preparation method were noted for any of the investigated formulations. Instead, different wetting behaviour appears for thin films compared to thick films – faster spreading on the surface and overall lower  $\Delta CA$  correlated with wetting taking place only in the x,y-dimension. The model of spreading and absorption provided less accurate fits for 99PVA samples.

Glycerol present in the matrix plasticises polymer chains and results in faster changes of CA, with spreading playing a more significant role compared to unplasticised samples. It is suggested that plasticisation has a more global effect in 87PVA (increases free volume and flexibility of the chains) compared to 99PVA. Higher chain entanglement, expected lower cavity radius, and higher amount of hydrogen bond donating -OH groups result in step-like changes in CA for the latter polymer due to abrupt changes in liquid surface tension as the polymer solvates.

Wetting was accelerated when using surfactant solutions compared to water, with both ionic surfactants showing similar trends in CA evolution and nonionic surfactant resulting in the most substantial changes comparable to these of dodecane. Linear structure, lack of head group charge and weaker polymer-surfactant interactions are likely the cause of this behaviour, enabling CA to be lowered more quickly and creating intermolecular ‘sandwiches’ that accelerate water infiltration into the system. The importance of water infiltration was highlighted while investigating thin films – as surfactant solutions on the surface did not cause acceleration of CA evolution with the exception of 99PVA films. Indeed, also for thick films, 99PVA-based formulations (both plasticised and unplasticised) were more susceptible to changes upon replacing water with surfactant solutions. Higher amount of -OH groups



compared to 87PVA and consequent changes of surface hydrophilicity are likely to be the reason for this behaviour.

Aging PVA samples at 4% and 45% RH did not cause significant changes in either CA evolution or in FTIR spectrum, although droplet instabilities were observed at the beginning of the process. This is likely due to insufficient water infiltration into the PVA film from the atmosphere to exceed the threshold of nonfreezing water in the system. It is further expected that changes in glycerol concentration on the film surface affect CA evolution. For 100% RH, the initial stages of PVA dissolution as a consequence of water absorption were observed, with measurements being impossible to perform due to nonuniformities of the surface. Again, molecular arrangement and properties of the matrix (chain entanglement, crystal structure, cavity radius, DH) are believed to be the reason for swollen polymer and gel-like behaviour for 99PVA and 87PVA-based formulations, respectively.

## Chapter 8. Conclusions

### 8.1. Motivation

This project aimed to understand molecular migration in multi-component, PVA-based systems both in two- (lateral, x,y-migration) and three dimensional (vertical, z-migration) contexts, exploring the effects of chemical composition, environmental conditions (RH, temperature), and adjacent liquid media on molecular migration. To this end, diffusive behaviour of migrants was investigated both in solid and liquid environments, introducing complexity into the system piecemeal to determine differences between thin- and thick films. By investigating the influence of each individual component on system morphology, chemistry, and inter-species interactions, it was possible not only to investigate the migration time scales, but also the importance of compatibility between each component in the system. On the basis of these findings, general rules for the formulation and storage conditions of PVA-based packaging materials could be derived.

### 8.2. Main findings

In PVA-based solutions containing charged molecules, intermolecular interactions play a crucial role in tracer migration rate. Favourable interactions lead to the formation of complex-like structures, with an effective slowdown in migration because of larger diameter of the molecule or longer time required to break this favourable interaction. In formulations where charged interactions are either less prominent or absent, steric effects play a dominant role and have an overriding effect on molecular diffusion in the system.

Specific intermolecular interactions and steric effects become more pronounced once solutions are spin coated into thin PVA-based films, especially as the compatibility threshold is achieved, e.g. upon excess plasticisation. Phase segregation, either in the form of plasticiser

aggregation or surfactant blooming, leads to increased variability in tracer diffusivity albeit with consistently lower diffusion rates than pure PVA or compatible PVA-glycerol formulations.

Aging thin films at elevated RH seems to increase plasticisation in the system and leads to faster migration of non-compatible additives to the surface. Surfactant presence does not influence overall water sorption behaviour, however induces surface segregation at different concentrations depending on head group chemistry. Temperature, on the other hand, increases overall compatibility in the system, leading to surfactant migration into the bulk of the system rather than to the air-film interface. The compatibility is also a function of DH and  $M_w$  of the polymer, with more significant morphological changes observed for 99PVA compared to the counterpart of lower  $M_w$  and DH. Despite these differences, model surfactant additives arrange themselves similarly in films spun from either polymer, demonstrating the formulation independent nature of the intermolecular interactions in the system.

In addition to the aforementioned environmental conditions, molecular arrangement and compatibility are significantly affected as more additives are introduced into the system. When ionic and nonionic surfactants are combined as additives in PVA-based films, overall system compatibility increases leading to reduced segregation. Conversely, when ionic surfactants with opposing head group charges are mixed, segregation is promoted. Similar findings are observed in RhB-surfactant systems, i.e. where both additives contained opposite charges. Electrostatic interactions between differently charged molecules again highlight the importance of both compatibility and interactions as the main factors influencing system behaviour.

Physical properties of the matrix also determine the PVA-based system response to outside influence i.e. wetting behaviour on contact with various liquid media. For films based

on PVA with higher  $M_w$  and DH, slower wetting kinetics were observed despite more hydrophilic character of the formulation. Although these changes can be explained by lower solubility in water and tighter molecular packing of 99PVA compared to 87PVA, these systems more promptly wet upon introducing surfactant solutions to the system, once more highlighting the importance of intermolecular interactions and their complex behaviour in the studied systems.

### 8.3. Final remarks

Although the majority of this work focuses on thin films with fewer additives than industrially-relevant formulations, it highlights the importance of aging conditions as well as additive choice on material performance. From the findings specific to the formulations studied here, conclusions about the behaviour of not only PVA-based packaging materials, but also a variety of other complex mixtures can be drawn:

- Compatibility is the primary driving force for segregation in polymer formulations, although supplementary additives can reduce phase separation in cases where the limits have been reached.
- Specific (charge-matching) interactions between additives lead to system phase segregation and can have subsequent effects on the migratory behaviour of additives in each of the two resultant phases.
- Aging polymer films at high RH conditions leads to significant water ingress, accelerating phase separation in incompatible systems and additive migration in general.
- Elevated temperature at low RH typically increases film compatibility, as solubility limits are increased.

- Matrix properties (i.e. chain entanglement and crystallinity) and polymer chemistry significantly affect behaviour upon contact with adjacent liquid media, enabling tuning to the desired application and known solute composition.

Presented studies can be further translated to even more complicated systems in order to improve environmental impact, mechanical properties and shelf life of future packaging materials.

## Chapter 9. Future work

To complete the methodology outlined in this thesis and provide a full picture of additive migration, further experiments should be undertaken to investigate the case of surfactant migration from adjacent nonaqueous media (e.g. concentrated surfactant solutions), with the possibility of extending the scope to more diverse applications. Preliminary results and suggestions are presented in Appendix E.

Investigations into z-directional migration from adjacent media to the polymer film can be performed using a fluorophore as a model migrating molecule (as seen in Chapters 3, and 4) and a confocal microscope. The concentration of fluorophore would be represented as changes in intensity of the signal (within the instrument detection limit). A proof of concept experiment performed on a fluorescence microscope has shown that the differences in surface fluorescence intensity (indicating migration of fluorophore) are a function of temperature, RH, and head group chemistry of surfactant used as a dopant. Therefore, exploring this area further using fluorophores of various sizes and side chain chemistry will provide useful insight into migration of model substances both within the film and from adjacent media to the film.

This thesis focuses on the migration behaviour in model systems that imitate industrial single dose detergents and their packaging materials. To make these systems more industrially relevant, presented models need to be extended by including more additives as well as broader range of surfactants (both within investigated groups as well as zwitterionic surfactants). Moreover, it would be worthwhile to perform measurements on migration from adjacent media to the film (as described above) using industrial prototype films (within a confidentiality agreement).

Within such complicated systems, PVA would interact with additives in a variety of ways that are likely to result in a range of morphologies displayed by these formulations. Therefore,

it is of interest to investigate the nature of PVA interactions with other additives. For that purpose, FTIR (or near-ambient X-ray photoelectron spectroscopy) coupled with AFM can reveal the nature of these interactions correlated with resultant morphological changes. Moreover, to obtain an even broader image of the investigated system, confocal Raman spectroscopy can provide the information of interaction changes with thickness change, while optical microscopy or SEM can measure changes in the morphology on longer length scales than AFM.

Evaporation of the plasticiser from the system is an important problem that changes the properties of the investigated formulations. In-depth investigations into this problem in thick films should be undertaken in a similar manner as presented in Chapter 5 to describe the kinetics of evaporation. This should be coupled with a tracing technique for glycerol (e.g. Raman spectroscopy using deuterated glycerol). As  $C_{12}E_x$  surfactants also have tendency to evaporate from the system, similar steps should be taken to track their evolution from the film in parallel to glycerol.

Contact angle was shown to be a useful tool to investigate the water infiltration and spreading kinetics. In industrial applications, polymeric films are doped with small concentration of surfactant that changes interfacial properties of the film. Therefore, the work carried out in Chapter 7 could be extended to see how addition of surfactant into the matrix will influence initial kinetics of water spreading on the surface. This information would be important to understand sealing of polymer films in greater detail.

Chapter 5 shows that morphology of samples containing SDS or CTAB is very sensitive to the concentration of surfactant in the system, leading to creation of various morphological features. Evolution of surfactant blooms and lamellae as a function of concentration as well as presence of other additives should be further investigated. For thin films, Neutron

Reflectometry (NR) or Ion Beam Analysis (IBA) can be used to measure the distribution of a given chemical in the system in the z-direction. By obtaining information for more than one chemical in the system, the influence of other additives on changes in molecular arrangement can also be concluded.

Finally, crystallinity in PVA is an important industrial problem that significantly influences both mechanical properties of the films and migration behaviour within. Therefore, detailed investigations into the influence of crystallinity on additive migration in the system should be performed by combining techniques that measure crystallinity on short- (FTIR) and long length scales (XRD), as well as thermal behaviour of the sample under elevated temperatures and its influence on recrystallization in the system (DSC). Coupling these techniques with AFM, Raman spectroscopy, or NR/IBA can provide the distribution of additives as a function of polymer crystallinity (induced by chemical or physical methods), as well as influence of other additives on crystallite behaviour, possibly under various environmental conditions.

The research carried out in this thesis only considered PVA as a polymer matrix, however the methodology used – piecemeal introduction of complexity from solutions, through thin films to thick films, then considering environmental contaminants – can be applied generally regardless of polymer chemistry. For example, studies on bio-derived polymers or their blends with PVA could be performed to investigate low-carbon alternatives to oil-derived polymers.



## Bibliography

- (1) Moraes, I. C. F.; Carvalho, R. A.; Bittante, A. M. Q. B.; Solorza-Feria, J.; Sobral, P. J. A. Film Forming Solutions Based on Gelatin and Poly(Vinyl Alcohol) Blends: Thermal and Rheological Characterizations. *J. Food Eng.* **2009**, *95* (4), 588–596.
- (2) Hasimi, A.; Stavropoulou, A.; Papadokostaki, K. G.; Sanopoulou, M. Transport of Water in Polyvinyl Alcohol Films: Effect of Thermal Treatment and Chemical Crosslinking. *Eur. Polym. J.* **2008**, *44* (12), 4114–4123.
- (3) Lim, M.; Kwon, H.; Kim, D.; Seo, J.; Han, H.; Khan, S. B. Highly-Enhanced Water Resistant and Oxygen Barrier Properties of Cross-Linked Poly(Vinyl Alcohol) Hybrid Films for Packaging Applications. *Prog. Org. Coatings* **2015**, *85*, 68–75.
- (4) Bergo, P.; Moraes, I. C. F.; Sobral, P. J. A. Effects of Different Moisture Contents on Physical Properties of PVA-Gelatin Films. *Food Biophys.* **2012**, *7* (4), 354–361.
- (5) Kawai, F.; Hu, X. Biochemistry of Microbial Polyvinyl Alcohol Degradation. *Appl. Microbiol. Biotechnol.* **2009**, *84* (2), 227–237.
- (6) Kim, D. Y.; Rhee, Y. H. Biodegradation of Microbial and Synthetic Polyesters by Fungi. *Appl. Microbiol. Biotechnol.* **2003**, *61* (4), 300–308.
- (7) Lim, L. Y.; Wan, L. S. C. The Effect of Plasticizers on the Properties of Polyvinyl Alcohol Films. *Drug Dev. Ind. Pharm.* **1994**, *20* (6), 1007–1020.
- (8) Hahladakis, J. N.; Velis, C. A.; Weber, R.; Iacovidou, E.; Purnell, P. An Overview of Chemical Additives Present in Plastics: Migration, Release, Fate and Environmental Impact during Their Use, Disposal and Recycling. *J. Hazard. Mater.* **2018**, *344*, 179–199.
- (9) El-Nasser, H. M. Effects of Methyl Red Acidity and UV Illumination on Absorption Coefficient of MR/PVA Thin Films. *Phys. B Condens. Matter* **2011**, *406* (10), 1940–1943.
- (10) Konidari, M. V.; Papadokostaki, K. G.; Sanopoulou, M. Moisture-Induced Effects on the Tensile Mechanical Properties and Glass-Transition Temperature of Poly(Vinyl Alcohol) Films. *J. Appl. Polym. Sci.* **2011**, *120* (6), 3381–3386.
- (11) Hodge, R. M.; Bastow, T. J.; Edward, G. H.; Simon, G. P.; Hill, A. J. Free Volume and the Mechanism of Plasticization in Water-Swollen Poly(Vinyl Alcohol). *Macromolecules* **1996**, *29* (25), 8137–8143.
- (12) Yao, L.; Haas, T. W.; Guiseppi-Elie, A.; Bowlin, G. L.; Simpson, D. G.; Wnek, G. E. Electrospinning and Stabilization of Fully Hydrolyzed Poly(Vinyl Alcohol) Fibers. *Chem. Mater.* **2003**, *15* (9), 1860–1864.
- (13) I Baker, M.; P Walsh, S.; Schwartz, Z.; Boyan, B. D.; Baker, M. I.; Walsh, S. P.; Schwartz, Z.; Boyan, B. D. A Review of Polyvinyl Alcohol and Its Uses in Cartilage and Orthopedic Applications. *J. Biomed. Mater. Res. Part B Appl. Biomater.* **2012**, *100B* (5), 1451–1457.
- (14) Kaplan, D. L.; Mayer, J. M.; Ball, D.; McCassie, J.; Stenhouse, S. Fundamentals of Biodegradable Polymers. In *Biodegradable Polymers and Packaging*; Lancaster, 1993; p 152.
- (15) Hassan, C. M.; Steward, J. E.; Peppas, N. A. Diffusional Characteristics of Freeze/Thawed Poly(Vinyl Alcohol) Hydrogels: Applications to Protein Controlled Release from Multilaminate Devices. *Eur. J. Pharm. Biopharm.* **2000**, *49*, 161–165.
- (16) Ollier, R.; Pérez, C. J.; Alvarez, V. Effect of Relative Humidity on the Mechanical Properties of Micro and Nanocomposites of Polyvinyl Alcohol. *Procedia Mater. Sci.* **2012**, *1*, 499–505.
- (17) Briddick, A.; Fong, R. J.; Sabattié, E. F. D.; Li, P.; Skoda, M. W. A.; Courchay, F.; Thompson, R. L. Blooming of Smectic Surfactant/Plasticizer Layers on Spin-Cast Poly(Vinyl Alcohol) Films. *Langmuir* **2018**, *34* (4), 1410–1418.
- (18) Mukherjee, G. S. Modification of Poly(Vinyl Alcohol) for Improvement of Mechanical Strength and Moisture Resistance. *J. Mater. Sci.* **2005**, *40* (11), 3017–3019.
- (19) Kanaya, T.; Ohkura, M.; Kaji, K.; Furusaka, M.; Misawa, M. Structure of Poly(Vinyl Alcohol) Gels Studied by Wide- and Small-Angle Neutron Scattering. *Macromolecules* **1994**, *27* (20), 5609–5615.
- (20) Rodler, M.; Bander, A. Structure of Syn-Vinyl Alcohol Determined by Microwave Spectroscopy. *J. Am. Chem. Soc.* **1984**, *106* (14), 4025–4028.
- (21) Wittcoff, H. A. Acetaldehyde: A Chemical Whose Fortunes Have Changed. *J. Chem. Educ.* **1983**, *60* (12), 1044–1047.
- (22) Pu-you, J.; Cai-ying, B.; Li-hong, H.; Yong-hong, Z. Properties of Poly(Vinyl Alcohol) Plasticized by Glycerin. *J. For. Prod. Ind.* **2014**, *3* (3), 151–153.
- (23) Atkins, P. Molecular Substances. In *The Elements of Physical Chemistry*; Oxford University Press: Oxford, 2001; p 392.
- (24) Finch, C. A. Biopolymers, PVA Hydrogels, Anionic Polymerisation, Nanocomposites. In *Advances in*

- polymer science*; John Wiley & Sons, Ltd, 2003.
- (25) Chan, L. W.; Hao, J. S.; Heng, P. W. S. Evaluation of Permeability and Mechanical Properties of Composite Polyvinyl Alcohol Films. *Chem. Pharm. Bull.* **1999**, *47* (10), 1412–1416.
- (26) Watase, M.; Nishinari, K. Effect of the Degree of Saponification on the Rheological and Thermal Properties of Poly(Vinyl Alcohol) Gels. *Makromol. Chem.* **1989**, *190*, 155–163.
- (27) Colvin, B. G. Crystal Structure of Polyvinyl Alcohol. *Nature* **1974**, *248* (April), 756–759.
- (28) Van Etten, E. A.; Ximenes, E. S.; Tarasconi, L. T.; Garcia, I. T. S.; Forte, M. M. C.; Boudinov, H. Insulating Characteristics of Polyvinyl Alcohol for Integrated Electronics. *Thin Solid Films* **2014**, *568* (1), 111–116.
- (29) Cozzolino, C. A.; Blomfeldt, T. O. J.; Nilsson, F.; Piga, A.; Piergiovanni, L.; Farris, S. Dye Release Behavior from Polyvinyl Alcohol Films in a Hydro-Alcoholic Medium: Influence of Physicochemical Heterogeneity. *Colloids Surfaces A Physicochem. Eng. Asp.* **2012**, *403*, 45–53.
- (30) Frisch, H. L.; Al-Madfai, S. Surface Tension of Synthetic High Polymer Solutions1. *J. Am. Chem. Soc.* **1958**, *80* (14), 3561–3565.
- (31) Figueiredo, K. C. S.; Alves, T. L. M.; Borges, C. P. Poly(Vinyl Alcohol) Films Crosslinked by Glutaraldehyde Under Mild Conditions. *J. Appl. Polym. Sci.* **2009**, *111* (5), 3074–3080.
- (32) Peppas, N. A. Crystallization of Polyvinyl Alcohol-Water Films by Slow Dehydration. *Eur. Polym. J.* **1976**, *1* (8), 1–4.
- (33) Krumova, M.; López, D.; Benavente, R.; Mijangos, C.; Pereña, J. M. Effect of Crosslinking on the Mechanical and Thermal Properties of Poly(Vinyl Alcohol). *Polymer (Guildf)*. **2000**, *41* (26), 9265–9272.
- (34) Wong, D.; Parasrampur, J. Polyvinyl Alcohol. *Anal. Profiles Drug Subst. Excipients* **2007**, *24*, 397–441.
- (35) Fukumori, T.; Nakaoki, T. Significant Improvement of Mechanical Properties for Polyvinyl Alcohol Film Prepared from Freeze/Thaw Cycled Gel. *Open J. Org. Polym. Mater.* **2013**, *03* (04), 110–116.
- (36) Fukumori, T.; Nakaoki, T. High-Tensile-Strength Polyvinyl Alcohol Films Prepared from Freeze/Thaw Cycled Gels. *J. Appl. Polym. Sci.* **2014**, *131* (15), 1–8.
- (37) Bhat, N. V.; Nate, M. M.; Kurup, M. B.; Bambole, V. A.; Sabharwal, S. Effect of  $\gamma$ -Radiation on the Structure and Morphology of Polyvinyl Alcohol Films. *Nucl. Instruments Methods Phys. Res. Sect. B Beam Interact. with Mater. Atoms* **2005**, *237* (3–4), 585–592.
- (38) El-Sawy, N. M.; El-Arnaouty, M. B.; Abdel Ghaffar, A. M.  $\Gamma$ -Irradiation Effect on the Non-Cross-Linked and Cross-Linked Polyvinyl Alcohol Films. *Polym. - Plast. Technol. Eng.* **2010**, *49* (2), 169–177.
- (39) Tretinnikov, O. N.; Zagorskaya, S. A. Determination of the Degree of Crystallinity. *J. Appl. Spectrosc.* **2012**, *79* (4), 538–543.
- (40) Assender, H. E.; Windle, A. H. Crystallinity in Poly(Vinyl Alcohol). 1. An X-Ray Diffraction Study of Atactic PVOH. *Polymer (Guildf)*. **1998**, *39* (18), 4295–4302.
- (41) Shah, Y. T.; Porter, J. H. A Model for Gel Drying. *J. Appl. Polym. Sci.* **1973**, *17* (2), 605–618.
- (42) Peppas, N. A.; Hansen, P. J. Crystallization Kinetics of Poly ( Vinyl Alcohol ). *J. Appl. Polym. Sci.* **2020**, *27*, 2020.
- (43) Wong, S. S.; Altinkaya, S. A.; Mallapragada, S. K. Understanding the Effect of Skin Formation on the Removal of Solvents from Semicrystalline Polymers. *J. Polym. Sci. Part B Polym. Phys.* **2005**, *43* (22), 3191–3204.
- (44) Ciampi, E.; McDonald, P. J. Skin Formation and Water Distribution in Semicrystalline Polymer Layers Cast from Solution: A Magnetic Resonance Imaging Study. *Macromolecules* **2003**, *36*, 8398–8405.
- (45) Wong, S.-S.; Altinkaya, S. A.; Mallapragada, S. K. Crystallization of Poly(Vinyl Alcohol) During Solvent Removal: Infrared Characterization and Mathematical Modeling. *J. Polym. Sci.* **2007**, *45*, 930–935.
- (46) Masuda, K.; Kaji, H.; Horii, F. CP / MAS 13 C NMR Analyses of Hydrogen Bonding and the Chain Conformation in the Crystalline and Noncrystalline Regions for Poly ( Vinyl Alcohol ) Films. **1999**, 1–9.
- (47) Heise, B.; Kilian, H. G.; Pietralla, M. Orientation — Strain Relations in Partially Crystallized Polymers. In *Mehrphasige Polymersysteme*; Steinkopff: Darmstadt, 1977; Vol. 36, pp 16–36.
- (48) Galeski, A. Strength and Toughness of Crystalline Polymer Systems. *Prog. Polym. Sci.* **2003**, *28* (12), 1643–1699.
- (49) Miyazaki, T.; Hoshiko, A.; Akasaka, M.; Sakai, M.; Takeda, Y.; Sakurai, S. Structure Model of a Poly(Vinyl Alcohol) Film Uniaxially Stretched in Water and the Role of Crystallites on the Stress-Strain Relationship. *Macromolecules* **2007**, *40* (23), 8277–8284.
- (50) Packter, A.; Nerurkar, M. S. Crystallization in Films of Polar Vinyl Polymers - I. Crystallinity of Polyvinyl Alcohol Films Prepared by Evaporation of Aqueous Solutions. *Eur. Polym. J.* **1968**, *4*, 685–693.
- (51) Fong, R. J.; Robertson, A.; Mallon, P. E.; Thompson, R. L. Polymers The Impact of Plasticizer and Degree of Hydrolysis on Free Volume of Poly ( Vinyl Alcohol ) Films. **2018**, 1–15.
- (52) Balani, K.; Verma, V.; Agarwal, A.; Narayan, R. Physical, Thermal, and Mechanical Properties of

- Polymers. *Biosurfaces* **2015**, 329–344.
- (53) Tadokoro, H.; Seki, S.; Nitta, I. The Crystallinity of Solid High Polymers. I. The Crystallinity of Polyvinyl Alcohol Film. *Bull. Chem. Soc. Jpn.* **1955**, *28* (8), 559–564.
- (54) Horii, F.; Hu, S.; Ito, T.; Odani, H.; Kitamaru, R.; Matsuzawa, S.; Yamaura, K. Cross Polarization/Magic Angle Spinning <sup>13</sup>C n.m.r. Study of Solid Structure and Hydrogen Bonding of Poly(Vinyl Alcohol) Films with Different Tacticities. *Polymer (Guildf)*. **1992**, *33* (11), 2299–2306.
- (55) Hu, S.; Tsuji, M.; Horii, F. Phase Structure of Poly(Vinyl Alcohol) Single Crystals as Revealed by High-Resolution Solid-State <sup>13</sup>C n.m.r. Spectroscopy. *Polymer (Guildf)*. **1994**, *35* (12), 2516–2522.
- (56) Masuda, K.; Horii, F. CP/MAS <sup>13</sup>C NMR Analyses of the Chain Conformation and Hydrogen Bonding for Frozen Poly(Vinyl Alcohol) Solutions. *Macromolecules* **1998**, *31* (17), 5810–5817.
- (57) Thomas, D.; Zhuravlev, E.; Wurm, A.; Schick, C.; Cebe, P. Fundamental Thermal Properties of Polyvinyl Alcohol by Fast Scanning Calorimetry. *Polymer (Guildf)*. **2018**, *137*, 145–155.
- (58) Lue, S. J.; Chen, J. Y.; Yang, J. M. Crystallinity and Stability of Poly(Vinyl Alcohol)-Fumed Silica Mixed Matrix Membranes. *J. Macromol. Sci. Part B Phys.* **2008**, *47* (1), 39–51.
- (59) Sakurada, I.; Fuchino, K.; Okada, N. Crystal Structure of Polyvinyl Alcohol. *Dep. Bull. Pap. Kyoto Univ.* **1950**, *23*, 78–79.
- (60) Bunn, C. W. Crystal Structure of Polyvinyl Alcohol. *Nature* **1948**, *161*, 929–930.
- (61) Colvin, B. G. Crystal Structure of Polyvinyl Alcohol. *Nature* **1974**, *248* (April), 756–759.
- (62) Keller, A. A Note on Single Crystals in Polymers: Evidence for a Folded Chain Configuration. *Philos. Mag.* **1957**, *2* (21), 1171–1175.
- (63) Hassan, C. M.; Peppas, N. A. Structure and Applications of Poly (Vinyl Alcohol) Hydrogels Produced by Conventional Crosslinking or by Freezing / Thawing Methods. *Adv. Polym. Sci.* **2000**, *153*, 37–65.
- (64) Ma, Y.; Hu, W.; Reiter, G. Lamellar Crystal Orientations Biased by Crystallization Kinetics in Polymer Thin Films. *Macromolecules* **2006**, *39* (15), 5159–5164.
- (65) Alsleben, M.; Schick, C. The Melting of Polymers - a Three-Phase Approach. *Thermochim. Acta* **1994**, *238* (C), 203–227.
- (66) Krimm, S.; Liang, C. Y.; Sutherland, G. B. B. M. Infrared Spectra of High Polymers. V. Polyvinyl Alcohol. *J. Polym. Sci.* **1956**, *22* (10), 227–247.
- (67) Assender, H. E.; Windle, A. H. Crystallinity in Poly(Vinyl Alcohol) 2. Computer Modelling of Crystal Structure over a Range of Tacticities. *Polymer (Guildf)*. **1998**, *39* (18), 4303–4312.
- (68) Cho, J. D.; Lyoo, W. S.; Chvalun, S. N.; Blackwell, J. X-Ray Analysis and Molecular Modeling of Poly(Vinyl Alcohol)s with Different Stereoregularities. *Macromolecules* **1999**, *32* (19), 6236–6241.
- (69) Kenney, J. F.; Willcockson, G. W. Structure–Property Relationships of Poly(Vinyl Alcohol). III. Relationships between Stereo-Regularity, Crystallinity, and Water Resistance in Poly(Vinyl Alcohol). *J. Polym. Sci. Part A-1 Polym. Chem.* **1966**, *4* (3), 679–698.
- (70) De Kesel, C.; Lefèvre, C.; Nagy, J. B.; David, C. Blends of Polycaprolactone with Polyvinylalcohol: A DSC, Optical Microscopy and Solid State NMR Study. *Polymer (Guildf)*. **1999**, *40* (8), 1969–1978.
- (71) Heberer, D. P.; Cheng, S. Z. D.; Barley, J. S.; Lien, S. H. S.; Bryant, R. G.; Harris, F. W. Crystallization and Morphology of Semicrystalline Polyimides. *Macromolecules* **1991**, *24* (8), 1890–1898.
- (72) Cheng, S. Z. D.; Cao, M. Y.; Wunderlich, B. Glass Transition and Melting Behavior of Poly(Oxy-1,4-Phenyleneoxy-1,4-Phenylenecarbonyl-1,4-Phenylene). *Macromolecules* **1986**, *19* (7), 1868–1876.
- (73) Roberts, J. D.; Caserio, M. C. *Basic Principles of Organic Chemistry*; 1977.
- (74) Finch, C. A. *Polyvinyl Alcohol: Properties and Applications*; Wiley, New York, 1973.
- (75) Flory, P. J.; Mark, J. E.; Abe, A. Random-Coil Configurations of Vinyl Polymer Chains. The Influence of Stereoregularity on the Average Dimensions. *J. Am. Chem. Soc.* **1966**, *88* (4), 639–650.
- (76) Carraher, C. E. *Polymer Chemistry. Sixth Edition Revised and Expanded*; Lagowski, J. J., Ed.; New York, 2003.
- (77) Masuda, K.; Kaji, H.; Horii, F. CP/MAS <sup>13</sup>C NMR Analyses of Hydrogen Bonding and the Chain Conformation in the Crystalline and Noncrystalline Regions for Poly(Vinyl Alcohol) Films. *J. Polym. Sci. Part B Polym. Phys.* **2000**, *38* (1), 1.
- (78) Bhunia, K.; Sablani, S. S.; Tang, J.; Rasco, B. Migration of Chemical Compounds from Packaging Polymers during Microwave, Conventional Heat Treatment, and Storage. *Compr. Rev. Food Sci. Food Saf.* **2013**, *12* (5), 523–545.
- (79) Dey, A. S. Thermal Properties of Polymers <https://textilestudycenter.com/thermal-properties-of-polymers/> (accessed 2021 -06 -01).
- (80) Mohsin, M.; Hossin, A.; Haik, Y. Thermal and Mechanical Properties of Poly(Vinyl Alcohol) Plasticized with Glycerol. *J. Appl. Polym. Sci.* **2011**, *122* (5), 3102–3109.
- (81) Verrall, A. P.; Bening, P. S.; Kugler, K. A. Polyvinyl Alcohol Complymer Film for Packaging Liquid

- Products and Having an Improved Shelf-Life, 2010.
- (82) Jang, J.; Lee, D. K. Plasticizer Effect on the Melting and Crystallization Behavior of Polyvinyl Alcohol. *Polymer (Guildf)*. **2003**, *44* (26), 8139–8146.
- (83) Liang, S.; Huang, Q.; Liu, L.; Yam, K. L. Microstructure and Molecular Interaction in Glycerol Plasticized Chitosan/Poly(Vinyl Alcohol) Blending Films. *Macromol. Chem. Phys.* **2009**, *210* (10), 832–839.
- (84) Dai, L.; Li, J.; Yamada, E. Effect of Glycerin on Structure Transition of PVA/SF Blends. *J. Appl. Polym. Sci.* **2002**, *86* (9), 2342–2347.
- (85) Sakellariou, P.; Hassan, A.; Rowe, R. C. Plasticization of Aqueous Poly(Vinyl Alcohol) and Hydroxypropyl Methylcellulose with Polyethylene Glycols and Glycerol. *Eur. Polym. J.* **1993**, *29* (7), 937–943.
- (86) Marcilla, A.; Beltran, M.; Wypych, G. 5. Mechanism of Plasticizers Action - Handbook of Plasticizers (Second Edition); William Andrew Publishing: Boston, 2012; pp 119–133.
- (87) Daniels, P. H. A Brief Overview of Theories of PVC Plasticization and Methods Used to Evaluate PVC-Plasticizer Interaction. *J. Vinyl Addit. Technol.* **2009**, *15* (4), 219–223.
- (88) Ueberreiter, K.; Kanig, G. Self-Plasticization of Polymers. *J. Colloid Sci.* **1952**, *7* (6), 569–583.
- (89) Lourdin, D.; Coignard, L.; Bizot, H.; Colonna, P. Influence of Equilibrium Relative Humidity and Plasticizer Concentration on the Water Content and Glass Transition of Starch Materials. *Polymer (Guildf)*. **1997**, *38* (21), 5401–5406.
- (90) Lipson, J. E. G. Global and Local Views of the Glass Transition in Mixtures. *Macromolecules* **2020**, *53* (17), 7219–7223.
- (91) Stukalin, E. B.; Douglas, J. F.; Freed, K. F. Plasticization and Antiplasticization of Polymer Melts Diluted by Low Molar Mass Species. *J. Chem. Phys.* **2010**, *132* (8), 84504.
- (92) Mascia, L.; Kouparitsas, Y.; Nocita, D.; Bao, X. Antiplasticization of Polymer Materials: Structural Aspects and Effects on Mechanical and Diffusion-Controlled Properties. *Polymers (Basel)*. **2020**, *12* (4).
- (93) Wypych, G. 7. Plasticizer Motion and Diffusion - Handbook of Plasticizers (Second Edition). William Andrew Publishing: Boston 2012, pp 165–185.
- (94) Arvanitoyannis, I. S.; Bosnea, L. Migration of Substances from Food Packaging Materials to Foods. *Crit. Rev. Food Sci. Nutr.* **2004**, *44* (2), 63–76.
- (95) Wei, X.-F.; Linde, E.; Hedenqvist, M. S. Plasticiser Loss from Plastic or Rubber Products through Diffusion and Evaporation. *npj Mater. Degrad.* **2019**, *3* (1), 18.
- (96) Bellobono, I. R.; Marcandalli, B.; Selli, E.; Polissi, A.; Leidi, G. A Model Study for Release of Plasticizers from Polymer Films through Vapor Phase. *J. Appl. Polym. Sci.* **1984**, *29* (10), 3185–3195.
- (97) Sinha, A.; Sharma, B. P. Preparation of Copper Powder by Glycerol Process. *Mater. Res. Bull.* **2002**, *37* (3), 407–416.
- (98) Mo, C.; Yuan, W.; Lei, W.; Shijiu, Y. Effects of Temperature and Humidity on the Barrier Properties of Biaxially-Oriented Polypropylene and Polyvinyl Alcohol Films. **2014**, *6* (1), 40–46.
- (99) Wu, S.; Yan, G.; Lian, Z.; Chen, X.; Zhou, B.; He, S. An Open-Cavity Fabry-Perot Interferometer with PVA Coating for Simultaneous Measurement of Relative Humidity and Temperature. *Sensors Actuators B Chem.* **2016**, *225*, 50–56.
- (100) Zhang, W. Z.; Satoh, M.; Komiyama, J. A Differential Scanning Calorimetry Study of the States of Water in Swollen Poly(Vinyl Alcohol) Membranes Containing Nonvolatile Additives. *J. Memb. Sci.* **1989**, *42* (3), 303–314.
- (101) Hodge, R. M.; Edward, G. H.; Simon, G. P. Water Absorption and States of Water in Semicrystalline Poly(Vinyl Alcohol) Films. *Polymer (Guildf)*. **1996**, *37* (8), 1371–1376.
- (102) Renugopalakrishnan, V.; Chandrakasan, G.; Moore, S.; Hutson, T. B.; Berney, C. V.; Bhatnagar, R. S. Bound Water in Collagen: Evidence from Fourier Transform Infrared and Fourier Transform Infrared Photoacoustic Spectroscopic Study. *Macromolecules* **1989**, *22* (10), 4121–4124.
- (103) Kumaki, J.; Nishikawa, Y.; Hashimoto, T. Visualization of Single-Chain Conformations of a Synthetic Polymer with Atomic Force Microscopy. *J. Am. Chem. Soc.* **1996**, *118* (13), 3321–3322.
- (104) Panaitescu, D. M.; Frone, A. N.; Ghiurea, M.; Chiulan, I. Influence of Storage Conditions on Starch/PVA Films Containing Cellulose Nanofibers. *Ind. Crops Prod.* **2015**, *70*, 170–177.
- (105) Manoli, K.; Goustouridis, D.; Chatzandroulis, S.; Raptis, I.; Valamontes, E. S.; Sanopoulou, M. Vapor Sorption in Thin Supported Polymer Films Studied by White Light Interferometry. *Polymer (Guildf)*. **2006**, *47* (17), 6117–6122.
- (106) Ji, Y.; Hui, F.; Shi, Y.; Han, T.; Song, X.; Pan, C.; Lanza, M. Note: Fabrication of a Fast-Response and User-Friendly Environmental Chamber for Atomic Force Microscopes. *Rev. Sci. Instrum.* **2015**, *86* (10), 106105.
- (107) Maxwell, J. M.; Huson, M. G. Using the Scanning Probe Microscope to Measure the Effect of Relative

- Humidity on Sample Stiffness. *Rev. Sci. Instrum.* **2002**, 73 (10), 3520–3524.
- (108) Lievonon, J.; Ranttila, K.; Ahlskog, M. Environmental Chamber for an Atomic Force Microscope. *Rev. Sci. Instrum.* **2007**, 78 (4), 43703.
- (109) McGill, R. A.; Paley, M. S.; Harris, J. M. Solvatochromic Characterization of Polymers. Effects of Relative Humidity. *Macromolecules* **1992**, 25 (12), 3015–3019.
- (110) Zepeda, S.; Yeh, Y.; Orme, C. A. Atomic Force Microscope Chamber for in Situ Studies of Ice. *Rev. Sci. Instrum.* **2001**, 72 (11), 4159–4163.
- (111) Greenspan, L. Low Frost-Point Humidity Generator. *J. Res. Natl. Bureau Stand. - A. Phys. Chem.* **1973**, 77A (5).
- (112) Alfa1; Kishan, H.; Singh, B. Mixed Flow Relative Humidity Generator. *MAPAN-Journal Metrol. Soc. India* **2017**, 23 (1), 1–4.
- (113) Hansen, K. V.; Wu, Y.; Jacobsen, T.; Mogensen, M. B.; Theil Kuhn, L. Improved Controlled Atmosphere High Temperature Scanning Probe Microscope. *Rev. Sci. Instrum.* **2013**, 84 (7), 73701.
- (114) Tolstikhina, A. L.; Gainutdinov, R. V.; Zhanavskina, M. L.; Sorokina, K. L.; Belugina, N. V.; Grishchenko, Y. V.; Shestakov, V. D. Clean Boxes with Artificial Climate for Atomic Force Microscopy: New Possibilities for Diagnostics of Nanodimensional Objects. *Russ. Microelectron.* **2009**, 38 (2), 110–117.
- (115) Wexler, A.; Hasegawa, S. Relative Humidity-Temperature Relationships of Some Saturated Salt Solutions in the Temperature Range 0 Degree to 50 Degrees C. **2011**, 1–8.
- (116) Carr, D. S.; Harris, B. L. Solutions for Maintaining Constant Relative Humidity. *Ind. Eng. Chem.* **1949**, 41 (9), 2014–2015.
- (117) Young, J. F. Humidity Control in the Laboratory Using Salt Solutions—a Review. *J. Appl. Chem.* **1967**, 17 (9), 241–245.
- (118) Kosswig, K. Surfactants. In *Ullmann's Encyclopedia of Industrial Chemistry*; Wiley-VCH Verlag GmbH & Co. KGaA: Weinheim, Germany, 2000; p 18.
- (119) Zheng, Y.; Zheng, M.; Ma, Z.; Xin, B.; Guo, R.; Xu, X. Sugar Fatty Acid Esters. In *Polar Lipids*; Elsevier, 2015; pp 215–243.
- (120) Griffin, W. C. Classification of Surface-Active Agents by HLB. *J. Soc. Cosmet. Chem.* **1949**, 1 (5), 311–326.
- (121) Griffin, W. C. Calculation of HLB Values of Non-Ionic Surfactants. *J. Soc. Cosmet. Chem.* **1954**, 5 (4), 249–256.
- (122) Fong, R. Blooming Surfactants: Small Molecule Segregation from PVA Films, University of Durham, 2020.
- (123) Davies, J. T. Gas/Liquid and Liquid/Liquid Interface. *Proc. 2nd Int. Congr. Surf. Act.* **1957**, 1.
- (124) Baldwin, R. L. The New View of Hydrophobic Free Energy. *FEBS Lett.* **2013**, 587 (8), 1062–1066.
- (125) Hansson, P.; Lindman, B. Surfactant-Polymer Interactions. *Curr. Opin. Colloid Interface Sci.* **1996**, 1 (5), 604–613.
- (126) de la Guardia, M.; Armenta, S. Chapter 5 - Greening Sample Treatments. In *Green Analytical Chemistry*; Guardia, M. D. La, Armenta, S. B. T.-C. A. C., Eds.; Elsevier, 2011; Vol. 57, pp 87–120.
- (127) Shirahama, K.; Ide, N. The Interaction between Sodium Alkylsulfates and Poly(Ethylene Oxide) in 0.1 M NaCl Solutions. **1976**, 54 (3), 450–452.
- (128) Edler, K. J.; Wasbrough, M. J.; Holdaway, J. A.; O'Driscoll, B. M. D. Self-Assembled Films Formed at the Air - Water Interface from CTAB/SDS Mixtures with Water-Soluble Polymers. *Langmuir* **2009**, 25 (7), 4047–4055.
- (129) Campbell, R. A.; Edler, K. J. Growth-Collapse Mechanism of PEI-CTAB Films at the Air-Water Interface. *Soft Matter* **2011**, 7 (23), 11125–11132.
- (130) Tadros, T. F. The Interaction of Cetyltrimethylammonium Bromide and Sodium Dodecylbenzene Sulfonate with Polyvinyl Alcohol. Adsorption of the Polymer-Surfactant Complexes on Silica. *J. Colloid Interface Sci.* **1974**, 46 (3), 528–540.
- (131) Lee, L. T. Polymer-Surfactant Interactions: Neutron Scattering and Reflectivity. *Curr. Opin. Colloid Interface Sci.* **1999**, 4 (3), 205–213.
- (132) El Feky, A. A.; Shalaby, M. N.; El-Shamy, O. A. A.; Selim, S. A. Adsorption of Some Surfactants onto Polyvinyl Alcohol as Hydrophobic Polymer Surface. *J. Dispers. Sci. Technol.* **2010**, 31 (8), 1091–1099.
- (133) Penfold, J.; Tucker, I.; Thomas, R. K.; Zhang, J. Adsorption of Polyelectrolyte / Surfactant Mixtures at the Air - Water Interface : Modified Poly ( Ethyleneimine ) and Sodium Dodecyl Sulfate. *Langmuir* **2005**, 21 (22), 10061–10073.
- (134) Arai, H.; Horin, S.; Goods, H. Interaction between Polymer and Detergent in Aqueous Solution. *J. Colloid Interface Sci.* **1969**, 30 (3), 372–377.
- (135) Atanase, L. I.; Riess, G. Poly(Vinyl Alcohol-Co-Vinyl Acetate) Complex Formation with Anionic

- Surfactants Particle Size of Nanogels and Their Disaggregation with Sodium Dodecyl Sulfate. *Colloids Surfaces A Physicochem. Eng. Asp.* **2010**, 355 (1–3), 29–36.
- (136) Shirahama, K.; Nagao, S. Binding of Tetradecylpyridinium Bromide to Poly(Vinyl Alcohol) with Various Degrees of Acetylation. *Colloids and Surfaces* **1992**, 66 (4), 275–279.
- (137) Schaub, T. F.; Kellogg, G. J.; Mayes, A. M.; Kulasekera, R.; Ankner, J. F.; Kaiser, H. Surface Modification via Chain End Segregation in Polymer Blends. *Macromolecules* **1996**, 29 (11), 3982–3990.
- (138) Rezaei Kolahchi, A.; Ajji, A.; Carreau, P. J. Surface Morphology and Properties of Ternary Polymer Blends: Effect of the Migration of Minor Components. *J. Phys. Chem. B* **2014**, 118 (23), 6316–6323.
- (139) Hamley, I. W. Introduction to Soft Matter: Synthetic and Biological Self-Assembling Materials; John Wiley & Sons, 2013.
- (140) Lee, H.; Archer, L. A. Functionalizing Polymer Surfaces by Surface Migration of Copolymer Additives: Role of Additive Molecular Weight. *Polymer (Guildf)*. **2002**, 43 (9), 2721–2728.
- (141) Zanjanijam, A. R.; Hakim, S.; Azizi, H. Migration of the Plasticizer in the Compatibilized PP/PVB Blends: Characterization and Thermodynamic Calculations. *Polym. Bull.* **2018**, 75 (10), 4671–4689.
- (142) Harkins, W. D.; Fieldman, A.; Feldman, A. Films. The Spreading of Liquids and the Spreading Coefficient. *J. Am. Chem. Soc.* **1922**, 44 (12), 2665–2685.
- (143) Taguet, A.; Huneault, M. A.; Favis, B. D. Interface/Morphology Relationships in Polymer Blends with Thermoplastic Starch. *Polymer (Guildf)*. **2009**, 50 (24), 5733–5743.
- (144) Larson, R. G. Self-assembly of Surfactant Liquid Crystalline Phases by Monte Carlo Simulation. *J. Chem. Phys.* **1989**, 91 (4), 2479–2488.
- (145) Krause, S. Polymer–Polymer Compatibility. In *Polymer Blends*; Elsevier, 1978; pp 15–113.
- (146) Liu, Y.; Wu, Z.; Zhao, Y. Liquid-Liquid Equilibrium Correlation of Aqueous Two-Phase Systems Composed of Polyethylene Glycol and Nonionic Surfactant. *Thermochim. Acta* **2015**, 602, 78–86.
- (147) Hildebrand, J. H. A Critique of the Theory of Solubility of Non-Electrolytes. *Chem. Rev.* **1948**, 37–45.
- (148) Leighton, D.; Acrivos, A. The Shear-Induced Migration of Particles in Concentrated Suspensions. *J. Fluid Mech.* **1987**, 181, 415–439.
- (149) Jendrejack, R. M.; Schwartz, D. C.; De Pablo, J. J.; Graham, M. D. Shear-Induced Migration in Flowing Polymer Solutions: Simulation of Long-Chain Deoxyribose Nucleic Acid in Microchannels. *J. Chem. Phys.* **2004**, 120 (5), 2513–2529.
- (150) Agarwal, U. S.; Dutta, A.; Mashelkar, R. A. Migration of Macromolecules under Flow: The Physical Origin and Engineering Implications. *Chem. Eng. Sci.* **1994**, 49 (11), 1693–1717.
- (151) Hsu, S. C.; Lin-Vien, D.; French, R. N. Probing the Concentration Profiles of Additives in Polymers by IR Microspectroscopy: The Diffusion of Cyasorb UV531 in Polypropylene. *Appl. Spectrosc.* **1992**, 46 (2), 225–228.
- (152) Haider, N.; Karlsson, S. Kinetics of Migration of Antioxidants from Polyolefins in Natural Environments as a Basis for Bioconversion Studies. *Biomacromolecules* **2000**, 1 (3), 481–487.
- (153) Research, D.-G. for; European Commission, I. Evaluation of Migration Models to Be Used under Directive 90/128/EEC.; Publications Office of the European Union, 2004.
- (154) Fang, X.; Vitrac, O. Predicting Diffusion Coefficients of Chemicals in and through Packaging Materials. *Crit. Rev. Food Sci. Nutr.* **2015**, 57 (2), 275–312.
- (155) Fick, A. V. On I, Iquid Diffusion. *London, Edinburgh, Dublin Philos. Mag. J. Sci.* **1855**, 10 (63), 30–39.
- (156) Hansen, C. M. The Significance of the Surface Condition in Solutions to the Diffusion Equation: Explaining “Anomalous” Sigmoidal, Case II, and Super Case II Absorption Behavior. *Eur. Polym. J.* **2010**, 46 (4), 651–662.
- (157) Thomas, N. .; Windle, A. . A Theory of Case II Diffusion. *Polymer (Guildf)*. **1982**, 23 (4), 529–542.
- (158) Hui, C. -Y.; Wu, K. -C.; Lasky, R. C.; Kramer, E. J. Case-II Diffusion in Polymers. I. Transient Swelling. *J. Appl. Phys.* **1987**, 61 (11), 5129–5136.
- (159) Miller, C. C.; A, P. R. S. L. The Stokes-Einstein Law for Diffusion in Solution. *Proc. R. Soc. London. Ser. A, Contain. Pap. a Math. Phys. Character* **1924**, 106 (740), 724–749.
- (160) Masuda, A.; Ushida, K.; Okamoto, T. New Fluorescence Correlation Spectroscopy (FCS) Suitable for the Observation of Anomalous Diffusion in Polymer Solution: Time and Space Dependences of Diffusion Coefficients. *J. Photochem. Photobiol. A Chem.* **2006**, 183 (3), 304–308.
- (161) Michelman-Ribeiro, A.; Horkay, F.; Nossal, R.; Boukari, H. Probe Diffusion in Aqueous Poly(Vinyl Alcohol) Solutions Studied by Fluorescence Correlation Spectroscopy. *Biomacromolecules* **2007**, 8 (5), 1595–1600.
- (162) Bu, Z.; Russo, P. S. Diffusion of Dextran in Aqueous (Hydroxypropyl)Cellulose. *Macromolecules* **1994**, 27 (5), 1187–1194.
- (163) Li, X.; Sakai, T. Mass Transport in Polymer Gels. In *Physics of Polymer Gels*; Wiley, 2020; pp 137–150.

- (164) Amsden, B. Solute Diffusion in Hydrogels. An Examination of the Retardation Effect. *Polym. Gels Networks* **1998**, *6* (1), 13–43.
- (165) Mustafa, M. B.; Tipton, D. L.; Barkley, M. D.; Russo, P. S.; Blum, F. D. Dye Diffusion in Isotropic and Liquid Crystalline Aqueous (Hydroxypropyl)Cellulose. *Macromolecules* **1993**, *26* (2), 370–378.
- (166) Phillies, G. D. J. Universal Scaling Equation for Self-Diffusion by Macromolecules in Solution. *Macromolecules* **1986**, *19* (9), 2367–2376.
- (167) Vrentas, J. S.; Duda, J. L. Diffusion in Polymer-Solvent Systems. I. Reexamination of the Free-Volume Theory. *J. Polym. Sci. Polym. Phys. Ed.* **1977**, *15*, 403–416.
- (168) Vrentas, J. S.; Duda, J. L. Diffusion in Polymer-Solvent Systems. II. A Predictive Theory for the Dependence of Diffusion Coefficient on Temperature, Concentration, and Molecular Weight. *J. Polym. Sci. Polym. Phys. Ed.* **1977**, *15* (12), 417–439.
- (169) Cohen, M. H.; Turnbull, D. Molecular Transport in Liquids and Glasses. *J. Chem. Phys.* **1959**, *31* (5), 1164–1169.
- (170) Masaro, L.; Zhu, X. X. Physical Models of Diffusion for Polymer Solutions, Gels and Solids. *Prog. Polym. Sci.* **1999**, *24* (5), 731–775.
- (171) Park, I. H.; Johnson, C. S.; Hill, C.; Carolina, N.; Gabriel, D. A. Probe Diffusion in Polyacrylamide Gels As Observed by Means of Holographic Relaxation Methods: Search for a Universal Equation. *Macromolecules* **1990**, *23* (5), 1548–1553.
- (172) Bucknall, D. G.; Higgins, J. S.; Butler, S. A. Real-Time Neutron Reflectivity Study of the Early Stages of Diffusion into and Dissolution of Glassy Polymers. *J Polym Sci Part B Polym Phys* **2004**, *42*, 3267–3281.
- (173) Tseng, K. C.; Turro, N. J.; Durning, C. J. Molecular Mobility in Polymer Thin Films. *Phys. Rev. E* **2000**, *61* (2), 1800–1811.
- (174) Petri, D. F. S. Characterization of Spin-Coated Polymer Films. *J. Braz. Chem. Soc.* **2002**, *13* (5), 695–699.
- (175) Kojima, Y.; Furuhashi, K.; Miyasaka, K. Diffusive Permeability of Solutes in Poly(Vinyl Alcohol) Membranes as a Function of the Degree of Hydration. *J. Appl. Polym. Sci.* **1983**, *29* (2), 533–546.
- (176) J Crank. *The Mathematics of Diffusion*; 1979.
- (177) Morita, R.; Honda, R.; Takahashi, Y. Development of Oral Controlled Release Preparations, a PVA Swelling Controlled Release System (SCRS). I. Design of SCRS and Its Release Controlling Factor. *J. Control. Release* **2000**, *63* (3), 297–304.
- (178) Siepmann, J.; Peppas, N. A. Higuchi Equation: Derivation, Applications, Use and Misuse. *Int. J. Pharm.* **2011**, *418* (1), 6–12.
- (179) Wan, L. S. C.; Lim, L. Y. Drug Release from Heat-Treated Polyvinyl Alcohol Films. *Drug Dev. Ind. Pharm.* **1992**, *18* (17), 1895–1906.
- (180) Lopes, J. F. A.; Simoneau, C. Solubility of Polyvinyl Alcohol in Ethanol. *EFSA Support. Publ.* **2014**, *11* (9).
- (181) Briddick, A. Exploring Surfactant and Plasticiser Segregation in Thin PVA Films, University of Durham, 2017.
- (182) Zhang, Z.; Moxey, M.; Alswieleh, A.; Morse, A. J.; Lewis, A. L.; Geoghegan, M.; Leggett, G. J. Effect of Salt on Phosphorylcholine-Based Zwitterionic Polymer Brushes. *Langmuir* **2016**, *32* (20), 5048–5057.
- (183) Alessandrini, A.; Facci, P. AFM: A Versatile Tool in Biophysics. *Meas. Sci. Technol.* **2005**, *16* (6), R65–R92.
- (184) Liu, S.; Wang, Y. Application of AFM in Microbiology: A Review. *Scanning* **2010**, *32* (2), 61–73.
- (185) NanoAndMore GMBH. What is Atomic Force Microscopy (AFM) <https://www.nanoandmore.com/what-is-atomic-force-microscopy> (accessed 2021 -06 -01).
- (186) Liamas, E. Interactions between Proteins and Biomaterials - an Experimental and Computational Multiscale Study, University of Birmingham, 2017.
- (187) Gan, Y. Atomic and Subnanometer Resolution in Ambient Conditions by Atomic Force Microscopy. *Surf. Sci. Rep.* **2009**, *64* (3), 99–121.
- (188) Kawai, A. Cohesion Property of Polymer Aggregates in Resist Pattern Analyzed by Atomic Force Microscope (AFM). *J. Photopolym. Sci. Technol.* **2002**, *15* (3), 371–376.
- (189) Ton-That, C.; Shard, A. G.; Bradley, R. H. Thickness of Spin-Cast Polymer Thin Films Determined by Angle-Resolved XPS and AFM Tip-Scratch Methods. *Langmuir* **2000**, *16* (5), 2281–2284.
- (190) Kiriy, A.; Gorodyska, G.; Minko, S.; Tsitsilianis, C.; Jaeger, W.; Stamm, M. Chemical Contrasting in a Single Polymer Molecule AFM Experiment. *J. Am. Chem. Soc.* **2003**, *125* (37), 11202–11203.
- (191) Murat, M.; Grest, G. S. Molecular Dynamics Simulations of the Force between a Polymer Brush and an AFM Tip. *Macromolecules* **1996**, *29* (25), 8282–8284.
- (192) Fractured Polymer/Silica Fiber Surface Studied by Tapping Mode Atomic Force Microscopy. *Surf. Sci.* **1993**, *290* (1–2), L688–L692.

- (193) Haugstad, G.; Jones, R. R. Mechanisms of Dynamic Force Microscopy on Polyvinyl Alcohol: Region-Specific Non-Contact and Intermittent Contact Regimes. *Ultramicroscopy* **1999**, *76* (1–2), 77–86.
- (194) Strawhecker, K. E.; Manias, E. AFM of Poly(Vinyl Alcohol) Crystals Next to an Inorganic Surface. *Macromolecules* **2001**, *34* (24), 8475–8482.
- (195) Ton-That, C.; Shard, A. G.; Teare, D. O. H.; Bradley, R. H. XPS and AFM Surface Studies of Solvent-Cast PS/PMMA Blends. *Polymer (Guildf)*. **2001**, *42* (3), 1121–1129.
- (196) Lee, K. S.; Ivanova, N.; Starov, V. M.; Hilal, N.; Dutschk, V. Kinetics of Wetting and Spreading by Aqueous Surfactant Solutions. *Adv. Colloid Interface Sci.* **2008**, *144* (1–2), 54–65.
- (197) Thundat, T.; Zheng, X. Y.; Chen, G. Y.; Warmack, R. J. Role of Relative Humidity in Atomic Force Microscopy Imaging. *Surf. Sci. Lett.* **2017**, *294* (1–2), L939–L943.
- (198) Sugawara, Y.; Ohta, M.; Konishi, T.; Morita, S.; Suzuki, M.; Enomoto, Y. Effects of Humidity and Tip Radius on the Adhesive Force Measured with Atomic Force Microscopy. *Wear* **1993**, *168* (1–2), 13–16.
- (199) Ondarçuhu, T.; Fabié, L. Capillary Forces in Atomic Force Microscopy and Liquid Nanodispensing. In *Surface Tension in Microsystems. Microtechnology and MEMS*; 2013; pp 279–305.
- (200) Zitzler, L.; Herminghaus, S.; Mugele, F. G. Capillary forces in tapping mode atomic force microscopy. *Phys. Rev. B* **2002**, *66* (15), 8432.
- (201) Belikov, S.; Alexander, J.; Wall, C.; Yermolenko, I.; Magonov, S.; Malovichko, I. Thermal Tune Method for AFM Oscillatory Resonant Imaging in Air and Liquid. In *2014 American Control Conference*; IEEE, 2014; pp 1009–1014.
- (202) Badia, A.; Demers, L.; Dickinson, L.; Morin, F. G.; Lennox, R. B.; Reven, L. Gold–Sulfur Interactions in Alkylthiol Self-Assembled Monolayers Formed on Gold Nanoparticles Studied by Solid-State NMR. *J. Am. Chem. Soc.* **1997**, *119* (45), 11104–11105.
- (203) Wang, H.; Chen, S.; Li, L.; Jiang, S. Improved Method for the Preparation of Carboxylic Acid and Amine Terminated Self-Assembled Monolayers of Alkanethiolates. *Langmuir* **2005**, *21* (7), 2633–2636.
- (204) Frank, B.; Gast, A. P.; Russell, T. P.; Brown, H. R.; Hawker, C. Polymer Mobility in Thin Films. *Macromolecules* **1996**, *29* (20), 6531–6534.
- (205) Jourdainne, L.; Lecuyer, S.; Arntz, Y.; Picart, C.; Schaaf, P.; Senger, B.; Voegel, J.-C.; Lavalle, P.; Charitat, T. Dynamics of Poly(1-Lysine) in Hyaluronic Acid/Poly(1-Lysine) Multilayer Films Studied by Fluorescence Recovery after Pattern Photobleaching. *Langmuir* **2008**, *24* (15), 7842–7847.
- (206) Raz-Ben Aroush, D.; Ofer, N.; Abu-Shah, E.; Allard, J.; Krichevsky, O.; Mogilner, A.; Keren, K. Actin Turnover in Lamellipodial Fragments. *Curr. Biol.* **2017**, *27* (19), 2963–2973.
- (207) Hauser, G. I.; Seiffert, S.; Opperman, W. Systematic Evaluation of FRAP Experiments Performed in a Confocal Laser Scanning Microscope – Part II: Multiple Diffusion Processes. *J. Microsc.* **2008**, *230* (3), 353–362.
- (208) Van Keuren, E.; Schrof, W. Fluorescence Recovery after Two-Photon Bleaching for the Study of Dye Diffusion in Polymer Systems. *Macromolecules* **2003**, *36* (13), 5002–5007.
- (209) Pinte, J.; Joly, C.; Plé, K.; Dole, P.; Feigenbaum, A. Proposal of a Set of Model Polymer Additives Designed for Confocal FRAP Diffusion Experiments. *J. Agric. Food Chem.* **2008**, *56* (21), 10003–10011.
- (210) Seiffert, S.; Oppermann, W. Diffusion of Linear Macromolecules and Spherical Particles in Semidilute Polymer Solutions and Polymer Networks. *Polymer (Guildf)*. **2008**, *49* (19), 4115–4126.
- (211) Van Keuren, E.; Schrof, W. Two-Photon Pattern Bleaching for Characterizing Structural Changes in Polymer Films. *Macromol. Rapid Commun.* **2002**, *23* (18), 1138–1140.
- (212) Ishitobi, H.; Shoji, S.; Hiramatsu, T.; Sun, H.-B.; Sekkat, Z.; Kawata, S. Two-Photon Induced Polymer Nanomovement. *Opt. Express* **2008**, *16* (18), 14106–14114.
- (213) Kang, M.; Day, C. A.; Kenworthy, A. K.; DiBenedetto, E. Simplified Equation to Extract Diffusion Coefficients from Confocal FRAP Data. *Traffic* **2012**, *13* (12), 1589–1600.
- (214) Schwille, P.; Haustein, E. Fluorescence Correlation Spectroscopy. An Introduction to Its Concepts and Applications. *Doi:10.1002/Lpor.200910041* **2001**, 1–33.
- (215) Wöll, D. Fluorescence Correlation Spectroscopy in Polymer Science. *RSC Adv.* **2014**, *4* (5), 2447–2465.
- (216) Molecular Biophysics Fradin Research Group. Fluorescence Correlation Spectroscopy <https://physwww.physics.mcmaster.ca/~biophys/molbiophys/FCS.html> (accessed 2021 -06 -01).
- (217) Picoquant. Fluorescence Correlation Spectroscopy (FCS) <https://www.picoquant.com/applications/category/life-science/fluorescence-correlation-spectroscopy-fcs> (accessed 2021 -06 -01).
- (218) Tomaszewska, E.; Soliwoda, K.; Kadziola, K.; Tkacz-Szczesna, B.; Celichowski, G.; Cichomski, M.; Szmaja, W.; Grobelny, J. Detection Limits of DLS and UV-Vis Spectroscopy in Characterization of Polydisperse Nanoparticles Colloids. *J. Nanomater.* **2013**, *2013*, 1–10.
- (219) Hassan, P. A.; Rana, S.; Verma, G. Making Sense of Brownian Motion: Colloid Characterization by



- Dynamic Light Scattering. *Langmuir* **2015**, *31* (1), 3–12.
- (220) Stetefeld, J.; McKenna, S. A.; Patel, T. R. Dynamic Light Scattering: A Practical Guide and Applications in Biomedical Sciences. *Biophys. Rev.* **2016**, *8* (4), 409–427.
- (221) Malvern Instruments. Calculating Volume Distributions from Dynamic Light Scattering Data; 2021.
- (222) Malvern Instruments Worldwide. A Basic Introduction to Rheology <https://cdn.technologynetworks.com/TN/Resources/PDF/WP160620BasicIntroRheology.pdf> (accessed 2021 -06 -01).
- (223) Pamies, R.; Lopez Martinez, M. C.; Hernandez Cifre, J. G.; Garcia de la Torre, J. Non-Newtonian Viscosity of Dilute Polymer Solutions. *Macromolecules* **2005**, *38* (4), 1371–1377.
- (224) Shakouri, A.; Ahmari, H.; Hojjat, M.; Zeinali Heris, S. Effect of TiO<sub>2</sub> Nanoparticle on Rheological Behavior of Poly(Vinyl Alcohol) Solution. *J. Vinyl Addit. Technol.* **2017**, *23* (3), 234–240.
- (225) Wilkinson, J. The Latest Developments in Dynamic Vapour Sorption (DVS) <https://www.azom.com/article.aspx?ArticleID=13001> (accessed 2021 -06 -01).
- (226) Good, R. J. Contact Angle, Wetting, and Adhesion: A Critical Review. *J. Adhes. Sci. Technol.* **1992**, *6* (12), 1269–1302.
- (227) DataPhysics Instruments GmbH. Contact angle <https://www.dataphysics-instruments.com/knowledge/understanding-interfaces/contact-angle/>. (accessed 2021 -06 -01).
- (228) Marmur, A. Advances in Colloid and Interface Science, 19 (1983) 75–102. **1983**, *19*, 75–102.
- (229) Dutschik, V.; Sabbatovskiy, K. G.; Stolz, M.; Grundke, K.; Rudoy, V. M. Unusual Wetting Dynamics of Aqueous Surfactant Solutions on Polymer Surfaces. **2003**, *267*, 456–462.
- (230) Farris, S.; Introzzi, L.; Biagioni, P.; Holz, T.; Schiraldi, A.; Piergiovanni, L. Wetting of Biopolymer Coatings: Contact Angle Kinetics and Image Analysis Investigation. *Langmuir* **2011**, *27* (12), 7563–7574.
- (231) Hejda, F.; Solař, P.; Kousal, J. Surface Free Energy Determination by Contact Angle Measurements – A Comparison of Various Approaches. *WDS'10 Proc. Contrib. Pap.* **2010**, No. 3, 25–30.
- (232) Binks, B. P.; Clint, J. H. Solid Wettability from Surface Energy Components: Relevance to Pickering Emulsions. *Langmuir* **2002**, *18* (4), 1270–1273.
- (233) Jańczuk, B.; Wójcik, W.; Zdziennicka, A. Determination of the Components of the Surface Tension of Some Liquids from Interfacial Liquid-Liquid Tension Measurements. *J. Colloid Interface Sci.* **1993**, *157* (2), 384–393.
- (234) Shimizu, R. N.; Demarquette, N. R. Evaluation of Surface Energy of Solid Polymers Using Different Models. *J. Appl. Polym. Sci.* **2000**, *76* (12), 1831–1845.
- (235) Bradley, M. Introduction to FTIR spectroscopy <https://www.thermofisher.com/uk/en/home/industrial/spectroscopy-elemental-isotope-analysis/spectroscopy-elemental-isotope-analysis-learning-center/molecular-spectroscopy-information/ftir-information/ftir-basics.html> (accessed 2021 -06 -01).
- (236) Kann, Y.; Shurgalin, M.; Krishnaswamy, R. K. FTIR Spectroscopy for Analysis of Crystallinity of Poly(3-Hydroxybutyrate-Co-4 -Hydroxybutyrate) Polymers and Its Utilization in Evaluation of Aging, Orientation and Composition. *Polym. Test.* **2014**, *40*, 218–224.
- (237) Mallapragada, S. K.; Narasimhan, B. Infrared Spectroscopy in Analysis of Polymer Crystallinity. *Encycl. Anal. Chem.* **2006**, 1–14.
- (238) Khanna, Y. P. Estimation of Polymer Crystallinity by Dynamic Mechanical Techniques. *J. Appl. Polym. Sci.* **1989**, *37* (9), 2719–2726.
- (239) Runt, J.; Kanchanasopa, M. Crystallinity Determination. *Encycl. Polym. Sci. Technol.* **2004**, *9* (2), 446–464.
- (240) Sreekumar, P. A.; Al-Harathi, M. A.; De, S. K. Effect of Glycerol on Thermal and Mechanical Properties of Polyvinyl Alcohol/Starch Blends. *J. Appl. Polym. Sci.* **2012**, *123* (1), 135–142.
- (241) Lee, J.; Jin Lee, K.; Jang, J. Effect of Silica Nanofillers on Isothermal Crystallization of Poly(Vinyl Alcohol): In-Situ ATR-FTIR Study. *Polym. Test.* **2008**, *27* (3), 360–367.
- (242) Mansur, H. S.; Sadahira, C. M.; Souza, A. N.; Mansur, A. A. P. FTIR Spectroscopy Characterization of Poly (Vinyl Alcohol) Hydrogel with Different Hydrolysis Degree and Chemically Crosslinked with Glutaraldehyde. *Mater. Sci. Eng. C* **2008**, *28* (4), 539–548.
- (243) Chan, K. S.; Senin, H. B.; Naimah, I. Structural and Mechanical Properties of Polyvinyl Alcohol (PVA) Thin Film. *AIP Conf. Proc.* **2009**, *1136*, 366–369.
- (244) Döppers, L. M.; Breen, C.; Sammon, C. Diffusion of Water and Acetone into Poly(Vinyl Alcohol)-Clay Nanocomposites Using ATR-FTIR. *Vib. Spectrosc.* **2004**, *35* (1–2), 27–32.
- (245) Zhang, Z. M.; Chen, S.; Liang, Y. Z. Baseline Correction Using Adaptive Iteratively Reweighted Penalized Least Squares. *Analyst* **2010**, *135* (5), 1138–1146.
- (246) Senanayake, K. K.; Fakhrabadi, E. A.; Liberatore, M. W.; Mukhopadhyay, A. Diffusion of Nanoparticles

- in Entangled Poly(Vinyl Alcohol) Solutions and Gels. *Macromolecules* **2019**, *52* (3), 787–795.
- (247) Slim, A. H.; Poling-Skutvik, R.; Conrad, J. C. Local Confinement Controls Diffusive Nanoparticle Dynamics in Semidilute Polyelectrolyte Solutions. *Langmuir* **2020**, *36* (31), 9153–9159.
- (248) Chan, T. C.; Li, H. T.; Li, K. Y. Effects of Shapes of Solute Molecules on Diffusion: A Study of Dependences on Solute Size, Solvent, and Temperature. *J. Phys. Chem. B* **2015**, *119* (51), 15718–15728.
- (249) Wypych, G. 8. Effect of Plasticizers on Other Components of Formulations - Handbook of Plasticizers (Second Edition); 2017.
- (250) Gratz, M.; Tschöpe, A. Size Effects in the Oscillatory Rotation Dynamics of Ni Nanorods in Poly(Ethylene Oxide) Solutions. *Macromolecules* **2019**, *52* (17), 6600–6612.
- (251) Cherdhirankorn, T.; Harmandaris, V.; Juhari, A.; Voudouris, P.; Fytas, G.; Kremer, K.; Koynov, K. Fluorescence Correlation Spectroscopy Study of Molecular Probe Diffusion in Polymer Melts. *Macromolecules* **2009**, *42* (13), 4858–4866.
- (252) Senanayake, K. K.; Shokeen, N.; Fakhrabadi, E. A.; Liberatore, M. W.; Mukhopadhyay, A. Diffusion of Nanoparticles within a Semidilute Polyelectrolyte Solution. *Soft Matter* **2019**, *15* (38), 7616–7622.
- (253) Wang, W.; Barkai, E.; Burov, S. Large Deviations for Continuous Time Random Walks. *Entropy* **2020**, *22* (6), 697–719.
- (254) Xue, C.; Shi, X.; Tian, Y.; Zheng, X.; Hu, G. Diffusion of Nanoparticles with Activated Hopping in Crowded Polymer Solutions. *Nano Lett.* **2020**, *20* (5), 3895–3904.
- (255) Jia, D.; Muthukumar, M. Electrostatically Driven Topological Freezing of Polymer Diffusion at Intermediate Confinements. *Phys. Rev. Lett.* **2021**, *126* (5), 057802.
- (256) Banks, D. S.; Tressler, C.; Peters, R. D.; Höfling, F.; Fradin, C. Characterizing Anomalous Diffusion in Crowded Polymer Solutions and Gels over Five Decades in Time with Variable-Lengthscale Fluorescence Correlation Spectroscopy. *Soft Matter* **2016**, *12* (18), 4190–4203.
- (257) Guillemet, F.; Piculell, L. Interactions in Aqueous Mixtures of Hydrophobically Modified Polyelectrolyte and Oppositely Charged Surfactant. Mixed Micelle Formation and Associative Phase Separation. *J. Phys. Chem.* **1995**, *99* (22), 9201–9209.
- (258) Langevin, D. Complexation of Oppositely Charged Polyelectrolytes and Surfactants in Aqueous Solutions. A Review. *Adv. Colloid Interface Sci.* **2009**, *147–148*, 170–177.
- (259) Lewis, K. E.; Robinson, C. P. The Interaction of Sodium Dodecyl Sulfate with Methyl Cellulose and Polyvinyl Alcohol. *J. Colloid Interface Sci.* **1970**, *32* (3), 539–546.
- (260) Qiu, L.; Cheng, M.; Xie, A.; Shen, Y. Study on the Viscosity of Cationic Gemini Surfactant–Nonionic Polymer Complex in Water. *J. Colloid Interface Sci.* **2004**, *278* (1), 40–43.
- (261) Negm, N. A.; Mohamed, A. S.; Ahmed, S. M.; El-Raouf, M. A. Polymer–Cationic Surfactant Interaction: 1. Surface and Physicochemical Properties of Polyvinyl Alcohol (PVA)-S-Alkyl Isothiouonium Bromide Surfactant Mixed Systems. *J. Surfactants Deterg.* **2015**, *18* (2), 245–250.
- (262) Trabelsi, S.; Guillot, S.; Ritacco, H.; Boué, F.; Langevin, D. Nanostructures of Colloidal Complexes Formed in Oppositely Charged Polyelectrolyte/Surfactant Dilute Aqueous Solutions. *Eur. Phys. J. E* **2007**, *23* (3), 305–311.
- (263) Babak, V. G.; Merkovich, E. A.; Desbrières, J.; Rinaudo, M. Formation of an Ordered Nanostructure in Surfactant–Polyelectrolyte Complexes Formed by Interfacial Diffusion. *Polym. Bull.* **2000**, *45*, 77–81.
- (264) Zana, R.; Lianos, P.; Lang, J. Fluorescence Probe Studies of the Interactions between Poly(Oxyethylene) and Surfactant Micelles and Microemulsion Droplets in Aqueous Solutions. *J. Phys. Chem.* **1985**, *89* (1), 41–44.
- (265) Annunziata, O.; Buzatu, D.; Albright, J. G. Protein Diffusion Coefficients Determined by Macroscopic-Gradient Rayleigh Interferometry and Dynamic Light Scattering. *Langmuir* **2005**, *21* (26), 12085–12089.
- (266) Ivanov, D. A.; Grossmann, T.; Winkelmann, J. Comparison of Ternary Diffusion Coefficients Obtained from Dynamic Light Scattering and Taylor Dispersion. *Fluid Phase Equilib.* **2005**, *228–229*, 283–291.
- (267) Wang, S.; Sun, P.; Zhang, R.; Lu, A.; Liu, M.; Zhang, L. Cation/Macromolecule Interaction in Alkaline Cellulose Solution Characterized with Pulsed Field-Gradient Spin-Echo NMR Spectroscopy. *Phys. Chem. Chem. Phys.* **2017**, *19* (11), 7486–7490.
- (268) Baldwin, R. L.; Ogston, A. G. The Diffusion and Sedimentation Coefficients of a Liquid Two-Component System in Terms of Macroscopic Properties of the System. *Trans. Faraday Soc.* **1954**, *50*, 749–755.
- (269) Ono, M.; Mashim, T. Sedimentation Process for Atoms in a Bi-Sb System Alloy under a Strong Gravitational Field: A New Type of Diffusion of Substitutional Solutes. *Philos. Mag. A Phys. Condens. Matter, Struct. Defects Mech. Prop.* **2002**, *82* (3), 591–600.
- (270) Zettl, U.; Hoffmann, S. T.; Koberling, F.; Krausch, G. Self-Diffusion and Cooperative Diffusion in Semidilute Polymer Solutions As Measured by Fluorescence Correlation Spectroscopy. *Macromolecules* **2009**, *42* (24), 9537–9547.

- (271) Giacin, J. R. Evaluation of Plastics Packaging Materials for Food Packaging Applications: Food Safety Considerations. *J. Food Saf.* **1980**, *2* (4), 257–276.
- (272) Liu, R.; Gao, X.; Adams, J.; Oppermann, W. A Fluorescence Correlation Spectroscopy Study on the Self-Diffusion of Polystyrene Chains in Dilute and Semidilute Solution. *Macromolecules* **2005**, *38* (21), 8845–8849.
- (273) Zettl, H.; Zettl, U.; Krausch, G.; Enderlein, J.; Ballauff, M. Direct Observation of Single Molecule Mobility in Semidilute Polymer Solutions. *Phys. Rev. E* **2007**, *75* (6), 194–196.
- (274) Zettl, H.; Häfner, W.; Böker, A.; Schmalz, H.; Lanzendörfer, M.; Müller, A. H. E.; Krausch, G. Fluorescence Correlation Spectroscopy of Single Dye-Labeled Polymers in Organic Solvents. *Macromolecules* **2004**, *37* (5), 1917–1920.
- (275) Cai, L.; Panyukov, S.; Rubinstein, M. Mobility of Nonsticky Nanoparticles in Polymer Liquids. *Macromolecules* **2011**, *44* (19), 7853–7863.
- (276) Cherdhirankorn, T.; Best, A.; Koynov, K.; Peneva, K.; Muellen, K.; Fytas, G. Diffusion in Polymer Solutions Studied by Fluorescence Correlation Spectroscopy. *J. Phys. Chem. B* **2009**, *113* (11), 3355–3359.
- (277) Boukari, H.; Nossal, R.; Sackett, D.; Schuck, P. Hydrodynamics of Nanoscopic Tubulin Rings in Dilute Solutions. *Phys. Rev. Lett.* **2004**, *93* (9), 098106.
- (278) Michelman-Ribeiro, A.; Boukari, H.; Nossal, R.; Horkay, F. Fluorescence Correlation Spectroscopy Study of Probe Diffusion in Poly(Vinyl Alcohol) Solutions and Gels. *Macromol. Symp.* **2005**, *227* (1), 221–230.
- (279) Pristinski, D.; Kozlovskaya, V.; Sukhishvili, S. A. Fluorescence Correlation Spectroscopy Studies of Diffusion of a Weak Polyelectrolyte in Aqueous Solutions. *J. Chem. Phys.* **2005**, *122* (1), 14907–14910.
- (280) Zhao, J. J.; Bae, S. C.; Xie, F.; Granick, S. Diffusion of Polymer-Coated Nanoparticles Studied by Fluorescence Correlation Spectroscopy. *Macromolecules* **2001**, *34* (10), 3123–3126.
- (281) Enderlein, J.; Gregor, I.; Patra, D.; Dertinger, T.; Kaupp, U. B. Performance of Fluorescence Correlation Spectroscopy for Measuring Diffusion and Concentration. *ChemPhysChem* **2005**, *6* (11), 2324–2336.
- (282) Zustiak, S. P.; Nossal, R.; Sackett, D. L. Hindered Diffusion in Polymeric Solutions Studied by Fluorescence Correlation Spectroscopy. *Biophys. J.* **2011**, *101* (1), 255–264.
- (283) Rusu, L.; Lumma, D.; Rädler, J. O. Charge and Size Dependence of Liposome Diffusion in Semidilute Biopolymer Solutions. *Macromol. Biosci.* **2010**, *10* (12), 1465–1472.
- (284) Vagias, A.; Raccis, R.; Koynov, K.; Jonas, U.; Butt, H.-J.; Fytas, G.; Košován, P.; Lenz, O.; Holm, C. Complex Tracer Diffusion Dynamics in Polymer Solutions. *Phys. Rev. Lett.* **2013**, *111* (8), 088301.
- (285) Omari, R. A.; Aneese, A. M.; Grabowski, C. A.; Mukhopadhyay, A. Diffusion of Nanoparticles in Semidilute and Entangled Polymer Solutions. *J. Phys. Chem. B* **2009**, *113* (25), 8449–8452.
- (286) Rashid, R.; Chee, S. M. L.; Raghunath, M.; Wohland, T. Macromolecular Crowding Gives Rise to Microviscosity, Anomalous Diffusion and Accelerated Actin Polymerization. *Phys. Biol.* **2015**, *12* (3), 034001.
- (287) Ochab-Marcinek, A.; Hołyst, R. Scale-Dependent Diffusion of Spheres in Solutions of Flexible and Rigid Polymers: Mean Square Displacement and Autocorrelation Function for FCS and DLS Measurements. *Soft Matter* **2011**, *7* (16), 7366–7369.
- (288) Dong, Y.; Feng, X.; Zhao, N.; Hou, Z. Diffusion of Nanoparticles in Semidilute Polymer Solutions: A Mode-Coupling Theory Study. *J. Chem. Phys.* **2015**, *143* (2), 024903.
- (289) Merouani, S.; Hamdaoui, O.; Saoudi, F.; Chiha, M. Sonochemical Degradation of Rhodamine B in Aqueous Phase: Effects of Additives. *Chem. Eng. J.* **2010**, *158* (3), 550–557.
- (290) Arbeloa, I. L.; Ojeda, P. R. Molecular Forms of Rhodamine B. *Chem. Phys. Lett.* **1981**, *79* (2), 347–350.
- (291) Soares, E. T.; Lansarin, M. A.; Moro, C. C. A Study of Process Variables for the Photocatalytic Degradation of Rhodamine B. *Brazilian J. Chem. Eng.* **2007**, *24* (1), 29–36.
- (292) Mchedlov-Petrossyan, N. O.; Vodolazkaya, N. A.; Doroshenko, A. O. Ionic Equilibria of Fluorophores in Organized Solutions: The Influence of Micellar Microenvironment on Protolytic and Photophysical Properties of Rhodamine B. *J. Fluoresc.* **2003**, *13* (3), 235–248.
- (293) Goins, A. B.; Sanabria, H.; Waxham, M. N. Macromolecular Crowding and Size Effects on Probe Microviscosity. *Biophys. J.* **2008**, *95* (11), 5362–5373.
- (294) Phillies, G. D. J. Dynamics of Macromolecules in Concentrated Solutions: The Universal Scaling Function Derived. *Macromolecules* **1987**, *20*, 558–564.
- (295) Briddick, A.; Li, P.; Hughes, A.; Courchay, F.; Martinez, A.; Thompson, R. L. Surfactant and Plasticizer Segregation in Thin Poly(Vinyl Alcohol) Films. *Langmuir* **2016**, *32* (3), 864–872.
- (296) Leong, Y. K. Depletion Interaction in Colloidal Suspensions: A Comparison between Theory and Experiment. *Colloids Surfaces A Physicochem. Eng. Asp.* **1996**, *118* (1–2), 107–114.
- (297) Sozański, K.; Wiśniewska, A.; Kalwarczyk, T.; Hołyst, R. Activation Energy for Mobility of Dyes and

- Proteins in Polymer Solutions: From Diffusion of Single Particles to Macroscale Flow. *Phys. Rev. Lett.* **2013**, *111* (22), 228301.
- (298) Ohta, T.; Nakanishi, A. Theory of Semi-Dilute Polymer Solutions. I. Static Property in a Good Solvent. *J. Phys. A. Math. Gen.* **1983**, *16* (17), 4155–4170.
- (299) Korosi, A.; Fabuss, B. M. Viscosity of Liquid Water from 25 to 150C. Measurements in Pressurized Glass Capillary Viscometer. *Anal. Chem.* **1968**, *40* (1), 157–162.
- (300) Kjøniksen, A. L.; Nyström, B. Dynamic Light Scattering of Poly(Vinyl Alcohol) Solutions and Their Dynamical Behavior during the Chemical Gelation Process. *Macromolecules* **1996**, *29* (22), 7116–7123.
- (301) Taylor, S. J.; Haw, M. D.; Sefcik, J.; Fletcher, A. J. Gelation Mechanism of Resorcinol-Formaldehyde Gels Investigated by Dynamic Light Scattering. *Langmuir* **2014**, *30* (34), 10231–10240.
- (302) Kok, C. M.; Rudin, A. Relationship between the Hydrodynamic Radius and the Radius of Gyration of a Polymer in Solution. *Die Makromol. Chemie, Rapid Commun.* **1981**, *2* (11), 655–659.
- (303) Hong, P.; Chou, C.; He, C. Solvent Effects on Aggregation Behavior of Polyvinyl Alcohol Solutions. *Polymer (Guildf)*. **2001**, *42* (14), 6105–6112.
- (304) Sheely, M. L. Glycerol Viscosity Tables. *Ind. Eng. Chem.* **1932**, *24* (9), 1060–1064.
- (305) Tajalli, H.; Ghanadzadeh Gilani, A.; Zakerhamidi, M. S.; Moghadam, M. Effects of Surfactants on the Molecular Aggregation of Rhodamine Dyes in Aqueous Solutions. *Spectrochim. Acta Part A Mol. Biomol. Spectrosc.* **2009**, *72* (4), 697–702.
- (306) McHedlov-Petrosyan, N. O.; Kholin, Y. V. Aggregation of Rhodamine B in Water. *Russ. J. Appl. Chem.* **2004**, *77* (3), 414–422.
- (307) Haglund, B. O.; Sundelöf, L.-O.; Upadrashta, S. M.; Wurster, D. E. Effect of SDS Micelles on Rhodamine-B Diffusion in Hydrogels. *J. Chem. Educ.* **1996**, *73* (9), 889.
- (308) Saito, S.; Yukawa, M. Interactions of Polymers and Cationic Surfactants with Thiocyanate as Counterions. *J. Colloid Interface Sci.* **1969**, *30* (2), 211–218.
- (309) Saito, S.; Kitamura, K. Counterion Effect of Tetraalkylammonium and Long-Chain Alkylammonium Salts in the Interaction with Nonionic Polymers. *J. Colloid Interface Sci.* **1971**, *35* (2).
- (310) Nakagaki, M.; Ninomiya, Y. Colloid Chemical Studies of Starching Materials. VI. Viscometric Studies of the Interaction between Polyvinyl Alcohol and Sodium Dodecyl Sulfate. *Bull. Chem. Soc. Jpn.* **1964**, *37* (6), 817–821.
- (311) Isemura, T.; Imanishi, A. The Dissolution of Water-Insoluble Polymers in the Surfactant Solution. The Polyelectrolyte-like Behavior of the Dissolved Polymers. *J. Polym. Sci.* **1958**, *33* (126), 337–352.
- (312) Jia, L.; Qin, X. The Effect of Different Surfactants on the Electrospinning Poly(Vinyl Alcohol) (PVA) Nanofibers. *J. Therm. Anal. Calorim.* **2013**, *112* (2), 595–605.
- (313) Flory, P. J. Thermodynamics of High Polymer Solutions. *J. Chem. Phys.* **1942**, *10* (1), 51–61.
- (314) Huggins, M. L. Solutions of Long Chain Compounds. *J. Chem. Phys.* **1941**, *9* (5), 440.
- (315) Krawczyk, J.; Croce, S.; McLeish, T. C. B.; Chakrabarti, B. Elasticity Dominated Surface Segregation of Small Molecules in Polymer Mixtures. *Phys. Rev. Lett.* **2016**, *116* (20), 208301.
- (316) Gundabala, V. R.; Zimmerman, W. B.; Routh, A. F. A Model for Surfactant Distribution in Latex Coatings. *Langmuir* **2004**, *20* (20), 8721–8727.
- (317) Gromer, A.; Thalmann, F.; Hébraud, P.; Holl, Y. Simulation of Vertical Surfactant Distributions in Drying Latex Films. *Langmuir* **2017**, *33* (2), 561–572.
- (318) F, A.; B, I.-H.; H, T. Migration of Additives in Rubber. *Gummi Fasern Kunststoff* **2004**, No. 10, 653–662.
- (319) Wypych, G. 15. Specialized Analytical Methods in Plasticizer Testing A2 - Handbook of Plasticizers (Second Edition). William Andrew Publishing: Boston 2012, pp 563–571.
- (320) Budkowski, A. Interfacial Phenomena in Thin Polymer Films: Phase Coexistence and Segregation: Interfaces Crystallization Viscoelasticity. *Adv. Polym. Sci.* **1999**, *148*, 1–111.
- (321) Geoghegan, M.; Krausch, G. Wetting at Polymer Surfaces and Interfaces. *Prog. Polym. Sci.* **2003**, *28* (2), 261–302.
- (322) Poças, M. F.; Oliveira, J. C.; Oliveira, F. A. R.; Hogg, T. A Critical Survey of Predictive Mathematical Models for Migration from Packaging. *Crit. Rev. Food Sci. Nutr.* **2008**, *48* (10), 913–928.
- (323) O'Brien, A.; Goodson, A.; Cooper, I. Polymer Additive Migration to Foods - a Direct Comparison of Experimental Data and Values Calculated from Migration Models for High Density Polyethylene (HDPE). *Food Addit. Contam.* **1999**, *16* (9), 367–380.
- (324) O'Brien, A.; Cooper, I. Polymer Additive Migration to Foods - a Direct Comparison of Experimental Data and Values Calculated from Migration Models for Polypropylene. *Food Addit. Contam.* **2001**, *18* (4), 343–355.
- (325) Begley, T.; Castle, L.; Feigenbaum, A.; Franz, R.; Hinrichs, K.; Lickly, T.; Mercea, P.; Milana, M.;

- O'Brien, A.; Rebre, S.; Rijk, R.; Piringer, O. Evaluation of Migration Models That Might Be Used in Support of Regulations for Food-Contact Plastics. *Food Addit. Contam.* **2005**, *22* (1), 73–90.
- (326) Zhu, S.; Welsh, N.; Hirt, D. E. Determination of the Diffusivity of a Hydrophilic Migratory Additive in Ipp Films. *J. Plast. Film Sheeting* **2007**, *23* (3), 187–201.
- (327) Schrof, W.; Klingler, J.; Rozouvan, S.; Horn, D. Raman Correlation Spectroscopy: A Method for Studying Chemical Composition and Dynamics of Disperse Systems. *Phys. Rev. E - Stat. Physics, Plasmas, Fluids, Relat. Interdiscip. Top.* **1998**, *57* (3), R2523–R2526.
- (328) Vural, H.; Maisch, J.; Gerhardt, I.; Jetter, M.; Portalupi, S. L.; Michler, P. Characterization of Spectral Diffusion by Slow-Light Photon-Correlation Spectroscopy. *Phys. Rev. B* **2020**, *101* (16), 1–6.
- (329) Kowert, B. A.; Dang, N. C.; Sobush, K. T.; Seele, L. G. Diffusion of Aromatic Hydrocarbons in N-Alkanes and Cyclohexanes. *J. Phys. Chem. A* **2001**, *105* (8), 1232–1237.
- (330) Duval, F. P.; Porion, P.; Van Damme, H. Microscale and Macroscale Diffusion of Water in Colloidal Gels. a Pulsed Field Gradient and NMR Imaging Investigation. *J. Phys. Chem. B* **1999**, *103* (27), 5730–5735.
- (331) Veniaminov, A.; Jahr, T.; Sillescu, H.; Bartsch, E. Length Scale Dependent Probe Diffusion in Drying Acrylate Latex Films. *Macromolecules* **2002**, *35* (3), 808–819.
- (332) Seiffert, S.; Opperman, W. Systematic Evaluation of FRAP Experiments Performed in a Confocal Laser Scanning Microscope. *J. Microsc.* **2005**, *220* (1), 20–30.
- (333) Jönsson, P.; Jonsson, M. P.; Tegenfeldt, J. O.; Höök, F. A Method Improving the Accuracy of Fluorescence Recovery after Photobleaching Analysis. *Biophys. J.* **2008**, *95* (11), 5334–5348.
- (334) Jones, R. A. L. The Dynamics of Thin Polymer Films. *Curr. Opin. Colloid Interface Sci.* **1999**, *4* (2), 153–158.
- (335) Flier, B. M. I.; Baier, M. C.; Huber, J.; Müllen, K.; Mecking, S.; Zumbusch, A.; Wöll, D. Heterogeneous Diffusion in Thin Polymer Films as Observed by High-Temperature Single-Molecule Fluorescence Microscopy. *J. Am. Chem. Soc.* **2012**, *134* (1), 480–488.
- (336) Edwards, D. A. Non-Fickian Diffusion in Thin Polymer Films. *J. Polym. Sci. Part B Polym. Phys.* **1996**, *34* (5), 981–997.
- (337) Zhang, W.; Yu, L. Surface Diffusion of Polymer Glasses. *Macromolecules* **2016**, *49* (2), 731–735.
- (338) Bansal, A.; Yang, H.; Li, C.; Cho, K.; Benicewicz, B. C.; Kumar, S. K.; Schadler, L. S. Quantitative Equivalence between Polymer Nanocomposites and Thin Polymer Films. *Nat. Mater.* **2005**, *4* (9), 693–698.
- (339) Karbowski, T.; Hervet, H.; Léger, L.; Champion, D.; Debeaufort, F.; Voilley, A. Effect of Plasticizers (Water and Glycerol) on the Diffusion of a Small Molecule in Iota-Carrageenan Biopolymer Films for Edible Coating Application. *Biomacromolecules* **2006**, *7* (6), 2011–2019.
- (340) Sprague, B.; McNally, J. FRAP Analysis of Binding: Proper and Fitting. *Trends Cell Biol.* **2005**, *15* (2), 84–91.
- (341) Stavreva, D. A.; McNally, J. G. Fluorescence Recovery after Photobleaching (FRAP) Methods for Visualizing Protein Dynamics in Living Mammalian Cell Nuclei. *Methods Enzymol.* **2003**, *375* (1976), 443–455.
- (342) Sprague, B. L.; Pego, R. L.; Stavreva, D. A.; McNally, J. G. Analysis of Binding Reactions by Fluorescence Recovery after Photobleaching. *Biophys. J.* **2004**, *86* (6), 3473–3495.
- (343) Chang, P.; Torres, J.; Lewis, R. A.; Mowry, K. L.; Houlston, E.; King, M. Lou. Localization of RNAs to the Mitochondrial Cloud in Xenopus Oocytes through Entrapment and Association with Endoplasmic Reticulum. *Mol. Biol. Cell* **2004**, *15* (10), 4669–4681.
- (344) Sakai, Y.; Kawahigashi, M.; Minami, T.; Inoue, T.; Hirayama, S. Deconvolution of Non-Exponential Emission Decays Arising from Reabsorption of Emitted Light. *J. Lumin.* **1989**, *42* (6), 317–324.
- (345) Yang, L.-X. X.; Zhu, Y.-J. J.; Tong, H.; Wang, W.-W. W. Submicrocubes and Highly Oriented Assemblies of MnCO<sub>3</sub> Synthesized by Ultrasound Agitation Method and Their Thermal Transformation to Nanoporous Mn<sub>2</sub>O<sub>3</sub>. *Ultrason. Sonochem.* **2007**, *14* (2), 259–265.
- (346) Reynier, A.; Dole, P.; Feigenbaum, A. Additive Diffusion Coefficients in Polyolefins. II. Effect of Swelling and Temperature on the D = f(M) Correlation. *J. Appl. Polym. Sci.* **2001**, *82* (10), 2434–2443.
- (347) Zhang, Q. G.; Liu, Q. L.; Chen, Y.; Wu, J. Y.; Zhu, A. M. Microstructure Dependent Diffusion of Water–Ethanol in Swollen Poly(Vinyl Alcohol): A Molecular Dynamics Simulation Study. *Chem. Eng. Sci.* **2009**, *64* (2), 334–340.
- (348) Lim, M.; Kim, D.; Han, H.; Khan, S. B.; Seo, J. Water Sorption and Water-Resistance Properties of Poly(Vinyl Alcohol)/Clay Nanocomposite Films: Effects of Chemical Structure and Morphology. *Polym. Compos.* **2015**, *36* (4), 660–667.
- (349) Kulagina, G. S.; Chalykh, A. E.; Gerasimov, V. K.; Chalykh, K. A.; Puryaeva, T. P. Sorption of Water by Poly(Vinyl Alcohol). *Polym. Sci. - Ser. A* **2007**, *49* (4), 425–432.

- (350) Long, F. A.; Thompson, L. J. Diffusion of Water Vapor in Polymers. *J. Polym. Sci.* **1955**, *15* (80), 413–426.
- (351) Gliemann, H.; Almeida, A. T.; Petri, D. F. S.; Schimmel, T. Nanostructure Formation in Polymer Thin Films Influenced by Humidity. *Surf. Interface Anal.* **2006**, *39* (1), 1–8.
- (352) Wang, D.; Russell, T. P. Advances in Atomic Force Microscopy for Probing Polymer Structure and Properties. *Macromolecules* **2018**, *51* (1), 3–24.
- (353) Noy, A.; Vezenov, D. V.; Lieber, C. M. Chemical Force Microscopy. *Annu. Rev. Mater. Sci.* **1997**, *27* (1), 381–421.
- (354) Wu, W. R.; Su, C. J.; Chuang, W. T.; Huang, Y. C.; Yang, P. W.; Lin, P. C.; Chen, C. Y.; Yang, T. Y.; Su, A. C.; Wei, K. H.; Liu, C. M.; Jeng, U. S. Surface Layering and Supersaturation for Top-Down Nanostructural Development during Spin Coating of Polymer/Fullerene Thin Films. *Adv. Energy Mater.* **2017**, *7* (14), 1–11.
- (355) Yu, J.; Hu, D.; Barbara, P. F. Unmasking Electronic Energy Transfer of Conjugated Polymers by Suppression of O<sub>2</sub> Quenching. *Science* (80-. ). **2000**, *289* (5483), 1327–1330.
- (356) Reiter, G.; Napolitano, S. Possible Origin of Thickness-Dependent Deviations from Bulk Properties of Thin Polymer Films. *J. Polym. Sci. Part B Polym. Phys.* **2010**, *48* (24), 2544–2547.
- (357) Geoghegan, M.; Jones, R. A. L.; Clough, A. S. Surface Directed Spinodal Decomposition in a Partially Miscible Polymer Blend. *J. Chem. Phys.* **1995**, *103* (7), 2719–2724.
- (358) Aguirreurreta, Z.; de la Cal, J. C.; Leiza, J. R. Preparation of High Solids Content Waterborne Acrylic Coatings Using Polymerizable Surfactants to Improve Water Sensitivity. *Prog. Org. Coatings* **2017**, *112* (December 2016), 200–209.
- (359) Vautier-Giongo, C.; Bales, B. L. Estimate of the Ionization Degree of Ionic Micelles Based on Krafft Temperature Measurements. *J. Phys. Chem. B* **2003**, *107* (23), 5398–5403.
- (360) Coppola, L.; Gianferri, R.; Nicotera, I.; Oliviero, C. Structural Changes in CTAB/H<sub>2</sub>O Mixtures Using a Rheological Approach. **2004**.
- (361) Tam, K. C.; Ragaram, S.; Pelton, R. H. Interaction of Surfactants with Poly(N-Isopropylacrylamide) Microgel Latexes. *Langmuir* **1994**, *10* (2), 418–422.
- (362) Coiro, V. M.; Manigrasso, M.; Mazza, F.; Pochetti, G. Structure of a Triclinic Phase of Sodium Dodecyl Sulfate Monohydrate. A Comparison with Other Sodium Dodecyl Sulfate Crystal Phases. *Acta Crystallogr. Sect. C* **1987**, *43* (5), 850–854.
- (363) Bagheri, F.; Radi, M.; Amiri, S. Drying Conditions Highly Influence the Characteristics of Glycerol-Plasticized Alginate Films. *Food Hydrocoll.* **2019**, *90*, 162–171.
- (364) Trevoy, D. J. Rate of Evaporation of Glycerol in High Vacuum. *Ind. Eng. Chem.* **1953**, *45* (10), 2366–2369.
- (365) Matthews, L.; Przybyłowicz, Ż.; Rogers, S. E.; Bartlett, P.; Johnson, A. J.; Sochon, R.; Briscoe, W. H. The Curious Case of SDS Self-Assembly in Glycerol: Formation of a Lamellar Gel. *J. Colloid Interface Sci.* **2020**, *572*, 384–395.
- (366) Matthews, L.; Stevens, M. C.; Schweins, R.; Bartlett, P.; Johnson, A. J.; Sochon, R.; Briscoe, W. H. Unexpected Observation of an Intermediate Hexagonal Phase upon Fluid-to-Gel Transition: SDS Self-Assembly in Glycerol. *Colloid Interface Sci. Commun.* **2021**, *40*, 100342.
- (367) Cosby, J.; Starck, P.; Littlewood, D.; Mykhaylyk, O. O.; Ryan, A. J. Co-Assembly and Structure of Sodium Dodecylsulfate and Other n-Alkyl Sulfates in Glycerol: N-Alkyl Sulfate-Glycerol Crystal Phase. *J. Colloid Interface Sci.* **2021**, *596*, 442–454.
- (368) Huang, Y.; Paul, D. R. Physical Aging of Thin Glassy Polymer Films Monitored by Gas Permeability. *Polymer (Guildf).* **2004**, *45* (25), 8377–8393.
- (369) Butt, H. J.; Cappella, B.; Kappl, M. Force Measurements with the Atomic Force Microscope: Technique, Interpretation and Applications. *Surf. Sci. Rep.* **2005**, *59* (1–6), 1–152.
- (370) Wilbur, J. L.; Biebuyck, H. A.; Macdonald, J. C.; Whitesides, G. M. Scanning Force Microscopies Can Image Patterned Self-Assembled Monolayers. *Langmuir* **1995**, *11* (3), 825–831.
- (371) Bowen, J.; Cheneler, D.; Andrews, J. W.; Avery, A. R.; Zhang, Z.; Ward, M. C. L.; Adams, M. J. Application of Colloid Probe Atomic Force Microscopy to the Adhesion of Thin Films of Viscous and Viscoelastic Silicone Fluids. *Langmuir* **2011**, *27* (18), 11489–11500.
- (372) Higuchi, A.; Iijima, T. D.s.c. Investigation of the States of Water in Poly(Vinyl Alcohol) Membranes. *Polymer (Guildf).* **1985**, *26* (8), 1207–1211.
- (373) Cha, W.-I.; Hyon, S.-H.; Ikada, Y. Microstructure of Poly(Vinyl Alcohol) Hydrogels Investigated with Differential Scanning Calorimetry. *Die Makromol. Chemie* **1993**, *194* (9), 2433–2441.
- (374) Chen, L.; Imam, S. H.; Gordon, S. H.; Greene, R. V. Starch-Polyvinyl Alcohol Crosslinked Film-Performance and Biodegradation. *J. Environ. Polym. Degrad.* **1997**, *5* (2), 111–117.

- (375) Nakamae, K.; Nishino, T.; Ohkubo, H. Studies on the Temperature Dependence of the Elastic Modulus of Crystalline Regions of Polymers: 14. Poly(Vinyl Alcohol) with Different Tacticities. *Polymer (Guildf)*. **1992**, *33* (12), 2581–2586.
- (376) Duan, Y.; Jiang, Y.; Jiang, S.; Li, L.; Yan, S.; Schultz, J. M. Depletion-Induced Nonbirefringent Banding in Thin Isotactic Polystyrene Thin Films. *Macromolecules* **2004**, *37* (24), 9283–9286.
- (377) Tung, W. S.; Griffin, P. J.; Meth, J. S.; Clarke, N.; Composto, R. J.; Winey, K. I. Temperature-Dependent Suppression of Polymer Diffusion in Polymer Nanocomposites. *ACS Macro Lett.* **2016**, *5* (6), 735–739.
- (378) Deppe, D. D.; Dhinojwala, A.; Torkelson, J. M. Small Molecule Probe Diffusion in Thin Polymer Films near the Glass Transition: A Novel Approach Using Fluorescence Nonradiative Energy Transfer. *Macromolecules* **1996**, *29* (11), 3898–3908.
- (379) Gam, S.; Meth, J. S.; Zane, S. G.; Chi, C.; Wood, B. A.; Seitz, M. E.; Winey, K. I.; Clarke, N.; Composto, R. J. Macromolecular Diffusion in a Crowded Polymer Nanocomposite. *Macromolecules* **2011**, *44* (9), 3494–3501.
- (380) Gam, S.; Meth, J. S.; Zane, S. G.; Chi, C.; Wood, B. A.; Winey, K. I.; Clarke, N.; Composto, R. J. Polymer Diffusion in a Polymer Nanocomposite: Effect of Nanoparticle Size and Polydispersity. *Soft Matter* **2012**, *8* (24), 6512–6520.
- (381) Lin, C. C.; Gam, S.; Meth, J. S.; Clarke, N.; Winey, K. I.; Composto, R. J. Do Attractive Polymer-Nanoparticle Interactions Retard Polymer Diffusion in Nanocomposites? *Macromolecules* **2013**, *46* (11), 4502–4509.
- (382) Xu, W.; Deng, Z. H.; Zhang, X. Z.; Wan, G. X. The Influence of the Compatibility of Plasticizers with Polymer Ionic Conductors on Ionic Conduction. *J. Solid State Electrochem.* **1998**, *2* (4), 257–261.
- (383) Fortunati, E.; Luzi, F.; Dugo, L.; Fanali, C.; Tripodo, G.; Santi, L.; Kenny, J. M.; Torre, L.; Bernini, R. Effect of Hydroxytyrosol Methyl Carbonate on the Thermal, Migration and Antioxidant Properties of PVA-Based Films for Active Food Packaging. *Polym. Int.* **2016**, *65* (8), 872–882.
- (384) Monjazebe Marvdashti, L.; Yavarmanesh, M.; Koocheki, A. In Vitro Release Study of Nisin from Active Polyvinyl Alcohol-Alyssum Homolocarpum Seed Gum Films at Different Temperatures. *Polym. Test.* **2019**, *79* (March), 106032.
- (385) Costello, L. M.; Koros, W. J. Temperature Dependence of Gas Sorption and Transport Properties in Polymers: Measurement and Applications. *Ind. Eng. Chem. Res.* **1992**, *31* (12), 2708–2714.
- (386) Kanatt, S. R.; Rao, M. S.; Chawla, S. P.; Sharma, A. Active Chitosan-Polyvinyl Alcohol Films with Natural Extracts. *Food Hydrocoll.* **2012**, *29* (2), 290–297.
- (387) Limm, W.; Hollifield, H. C. Modelling of Additive Diffusion in Polyolefins. *Food Addit. Contam.* **1996**, *13* (8), 949–967.
- (388) Jiao, S. xi; Zhao, Y.; Gu, J. jin. Simultaneous Measurement of Humidity and Temperature Using a Polyvinyl Alcohol Tapered Fiber Bragg Grating. *Instrum. Sci. Technol.* **2018**, *46* (5), 463–474.
- (389) Hemalatha, K. S.; Sriprakash, G.; Ambika Prasad, M. V. N.; Damle, R.; Rukmani, K. Temperature Dependent Dielectric and Conductivity Studies of Polyvinyl Alcohol-ZnO Nanocomposite Films by Impedance Spectroscopy. *J. Appl. Phys.* **2015**, *118* (15).
- (390) Mao, L.; Imam, S.; Gordon, S.; Cinelli, P.; Chiellini, E. Extruded Cornstarch-Glycerol-Polyvinyl Alcohol Blends: Mechanical Properties, Morphology, and Biodegradability. *J. Polym. Environ.* **2000**, *8* (4), 205–211.
- (391) Holland, B. J.; Hay, J. N. The Thermal Degradation of Poly ( Vinyl Alcohol ). **2001**, *42*, 6775–6783.
- (392) Lenntech. Relative humidity calculator <https://www.lennotech.com/calculators/humidity/relative-humidity.htm>.
- (393) Berkelaar, R. P.; Bampoulis, P.; Dietrich, E.; Jansen, H. P.; Zhang, X.; Kooij, E. S.; Lohse, D.; Zandvliet, H. J. W. Water-Induced Blister Formation in a Thin Film Polymer. *Langmuir* **2015**, *31* (3), 1017–1025.
- (394) Calvert, P. D.; Billingham, N. C. Loss of Additives from Polymers: A Theoretical Model. *J. Appl. Polym. Sci.* **1979**, *24* (2), 357–370.
- (395) Tah, B.; Pal, P.; Mahato, M.; Talapatra, G. B. Aggregation Behavior of SDS/CTAB Catanionic Surfactant Mixture in Aqueous Solution and at the Air/Water Interface. *J. Phys. Chem. B* **2011**, *115* (26), 8493–8499.
- (396) Marten, F. L. Vinyl Alcohol Polymers. In Kirk-Othmer Encyclopedia of Chemical Technology; John Wiley & Sons, Inc.: Hoboken, NJ, USA, 2000.
- (397) Shuler, C. A.; Janorkar, A. V.; Hirt, D. E. Fate of Erucamide in Polyolefin Films at Elevated Temperature. *Polym. Eng. Sci.* **2004**, *44* (12), 2247–2253.
- (398) Khan, H.; Seddon, J. M.; Law, R. V.; Brooks, N. J.; Robles, E.; Cabral, J. T.; Ces, O. Effect of Glycerol with Sodium Chloride on the Krafft Point of Sodium Dodecyl Sulfate Using Surface Tension. *J. Colloid Interface Sci.* **2019**, *538*, 75–82.
- (399) Rosen, M. J.; Zhou, Q. Surfactant-Surfactant Interactions in Mixed Monolayer and Mixed Micelle

- Formation. *Langmuir* **2002**, *17* (12), 3532–3537.
- (400) Tsujii, K.; Saito, N.; Takeuchi, T. Krafft Points of Anionic Surfactants and Their Mixtures with Special Attention to Their Applicability in Hard Water. *J. Phys. Chem.* **1980**, *84* (18), 2287–2291.
- (401) Doan, T.; Acosta, E.; Scamehorn, J. F.; Sabatini, D. A. Formulating Middle-Phase Microemulsions Using Mixed Anionic and Cationic Surfactant Systems. *J. Surfactants Deterg.* **2003**, *6* (3), 215–224.
- (402) Nakayama, H.; Shinoda, K. The Effect of Added Salts on the Solubilities and Krafft Points of Sodium Dodecyl Sulfate and Potassium Perfluoro-Octanoate. *Bull. Chem. Soc. Jpn.* **1967**, *40* (8), 1797–1799.
- (403) Tartar, H. V.; Cadle, R. D. Studies of Sulfonates. VI. *J. Phys. Chem.* **1939**, 1173–1179.
- (404) Jingliang, L. I. The Influence of Surfactants on The Solubilization, Exreaction and Biodergradation of Model Polycyclic Aromatic Hydrocarbons. *Biomol. Eng.* **2004**, 245.
- (405) Waheed, Z.; Dong, Y.; Han, N.; Liu, S. Water and Gas Barrier Properties of Polyvinyl Alcohol ( PVA )/ Starch ( ST )/ Glycerol ( GL )/ Halloysite Nanotube ( HNT ) Bionanocomposite Films : Experimental Characterisation and Modelling Approach. *Compos. Part B* **2019**, *174* (February), 107033.
- (406) Asem, M.; Nawawi, W. M. F. W.; Jimat, D. N. Evaluation of Water Absorption of Polyvinyl Alcohol-Starch Biocomposite Reinforced with Sugarcane Bagasse Nanofibre: Optimization Using Two-Level Factorial Design. *IOP Conf. Ser. Mater. Sci. Eng.* **2018**, *368*, 012005.
- (407) Thomas, P. S.; Stuart, B. H. A Fourier Transform Raman Spectroscopy Study of Water Sorption by Poly(Vinyl Alcohol). *Spectrochim. Acta - Part A Mol. Biomol. Spectrosc.* **1997**, *53* (13), 2275–2278.
- (408) Shafee, E. El; Naguib, H. F. Water Sorption in Cross-Linked Poly ( Vinyl Alcohol ) Networks. **2003**, *44*, 1647–1653.
- (409) Tanigami, T.; Yano, K.; Yamaura, K.; Matsuzawa, S. Anomalous Swelling of Poly(Vinyl Alcohol) Film in Mixed Solvents of Dimethylsulfoxide and Water. *Polymer (Guildf)*. **1995**, *36* (15), 2941–2946.
- (410) Shi, S. Q.; Gardner, D. J. Dynamic Adhesive Wettability of Wood. *Wood Fiber Sci.* **2001**, *33* (1), 58–68.
- (411) Liu, T.; Hao, J.; Yang, B.; Hu, B.; Cui, Z.; Li, S. Contact Angle Measurements: An Alternative Approach Towards Understanding the Mechanism of Increased Drug Dissolution from Ethylcellulose Tablets Containing Surfactant and Exploring the Relationship Between Their Contact Angles and Dissolution Behaviors. *AAPS PharmSciTech* **2018**, *19* (4), 1582–1591.
- (412) Shanahan, M. E. R.; Bourgès, C. Effects of Evaporation on Contact Angles on Polymer Surfaces. *Int. J. Adhes. Adhes.* **1994**, *14* (3), 201–205.
- (413) Theodorakis, P. E.; Mu, E. A.; Craster, R. V.; Matar, O. K. Superspreading: Mechanisms and Molecular Design. **2015**, 27–32.
- (414) Szymczyk, K.; Zdziennicka, A.; Krawczyk, J.; Ja, B. Applied Surface Science Correlation between Wetting , Adhesion and Adsorption in the Polymer – Aqueous Solutions of Ternary Surfactant Mixtures – Air Systems. **2014**, *288*, 488–496.
- (415) Stoebe, T.; Lin, Z.; Hill, R. M.; Ward, M. D.; Davis, H. T. Surfactant-Enhanced Spreading. *Langmuir* **1996**, *12* (2), 337–344.
- (416) Kovalchuk, N. M.; Trybala, A.; Arjmandi-tash, O.; Starov, V. Surfactant-Enhanced Spreading : Experimental Achievements and Possible Mechanisms. *Adv. Colloid Interface Sci.* **2016**, *233*, 155–160.
- (417) Campus, S. K.; Campus, S. K. *On Surfactant-Enhanced Spreading and Superspreading of Liquid Drops on Solid Surfaces*; 2011; Vol. 670.
- (418) Woodward, J. T.; Schwartz, D. K. Dewetting Modes of Surfactant Solution as a Function of the Spreading Coefficient. *Langmuir* **1997**, *13* (26), 6873–6876.
- (419) Sarker, D.; Bergeron, V.; Meunier, J.; Bonn, D. Superspreading: Aqueous Surfactant Drops Spreading on Hydrophobic Surfaces. **2002**, No. 10, 10486–10488.
- (420) Marangoni, A. *Fat Crystal Networks*; New York, 2005.
- (421) Muscat, D.; Drew, R. A. L. Modeling the Infiltration Kinetics of Molten Aluminum into Porous Titanium Carbide. *Metall. Mater. Trans. A* **1994**, *25* (11), 2357–2370.
- (422) Newman, S. Kinetics of Wetting of Surfaces by Polymers; Capillary Flow. *J. Colloid Interface Sci.* **1968**, *26* (2), 209–213.
- (423) Blake, T. D.; Clarke, A. Contact Angle Relaxation during Droplet Spreading : **1997**, *121* (11), 2164–2166.
- (424) Yin, T. P. The Kinetics of Spreading. *J. Phys. Chem.* **1969**, *73* (7), 2413–2417.
- (425) Oene, H. Van; Chang, Y. F.; Newman, S. The Rheology of Wetting By Polymer Melts. *J. Adhes.* **1969**, *1* (1), 54–68.
- (426) Lelah, M. D.; Marmur, A. Spreading Kinetics of Drops on Glass. *J. Colloid Interface Sci.* **1981**, *82* (2), 518–525.
- (427) Cherry, B. W.; Holmes, C. M. Kinetics of Wetting of Surfaces by Polymers. *J. Colloid Interface Sci.* **1969**, *29* (1), 174–176.
- (428) Schonhorn, H.; Frisch, H. L.; Kwei, T. K. Kinetics of Wetting of Surfaces by Polymer Melts. *J. Appl.*



- Phys.* **1966**, 37 (13), 4967–4973.
- (429) Litwinowicz, M. A.; Rogers, S.; Tellam, J.; Thompson, R. L. Tuning the Bulk and Surface Properties of PDMS Networks through Cross-Linker and Surfactant Concentration. *Prep.*
- (430) Li, A.-J.; Nussinov, R. A Set of van Der Waals and Coulombic Radii of Protein Atoms for Molecular and Solvent-Accessible Surface Calculation, Packing Evaluation, and Docking. *Proteins Struct. Funct. Genet.* **1998**, 32 (1), 111–127.
- (431) Camós Noguera, A.; Olsen, S. M.; Hvilsted, S.; Kiil, S. Diffusion of Surface-Active Amphiphiles in Silicone-Based Fouling-Release Coatings. *Prog. Org. Coatings* **2017**, 106, 77–86.
- (432) Peppas, N. Infrared Spectroscopy of Semicrystalline Poly(Vinyl Alcohol) Networks. *Die Makromol. Chemie* **1977**, 178 (2), 595–601.
- (433) Ruckenstein, E. Colloids and Surfaces A : Physicochemical and Engineering Aspects Superspreading : A Possible Mechanism. *Colloids Surfaces A Physicochem. Eng. Asp.* **2012**, 412, 36–37.
- (434) Sritapunya, T.; Kitiyanan, B.; Scamehorn, J. F.; Grady, B. P.; Chavadej, S. Colloids and Surfaces A : Physicochemical and Engineering Aspects Wetting of Polymer Surfaces by Aqueous Surfactant Solutions. *Colloids Surfaces A Physicochem. Eng. Asp.* **2012**, 409, 30–41.
- (435) De Oliveira, H. P. M.; Gehlen, M. H. Characterization of Mixed Micelles of Sodium Dodecyl Sulfate and Tetraoxyethylene Dodecyl Ether in Aqueous Solution. *Langmuir* **2002**, 18 (10), 3792–3796.
- (436) Hu, C.; Li, R.; Yang, H.; Wang, J. Properties of Binary Surfactant Systems of Nonionic Surfactants C12E10, C12E23, and C12E42 with a Cationic Gemini Surfactant in Aqueous Solutions. *J. Colloid Interface Sci.* **2011**, 356 (2), 605–613.
- (437) Warisnoicharoen, W.; Lansley, A. B.; Lawrence, M. J. Light-Scattering Investigations on Dilute Nonionic Oil-in-Water Microemulsions. *AAPS PharmSci* **2000**, 2 (2), 16–26.
- (438) Bharmoria, P.; Vaneet; Banipal, P. K.; Kumar, A.; Kang, T. S. Modulation of Micellization Behavior of Cetyltrimethylammonium Bromide (CTAB) by Organic Anions in Low Concentration Regime. *J. Solution Chem.* **2015**, 44 (1), 16–33.
- (439) Hadad, S.; Goli, S. A. H. Fabrication and Characterization of Electrospun Nanofibers Using Flaxseed (*Linum Usitatissimum*) Mucilage. *Int. J. Biol. Macromol.* **2018**, 114, 408–414.
- (440) Miller-Chou, B. A.; Koenig, J. L. A Review of Polymer Dissolution. *Prog. Polym. Sci.* **2003**, 28 (8), 1223–1270.
- (441) Birkin, P. R.; Offin, D. G.; Leighton, T. G. *PCCP*. **2005**, 530–537.
- (442) Arakawa, K.; Takenaka, N. The Rheological Study of Aqueous Solutions of Polyvinyl Alcohol at Ultrasonic Frequencies. *Bull. Chem. Soc. Jpn.* **1966**, 404 (1962).
- (443) Zhang, S. J.; Yu, H. Q. Radiation-Induced Degradation of Polyvinyl Alcohol in Aqueous Solutions. *Water Res.* **2004**, 38 (2), 309–316.
- (444) Behnajady, M. A.; Modirshahla, N.; Tabrizi, S. B.; Molanee, S. Ultrasonic Degradation of Rhodamine B in Aqueous Solution: Influence of Operational Parameters. *J. Hazard. Mater.* **2008**, 152 (1), 381–386.
- (445) Coates, J. Interpretation of Infrared Spectral. In *Encyclopedia of Analytical Chemistry*; 2000.
- (446) Awada, H.; Daneault, C. Chemical Modification of Poly(Vinyl Alcohol) in Water. *Appl. Sci.* **2015**, 5 (4), 840–850.
- (447) Gross, S. F.; Kvecher, A.; Koster, J.; Coxey, M. Aqueous Laundry Liquid Suitable for Packaging in Polyvinyl Alcohol Pouches, 2012.
- (448) Dunlop, H. A.; Chaffee, R. H. Packet of Water-Soluble Film of Polyvinyl Alcohol Filled with Detergent Composition, 1965.
- (449) Bianco, T. S.; Kratz, H.; Kratz, Edouard, M. Polyvinyl Alcohol Compositions, 1994.
- (450) Illini, P.; Platz, G. Electric Field Induced Anisotropic Concentration Fluctuations in Solutions Containing 2-Butanol, 1-Butanol or 2-Methyl-1-Propanol, Water and Ionic Surfactants. *Berichte der Bunsengesellschaft/Physical Chem. Chem. Phys.* **1985**, 89 (2), 197–207.
- (451) Mettler Toledo. Raman Spectroscopy - Expand Understanding of Chemical Reactions [https://www.mt.com/gb/en/home/applications/L1\\_AutoChem\\_Applications/Raman-Spectroscopy.html#:~:text=The Raman Spectroscopy Principle,elastic scattering%2C or Rayleigh scattering.](https://www.mt.com/gb/en/home/applications/L1_AutoChem_Applications/Raman-Spectroscopy.html#:~:text=The Raman Spectroscopy Principle,elastic scattering%2C or Rayleigh scattering.) (accessed 2021-06-01)

## Chapter 10. Appendices

### Appendix A

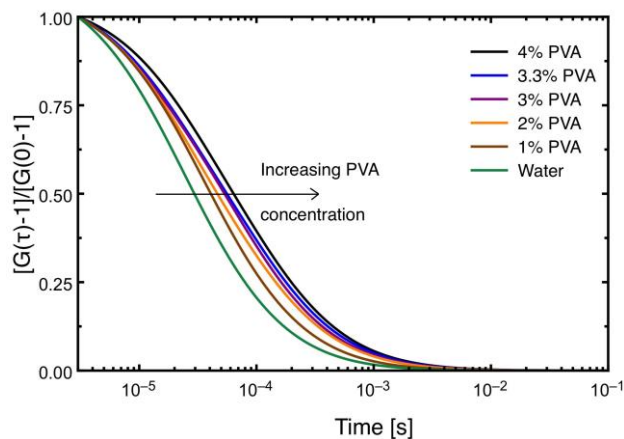


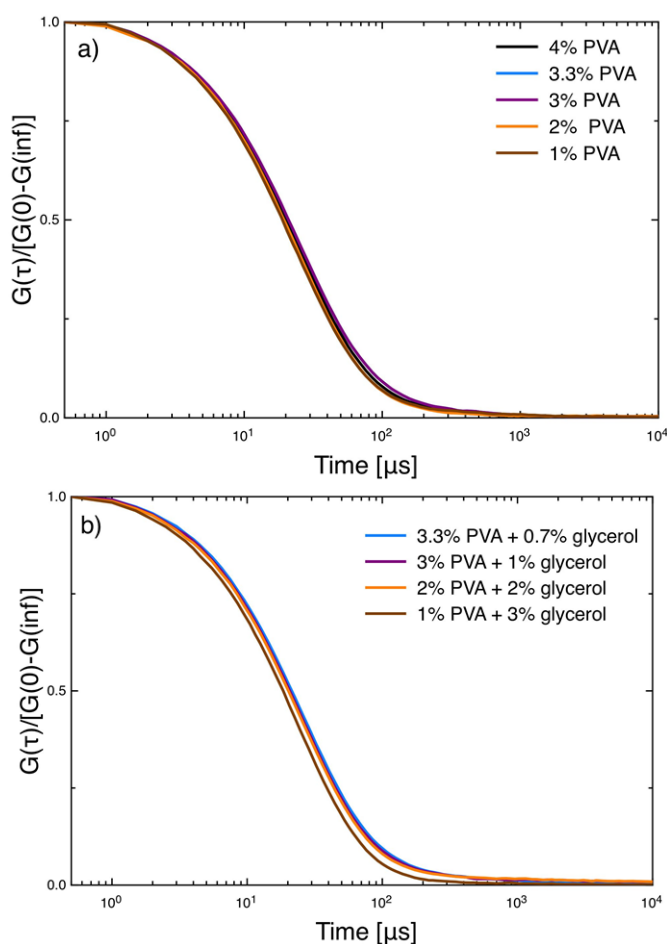
**Figure 10.1.** FCS autocorrelation functions of PVA solutions of various concentrations (compositions 2-6). The percentage of polymer in the graph is given in (w/v)%.

**Table 10.1.** Average diffusion coefficient of Rhodamine B in samples of various compositions ( $T \approx 28$  °C).

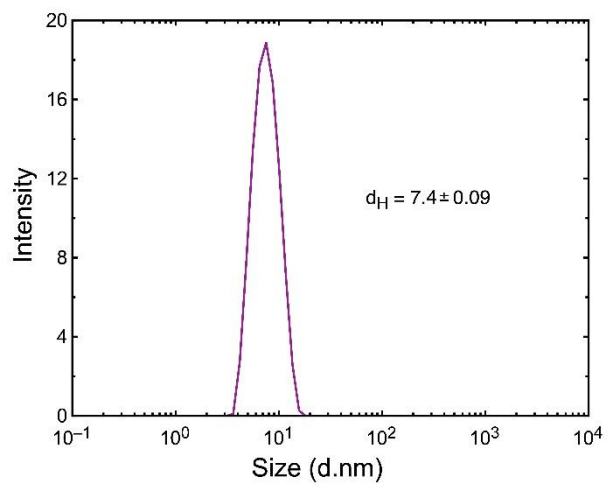
Sample	PVA concentration (wt%)	Glycerol concentration (wt%)	Average D ( $\mu\text{m}^2/\text{s}$ )
Addition of water	2	1.0	359.8 $\pm$ 13.7
	3	2.0	274.9 $\pm$ 9.3
	4	3.0	247.9 $\pm$ 6.5
	5	3.3	220.5 $\pm$ 5.1
	6	4.0	188.4 $\pm$ 3.8
Addition of glycerol solution	1a	0.0	416.6 $\pm$ 19.4
	2a	1.0	295.0 $\pm$ 13.1
	3a	2.0	259.5 $\pm$ 6.5
	4a	3.0	218.7 $\pm$ 7.0
	5a	3.3	208.5 $\pm$ 6.0

Equations 2.10-2.12 were used to calculate the diffusion coefficient of the analysed species and, accordingly, changes in their size with composition variations. For normalised autocorrelation functions, the diffusion coefficient can be obtained from fitting the curve to the single exponential decay (Equation 2.11). Presented autocorrelation functions are very similar in the first part of the curve – this region can be connected with the exponential decay of diffusion coefficient for particles of the highest intensities (diameter 1-15 nm). The value of this diffusion coefficient is approximately constant for all investigated PVA/glycerol

compositions (Figure 10.2), therefore the weighted average radius of the particles shows nearly linear dependence on the viscosity of the solution, increasing with decreasing viscosity. Autocorrelation functions together with decreasing solution viscosity result in larger particle sizes for solutions with higher glycerol content.

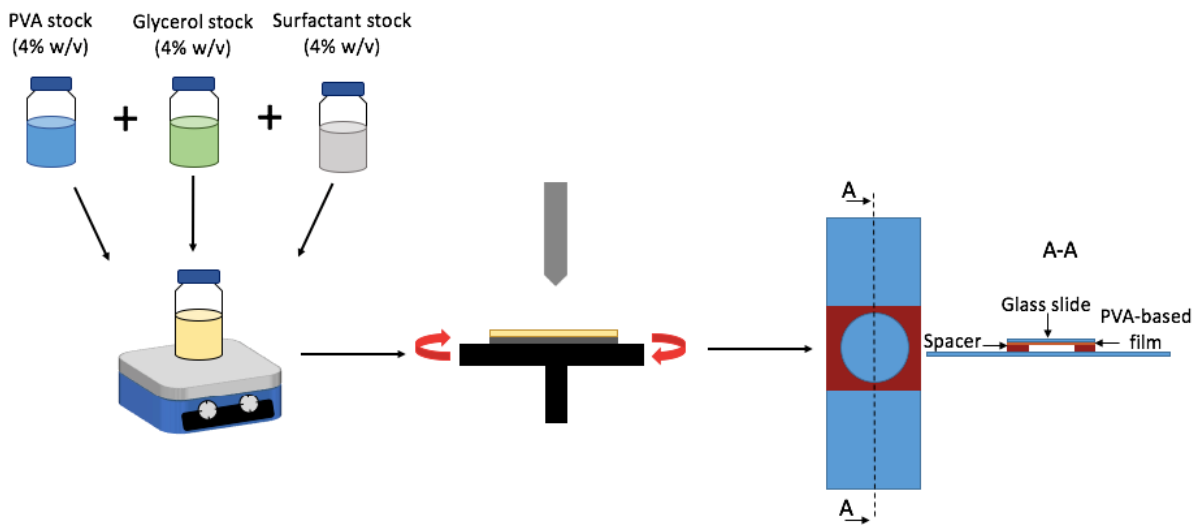


**Figure 10.2.** DLS autocorrelation functions of (a) PVA solutions of compositions 2-6 and (b) PVA/glycerol solution compositions 2a-5a. The percentage of polymer in the graph is given in (w/v)%.

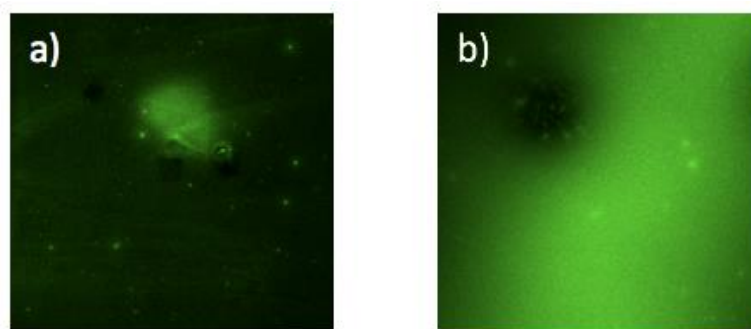


**Figure 10.3.** Average size distribution for C<sub>12</sub>E<sub>10</sub> stock solution investigated by DLS.

Appendix B

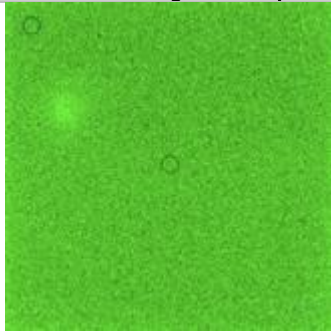
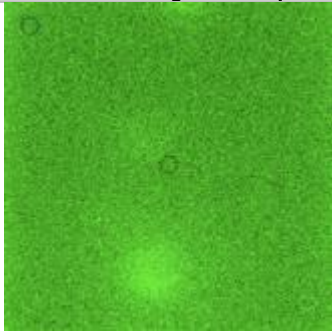
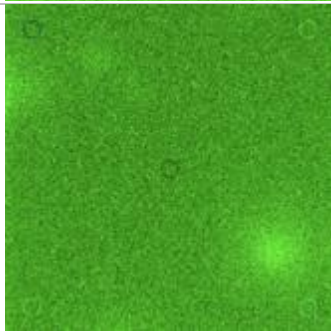
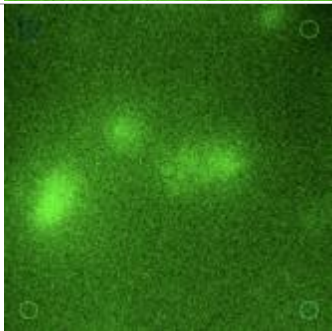
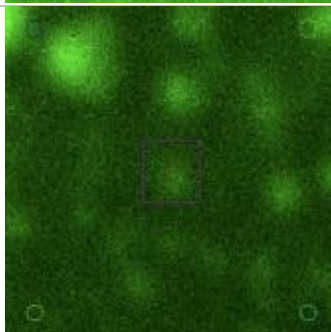
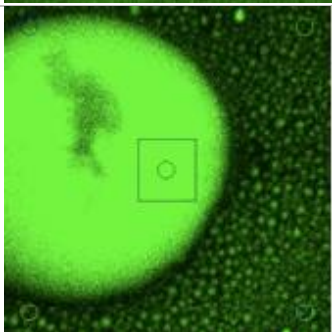
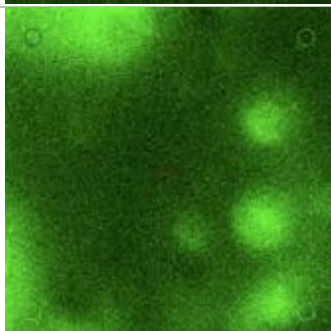
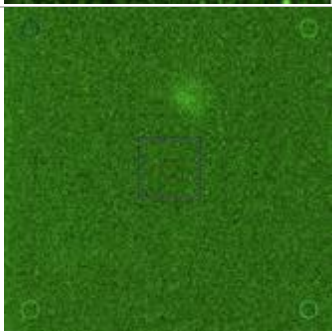
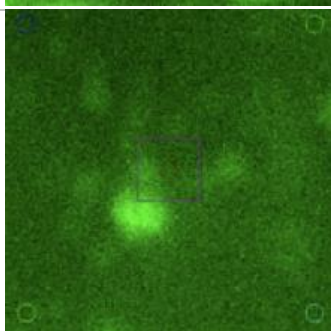


**Figure 10.4.** Sample preparation procedure used for FRAP measurements.



**Figure 10.5.** Films of composition D containing (a) Alexa 488 C5 Maleimide at 3.4 nM in the spin coating solution – image size 214  $\mu\text{m}$  and (b) Alexa 488 carboxylic acid at 3.4 nM in the spin coating solution – image size 60.7  $\mu\text{m}$ .

**Table 10.2.** Images obtained from confocal microscope for PVA/glycerol/surfactant films doped with RhB.

Composition	Image from confocal microscope (60.7 $\mu\text{m}$ )	Composition	Image from confocal microscope (60.7 $\mu\text{m}$ )
a)		b)	
c)		d)	
e)		f)	
g)		h)	
i)			

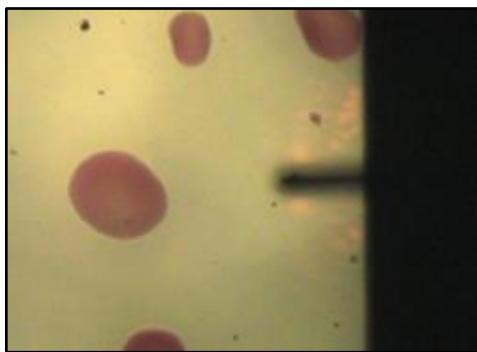


**Figure 10.6.** Morphology of the pure glycerol films doped with RhB –image obtained from optical microscope connected with AFM. The length of the protruding cantilever is ca. 125  $\mu\text{m}$ .

**Table 10.3.** Average radius of FRAP bleach for samples A-I.

Composition	Average resulting spot radius ( $\mu\text{m}$ )
A	$5.61 \pm 0.12$
B	$5.19 \pm 0.09$
C	$5.18 \pm 0.10$
D	$4.89 \pm 0.13$
E	$4.25 \pm 0.10$
F	$4.08 \pm 0.35$
G	$3.21 \pm 0.12$
H	$4.77 \pm 0.15$
I	$5.01 \pm 0.10$

### B1. Effect of sonicating spin coating solutions on eventual film properties

The preparation method is critical for establishing any properties of the resultant films. Sonication was chosen as an additional mixing method to make phase-separated samples as uniform as possible. This process can, however, affect the polymer elongation, tensile strength and Young's modulus, as well as induce physical and chemical changes in the substances due to high pressures connected with bubble cavitation.<sup>441</sup> Moreover, sonication generates more chemical bonds like hydrogen bonds and covalent bonds. To check if the sonication during preparation influences the film properties, sample C was prepared without sonication followed

by examination of 10 positions on the sample to calculate the RhB diffusion coefficient. Sonication does not seem to influence tracer diffusivity in the investigated composition, showing consistent results with its unsonicated counterpart (Table 10.4).

**Table 10.4.** The average diffusion coefficient for the sample C prepared from solution with and without sonication.

Composition	Averaged diffusion coefficient ( $\mu\text{m}^2/\text{s}$ )	Number of positions investigated (-)
C – sonicated	$0.712 \pm 0.036$	30
C – non-sonicated	$0.81 \pm 0.076$	10

It was proven for polymer solutions that while rheological properties change during sonication, they return to their original state after stopping the process.<sup>442,443</sup> Hence, while investigating polymer-based solutions sonication is expected to improve the level of molecular mixing without changing polymer properties. Moreover, while RhB was proven to be sensitive to sonication,<sup>289,444</sup> no observed changes in fluorescence for films prepared from sonicated and non-sonicated solutions were noted.

**Table 10.5.** Average half recovery times and normalised amplitude for fast and slow migrating molecules for investigated samples prepared from filtered solutions.

Composition	$I_{N,\text{fast}}$	$\tau_{1/2,\text{fast}} (\text{s})$	$I_{N,\text{slow}}$	$\tau_{1/2,\text{slow}} (\text{s})$
A	$0.33 \pm 0.0075$	$11.05 \pm 0.55$	$0.20 \pm 0.013$	$94.38 \pm 8.36$
B	$0.52 \pm 0.0063$	$4.94 \pm 0.23$	$0.12 \pm 0.0051$	$145.21 \pm 10.83$
C	$0.22 \pm 0.011$	$3.37 \pm 0.68$	$0.25 \pm 0.011$	$114.27 \pm 12.57$
D	$0.24 \pm 0.032$	$40.9 \pm 7.14$	$0.16 \pm 0.030$	$200.26 \pm 56.81$
E	$0.27 \pm 0.015$	$20.26 \pm 1.44$	$0.12 \pm 0.017$	$195.30 \pm 33.28$
G	$0.097 \pm 0.026$	$7.62 \pm 2.83$	$0.20 \pm 0.023$	$112.14 \pm 35.07$
H	$0.18 \pm 0.036$	$12.54 \pm 7.76$	$0.28 \pm 0.022$	$69.21 \pm 4.55$
I	$0.069 \pm 0.010$	$17.47 \pm 1.20$	$0.31 \pm 0.151$	$295.19 \pm 114.86$



### Appendix C



**Figure 10.7.** Optical microscope image of the bloom region (framed) in a plasticised PVA film containing 3 wt% CTAB after two months of sample storage. The length of the protruding cantilever is ca. 125  $\mu\text{m}$ .

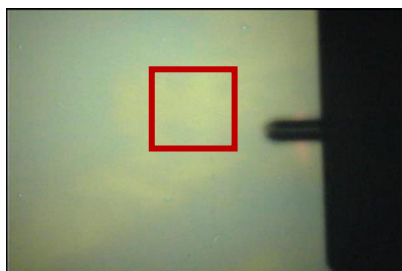


**Figure 10.8.** Optical microscope image of the bloom region (framed) for a film containing 4 wt% CTAB after 2 weeks of sample storage. The length of the protruding cantilever is ca. 125  $\mu\text{m}$ .

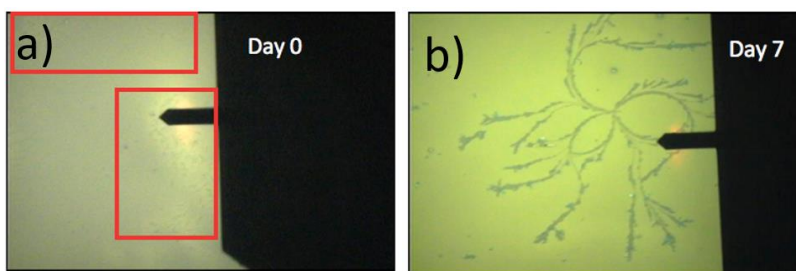


**Figure 10.9.** (a) Optical microscopy image of surfactant blooms and crystals visible on the surface of a film containing 5 wt% CTAB day 0 (framed). (b) Dendritic crystals visible on the surface of the same sample (and position) sample on day 7. The length of the protruding cantilever is ca. 125  $\mu\text{m}$ .

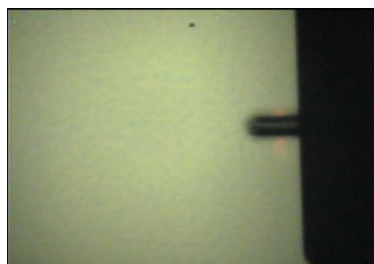


**Figure 10.10.** Optical microscope image of bloom region for a sample containing 2 wt% SDS on day 0. The length of the protruding cantilever is ca. 125  $\mu\text{m}$ .

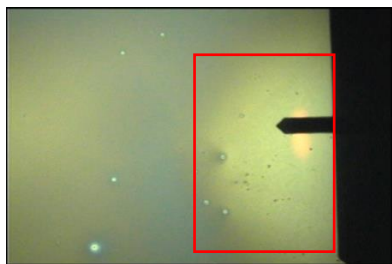


**Figure 10.11.** Optical microscope image of a bloom region (framed) for a sample containing 5 wt% SDS on day 0. The length of the protruding cantilever is ca. 125  $\mu\text{m}$ .

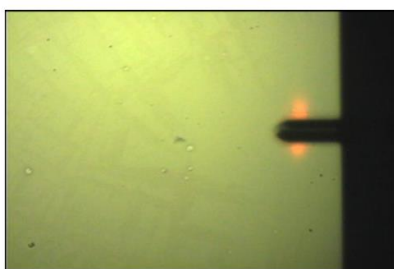


**Figure 10.12.** Optical microscope image of a bloom region for a sample containing 20 wt%  $\text{C}_{12}\text{E}_{10}$  on day 7. The length of the protruding cantilever is ca. 125  $\mu\text{m}$ .

**Table 10.6.** Thickness of PVA-based samples doped with surfactants of various head group chemistry and concentration investigated using AFM scratch test.

Addition of anionic surfactant (SDS)										
Sample→	PVA + glycerol + 1% SDS		PVA + glycerol + 2% SDS		PVA + glycerol + 3% SDS		PVA + glycerol + 4% SDS		PVA + glycerol + 5% SDS	
Time (day) ↓	Thickness (nm)	Error (nm)	Thickness (nm)	Error (nm)	Thickness (nm)	Error (nm)	Thickness (nm)	Error (nm)	Thickness (nm)	Error (nm)
1	82.0	0.5	95.6	1.6	87.1	2.3	80.0	0.7	97.4	1.4
7	71.3	1.4	79.6	1.1	68.2	1.1	58.9	1.1	58.3	0.5
14	69.6	1.4	73.9	2.4	67.7	2.6	60.0	0.4	58.4	0.7
Addition of nonionic surfactant (C <sub>12</sub> E <sub>10</sub> )										
Sample→	PVA + glycerol + 1% C <sub>12</sub> E <sub>10</sub>		PVA + glycerol + 2% C <sub>12</sub> E <sub>10</sub>		PVA + glycerol + 3% C <sub>12</sub> E <sub>10</sub>		PVA + glycerol + 4% C <sub>12</sub> E <sub>10</sub>		PVA + glycerol + 5% C <sub>12</sub> E <sub>10</sub>	
Time (day) ↓	Thickness (nm)	Error (nm)	Thickness (nm)	Error (nm)	Thickness (nm)	Error (nm)	Thickness (nm)	Error (nm)	Thickness (nm)	Error (nm)
1	124.0	1.2	104.6	1.5	95.3	2.0	86.2	2.2	87.5	1.1
7	104.5	1.5	83.5	1.7	80.6	2.6	68.1	2.9	74.1	1.3
14	104.2	1.7	80.4	1.2	83.3	1.7	68.4	2.6	68.5	0.8
Addition of cationic surfactant (CTAB)										
Sample→	PVA + glycerol + 1% CTAB		PVA + glycerol + 2% CTAB		PVA + glycerol + 3% CTAB		PVA + glycerol + 4% CTAB		PVA + glycerol + 5% CTAB	
Time (day) ↓	Thickness (nm)	Error (nm)	Thickness (nm)	Error (nm)	Thickness (nm)	Error (nm)	Thickness (nm)	Error (nm)	Thickness (nm)	Error (nm)
1	100.0	1.9	98.5	0.5	96.8	0.5	82.3	4.1	81.5	1.6
7	79.4	1.4	82.7	0.9	76.9	1.1	67.5	0.9	68.2	1.2
14	85.8	2.8	80.7	0.7	72.0	1.9	72.8	1.8	69.5	1.1
Control samples										
Sample→	PVA		PVA + glycerol							
Time (day) ↓	Thickness (nm)	Error (nm)	Thickness (nm)	Error (nm)						
1	128.6	2.2	116.6	0.1						
7	120.1	2.1	98.4	0.4						
14	124.8	1.9	96.8	0.5						

**Table 10.7.** Thickness (% changes) of the PVA-based samples doped with surfactants of various head group chemistry and concentration investigated as in Table 10.6.

Addition of anionic surfactant (SDS)										
Sample→	PVA + glycerol + 1% SDS		PVA + glycerol + 2% SDS		PVA + glycerol + 3% SDS		PVA + glycerol + 4% SDS		PVA + glycerol + 5% SDS	
Time (day) ↓	Thickness (%)	Error (%)	Thickness (%)	Error (%)	Thickness (%)	Error (%)	Thickness (%)	Error (%)	Thickness (%)	Error (%)
1	100.0	0.2	100.0	1.7	100.0	2.7	100.0	0.9	100.0	1.4
7	86.9	0.2	83.2	1.4	78.3	1.7	73.6	1.8	59.9	0.8
14	84.8	0.2	77.4	3.3	77.7	3.8	74.9	0.6	60.0	1.1
Addition of nonionic surfactant (C <sub>12</sub> E <sub>10</sub> )										
Sample→	PVA + glycerol + 1% C <sub>12</sub> E <sub>10</sub>		PVA + glycerol + 2% C <sub>12</sub> E <sub>10</sub>		PVA + glycerol + 3% C <sub>12</sub> E <sub>10</sub>		PVA + glycerol + 4% C <sub>12</sub> E <sub>10</sub>		PVA + glycerol + 5% C <sub>12</sub> E <sub>10</sub>	
Time (day) ↓	Thickness (%)	Error (%)	Thickness (%)	Error (%)	Thickness (%)	Error (%)	Thickness (%)	Error (%)	Thickness (%)	Error (%)
1	100.0	1.0	100.0	1.4	100.0	2.1	100.0	2.6	100.0	1.3
7	84.3	1.5	79.8	2.1	84.5	3.3	79.0	4.2	84.7	1.5
14	84.0	1.6	76.8	1.5	87.4	2.0	79.4	3.8	78.3	0.9
Addition of cationic surfactant (CTAB)										
Sample→	PVA + glycerol + 1% CTAB		PVA + glycerol + 2% CTAB		PVA + glycerol + 3% CTAB		PVA + glycerol + 4% CTAB		PVA + glycerol + 5% DGME	
Time (day) ↓	Thickness (%)	Error (%)	Thickness (%)	Error (%)	Thickness (%)	Error (%)	Thickness (%)	Error (%)	Thickness (%)	Error (%)
1	100.0	1.9	100.0	0.5	100.0	0.5	100.0	5.0	100.0	2.0
7	79.4	1.7	84.0	1.1	79.5	1.5	82.0	1.3	83.7	1.5
14	85.8	3.3	82.0	0.9	74.4	2.7	88.5	2.5	85.3	1.3
Control samples										
Sample→	PVA		PVA + glycerol							
Time (day) ↓	Thickness (%)	Error (%)	Thickness (%)	Error (%)						
1	100.0	1.7	100.0	0.1						
7	93.4	1.8	84.4	0.4						
14	97.0	1.5	83.0	0.5						

**Table 10.8.** Thickness of PVA-based samples doped with surfactants of various head group chemistry and concentration investigated using AFM scratch test.

15% RH										
Sample →	PVA		PVA + glycerol		PVA + glycerol + 1% SDS		PVA + glycerol + 1% CTAB		PVA + glycerol + 1% C <sub>12</sub> E <sub>10</sub>	
Time (day) ↓	Thickness (nm)	Error (nm)	Thickness (nm)	Error (nm)	Thickness (nm)	Error (nm)	Thickness (nm)	Error (nm)	Thickness (nm)	Error (nm)
1	116.2	2.7	100.5	1.1	85.1	1.0	89.6	0.7	111.7	0.4
7	-	-	-	-	72.4	0.6	-	-	-	-
14	116.5	1.6	80.6	0.8	69.7	0.8	73.4	0.6	88.9	0.5
21	-	-	-	-	68.4	1.1	-	-	-	-
28	116.0	1.8	80.1	1.1	68.8	0.8	72.9	0.2	89.1	0.9
35	-	-	-	-	68.2	1.2	-	-	-	-
42	116.7	2.2	80.8	0.4	68.4	0.5	73.0	0.6	88.4	0.6
25% RH										
Sample →	PVA		PVA + glycerol		PVA + glycerol + 1% SDS		PVA + glycerol + 1% CTAB		PVA + glycerol + 1% C <sub>12</sub> E <sub>10</sub>	
Time (day) ↓	Thickness (nm)	Error (nm)	Thickness (nm)	Error (nm)	Thickness (nm)	Error (nm)	Thickness (nm)	Error (nm)	Thickness (nm)	Error (nm)
1	120.0	2.4	113.5	1.2	89.9	2.7	75.5	0.7	118.6	1.3
7	119.2	2.2	94.0	0.8	72.3	2.0	62.8	0.2	95.1	0.6
14	125.6	1.4	93.6	1.4	70.9	2.6	60.7	0.6	96.3	1.0
21	122.7	2.7	91.0	1.6	69.9	2.6	60.9	1.3	94.9	1.5
28	120.2	1.1	92.4	0.5	72.6	1.7	61.7	1.2	94.1	0.3
35	118.3	1.4	90.4	1.2	71.5	2.5	59.2	1.1	90.2	1.0
42	122.6	2.1	92.7	2.2	70.4	3.7	63.7	2.7	94.2	2.0

**Table 10.8 (continuation).** Thickness of PVA-based samples doped with surfactants of various head group chemistry and concentration investigated using AFM scratch test.

35% RH										
Sample →	PVA		PVA + glycerol		PVA + glycerol + 1% SDS		PVA + glycerol + 1% CTAB		PVA + glycerol + 1% C <sub>12</sub> E <sub>10</sub>	
Time (day) ↓	Thickness (nm)	Error (nm)	Thickness (nm)	Error (nm)	Thickness (nm)	Error (nm)	Thickness (nm)	Error (nm)	Thickness (nm)	Error (nm)
1	127.6	1.5	107.9	0.8	88.8	1.5	102.5	1.7	104.5	3.8
7	126.2	3.1	92.5	2.5	70.0	2.0	89.4	3.7	90.2	2.4
14	124.5	2.1	91.2	1.4	74.7	1.5	87.4	4.4	87.2	3.3
21	125.4	1.5	93.4	2.2	71.3	1.1	84.2	1.8	84.8	4.0
28	126.2	1.6	85.6	1.0	70.7	0.8	84.3	1.0	84.4	3.4
35	122.1	1.9	89.5	1.3	71.1	0.5	83.7	1.4	86.5	3.8
42	126.4	1.8	86.5	1.4	71.8	0.7	87.7	4.2	85.3	3.7
45% RH										
Sample →	PVA		PVA + glycerol		PVA + glycerol + 1% SDS		PVA + glycerol + 1% CTAB		PVA + glycerol + 1% C <sub>12</sub> E <sub>10</sub>	
Time (day) ↓	Thickness (nm)	Error (nm)	Thickness (nm)	Error (nm)	Thickness (nm)	Error (nm)	Thickness (nm)	Error (nm)	Thickness (nm)	Error (nm)
1	103.6	3.3	94.8	0.9	83.9	1.1	92.2	1.1	107.8	1.2
3	103.3	1.7	81.1	1.0	65.2	2.1	76.6	0.5	88.0	0.6
7	103.7	2.3	79.8	0.7	67.0	1.4	73.8	0.9	88.0	0.8
14	106.8	1.9	78.1	0.6	62.1	1.9	74.2	0.7	86.9	1.5
21	103.6	1.1	78.3	2.5	65.0	2.3	74.4	0.5	88.6	1.4
28	106.7	2.3	79.1	0.9	64.8	1.5	74.3	0.8	88.0	1.6
35	106.2	2.7	76.6	0.5	64.1	1.1	73.9	0.5	87.4	1.0
42	104.6	1.4	80.5	0.5	63.5	1.0	76.5	0.8	87.3	0.9

**Table 10.8 (continuation).** Thickness of PVA-based samples doped with surfactants of various head group chemistry and concentration investigated using AFM scratch test.

55% RH										
Sample →	PVA		PVA + glycerol		PVA + glycerol + 1% SDS		PVA + glycerol + 1% CTAB		PVA + glycerol + 1% C <sub>12</sub> E <sub>10</sub>	
Time (day) ↓	Thickness (nm)	Error (nm)	Thickness (nm)	Error (nm)	Thickness (nm)	Error (nm)	Thickness (nm)	Error (nm)	Thickness (nm)	Error (nm)
1	133.1	1.3	127.2	2.0	97.6	0.9	96.4	1.0	128.9	1.1
3	126.9	3.3	104.2	1.5	80.5	0.6	81.5	0.7	107.8	0.5
7	131.6	4.1	101.8	1.1	77.4	1.6	83.1	0.7	107.5	0.7
14	127.8	3.7	98.5	1.0	79.1	1.0	80.2	1.0	102.2	0.7
21	126.3	2.1	98.7	0.3	76.7	1.2	78.8	0.5	102.4	0.6
28	129.9	2.7	100.9	2.0	77.8	0.8	79.7	0.7	102.0	0.5
35	131.2	4.5	96.8	1.1	75.7	2.1	78.0	0.6	101.0	1.3
42	129.9	2.4	97.9	2.7	78.2	3.8	75.3	1.4	100.4	1.7

**Table 10.9.** Thickness (% changes) of PVA-based samples doped with surfactants of various head group chemistry and concentration investigated as in Table 10.8.

15% RH										
Sample →	PVA		PVA + glycerol		PVA + glycerol + 1% SDS		PVA + glycerol + 1% CTAB		PVA + glycerol + 1% C <sub>12</sub> E <sub>10</sub>	
Time (day) ↓	Thickness (%)	Error (%)	Thickness (%)	Error (%)	Thickness (%)	Error (%)	Thickness (%)	Error (%)	Thickness (%)	Error (%)
1	100.0	2.3	100.0	1.1	100.0	1.1	100.0	0.8	100.0	0.4
7	-	-	-	-	85.1	0.8	-	-	-	-
14	100.3	1.4	80.2	1.0	81.9	1.2	81.9	0.9	79.6	0.5
21	-	-	-	-	80.4	1.6	-	-	-	-
28	99.8	1.5	79.8	1.3	80.9	1.2	81.4	0.3	79.8	1.0
35	-	-	-	-	80.2	1.8	-	-	-	-
42	100.4	1.9	80.5	0.5	80.4	0.7	81.5	0.8	79.1	0.7

**Table 10.9 (continuation).** Thickness (% changes) of PVA-based samples doped with surfactants of various head group chemistry and concentration investigated as in Table 10.8.

25% RH										
Sample →	PVA		PVA + glycerol		PVA + glycerol + 1% SDS		PVA + glycerol + 1% CTAB		PVA + glycerol + 1% C <sub>12</sub> E <sub>10</sub>	
Time (day) ↓	Thickness (%)	Error (%)	Thickness (%)	Error (%)	Thickness (%)	Error (%)	Thickness (%)	Error (%)	Thickness (%)	Error (%)
1	100.0	2.0	100.0	1.0	100.0	3.0	100.0	0.9	100.0	1.1
7	99.3	1.8	82.8	0.9	80.4	2.7	83.2	0.4	80.2	0.7
14	104.7	1.1	82.5	1.4	78.9	3.6	80.4	0.9	81.2	1.0
21	102.3	2.2	80.2	1.8	77.7	3.7	80.6	2.1	80.0	1.6
28	100.2	0.9	81.4	0.5	80.7	2.3	81.7	2.0	79.4	0.3
35	98.6	1.2	79.7	1.4	79.6	3.5	78.3	1.9	76.1	1.1
42	102.2	1.7	81.7	2.4	78.3	5.3	84.4	4.2	79.5	2.1
35% RH										
Sample →	PVA		PVA + glycerol		PVA + glycerol + 1% SDS		PVA + glycerol + 1% CTAB		PVA + glycerol + 1% C <sub>12</sub> E <sub>10</sub>	
Time (day) ↓	Thickness (%)	Error (%)	Thickness (%)	Error (%)	Thickness (%)	Error (%)	Thickness (%)	Error (%)	Thickness (%)	Error (%)
1	100.0	1.2	100.0	0.7	100.0	1.7	100.0	1.6	100.0	3.6
7	99.0	2.4	85.8	2.7	78.8	2.9	87.3	4.1	86.4	2.7
14	97.6	1.7	84.5	1.5	84.1	2.1	85.3	5.0	83.5	3.8
21	98.3	1.2	86.6	2.3	80.3	1.5	82.2	2.2	81.2	4.7
28	98.9	1.3	79.3	1.2	79.6	1.1	82.3	1.1	80.8	4.1
35	95.7	1.6	82.9	1.5	80.0	0.7	81.7	1.7	82.8	4.4
42	99.1	1.5	80.2	1.6	80.9	1.0	85.5	4.7	81.7	4.3



**Table 10.9 (continuation).** Thickness (% changes) of PVA-based samples doped with surfactants of various head group chemistry and concentration investigated as in Table 10.8.

45% RH										
Sample →	PVA		PVA + glycerol		PVA + glycerol + 1% SDS		PVA + glycerol + 1% CTAB		PVA + glycerol + 1% C <sub>12</sub> E <sub>10</sub>	
Time (day) ↓	Thickness (%)	Error (%)	Thickness (%)	Error (%)	Thickness (%)	Error (%)	Thickness (%)	Error (%)	Thickness (%)	Error (%)
1	100.0	3.2	100.0	0.9	100.0	1.3	100.0	1.2	100.0	1.1
3	99.7	1.6	85.6	1.2	77.7	3.2	83.1	0.7	81.6	0.7
7	100.1	2.2	84.2	0.9	79.9	2.0	80.0	1.2	81.7	0.9
14	103.1	1.8	82.4	0.7	74.0	3.0	80.5	1.0	80.6	1.7
21	100.0	1.1	82.6	3.2	77.5	3.6	80.7	0.7	82.2	1.6
28	103.0	2.1	83.5	1.1	77.2	2.4	80.6	1.1	81.6	1.8
35	102.6	2.5	80.8	0.7	76.4	1.7	80.1	0.6	81.1	1.1
42	100.9	1.3	85.0	0.7	75.7	1.6	83.0	1.0	81.0	1.0
55% RH										
Sample →	PVA		PVA + glycerol		PVA + glycerol + 1% SDS		PVA + glycerol + 1% CTAB		PVA + glycerol + 1% C <sub>12</sub> E <sub>10</sub>	
Time (day) ↓	Thickness (%)	Error (%)	Thickness (%)	Error (%)	Thickness (%)	Error (%)	Thickness (%)	Error (%)	Thickness (%)	Error (%)
1	100.0	0.9	100.0	1.6	100.0	1.0	100.0	1.1	100.0	0.8
3	95.3	2.6	82.0	1.4	82.4	0.7	84.5	0.9	83.6	0.5
7	98.9	3.1	80.1	1.1	79.3	2.0	86.2	0.8	83.4	0.6
14	96.0	2.9	77.5	1.1	81.0	1.2	83.2	1.3	79.3	0.7
21	94.9	1.7	77.6	0.4	78.6	1.6	81.7	0.6	79.5	0.6
28	97.6	2.1	79.3	2.0	79.7	1.0	82.7	0.9	79.1	0.5
35	98.6	3.5	76.1	1.1	77.6	2.8	80.9	0.8	78.4	1.3
42	97.6	1.9	77.0	2.7	80.1	4.8	78.1	1.9	77.9	1.7

**Table 10.10.** Average thickness and thickness range of solution cast PVA-based samples doped with surfactants of various head group chemistry and concentration.

Sample	1% CTAB	1% C <sub>12</sub> E <sub>10</sub>	1% SDS	3% CTAB	3% C <sub>12</sub> E <sub>10</sub>	3% SDS
Average thickness (μm)	34.5 ± 7.3	36.4 ± 6.3	39.9 ± 10.5	42.3 ± 9.2	76.4 ± 10.6	57.8 ± 32.7
Range (μm)	12-55	19-69	15-80	3-70	38-108	2-142

**Table 10.10 (continuation).** Average thickness and thickness range of solution cast PVA-based samples doped with surfactants of various head group chemistry and concentration.

Sample	5% CTAB	5% C <sub>12</sub> E <sub>10</sub>	5% SDS	PVA	PVA + glycerol
Average thickness (μm)	34.3 ± 8.8	39.3 ± 8	68.5 ± 27.2	21.3 ± 1.5	33.6 ± 4.2
Range (μm)	10-60	31-50	2-179	15-27	24-49

**Table 10.11.** Time required to reach equilibrium (in minutes) for thick PVA-based samples doped with surfactants of various head group chemistry and concentration investigated using DVS.

RH (%)	PVA	PVA	PVA	PVA + glycerol	PVA + glycerol + 1% SDS	PVA + glycerol + 3% SDS	PVA + glycerol + 3% SDS	PVA + glycerol + 3% SDS
1	10.0	10.0	10.0	10.0	10.0	10.0	10.0	10.0
5	9.7	9.7	9.7	9.7	9.7	9.7	9.7	9.7
15	9.7	9.7	9.7	9.7	16.3	9.7	9.7	9.7
25	9.7	9.7	46.0	55.3	65.0	51.0	9.7	9.7
35	9.7	9.7	55.3	59.0	47.3	57.7	9.7	9.7
45	9.7	9.7	65.3	40.3	45.0	58.7	25.0	59.0
55	10.0	10.0	79.0	48.3	61.0	96.7	67.0	129.0
65	9.7	9.7	89.3	25.3	95.0	74.3	66.6	27.3
75	120.7	119.7	47.3	9.7	49.0	50.0	73.0	18.7
65	9.7	9.7	37.3	24.3	30.0	10.0	9.7	9.7
55	18.4	17.7	55.7	9.7	53.0	49.3	9.7	9.7
45	23.3	23.0	70.0	10.0	77.3	65.7	9.7	9.7
35	18.0	20.0	59.7	32.3	47.3	76.7	47.7	9.7
25	9.7	9.7	46.3	42.3	58.0	62.0	34.7	10.0
15	41.0	41.3	72.0	61.0	69.3	93.0	51.3	10.0
5	9.7	10.0	10.0	9.7	29.3	9.7	9.7	49.0
1	10.0	9.7	10.0	9.7	9.7	9.7	9.7	9.6
Change in mass after the whole cycle (%)	2.3	2.0	1.0	0.8	0.7	1.3	2.6	3.1

**Table 10.11 (continuation).** Time required to reach equilibrium (in minutes) for thick PVA-based samples doped with surfactants of various head group chemistry and concentration investigated using DVS.

RH (%)	PVA + glycerol + 5% SDS	PVA + glycerol + 1% C <sub>12</sub> E <sub>10</sub>	PVA + glycerol + 3% C <sub>12</sub> E <sub>10</sub>	PVA + glycerol + 5% C <sub>12</sub> E <sub>10</sub>	PVA + glycerol + 1% CTAB	PVA + glycerol + 3% CTAB	PVA + glycerol + 5% CTAB	PVA + glycerol + 5% CTAB
1	10.0	10.0	11.7	10.0	10.0	15.7	10.0	10.0
5	9.7	9.7	10.0	9.7	9.7	9.7	9.7	9.7
15	9.7	9.7	9.7	9.7	9.7	10.0	9.7	9.7
25	9.7	51.7	58.3	52.3	36.3	59.3	49.3	49.7
35	9.5	41.7	40.0	40.7	41.3	50.7	39.0	41.0
45	9.7	50.0	58.0	46.0	63.0	67.0	42.0	46.3
55	77.7	89.7	44.3	60.3	101.0	43.3	43.0	59.3
65	131.3	78.7	30.0	103.3	87.0	59.3	32.0	120.0
75	55.3	46.0	9.7	41.7	48.3	11.0	18.3	42.7
65	9.7	30.0	9.7	39.3	33.3	19.0	21.4	39.3
55	9.7	50.7	9.7	46.7	48.7	19.7	9.7	52.0
45	61.7	67.0	28.3	59.3	65.7	47.7	29.3	71.7
35	34.0	50.7	52.7	48.3	52.0	73.6	46.7	57.3
25	35.7	51.7	36.7	43.3	53.3	45.7	39.0	49.0
15	38.7	70.3	58.0	57.3	61.7	80.0	61.3	74.3
5	9.7	9.7	10.0	9.7	9.7	9.7	9.7	9.7
1	9.7	9.7	10.0	9.0	9.7	14.0	9.7	9.7
Change in mass after the whole cycle (%)	2.5	0.7	0.3	0.5	1.0	0.6	0.3	1.0

## Appendix D

**Table 10.12.** Thickness, roughness, SFE, and fit parameters to Equation 7.1 for PVA films with various compositions. Shaded cells correspond to spin-coated films.

Sample	Thickness ( $\mu\text{m}$ )	Roughness (nm)	k	n	R <sup>2</sup>	SFE <sub>0</sub> (mN/m)
87PVA	30.6±1.9	0.6±0.01	-0.119±0.014	0.171±0.011	0.915±0.012	45.214±0.396
	44.5±3.8	0.8±0.02	-0.080±0.019	0.206±0.031	0.938±0.033	39.419±0.236
	87.0±3.3	0.8±0.04	-0.100±0.012	0.205±0.012	0.927±0.009	40.092±0.637
	129.7±7.6	0.7 ±0.02	-0.039±0.007	0.302±0.018	0.969±0.007	43.491±0.629
	0.093±0.003	0.3±0.02	-0.369±0.007	0.275±0.013	0.880±0.009	50.202±0.268
	0.120±0.003	0.3±0.02	-0.279±0.021	0.328±0.016	0.891±0.008	48.275±0.510
Plasticised 87PVA	21.7±2.7	0.9 ± 0.02	-0.095±0.039	0.425±0.038	0.973±0.008	44.259±0.554
	39.3±5.5	0.9±0.02	-0.252±0.012	0.181±0.046	0.759±0.080	44.366±0.337
	73.5±4.5	0.8±0.01	-0.187±0.020	0.274±0.019	0.930±0.038	42.024±0.153
	108.8±3.0	1±0.03	-0.225±0.030	0.257±0.018	0.959±0.016	42.116±0.589
	0.078±0.001	0.3±0.01	-0.487±0.029	0.264±0.028	0.815±0.021	45.805±0.174
	0.118±0.001	0.3±0.01	-0.355±0.039	0.374±0.050	0.871±0.040	44.194±0.236
99PVA	52.8±2.3	1±0.02	-0.030±0.007	0.350±0.039	0.831±0.035	54.426±0.321
	88.3±4.6	1.2±0.02	-0.105±0.021	0.148±0.017	0.841±0.015	55.071±0.506
	129.7±3.3	0.9±0.01	-0.068±0.021	0.224±0.047	0.867±0.014	52.133±0.798
	208.5±2.2	1.0±0.01	-0.046±0.017	0.360±0.101	0.893±0.028	53.666±0.491
	0.149±0.009	0.4±0.02	-0.068±0.008	0.158±0.014	0.890±0.008	58.326±0.423
	0.192±0.013	0.6±0.02	-0.041±0.008	0.218±0.028	0.921±0.013	57.387±0.289
Plasticised 99PVA	33.1±3.3	1±0.03	-0.156±0.023	0.274±0.035	0.922±0.010	58.913±0.358
	65.8±3.0	0.9±0.03	-0.241±0.047	0.167±0.015	0.851±0.043	59.665±0.583
	119.8±2.1	0.9±0.03	-0.617±0.064	0.122±0.021	0.925±0.011	50.764±0.867
	169.2±4.1	1.4±0.03	-0.420±0.080	0.128±0.014	0.917±0.028	53.032±0.876
	0.124±0.001	0.7±0.05	-0.409±0.035	0.370±0.043	0.883±0.028	51.433±0.244
	0.181±0.003	0.8±0.04	-0.345±0.074	0.535±0.118	0.924±0.029	54.229±0.374

**Table 10.13.** CA evolution parameters for investigated compositions using water as the medium. Symbols represent:  $CA_0$  – initial CA,  $CA_e$  – contact angle at the end of the measurement,  $\Delta CA$  – difference between  $CA_0$  and  $CA_e$ ,  $\Delta V$  – change in the droplet volume,  $\Delta A$  – change in the liquid/solid contact area. For mechanisms, A+S stands for absorption and spreading, while S – for spreading (MS indicates mainly spreading). Shaded cells correspond to spin-coated films.

Sample	Thickness ( $\mu\text{m}$ )	$CA_0$ ( $^\circ$ )	$CA_e$ ( $^\circ$ )	$\Delta CA$ ( $^\circ$ )	$\Delta V$ ( $\mu\text{L}$ )	$\Delta A$ ( $\text{mm}^2$ )	Mechanism
87PVA	30.6 $\pm$ 1.9	62.54 $\pm$ 1.59	48.67 $\pm$ 0.55	-13.86 $\pm$ 1.18	-0.46 $\pm$ 0.08	1.32 $\pm$ 0.73	A+S
	44.5 $\pm$ 3.8	73.57 $\pm$ 0.97	61.23 $\pm$ 1.14	-12.34 $\pm$ 0.97	-0.17 $\pm$ 0.16	1.17 $\pm$ 0.33	A+S
	87.0 $\pm$ 3.3	71.66 $\pm$ 2.70	56.24 $\pm$ 1.94	-15.42 $\pm$ 1.23	-0.77 $\pm$ 0.06	2.26 $\pm$ 0.52	A+S
	129.7 $\pm$ 7.6	66.00 $\pm$ 2.40	57.21 $\pm$ 2.20	-8.79 $\pm$ 0.80	-0.31 $\pm$ 0.05	1.09 $\pm$ 0.15	A+S
	0.093 $\pm$ 0.003	54.34 $\pm$ 1.05	20.01 $\pm$ 0.51	-34.33 $\pm$ 1.23	-0.32 $\pm$ 0.22	12.84 $\pm$ 0.28	A+S (MS)
	0.120 $\pm$ 0.003	57.79 $\pm$ 1.88	19.91 $\pm$ 0.11	-37.88 $\pm$ 1.99	-0.65 $\pm$ 0.09	11.85 $\pm$ 0.70	A+S
Plasticised 87PVA	21.7 $\pm$ 2.7	64.41 $\pm$ 1.77	43.84 $\pm$ 5.24	-20.57 $\pm$ 6.91	-0.63 $\pm$ 0.19	2.81 $\pm$ 1.24	A+S
	39.3 $\pm$ 5.5	64.45 $\pm$ 1.26	39.88 $\pm$ 5.14	24.57 $\pm$ 5.42	-0.40 $\pm$ 0.18	5.04 $\pm$ 1.61	A+S
	73.5 $\pm$ 4.5	68.27 $\pm$ 0.60	39.46 $\pm$ 1.02	-28.81 $\pm$ 1.19	-0.94 $\pm$ 0.38	5.33 $\pm$ 1.02	A+S
	108.8 $\pm$ 3.0	68.54 $\pm$ 2.73	34.49 $\pm$ 1.33	-34.05 $\pm$ 3.63	-0.34 $\pm$ 0.14	5.12 $\pm$ 0.48	A+S (MS)
	0.078 $\pm$ 0.001	61.69 $\pm$ 0.64	18.54 $\pm$ 0.32	-43.16 $\pm$ 0.78	-0.40 $\pm$ 0.13	14.13 $\pm$ 0.77	A+S (MS)
	0.118 $\pm$ 0.001	64.51 $\pm$ 0.89	21.63 $\pm$ 1.63	-42.88 $\pm$ 2.01	-0.45 $\pm$ 0.23	11.91 $\pm$ 1.14	A+S (MS)
99PVA	52.8 $\pm$ 2.3	47.37 $\pm$ 1.13	40.52 $\pm$ 1.20	-6.84 $\pm$ 1.28	-0.29 $\pm$ 0.03	0.25 $\pm$ 0.06	A+S
	88.3 $\pm$ 4.6	45.72 $\pm$ 1.23	35.99 $\pm$ 1.57	-9.73 $\pm$ 1.21	-0.29 $\pm$ 0.04	0.34 $\pm$ 0.08	A+S
	129.7 $\pm$ 3.3	50.13 $\pm$ 2.81	41.53 $\pm$ 1.23	-8.60 $\pm$ 2.21	-0.35 $\pm$ 0.07	0.33 $\pm$ 0.13	A+S
	208.5 $\pm$ 2.2	47.19 $\pm$ 1.31	41.08 $\pm$ 1.09	-6.11 $\pm$ 1.09	-0.32 $\pm$ 0.04	0.27 $\pm$ 0.09	A+S
	0.149 $\pm$ 0.009	41.60 $\pm$ 0.99	36.36 $\pm$ 0.59	-5.24 $\pm$ 0.57	-0.33 $\pm$ 0.01	0.06 $\pm$ 0.01	A+S
	0.192 $\pm$ 0.013	43.05 $\pm$ 0.69	38.76 $\pm$ 0.62	-4.29 $\pm$ 0.34	-0.30 $\pm$ 0.02	0.10 $\pm$ 0.06	A+S
Plasticised 99PVA	33.1 $\pm$ 3.3	39.50 $\pm$ 1.13	27.45 $\pm$ 0.44	-12.05 $\pm$ 0.87	-1.12 $\pm$ 0.24	4.16 $\pm$ 1.43	A+S
	65.8 $\pm$ 3.0	38.23 $\pm$ 2.40	26.77 $\pm$ 0.34	-11.46 $\pm$ 2.49	-3.02 $\pm$ 0.81	3.45 $\pm$ 0.97	A+S
	119.8 $\pm$ 2.1	52.78 $\pm$ 2.66	19.56 $\pm$ 1.20	-33.21 $\pm$ 2.49	-0.96 $\pm$ 0.36	13.64 $\pm$ 2.92	A+S
	169.2 $\pm$ 4.1	47.49 $\pm$ 3.12	22.61 $\pm$ 1.30	-24.88 $\pm$ 3.72	-0.36 $\pm$ 0.19	7.94 $\pm$ 1.54	A+S
	0.124 $\pm$ 0.001	52.32 $\pm$ 0.87	22.15 $\pm$ 2.07	-30.17 $\pm$ 2.41	-3.22 $\pm$ 0.86	16.27 $\pm$ 4.67	A+S
	0.181 $\pm$ 0.003	47.75 $\pm$ 1.31	15.01 $\pm$ 0.84	-32.75 $\pm$ 1.78	-0.44 $\pm$ 0.08	28.28 $\pm$ 12.88	S

### D1. FTIR spectroscopy of PVA-based thick films

Data in the fingerprint region for analysed compositions (Figure 7.5) suggest that the spectrum is substantially altered both by presence of glycerol and changes in DH. For the unplasticised PVA spectra, the peak at 1050  $\text{cm}^{-1}$  (assigned to C-O stretching, Table 10.14) is much weaker compared to plasticised samples, evidently due to the glycerol presence. Conversely, peaks at 1250 and ca. 1735  $\text{cm}^{-1}$  were only detected in samples with lower DH (regardless of plasticisation), i.e. associated with carbonyl groups<sup>38</sup> – the C=O and C-O stretching from remaining acetate groups.<sup>242,445</sup> Three peaks present between 1320 and 1450  $\text{cm}^{-1}$ , corresponding to  $\text{CH}_2$  bending, show significant changes between samples of

different DH, but not between plasticised and unplasticised samples of the same DH. Presumably this reflects different relative abundances of CH<sub>2</sub> vibrational modes in the polymer backbone and acetate groups.

**Table 10.14.** FTIR absorption bands of PVA films.

Assignment	Wavenumber (cm <sup>-1</sup> )	Associated references
OH stretching (intramolecular and intramolecular hydrogen bonds) <sup>80,242</sup>	3200-3500	37,38,242,439
CH <sub>2</sub> stretching and bending	2900-2942	37,38,439
C=O and C-O stretching	1735-1750	242,445
CH <sub>2</sub> bending	1320, 1380, 1417-1461	38,242
C-O stretching	1050, 1094, 1100, 1250	39,439
C-C stretching	820-850, 1141-1143	37,38
C-O (crystallinity)	1141	242
C-O-C stretching*	1085-1150	242
C-OH stretching	950	439
CH <sub>2</sub> rocking	916-922	37

\*Associated with PVAc groups

Beyond the fingerprint region, the peak of 3300 cm<sup>-1</sup> is assigned to hydrogen bonding (and more generally -OH groups). In the literature, the intensity of this peak was reported to decrease with increasing glycerol concentration.<sup>80</sup> Although not a quantitative measure, here the intensity of this peak lowers with increasing glycerol concentration. Inverse behaviour can be observed in the 1094 cm<sup>-1</sup> peak (C-O stretching, Table 10.14). For both peaks, these changes may be correlated with the amount of glycerol and acetate groups in the system: the difference in peak intensity between plasticised and unplasticised samples appears constant regardless of DH and *vice versa*. The peaks observed at ca. 2840 cm<sup>-1</sup> and 2920 cm<sup>-1</sup> correspond to symmetric and antisymmetric stretching of C-H from alkyl groups, respectively,<sup>446</sup> shifting slightly with changes in the composition, although no correlation between peak intensity and film composition was observed. The ratio of 3300/2920 cm<sup>-1</sup> peaks increases with addition of glycerol for 87PVA films, but does not for 99PVA. When thinking of a film as a whole, this

stands to reason as the ratio of total -OH groups to -CH<sub>2</sub> groups is similar in plasticised and unplasticised 99PVA films, while this ratio increases significantly as glycerol is introduced to the 87PVA films. Moreover, for samples of a given composition, there was very little change in the spectra with changes of the sample thickness (Figure 10.13). For instance, some differences were visible in the 2850-3300 cm<sup>-1</sup> region, indicating slight variations in system water content.

**Table 10.15.** Average DC values for all investigated compositions.

Sample	Thickness (µm)	DC (1140/1425)	DC (Peppas et al.)	DC (1140/850)	DC (1140/1094)	DC (Tretinnikov et al.)
87PVA	30.6±1.9	106.67±0.39	45.84±0.45	127.38±0.35	47.24±0.04	29.18±0.04
	44.5±3.8	104.61±0.19	43.73±0.22	135.16±0.48	49.16±0.06	30.89±0.06
	87.0±3.3	105.41±0.27	44.55±0.31	132.66±0.76	48.37±0.18	30.19±0.18
	129.7±7.6	105.32±0.10	44.46±0.11	137.60±0.11	49.31±0.07	31.03 ± 0.06
Plasticised 87PVA	21.7±2.7	82.52±0.18	21.06±0.20	114.09±0.20	42.47±0.06	24.91±0.06
	39.3±5.5	76.75±0.42	15.15±0.48	107.15±0.46	39.76±0.17	22.49±0.17
	73.5±4.5	87.09±0.31	25.75±0.36	118.15±0.29	43.92±0.09	26.21±0.09
	108.8±3.0	87.37± 0.33	26.05±0.38	118.29±0.31	43.72±0.13	26.03±0.13
99PVA	52.8±2.3	113.20±0.35	52.54±0.40	126.82±0.37	49.51±0.14	31.21±0.14
	88.3±4.6	110.88±0.96	50.16±1.11	123.64±1.18	48.46±0.32	30.27±0.32
	129.7±3.3	101.95±0.13	41.00±0.15	116.02±0.23	46.45±0.06	28.47±0.06
	208.5±2.2	103.86±0.11	42.96±0.13	118.18±0.09	46.89±0.03	28.87±0.03
Plasticised 99PVA	33.1±3.3	86.88±0.18	25.54±0.21	102.62±0.31	41.59±0.12	24.12±0.12
	65.8±3.0	86.75±0.46	25.40±0.53	104.12±0.28	42.35±0.15	24.81±0.14
	119.8±2.1	94.86±0.32	33.72±0.37	111.95±0.05	45.85±0.04	27.94±0.04
	169.2±4.1	95.38±0.17	34.26±0.19	112.88±0.10	46.35±0.05	28.38±0.05



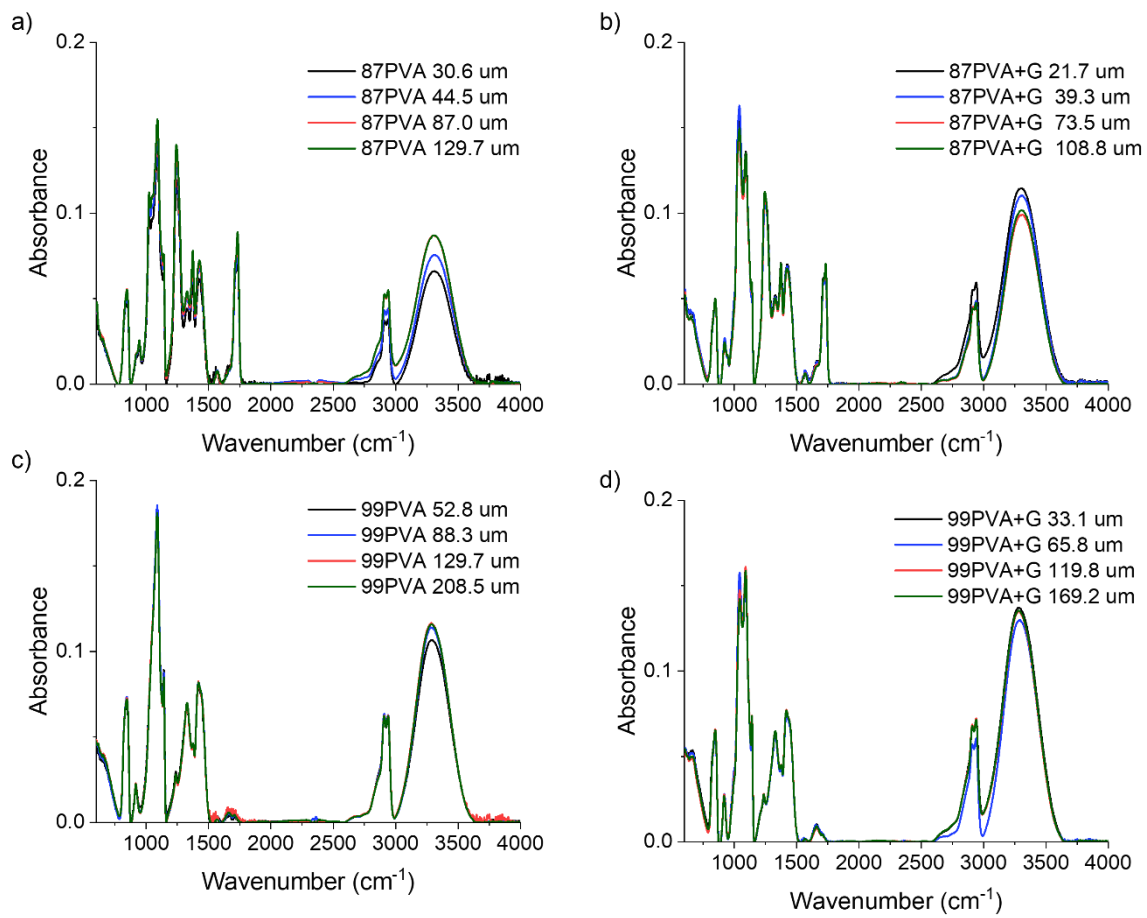


**Figure 10.13.** FTIR spectra of solution-cast PVA films, comparing between different thicknesses. (a) 87PVA, (b) plasticised 87PVA, (c) 99PVA, and (d) plasticised 99PVA.

**Table 10.16.** Fit parameters to Equation 7.1 for spreading of SDS solution on the surface of the films of various compositions. Shaded cells correspond to spin-coated films, while bCMC stands for surfactant solution below CMC.

Sample	Thickness ( $\mu\text{m}$ )	k	n	R <sup>2</sup>
87PVA	30.6 $\pm$ 1.9	-0.320 $\pm$ 0.043	0.074 $\pm$ 0.009	0.715 $\pm$ 0.042
	44.5 $\pm$ 3.8	-0.170 $\pm$ 0.068	0.149 $\pm$ 0.039	0.925 $\pm$ 0.024
	87.0 $\pm$ 3.3	-0.109 $\pm$ 0.035	0.227 $\pm$ 0.049	0.961 $\pm$ 0.005
	129.7 $\pm$ 7.6	-0.095 $\pm$ 0.032	0.231 $\pm$ 0.047	0.936 $\pm$ 0.019
	0.093 $\pm$ 0.003	-0.233 $\pm$ 0.046	0.371 $\pm$ 0.025	0.986 $\pm$ 0.002
	0.120 $\pm$ 0.003	-0.151 $\pm$ 0.011	0.426 $\pm$ 0.017	0.991 $\pm$ 0.001
	bCMC 30.6 $\pm$ 1.9	-0.115 $\pm$ 0.040	0.176 $\pm$ 0.038	0.913 $\pm$ 0.041
	bCMC 87.0 $\pm$ 3.3	-0.020 $\pm$ 0.003	0.298 $\pm$ 0.022	0.981 $\pm$ 0.003
Plasticised 87PVA	21.7 $\pm$ 2.7	-0.539 $\pm$ 0.029	0.182 $\pm$ 0.010	0.762 $\pm$ 0.010
	39.3 $\pm$ 5.5	-0.512 $\pm$ 0.074	0.170 $\pm$ 0.020	0.722 $\pm$ 0.026
	73.5 $\pm$ 4.5	-0.506 $\pm$ 0.083	0.196 $\pm$ 0.021	0.782 $\pm$ 0.035
	108.8 $\pm$ 3.0	-0.518 $\pm$ 0.041	0.164 $\pm$ 0.016	0.726 $\pm$ 0.026
	0.078 $\pm$ 0.001	-0.433 $\pm$ 0.047	0.255 $\pm$ 0.021	0.893 $\pm$ 0.008
	0.118 $\pm$ 0.001	-0.307 $\pm$ 0.025	0.267 $\pm$ 0.016	0.859 $\pm$ 0.017
	99PVA	52.8 $\pm$ 2.3	-0.719 $\pm$ 0.031	0.416 $\pm$ 0.045
88.3 $\pm$ 4.6	-0.744 $\pm$ 0.055	0.377 $\pm$ 0.036	0.903 $\pm$ 0.042	
129.7 $\pm$ 3.3	-0.755 $\pm$ 0.041	0.457 $\pm$ 0.061	0.951 $\pm$ 0.023	
208.5 $\pm$ 2.2	-0.972 $\pm$ 0.062	0.408 $\pm$ 0.050	0.899 $\pm$ 0.053	
0.149 $\pm$ 0.009	-0.558 $\pm$ 0.090	0.047 $\pm$ 0.011	0.710 $\pm$ 0.038	
0.192 $\pm$ 0.013	-0.521 $\pm$ 0.020	0.040 $\pm$ 0.001	0.691 $\pm$ 0.013	
bCBC 52.8 $\pm$ 2.3	-0.056 $\pm$ 0.027	0.265 $\pm$ 0.063	0.893 $\pm$ 0.005	
bCMC 129.7 $\pm$ 3.3	0.056 $\pm$ 0.027	0.265 $\pm$ 0.063	0.893 $\pm$ 0.005	
Plasticised 99PVA	33.1 $\pm$ 3.3	-0.675 $\pm$ 0.018	0.155 $\pm$ 0.008	0.930 $\pm$ 0.011
	65.8 $\pm$ 3.0	-0.738 $\pm$ 0.046	0.157 $\pm$ 0.025	0.858 $\pm$ 0.022
	119.8 $\pm$ 2.1	-0.694 $\pm$ 0.098	0.316 $\pm$ 0.005	0.930 $\pm$ 0.035
	169.2 $\pm$ 4.1	-0.778 $\pm$ 0.019	0.135 $\pm$ 0.020	0.633 $\pm$ 0.015
	0.124 $\pm$ 0.001	-0.252 $\pm$ 0.048	0.357 $\pm$ 0.081	0.915 $\pm$ 0.021
	0.181 $\pm$ 0.003	-0.501 $\pm$ 0.049	0.151 $\pm$ 0.014	0.643 $\pm$ 0.007

**Table 10.17.** Fit parameters to Equation 7.1 for spreading of CTAB solution on the surface of the films of various compositions. Shaded cells correspond to spin-coated films, while bCMC stands for surfactant solution below CMC.

Sample	Thickness ( $\mu\text{m}$ )	k	n	R <sup>2</sup>
87PVA	30.6 $\pm$ 1.9	-0.252 $\pm$ 0.054	0.092 $\pm$ 0.016	0.730 $\pm$ 0.061
	44.5 $\pm$ 3.8	-0.254 $\pm$ 0.038	0.076 $\pm$ 0.005	0.773 $\pm$ 0.032
	87.0 $\pm$ 3.3	-0.192 $\pm$ 0.025	0.090 $\pm$ 0.010	0.871 $\pm$ 0.015
	129.7 $\pm$ 7.6	-0.249 $\pm$ 0.048	0.080 $\pm$ 0.012	0.866 $\pm$ 0.015
	0.093 $\pm$ 0.003	-0.251 $\pm$ 0.020	0.303 $\pm$ 0.011	0.903 $\pm$ 0.006
	0.120 $\pm$ 0.003	-0.169 $\pm$ 0.010	0.405 $\pm$ 0.012	0.950 $\pm$ 0.004
	bCMC 87.0 $\pm$ 3.3	-0.050 $\pm$ 0.033	0.247 $\pm$ 0.081	0.965 $\pm$ 0.011
	bCMC 30.6 $\pm$ 1.9	-0.117 $\pm$ 0.040	0.163 $\pm$ 0.044	0.928 $\pm$ 0.020
Plasticised 87PVA	21.7 $\pm$ 2.7	-0.401 $\pm$ 0.020	0.317 $\pm$ 0.008	0.986 $\pm$ 0.001
	39.3 $\pm$ 5.5	-0.384 $\pm$ 0.019	0.310 $\pm$ 0.007	0.982 $\pm$ 0.003
	73.5 $\pm$ 4.5	-0.518 $\pm$ 0.051	0.269 $\pm$ 0.012	0.964 $\pm$ 0.007
	108.8 $\pm$ 3.0	-0.574 $\pm$ 0.035	0.244 $\pm$ 0.007	0.983 $\pm$ 0.004
	0.078 $\pm$ 0.001	-0.597 $\pm$ 0.019	0.192 $\pm$ 0.012	0.724 $\pm$ 0.031
	0.118 $\pm$ 0.001	-0.465 $\pm$ 0.041	0.202 $\pm$ 0.009	0.768 $\pm$ 0.004
99PVA	52.8 $\pm$ 2.3	-0.578 $\pm$ 0.040	0.548 $\pm$ 0.061	0.921 $\pm$ 0.051
	88.3 $\pm$ 4.6	-0.617 $\pm$ 0.051	0.344 $\pm$ 0.015	0.93 $\pm$ 0.002
	129.7 $\pm$ 3.3	-0.693 $\pm$ 0.062	0.529 $\pm$ 0.026	0.972 $\pm$ 0.012
	208.5 $\pm$ 2.2	-0.646 $\pm$ 0.052	0.555 $\pm$ 0.011	0.987 $\pm$ 0.003
	0.149 $\pm$ 0.009	-0.211 $\pm$ 0.038	0.080 $\pm$ 0.022	0.801 $\pm$ 0.078
	0.192 $\pm$ 0.013	-0.338 $\pm$ 0.046	0.039 $\pm$ 0.003	0.712 $\pm$ 0.025
	bCMC 52.8 $\pm$ 2.3	-0.006 $\pm$ 0.001	0.506 $\pm$ 0.084	0.867 $\pm$ 0.030
	bCMC 129.7 $\pm$ 3.3	-0.114 $\pm$ 0.045	0.084 $\pm$ 0.025	0.783 $\pm$ 0.021
Plasticised 99PVA	33.1 $\pm$ 3.3	-0.663 $\pm$ 0.066	0.390 $\pm$ 0.025	0.758 $\pm$ 0.149
	65.8 $\pm$ 3.0	-0.660 $\pm$ 0.057	0.407 $\pm$ 0.047	0.44 $\pm$ 0.101
	119.8 $\pm$ 2.1	-0.731 $\pm$ 0.002	0.408 $\pm$ 0.031	0.974 $\pm$ 0.011
	169.2 $\pm$ 4.1	-0.722 $\pm$ 0.036	0.358 $\pm$ 0.018	0.864 $\pm$ 0.006
	0.124 $\pm$ 0.001	-0.249 $\pm$ 0.042	0.421 $\pm$ 0.067	0.840 $\pm$ 0.057
	0.181 $\pm$ 0.003	-0.310 $\pm$ 0.016	0.244 $\pm$ 0.027	0.899 $\pm$ 0.030

**Table 10.18.** Fit parameters to Equation 7.1 for spreading of C<sub>12</sub>E<sub>10</sub> solution on the surface of the films of various compositions. Shaded cells correspond to spin-coated films, while bCMC stands for surfactant solution below CMC.

Sample	Thickness (μm)	k	n	R <sup>2</sup>
87PVA	30.6±1.9	-0.592±0.049	0.132±0.049	0.561±0.070
	44.5±3.8	-0.567±0.062	0.124±0.014	0.635±0.014
	87.0±3.3	-0.688±0.011	0.246±0.023	0.833±0.024
	129.7±7.6	-0.515±0.017	0.257±0.011	0.780±0.002
	0.093±0.003	-0.191±0.011	0.283±0.008	0.941±0.005
	0.120±0.003	-0.147±0.017	0.336±0.032	0.943±0.007
	bCMC 30.6±1.9	-0.085±0.028	0.149±0.033	0.951±0.003
Plasticised 87PVA	21.7±2.7	-0.707±0.038	0.193±0.015	0.701±0.038
	39.3±5.5	-0.757±0.035	0.245±0.007	0.577±0.020
	73.5±4.5	-0.515±0.046	0.388±0.020	0.985±0.007
	108.8±3.0	-0.526±0.023	0.318±0.010	0.995±0.004
	0.078±0.001	-0.458±0.030	0.143±0.006	0.782±0.002
	0.118±0.001	-0.352±0.012	0.165±0.005	0.772±0.005
	bCMC 73.5±4.5	-0.121±0.038	0.112±0.021	0.941±0.028
99PVA	52.8±2.3	-1.103±0.073	0.452±0.062	0.917±0.037
	88.3±4.6	-0.912±0.109	0.580±0.031	0.978±0.002
	129.7±3.3	-0.758±0.094	0.544±0.050	0.967±0.006
	208.5±2.2	-0.809±0.059	0.549±0.024	0.946±0.025
	0.149±0.009	-0.511±0.030	0.040±0.002	0.777±0.012
	0.192±0.013	-0.403±0.015	0.049±0.002	0.721±0.007
	bCMC 52.8±2.3	-0.308±0.049	0.392±0.035	0.910±0.039
Plasticised 99PVA	33.1±3.3	-0.929±0.023	0.342±0.015	0.857±0.079
	65.8±3.0	-0.938±0.042	0.342±0.020	0.903±0.048
	119.8±2.1	-0.922±0.069	0.334±0.038	0.875±0.066
	169.2±4.1	-1.001±0.090	0.371±0.026	0.980±0.004
	0.124±0.001	-0.755±0.113	0.077±0.032	0.744±0.047
	0.181±0.003	-0.982±0.052	0.144±0.022	0.756±0.036
	bCMC 119.8±2.1	-0.190±0.013	0.516±0.058	0.950±0.047

**Table 10.19.** Fit parameters to Equation 7.1 for spreading of dodecane on the surface of the films of various compositions. Shaded cells correspond to spin-coated films.

Sample	Thickness ( $\mu\text{m}$ )	k	n	R <sup>2</sup>
87PVA	30.6 $\pm$ 1.9	-1.015 $\pm$ 0.111	0.539 $\pm$ 0.010	0.975 $\pm$ 0.013
	44.5 $\pm$ 3.8	-0.938 $\pm$ 0.098	0.493 $\pm$ 0.020	0.968 $\pm$ 0.013
	87.0 $\pm$ 3.3	-1.217 $\pm$ 0.060	0.398 $\pm$ 0.048	0.926 $\pm$ 0.037
	129.7 $\pm$ 7.6	-0.966 $\pm$ 0.003	0.369 $\pm$ 0.015	0.964 $\pm$ 0.031
	0.093 $\pm$ 0.003	-1.024 $\pm$ 0.061	0.487 $\pm$ 0.006	0.987 $\pm$ 0.004
	0.120 $\pm$ 0.003	-0.988 $\pm$ 0.037	0.539 $\pm$ 0.025	0.987 $\pm$ 0.003
Plasticised 87PVA	21.7 $\pm$ 2.7	-0.751 $\pm$ 0.003	0.612 $\pm$ 0.015	0.996 $\pm$ 0.001
	39.3 $\pm$ 5.5	-0.780 $\pm$ 0.127	0.496 $\pm$ 0.010	0.939 $\pm$ 0.028
	73.5 $\pm$ 4.5	-1.036 $\pm$ 0.071	0.421 $\pm$ 0.028	0.928 $\pm$ 0.033
	108.8 $\pm$ 3.0	-1.069 $\pm$ 0.062	0.444 $\pm$ 0.027	0.951 $\pm$ 0.011
	0.078 $\pm$ 0.001	-1.228 $\pm$ 0.015	0.402 $\pm$ 0.031	0.985 $\pm$ 0.002
	0.118 $\pm$ 0.001	-1.129 $\pm$ 0.048	0.459 $\pm$ 0.031	0.988 $\pm$ 0.004
99PVA	52.8 $\pm$ 2.3	-0.962 $\pm$ 0.046	0.459 $\pm$ 0.029	0.959 $\pm$ 0.025
	88.3 $\pm$ 4.6	-0.948 $\pm$ 0.030	0.477 $\pm$ 0.045	0.963 $\pm$ 0.015
	129.7 $\pm$ 3.3	-0.757 $\pm$ 0.013	0.389 $\pm$ 0.029	0.961 $\pm$ 0.009
	208.5 $\pm$ 2.2	-0.969 $\pm$ 0.107	0.472 $\pm$ 0.035	0.971 $\pm$ 0.020
	0.149 $\pm$ 0.009	-1.172 $\pm$ 0.057	0.477 $\pm$ 0.043	0.990 $\pm$ 0.002
	0.192 $\pm$ 0.013	-1.334 $\pm$ 0.032	0.398 $\pm$ 0.027	0.985 $\pm$ 0.003
Plasticised 99PVA	33.1 $\pm$ 3.3	-1.083 $\pm$ 0.152	0.454 $\pm$ 0.070	0.969 $\pm$ 0.013
	65.8 $\pm$ 3.0	-1.147 $\pm$ 0.087	0.438 $\pm$ 0.026	0.978 $\pm$ 0.006
	119.8 $\pm$ 2.1	-1.285 $\pm$ 0.184	0.383 $\pm$ 0.016	0.987 $\pm$ 0.005
	169.2 $\pm$ 4.1	-0.978 $\pm$ 0.211	0.362 $\pm$ 0.020	0.967 $\pm$ 0.003
	0.124 $\pm$ 0.001	-1.158 $\pm$ 0.055	0.451 $\pm$ 0.048	0.987 $\pm$ 0.006
	0.181 $\pm$ 0.003	-1.098 $\pm$ 0.085	0.494 $\pm$ 0.029	0.980 $\pm$ 0.007

**Table 10.20.** CA evolution parameters for investigated compositions using CTAB solution as the medium. Symbols represent:  $CA_0$  – initial CA,  $CA_e$  – contact angle at the end of the measurement,  $\Delta CA$  – difference between  $CA_0$  and  $CA_e$ ,  $\Delta V$  – change in the droplet volume,  $\Delta A$  – change in the liquid/solid contact area. For mechanisms, A+S stands for absorption and spreading, while S – for spreading (MS indicates mainly spreading). Shaded cells correspond to spin-coated films, while bCMC stands for surfactant solution below CMC.

Sample	Thickness ( $\mu\text{m}$ )	$CA_0$ ( $^\circ$ )	$CA_e$ ( $^\circ$ )	$\Delta CA$ ( $^\circ$ )	$\Delta V$ ( $\mu\text{l}$ )	$\Delta A$ ( $\text{mm}^2$ )	Mechanism	
87PVA	30.6 $\pm$ 1.9	46.30 $\pm$ 2.16	32.34 $\pm$ 1.49	-13.96 $\pm$ 2.55	-0.65 $\pm$ 0.07	4.41 $\pm$ 1.10	A+S	
	44.5 $\pm$ 3.8	55.41 $\pm$ 4.71	35.68 $\pm$ 2.39	-19.73 $\pm$ 4.10	-0.63 $\pm$ 0.13	3.51 $\pm$ 0.71	A+S	
	87.0 $\pm$ 3.3	55.81 $\pm$ 2.60	41.99 $\pm$ 2.43	-13.83 $\pm$ 1.20	-0.68 $\pm$ 0.08	2.00 $\pm$ 0.18	A+S	
	129.7 $\pm$ 7.6	48.23 $\pm$ 1.60	33.79 $\pm$ 1.06	-14.44 $\pm$ 2.18	-0.55 $\pm$ 0.05	2.64 $\pm$ 0.38	A+S	
	0.093 $\pm$ 0.003	48.50 $\pm$ 1.72	19.62 $\pm$ 0.37	-28.88 $\pm$ 1.92	-0.58 $\pm$ 0.04	10.74 $\pm$ 0.63	A+S (MS)	
	0.120 $\pm$ 0.003	52.03 $\pm$ 2.08	20.32 $\pm$ 0.56	-31.72 $\pm$ 1.87	-0.38 $\pm$ 0.05	10.74 $\pm$ 0.77	A+S (MS)	
	bCMC 87.0 $\pm$ 3.3	72.17 $\pm$ 2.12	64.63 $\pm$ 0.92	-7.55 $\pm$ 2.57	-0.47 $\pm$ 0.01	0.14 $\pm$ 0.02	A+S	
	bCMC 30.6 $\pm$ 1.9	63.91 $\pm$ 2.24	52.61 $\pm$ 1.16	-11.30 $\pm$ 2.85	-0.45 $\pm$ 0.01	0.61 $\pm$ 0.06	A+S	
Plasticised 87PVA	21.7 $\pm$ 2.7	47.53 $\pm$ 1.90	8.90 $\pm$ 0.25	-38.63 $\pm$ 1.90	-2.36 $\pm$ 0.07	23.74 $\pm$ 0.79	A+S	
	39.3 $\pm$ 5.5	42.12 $\pm$ 0.75	9.13 $\pm$ 0.49	-32.99 $\pm$ 1.03	-2.49 $\pm$ 0.27	25.46 $\pm$ 1.25	A+S	
	73.5 $\pm$ 4.5	53.35 $\pm$ 4.89	11.44 $\pm$ 1.67	-41.92 $\pm$ 4.54	-1.72 $\pm$ 0.29	22.46 $\pm$ 2.33	A+S	
	108.8 $\pm$ 3.0	58.92 $\pm$ 2.52	11.21 $\pm$ 0.67	-47.71 $\pm$ 2.63	-1.98 $\pm$ 0.16	22.12 $\pm$ 3.06	A+S	
	0.078 $\pm$ 0.001	54.69 $\pm$ 1.63	14.61 $\pm$ 0.84	-40.08 $\pm$ 2.27	-0.87 $\pm$ 0.05	14.06 $\pm$ 0.28	A+S	
	0.118 $\pm$ 0.001	49.32 $\pm$ 5.51	16.86 $\pm$ 0.47	-32.46 $\pm$ 5.34	-1.58 $\pm$ 0.90	12.02 $\pm$ 1.58	A+S	
	99PVA	52.8 $\pm$ 2.3	31.44 $\pm$ 0.97	9.33 $\pm$ 3.61	-22.10 $\pm$ 3.92	-3.35 $\pm$ 1.15	29.96 $\pm$ 5.32	A+S
		88.3 $\pm$ 4.6	42.75 $\pm$ 5.16	29.05 $\pm$ 23.24	-38.65 $\pm$ 5.47	-3.61 $\pm$ 1.40	34.15 $\pm$ 4.45	A+S
129.7 $\pm$ 3.3		34.64 $\pm$ 0.99	3.60 $\pm$ 1.35	-31.04 $\pm$ 0.99	-6.71 $\pm$ 0.50	34.93 $\pm$ 6.08	A+S	
208.5 $\pm$ 2.2		33.66 $\pm$ 0.81	3.94 $\pm$ 0.74	-29.73 $\pm$ 1.50	-2.48 $\pm$ 0.76	44.56 $\pm$ 5.63	A+S	
0.149 $\pm$ 0.009		28.15 $\pm$ 1.17	18.71 $\pm$ 0.60	-9.44 $\pm$ 1.35	-1.24 $\pm$ 0.69	5.38 $\pm$ 0.72	A+S	
0.192 $\pm$ 0.013		28.73 $\pm$ 0.88	16.35 $\pm$ 1.11	-12.39 $\pm$ 1.94	-0.72 $\pm$ 0.15	8.08 $\pm$ 1.67	A+S	
bCMC 52.8 $\pm$ 2.3		36.05 $\pm$ 0.52	33.96 $\pm$ 0.67	-2.10 $\pm$ 0.40	-0.60 $\pm$ 0.03	0.17 $\pm$ 0.02	A+S	
bCMC 129.7 $\pm$ 3.3		41.91 $\pm$ 2.80	35.32 $\pm$ 0.69	-6.59 $\pm$ 2.11	-0.44 $\pm$ 0.12	0.54 $\pm$ 0.34	A+S	
Plasticised 99PVA	33.1 $\pm$ 3.3	26.89 $\pm$ 0.96	4.15 $\pm$ 1.72	-22.73 $\pm$ 1.79	-4.55 $\pm$ 1.43	29.39 $\pm$ 9.52	A+S	
	65.8 $\pm$ 3.0	25.40 $\pm$ 2.45	3.78 $\pm$ 1.51	-21.49 $\pm$ 2.59	-7.62 $\pm$ 0.45	22.77 $\pm$ 4.83	A+S	
	119.8 $\pm$ 2.1	30.22 $\pm$ 3.26	4.98 $\pm$ 2.09	-25.24 $\pm$ 1.24	-4.86 $\pm$ 1.48	22.78 $\pm$ 4.82	A+S	
	169.2 $\pm$ 4.1	31.33 $\pm$ 4.21	5.62 $\pm$ 2.31	-25.71 $\pm$ 3.41	-6.53 $\pm$ 0.70	27.28 $\pm$ 7.31	A+S	
	0.124 $\pm$ 0.001	37.77 $\pm$ 1.72	12.95 $\pm$ 1.17	-24.97 $\pm$ 1.98	-0.49 $\pm$ 0.08	15.66 $\pm$ 1.57	A+S (MS)	
	0.181 $\pm$ 0.003	33.81 $\pm$ 0.79	13.75 $\pm$ 0.94	-20.06 $\pm$ 1.37	-0.61 $\pm$ 0.10	13.91 $\pm$ 1.72	A+S	

**Table 10.21.** CA evolution parameters for investigated compositions using SDS solution as the medium.

Symbols represent:  $CA_0$  – initial CA,  $CA_e$  – contact angle at the end of the measurement,  $\Delta CA$  – difference between  $CA_0$  and  $CA_e$ ,  $\Delta V$  – change in the droplet volume,  $\Delta A$  – change in the liquid/solid contact area. For mechanisms, A+S stands for absorption and spreading, while S – for spreading (MS indicates mainly spreading).

Shaded cells correspond to spin-coated films, while bCMC stands for surfactant solution below CMC.

Sample	Thickness ( $\mu\text{m}$ )	$CA_0$ ( $^\circ$ )	$CA_e$ ( $^\circ$ )	$\Delta CA$ ( $^\circ$ )	$\Delta V$ ( $\mu\text{l}$ )	$\Delta A$ ( $\text{mm}^2$ )	Mechanism
87PVA	30.6 $\pm$ 1.9	57.31 $\pm$ 2.63	36.78 $\pm$ 1.36	-20.53 $\pm$ 2.51	-0.60 $\pm$ 0.16	3.91 $\pm$ 0.93	A+S
	44.5 $\pm$ 3.8	53.60 $\pm$ 3.84	40.99 $\pm$ 1.39	-12.62 $\pm$ 3.77	-0.15 $\pm$ 0.19	1.13 $\pm$ 0.31	A+S
	87.0 $\pm$ 3.3	50.92 $\pm$ 3.45	39.86 $\pm$ 1.47	-11.06 $\pm$ 2.90	-0.44 $\pm$ 0.06	1.56 $\pm$ 0.23	A+S
	129.7 $\pm$ 7.6	47.52 $\pm$ 4.01	37.64 $\pm$ 1.39	-9.87 $\pm$ 2.80	-0.71 $\pm$ 0.13	1.44 $\pm$ 0.29	A+S
	0.093 $\pm$ 0.003	44.67 $\pm$ 1.78	14.94 $\pm$ 0.17	-29.73 $\pm$ 1.81	-0.75 $\pm$ 0.05	13.05 $\pm$ 0.26	A+S
	0.120 $\pm$ 0.003	44.63 $\pm$ 1.80	16.83 $\pm$ 0.20	-27.80 $\pm$ 1.69	-0.73 $\pm$ 0.06	11.96 $\pm$ 0.50	A+S
bCMC	30.6 $\pm$ 1.9	64.27 $\pm$ 3.39	51.29 $\pm$ 1.44	-12.98 $\pm$ 2.91	-0.44 $\pm$ 0.04	1.18 $\pm$ 0.12	A+S
	87.0 $\pm$ 3.3	56.15 $\pm$ 2.72	51.83 $\pm$ 2.32	-4.32 $\pm$ 0.45	-0.44 $\pm$ 0.02	0.48 $\pm$ 0.05	A+S
Plasticised 87PVA	21.7 $\pm$ 2.7	51.28 $\pm$ 1.71	17.17 $\pm$ 0.41	-34.11 $\pm$ 1.66	-0.73 $\pm$ 0.08	12.84 $\pm$ 0.71	A+S
	39.3 $\pm$ 5.5	50.22 $\pm$ 5.17	18.77 $\pm$ 0.61	-31.45 $\pm$ 4.69	-0.70 $\pm$ 0.04	11.29 $\pm$ 0.41	A+S
	73.5 $\pm$ 4.5	54.29 $\pm$ 5.72	19.16 $\pm$ 0.15	-35.13 $\pm$ 5.59	-0.68 $\pm$ 0.06	11.63 $\pm$ 0.22	A+S
	108.8 $\pm$ 3.0	49.80 $\pm$ 2.37	18.83 $\pm$ 0.73	-30.97 $\pm$ 2.01	-0.75 $\pm$ 0.11	11.43 $\pm$ 0.83	A+S
	0.078 $\pm$ 0.001	47.91 $\pm$ 2.33	17.22 $\pm$ 0.59	-30.69 $\pm$ 2.49	-0.52 $\pm$ 0.18	13.09 $\pm$ 0.43	A+S
	0.118 $\pm$ 0.001	45.84 $\pm$ 0.82	20.67 $\pm$ 1.38	-25.17 $\pm$ 1.74	-0.37 $\pm$ 0.10	10.34 $\pm$ 0.99	A+S
99PVA	52.8 $\pm$ 2.3	37.07 $\pm$ 4.24	5.12 $\pm$ 0.65	-23.54 $\pm$ 0.88	-3.32 $\pm$ 0.61	20.90 $\pm$ 4.51	A+S
	88.3 $\pm$ 4.6	35.30 $\pm$ 3.39	8.12 $\pm$ 1.27	-27.18 $\pm$ 3.93	-1.59 $\pm$ 0.43	28.32 $\pm$ 5.29	A+S
	129.7 $\pm$ 3.3	45.42 $\pm$ 4.97	10.01 $\pm$ 1.81	-35.41 $\pm$ 5.55	-3.09 $\pm$ 1.12	30.12 $\pm$ 4.80	A+S
	208.5 $\pm$ 2.2	44.87 $\pm$ 4.46	5.75 $\pm$ 1.30	-39.11 $\pm$ 3.48	-2.50 $\pm$ 0.43	33.45 $\pm$ 4.60	A+S
	0.149 $\pm$ 0.009	27.57 $\pm$ 1.93	13.72 $\pm$ 0.49	-13.85 $\pm$ 2.08	-0.47 $\pm$ 0.10	10.27 $\pm$ 0.78	A+S
	0.192 $\pm$ 0.013	21.76 $\pm$ 0.65	11.68 $\pm$ 0.38	-10.07 $\pm$ 0.57	-0.79 $\pm$ 0.10	9.96 $\pm$ 1.38	A+S
bCMC	52.8 $\pm$ 2.3	39.64 $\pm$ 2.55	34.91 $\pm$ 1.42	-4.73 $\pm$ 1.45	-0.50 $\pm$ 0.05	0.78 $\pm$ 0.25	A+S
	129.7 $\pm$ 3.3	44.70 $\pm$ 4.67	36.38 $\pm$ 0.35	-8.31 $\pm$ 5.03	-0.91 $\pm$ 0.40	1.15 $\pm$ 0.89	A+S
Plasticised 99PVA	33.1 $\pm$ 3.3	24.57 $\pm$ 2.18	8.12 $\pm$ 0.12	-16.45 $\pm$ 2.11	-0.84 $\pm$ 0.14	25.23 $\pm$ 2.70	A+S
	65.8 $\pm$ 3.0	26.53 $\pm$ 1.25	7.10 $\pm$ 0.48	-18.59 $\pm$ 1.12	-2.37 $\pm$ 0.62	22.90 $\pm$ 2.92	A+S
	119.8 $\pm$ 2.1	31.57 $\pm$ 3.59	11.04 $\pm$ 2.62	-26.54 $\pm$ 2.35	-0.41 $\pm$ 0.14	29.65 $\pm$ 1.95	A+S (MS)
	169.2 $\pm$ 4.1	26.81 $\pm$ 2.85	8.72 $\pm$ 1.54	-18.09 $\pm$ 1.85	-1.03 $\pm$ 0.73	27.34 $\pm$ 8.45	A+S
	0.124 $\pm$ 0.001	27.30 $\pm$ 0.43	12.68 $\pm$ 1.00	-14.97 $\pm$ 0.94	-0.41 $\pm$ 0.18	10.22 $\pm$ 6.60	A+S
	0.181 $\pm$ 0.003	26.19 $\pm$ 0.36	10.43 $\pm$ 0.69	-15.76 $\pm$ 0.71	-1.08 $\pm$ 0.21	16.01 $\pm$ 0.98	A+S

**Table 10.22.** CA evolution parameters for investigated compositions using C<sub>12</sub>E<sub>10</sub> solution as the medium. Symbols represent: CA<sub>0</sub> – initial CA, CA<sub>e</sub> – contact angle at the end of the measurement, ΔCA – difference between CA<sub>0</sub> and CA<sub>e</sub>, ΔV – change in the droplet volume, ΔA – change in the liquid/solid contact area. For mechanisms, A+S stands for absorption and spreading, while S – for spreading (MS indicates mainly spreading). Shaded cells correspond to spin-coated films, while bCMC stands for surfactant solution below CMC.

Sample	Thickness (μm)	CA <sub>0</sub> (°)	CA <sub>e</sub> (°)	ΔCA (°)	ΔV (μl)	ΔA (mm <sup>2</sup> )	Mechanism
87PVA	30.6±1.9	49.34±4.09	20.50±1.71	-28.84±3.14	-0.83±0.21	10.36±1.12	A+S
	44.5±3.8	56.07±3.45	24.85±2.38	-31.22±2.69	-0.38±0.64	7.57±0.84	A+S (MS)
	87.0±3.3	60.74±3.06	27.88±4.01	-32.86±1.76	-0.35±0.11	7.88±1.01	A+S
	129.7±7.6	45.66±3.48	21.65±1.39	-24.01±2.98	-2.14±1.05	5.09±1.25	A+S
	0.093±0.003	39.94±0.85	20.93±0.36	-19.01±0.84	-0.34±0.06	7.86±0.25	A+S (MS)
	0.120±0.003	41.35±1.53	22.51±0.25	-18.84±1.59	-0.34±0.06	7.19±0.47	A+S (MS)
	bCMC 30.6±1.9	56.43±1.80	48.71±0.74	-7.72±1.65	-0.41±0.01	0.44±0.04	A+S
Plasticised 87PVA	21.7±2.7	42.06±1.98	9.89±0.26	-32.17±1.75	-1.34±0.08	20.19±0.39	A+S
	39.3±5.5	40.01±1.61	10.97±0.20	-29.04±1.49	-1.14±0.10	17.54±0.52	A+S
	73.5±4.5	46.46±4.57	10.72±0.64	-35.74±4.08	-1.37±0.28	18.02±2.35	A+S
	108.8±3.0	50.65±4.04	11.64±0.25	-39.01±4.03	-0.10±0.66	19.23±2.07	A+S
	0.078±0.001	39.45±0.87	17.13±0.37	-22.32±1.09	-0.62±0.02	9.73±0.42	A+S
	0.118±0.001	37.48±1.24	18.36±0.17	-19.12±1.30	-0.64±0.02	8.58±0.21	A+S
	bCMC 21.7±2.7	73.77±3.30	60.75±2.42	-13.02±3.19	-0.48±0.10	0.51±0.18	A+S
99PVA	52.8±2.3	33.43±3.64	4.49±1.31	-28.93±4.35	-1.98±0.38	30.88±4.37	A+S
	88.3±4.6	30.39±2.04	3.84±1.10	-26.55±1.70	-2.21±0.84	29.71±6.26	A+S
	129.7±3.3	32.01±1.38	9.28±1.66	-22.72±1.74	-2.20±0.86	22.05±3.47	A+S
	208.5±2.2	27.67±1.25	4.59±0.41	-23.09±1.50	-1.95±0.61	42.46±9.22	A+S
	0.149±0.009	23.20±1.23	12.32±0.45	-10.88±0.90	-0.78±0.08	9.40±0.46	A+S
	0.192±0.013	19.38±0.55	11.28±0.32	-8.10±0.42	-0.55±0.08	9.70±0.42	A+S
	bCMC 52.8±2.3	34.96±2.48	7.86±1.53	-29.85±6.17	-6.07±1.69	22.31±10.15	A+S
Plasticised 99PVA	33.1±3.3	25.51±1.30	4.61±1.46	-20.12±2.36	-5.93±0.13	20.08±1.83	A+S
	65.8±3.0	22.83±1.19	2.39±0.49	-20.44±0.88	-4.77±0.90	64.22±27.09	A+S
	119.8±2.1	27.80±0.50	2.47±0.56	-25.33±0.55	-3.60±0.63	33.60±5.90	A+S
	169.2±4.1	37.59±2.92	3.72±1.52	-33.86±2.12	-4.69±0.67	28.13±8.28	A+S
	0.124±0.001	26.14±1.03	9.02±0.81	-17.12±0.78	-1.39±0.16	16.52±1.66	A+S
	0.181±0.003	26.11±1.46	5.68±0.26	-20.43±1.37	-0.78±0.32	23.56±1.33	A+S
	bCMC 119.8±2.1	37.39±1.52	14.80±2.35	-22.59±3.87	-12.55±1.97	7.53±7.15	A+S



**Table 10.23.** CA evolution parameters for investigated compositions using dodecane as the medium. Symbols represent:  $CA_0$  – initial CA,  $CA_e$  – contact angle at the end of the measurement,  $\Delta CA$  – difference between  $CA_0$  and  $CA_e$ ,  $\Delta V$  – change in the droplet volume,  $\Delta A$  – change in the liquid/solid contact area. For mechanisms, A+S stands for absorption and spreading, while S – for spreading (MS indicates mainly spreading). Shaded cells correspond to spin-coated films.

Sample	Thickness ( $\mu\text{m}$ )	$CA_0$ ( $^\circ$ )	$CA_e$ ( $^\circ$ )	$\Delta CA$ ( $^\circ$ )	$\Delta V$ ( $\mu\text{l}$ )	$\Delta A$ ( $\text{mm}^2$ )	Mechanism
87PVA	30.6 $\pm$ 1.9	15.71 $\pm$ 0.75	1.48 $\pm$ 0.19	-14.23 $\pm$ 0.89	-5.13 $\pm$ 0.32	8.75 $\pm$ 0.81	A+S
	44.5 $\pm$ 3.8	16.96 $\pm$ 1.24	2.12 $\pm$ 0.29	-14.84 $\pm$ 1.27	-5.56 $\pm$ 0.85	21.01 $\pm$ 7.64	A+S
	87.0 $\pm$ 3.3	22.63 $\pm$ 2.06	2.55 $\pm$ 0.57	-20.08 $\pm$ 1.60	-5.18 $\pm$ 0.04	21.49 $\pm$ 3.81	A+S
	129.7 $\pm$ 7.6	19.05 $\pm$ 1.21	1.54 $\pm$ 0.31	-17.50 $\pm$ 0.96	-5.96 $\pm$ 1.16	22.18 $\pm$ 5.39	A+S
	0.093 $\pm$ 0.003	17.61 $\pm$ 0.78	0.64 $\pm$ 0.01	-17.05 $\pm$ 1.08	-4.01 $\pm$ 1.57	45.18 $\pm$ 14.70	A+S
	0.120 $\pm$ 0.003	16.11 $\pm$ 0.99	0.79 $\pm$ 0.25	-14.42 $\pm$ 0.50	-4.86 $\pm$ 1.21	17.69 $\pm$ 12.17	A+S
Plasticised 87PVA	21.7 $\pm$ 2.7	18.40 $\pm$ 4.64	1.31 $\pm$ 0.06	-17.08 $\pm$ 4.59	-6.07 $\pm$ 2.78	7.64 $\pm$ 3.88	A+S
	39.3 $\pm$ 5.5	16.98 $\pm$ 1.56	2.13 $\pm$ 0.60	-14.85 $\pm$ 1.61	-5.55 $\pm$ 0.36	13.23 $\pm$ 4.00	A+S
	73.5 $\pm$ 4.5	19.84 $\pm$ 0.98	2.57 $\pm$ 0.29	-16.91 $\pm$ 1.31	-6.17 $\pm$ 1.15	21.30 $\pm$ 6.66	A+S
	108.8 $\pm$ 3.0	17.79 $\pm$ 1.53	1.06 $\pm$ 0.17	-16.73 $\pm$ 1.47	-3.19 $\pm$ 1.55	25.94 $\pm$ 8.60	A+S
	0.078 $\pm$ 0.001	18.86 $\pm$ 0.61	1.99 $\pm$ 0.40	-16.87 $\pm$ 0.65	-3.73 $\pm$ 0.40	29.52 $\pm$ 1.58	A+S
	0.118 $\pm$ 0.001	18.88 $\pm$ 1.26	1.00 $\pm$ 0.18	-17.88 $\pm$ 1.13	-5.95 $\pm$ 0.24	13.28 $\pm$ 1.86	A+S
99PVA	52.8 $\pm$ 2.3	16.66 $\pm$ 1.27	2.00 $\pm$ 0.17	-14.66 $\pm$ 1.22	-4.85 $\pm$ 0.49	27.19 $\pm$ 5.70	A+S
	88.3 $\pm$ 4.6	20.32 $\pm$ 2.25	2.12 $\pm$ 0.23	-18.20 $\pm$ 2.23	-4.79 $\pm$ 1.29	9.69 $\pm$ 2.21	A+S
	129.7 $\pm$ 3.3	24.08 $\pm$ 1.48	2.10 $\pm$ 0.78	-22.87 $\pm$ 2.28	-5.24 $\pm$ 1.20	31.23 $\pm$ 7.92	A+S
	208.5 $\pm$ 2.2	20.02 $\pm$ 1.51	1.86 $\pm$ 0.22	-18.18 $\pm$ 1.43	-5.86 $\pm$ 0.76	21.48 $\pm$ 6.30	A+S
	0.149 $\pm$ 0.009	16.02 $\pm$ 1.83	0.75 $\pm$ 0.13	-15.28 $\pm$ 1.77	-3.17 $\pm$ 0.93	45.96 $\pm$ 3.87	A+S
	0.192 $\pm$ 0.013	14.12 $\pm$ 2.90	0.93 $\pm$ 0.21	-15.52 $\pm$ 3.82	-5.76 $\pm$ 0.23	33.23 $\pm$ 1.75	A+S
Plasticised 99PVA	33.1 $\pm$ 3.3	20.17 $\pm$ 2.13	1.76 $\pm$ 0.43	-18.41 $\pm$ 1.72	-4.93 $\pm$ 1.03	42.14 $\pm$ 9.41	A+S
	65.8 $\pm$ 3.0	18.47 $\pm$ 1.54	2.32 $\pm$ 0.21	-16.16 $\pm$ 1.65	-3.77 $\pm$ 0.69	30.39 $\pm$ 5.22	A+S
	119.8 $\pm$ 2.1	23.91 $\pm$ 1.40	1.05 $\pm$ 0.30	-23.76 $\pm$ 2.14	-2.87 $\pm$ 0.78	35.25 $\pm$ 16.58	A+S
	169.2 $\pm$ 4.1	27.16 $\pm$ 2.25	3.50 $\pm$ 0.63	-23.66 $\pm$ 1.81	-2.98 $\pm$ 0.88	34.16 $\pm$ 5.84	A+S
	0.124 $\pm$ 0.001	17.07 $\pm$ 1.57	2.57 $\pm$ 0.18	-14.50 $\pm$ 1.46	-4.23 $\pm$ 0.48	20.98 $\pm$ 2.65	A+S
	0.181 $\pm$ 0.003	17.50 $\pm$ 1.16	1.31 $\pm$ 0.31	-16.18 $\pm$ 0.96	-5.43 $\pm$ 1.92	25.03 $\pm$ 0.96	A+S
Pure dodecane	-	17.66 $\pm$ 1.18	1.96 $\pm$ 0.54	-15.70 $\pm$ 1.28	-0.49 $\pm$ 0.47	29.03 $\pm$ 10.04	S

## D2. Trends in $\Delta A$ and $\Delta V$ during ionic surfactant solution wetting

Fittings to the Farris model of spreading and infiltration can be corroborated by investigating droplet geometry over the course of the experiment for samples wetted by surfactant solutions. Higher values of  $\Delta A$  are noted for thick films compared to water wetting: for 99PVA films,  $\Delta A$  increases by factors of ca. 100 and 5 times for unplasticised and plasticised films, respectively for both SDS and CTAB wetting (Table 10.20, Table 10.21). For 87PVA formulations, more modest increases are seen:  $\Delta A$  increases for SDS wetting by factor of 2 for plasticised formulations and remains unchanged for unplasticised counterparts. For CTAB

solution, larger increase of 2 and 5 times (unplasticised and plasticised formulations, respectively) compared to water wetting were noted. Thin films again contrast in their behaviour, with only unplasticised 99PVA formulations showing any increase in  $\Delta A$  over water. When comparing the high value of  $\Delta A$  to the almost 0 value of  $n$  for these samples, the model of Farris et al is invalid. Evidently, geometric corroboration is essential for all samples to confirm the fittings generated.

Accordingly,  $\Delta V$  was also analysed to confirm absorption of the liquid medium into the films. Here again, introduction of ionic surfactants into the liquid medium increased  $\Delta V$  in 99PVA films: by factors of 10 (both CTAB and SDS) for unplasticised films or remained unchanged (for SDS) or increased by a factor of 5 (for CTAB) for plasticised films. For 87PVA films, no increase in  $\Delta V$  is seen for the unplasticised formulation, while a 5 times increase is observed in the plasticised formulation for CTAB only (Table 10.20, Table 10.21). Overall, these contrasts against the water medium show a change in absorption behaviour for the surfactant solutions into thick films, indicative of a change in the absorption mechanism.

### **D3. Trends in $\Delta A$ and $\Delta V$ during nonionic surfactant solution wetting**

Similar to charged surfactants, fittings of the Farris model to describe  $C_{12}E_{10}$  solutions spreading can be confirmed from droplet geometry as a function of time. In terms of solid-liquid contact areas, higher  $C_{12}E_{10}$  spreading (i.e.  $\Delta A$ ) was observed for all thick PVA formulations compared against pure water (Table 10.13, Table 10.22). Generally, for 87PVA formulations,  $\Delta A$  for  $C_{12}E_{10}$  was higher than both ionic surfactants (2 times and 4 times respectively for CTAB and SDS) – agreeing with the changes seen for  $k$  parameter (Figure 7.6a). Plasticised formulations of 87PVA showed higher  $\Delta A$  (ca. 4 times increase) for thick films compared to water, but no clear trend in  $\Delta A$  was observed between surfactant types. For

both plasticised and unplasticised formulations of 99PVA,  $\Delta A$  increased significantly for all surfactants equally – by a factor of ca. 6 compared to water – highlighting the similar kinetics of wetting independent of head group chemistry (agreeing with the data shown in Figure 7.7e and g). By contrast, only 87PVA thin films (both plasticised and unplasticised) showed a change in  $\Delta A$  as  $C_{12}E_{10}$  had a lower  $\Delta A$  than for ionic surfactants; no pattern could be discerned for 99PVA thin films between different surfactants. Absorption of  $C_{12}E_{10}$  into the thick films (measured using  $\Delta V$ ) was of the same magnitude as for other surfactants, in agreement with non-substantial changes of parameter  $n$ . Comparing surfactant absorption into thin PVA films was futile, as  $\Delta V$  was insignificant for these samples.

**Table 10.24.** Average DC values for all investigated compositions after one week of storage at controlled RH.

Sample	Thickness ( $\mu\text{m}$ )	DC (1140/1425)	DC (Peppas et al.)	DC (1140/850)	DC (1140/1094)	DC (Tretinnikov et al.)
Ambient 87PVA	129.7 $\pm$ 7.6	106.68 $\pm$ 0.19	45.85 $\pm$ 0.21	143.62 $\pm$ 0.51	50.36 $\pm$ 0.13	31.98 $\pm$ 0.13
Ambient plasticised 87PVA	108.8 $\pm$ 3.0	89.74 $\pm$ 0.36	28.47 $\pm$ 0.41	124.58 $\pm$ 0.28	45.89 $\pm$ 0.09	27.97 $\pm$ 0.09
Ambient 99PVA	208.5 $\pm$ 2.2	104.89 $\pm$ 0.18	44.02 $\pm$ 0.20	117.65 $\pm$ 0.09	46.87 $\pm$ 0.04	28.85 $\pm$ 0.04
Ambient plasticised 99PVA	169.2 $\pm$ 4.1	97.15 $\pm$ 0.19	36.08 $\pm$ 0.21	124.06 $\pm$ 0.29	46.70 $\pm$ 0.03	28.70 $\pm$ 0.03
4% RH 87PVA	30.6 $\pm$ 1.9	107.74 $\pm$ 0.21	46.95 $\pm$ 0.24	124.06 $\pm$ 0.29	46.70 $\pm$ 0.03	28.70 $\pm$ 0.03
4% RH plasticised 87PVA	21.7 $\pm$ 2.7	83.16 $\pm$ 0.62	21.72 $\pm$ 0.71	112.56 $\pm$ 0.35	41.57 $\pm$ 0.18	24.11 $\pm$ 0.18
4% RH 99PVA	52.8 $\pm$ 2.3	111.13 $\pm$ 0.40	50.41 $\pm$ 0.46	123.81 $\pm$ 0.62	48.69 $\pm$ 0.19	30.48 $\pm$ 0.19
4% RH plasticised 99PVA	33.1 $\pm$ 3.3	87.31 $\pm$ 0.23	25.97 $\pm$ 0.26	104.12 $\pm$ 0.11	41.93 $\pm$ 0.06	24.43 $\pm$ 0.06
45% RH 87PVA	44.5 $\pm$ 3.8	106.07 $\pm$ 0.13	45.23 $\pm$ 0.14	133.97 $\pm$ 0.21	48.02 $\pm$ 0.08	29.88 $\pm$ 0.08
45% RH plasticised 87PVA	39.3 $\pm$ 5.5	77.55 $\pm$ 0.22	15.97 $\pm$ 97	106.21 $\pm$ 0.08	39.16 $\pm$ 0.08	21.95 $\pm$ 0.08
45% RH 99PVA	88.3 $\pm$ 4.6	114.00 $\pm$ 0.27	53.36 $\pm$ 0.29	127.85 $\pm$ 0.41	49.45 $\pm$ 0.11	31.16 $\pm$ 0.11
45% RH plasticised 99PVA	65.8 $\pm$ 3.0	88.97 $\pm$ 0.27	27.68 $\pm$ 0.31	103.67 $\pm$ 0.19	42.26 $\pm$ 0.08	24.72 $\pm$ 0.08
100% RH 87PVA	87.0 $\pm$ 3.3	899.73 $\pm$ 37.96	859.53 $\pm$ 43.54	95.21 $\pm$ 0.54	100.0 $\pm$ 0.00	76.40 $\pm$ 0.00
100% RH plasticised 87PVA	73.5 $\pm$ 4.5	100.00 $\pm$ 0.00	59.00 $\pm$ 0.00	100.00 $\pm$ 0.00	100.00 $\pm$ 0.00	76.40 $\pm$ 0.00
100% RH 99PVA	129.7 $\pm$ 3.3	86.69 $\pm$ 0.47	25.35 $\pm$ 0.53	106.26 $\pm$ 0.75	41.33 $\pm$ 0.20	23.89 $\pm$ 0.20
100% RH plasticised 99PVA	119.8 $\pm$ 2.1	76.36 $\pm$ 0.42	14.75 $\pm$ 0.48	89.00 $\pm$ 0.62	36.66 $\pm$ 0.13	19.71 $\pm$ 0.13

**Table 10.25.** Fit parameters to Equation 7.1 for spreading of water on the surface of the films of various compositions after storing at 4% RH conditions.

Sample	Thickness ( $\mu\text{m}$ )	k	n	R <sup>2</sup>
87PVA	30.6 $\pm$ 1.9	-0.039 $\pm$ 0.011	0.341 $\pm$ 0.058	0.925 $\pm$ 0.018
	44.5 $\pm$ 3.8	-0.125 $\pm$ 0.017	0.174 $\pm$ 0.026	0.895 $\pm$ 0.050
	87.0 $\pm$ 3.3	-0.142 $\pm$ 0.026	0.167 $\pm$ 0.014	0.801 $\pm$ 0.102
	129.7 $\pm$ 7.6	-0.150 $\pm$ 0.024	0.200 $\pm$ 0.028	0.957 $\pm$ 0.010
Plasticised 87PVA	21.7 $\pm$ 2.7	-0.170 $\pm$ 0.017	0.247 $\pm$ 0.122	0.716 $\pm$ 0.204
	39.3 $\pm$ 5.5	-0.186 $\pm$ 0.013	0.340 $\pm$ 0.004	0.898 $\pm$ 0.047
	73.5 $\pm$ 4.5	-0.006 $\pm$ 0.010	0.589 $\pm$ 0.013	0.977 $\pm$ 0.007
	108.8 $\pm$ 3.0	-0.004 $\pm$ 0.009	0.619 $\pm$ 0.014	0.824 $\pm$ 0.004
99PVA	52.8 $\pm$ 2.3	-0.003 $\pm$ 0.001	0.836 $\pm$ 0.068	0.996 $\pm$ 0.002
	88.3 $\pm$ 4.6	-0.064 $\pm$ 0.034	0.429 $\pm$ 0.125	0.944 $\pm$ 0.026
	129.7 $\pm$ 3.3	-0.055 $\pm$ 0.032	0.591 $\pm$ 0.110	0.955 $\pm$ 0.021
	208.5 $\pm$ 2.2	-0.173 $\pm$ 0.045	0.302 $\pm$ 0.022	0.904 $\pm$ 0.010
Plasticised 99PVA	33.1 $\pm$ 3.3	-0.306 $\pm$ 0.063	0.175 $\pm$ 0.026	0.890 $\pm$ 0.032
	65.8 $\pm$ 3.0	-0.216 $\pm$ 0.047	0.255 $\pm$ 0.052	0.704 $\pm$ 0.059
	119.8 $\pm$ 2.1	-0.221 $\pm$ 0.030	0.137 $\pm$ 0.014	0.849 $\pm$ 0.080
	169.2 $\pm$ 4.1	-0.351 $\pm$ 0.030	0.108 $\pm$ 0.017	0.926 $\pm$ 0.014

**Table 10.26.** Fit parameters to Equation 7.1 for spreading of water on the surface of the films of various compositions after storing at 45% RH conditions.

Sample	Thickness ( $\mu\text{m}$ )	k	n	R <sup>2</sup>
87PVA	30.6 $\pm$ 1.9	-0.109 $\pm$ 0.019	0.227 $\pm$ 0.050	0.953 $\pm$ 0.016
	44.5 $\pm$ 3.8	-0.201 $\pm$ 0.026	0.195 $\pm$ 0.024	0.876 $\pm$ 0.021
	87.0 $\pm$ 3.3	-0.164 $\pm$ 0.032	0.197 $\pm$ 0.016	0.844 $\pm$ 0.046
	129.7 $\pm$ 7.6	-0.199 $\pm$ 0.029	0.196 $\pm$ 0.015	0.901 $\pm$ 0.020
Plasticised 87PVA	21.7 $\pm$ 2.7	-0.185 $\pm$ 0.006	0.366 $\pm$ 0.012	0.962 $\pm$ 0.006
	39.3 $\pm$ 5.5	-0.123 $\pm$ 0.026	0.510 $\pm$ 0.060	0.897 $\pm$ 0.035
	73.5 $\pm$ 4.5	-0.169 $\pm$ 0.014	0.362 $\pm$ 0.001	0.890 $\pm$ 0.025
	108.8 $\pm$ 3.0	-0.191 $\pm$ 0.031	0.384 $\pm$ 0.029	0.940 $\pm$ 0.020
99PVA	52.8 $\pm$ 2.3	-0.052 $\pm$ 0.013	0.239 $\pm$ 0.051	0.808 $\pm$ 0.057
	88.3 $\pm$ 4.6	-0.064 $\pm$ 0.014	0.184 $\pm$ 0.023	0.886 $\pm$ 0.008
	129.7 $\pm$ 3.3	-0.035 $\pm$ 0.012	0.321 $\pm$ 0.071	0.899 $\pm$ 0.020
	208.5 $\pm$ 2.2	-0.059 $\pm$ 0.022	0.328 $\pm$ 0.117	0.896 $\pm$ 0.028
Plasticised 99PVA	33.1 $\pm$ 3.3	-0.222 $\pm$ 0.056	0.259 $\pm$ 0.035	0.850 $\pm$ 0.059
	65.8 $\pm$ 3.0	-0.199 $\pm$ 0.026	0.238 $\pm$ 0.022	0.848 $\pm$ 0.042
	119.8 $\pm$ 2.1	-0.204 $\pm$ 0.014	0.145 $\pm$ 0.013	0.928 $\pm$ 0.007
	169.2 $\pm$ 4.1	-0.249 $\pm$ 0.029	0.188 $\pm$ 0.023	0.868 $\pm$ 0.030

**Table 10.27.** Fit parameters to Equation 7.1 for spreading of water on the surface of the films of various compositions after storing at 100% RH conditions.

Sample	Thickness ( $\mu\text{m}$ )	k	n	R <sup>2</sup>
87PVA	30.6 $\pm$ 1.9	-0.155 $\pm$ 0.019	0.356 $\pm$ 0.018	0.990 $\pm$ 0.004
	44.5 $\pm$ 3.8	-0.363 $\pm$ 0.073	0.281 $\pm$ 0.036	0.894 $\pm$ 0.043
	87.0 $\pm$ 3.3	-0.379 $\pm$ 0.082	0.296 $\pm$ 0.024	0.948 $\pm$ 0.019
	129.7 $\pm$ 7.6	-0.480 $\pm$ 0.090	0.346 $\pm$ 0.025	0.938 $\pm$ 0.046
Plasticised 87PVA	21.7 $\pm$ 2.7	-0.863 $\pm$ 0.369	0.247 $\pm$ 0.083	0.831 $\pm$ 0.014
	39.3 $\pm$ 5.5	-0.799 $\pm$ 0.096	0.423 $\pm$ 0.050	0.818 $\pm$ 0.152
	73.5 $\pm$ 4.5	-0.890 $\pm$ 0.057	0.354 $\pm$ 0.019	0.953 $\pm$ 0.004
	108.8 $\pm$ 3.0	-1.051 $\pm$ 0.223	0.555 $\pm$ 0.072	0.960 $\pm$ 0.023
99PVA	52.8 $\pm$ 2.3	-0.027 $\pm$ 0.064	0.240 $\pm$ 0.083	0.843 $\pm$ 0.072
	88.3 $\pm$ 4.6	-0.061 $\pm$ 0.053	0.150 $\pm$ 0.038	0.850 $\pm$ 0.089

**Table 10.28.** CA evolution parameters for investigated compositions stored at 4% RH using water as the medium. Symbols represent: CA<sub>0</sub> – initial CA, CA<sub>e</sub> – contact angle at the end of the measurement,  $\Delta$ CA – difference between CA<sub>0</sub> and CA<sub>e</sub>,  $\Delta$ V – change in the droplet volume,  $\Delta$ A – change in the liquid/solid contact area. For mechanisms, A+S stands for absorption and spreading, while S – for spreading (MS indicates mainly spreading). Shaded cells correspond to spin-coated films.

Sample	Thickness ( $\mu\text{m}$ )	CA <sub>0</sub> (°)	CA <sub>e</sub> (°)	$\Delta$ CA (°)	$\Delta$ V ( $\mu\text{l}$ )	$\Delta$ A (mm <sup>2</sup> )	Mechanism
87PVA	30.6 $\pm$ 1.9	62.82 $\pm$ 0.98	54.55 $\pm$ 0.82	-8.27 $\pm$ 1.11	-0.31 $\pm$ 0.01	0.24 $\pm$ 0.06	A+S
	44.5 $\pm$ 3.8	63.33 $\pm$ 0.82	49.35 $\pm$ 2.81	-13.98 $\pm$ 2.32	-0.33 $\pm$ 0.02	1.54 $\pm$ 0.85	A+S
	87.0 $\pm$ 3.3	65.18 $\pm$ 0.80	49.70 $\pm$ 2.89	-15.48 $\pm$ 2.92	-0.32 $\pm$ 0.04	1.40 $\pm$ 0.59	A+S
	129.7 $\pm$ 7.6	69.77 $\pm$ 1.64	47.92 $\pm$ 3.82	-21.85 $\pm$ 4.20	-0.36 $\pm$ 0.04	0.40 $\pm$ 0.10	A+S
Plasticised 87PVA	21.7 $\pm$ 2.7	61.44 $\pm$ 1.97	43.32 $\pm$ 7.61	-18.13 $\pm$ 8.65	-0.22 $\pm$ 0.08	4.89 $\pm$ 3.05	A+S
	39.3 $\pm$ 5.5	59.24 $\pm$ 2.11	36.09 $\pm$ 9.42	-	-0.33 $\pm$ 0.05	8.76 $\pm$ 0.58	A+S
	73.5 $\pm$ 4.5	38.73 $\pm$ 1.61	35.25 $\pm$ 1.57	-3.49 $\pm$ 0.08	-0.31 $\pm$ 0.02	0.15 $\pm$ 0.06	A+S
	108.8 $\pm$ 3.0	39.47 $\pm$ 0.66	36.54 $\pm$ 0.73	-2.93 $\pm$ 0.07	-0.22 $\pm$ 0.06	0.22 $\pm$ 0.09	A+S
99PVA	52.8 $\pm$ 2.3	39.83 $\pm$ 0.84	36.18 $\pm$ 16.94	-3.03 $\pm$ 0.38	-0.25 $\pm$ 0.05	0.21 $\pm$ 0.05	A+S
	88.3 $\pm$ 4.6	41.21 $\pm$ 2.56	34.95 $\pm$ 1.93	-6.26 $\pm$ 1.52	-0.32 $\pm$ 0.01	0.19 $\pm$ 0.01	A+S
	129.7 $\pm$ 3.3	50.42 $\pm$ 3.25	37.78 $\pm$ 3.26	-12.63 $\pm$ 5.89	-0.33 $\pm$ 0.02	0.05 $\pm$ 0.02	A+S
	208.5 $\pm$ 2.2	53.67 $\pm$ 4.64	33.31 $\pm$ 3.32	-20.36 $\pm$ 7.32	-0.29 $\pm$ 0.04	0.16 $\pm$ 0.15	A+S
Plasticised 99PVA	33.1 $\pm$ 3.3	40.31 $\pm$ 1.31	21.72 $\pm$ 1.34	-18.59 $\pm$ 2.45	-0.75 $\pm$ 0.51	4.28 $\pm$ 0.81	A+S
	65.8 $\pm$ 3.0	37.11 $\pm$ 2.40	20.97 $\pm$ 1.54	-16.14 $\pm$ 2.23	-0.27 $\pm$ 0.06	6.78 $\pm$ 1.49	A+S (MS)
	119.8 $\pm$ 2.1	38.46 $\pm$ 0.86	25.78 $\pm$ 0.60	-12.68 $\pm$ 0.94	-0.49 $\pm$ 0.07	3.57 $\pm$ 0.46	A+S
	169.2 $\pm$ 4.1	45.19 $\pm$ 2.10	25.44 $\pm$ 1.03	-19.75 $\pm$ 1.43	-0.32 $\pm$ 0.15	4.62 $\pm$ 0.67	A+S

**Table 10.29.** CA evolution parameters for investigated compositions stored at 45% RH using water as the medium. Symbols represent:  $CA_0$  – initial CA,  $CA_e$  – contact angle at the end of the measurement,  $\Delta CA$  – difference between  $CA_0$  and  $CA_e$ ,  $\Delta V$  – change in the droplet volume,  $\Delta A$  – change in the liquid/solid contact area. For mechanisms, A+S stands for absorption and spreading, while S – for spreading (MS indicates mainly spreading). Shaded cells correspond to spin-coated films.

Sample	Thickness ( $\mu\text{m}$ )	$CA_0$ ( $^\circ$ )	$CA_e$ ( $^\circ$ )	$\Delta CA$ ( $^\circ$ )	$\Delta V$ ( $\mu\text{l}$ )	$\Delta A$ ( $\text{mm}^2$ )	Mechanism
87PVA	30.6 $\pm$ 1.9	64.30 $\pm$ 0.97	53.33 $\pm$ 1.71	-10.98 $\pm$ 1.91	-0.30 $\pm$ 0.03	0.70 $\pm$ 0.16	A+S
	44.5 $\pm$ 3.8	69.08 $\pm$ 2.72	45.83 $\pm$ 2.85	-23.25 $\pm$ 3.65	-0.34 $\pm$ 0.03	1.40 $\pm$ 0.19	A+S
	87.0 $\pm$ 3.3	66.22 $\pm$ 0.98	46.50 $\pm$ 2.45	-19.72 $\pm$ 2.83	-0.35 $\pm$ 0.05	1.03 $\pm$ 0.25	A+S
	129.7 $\pm$ 7.6	64.75 $\pm$ 2.29	42.93 $\pm$ 2.93	-21.82 $\pm$ 3.86	-0.30 $\pm$ 0.03	2.64 $\pm$ 0.82	A+S
Plasticised 87PVA	21.7 $\pm$ 2.7	65.50 $\pm$ 0.76	25.70 $\pm$ 0.59	-39.80 $\pm$ 0.73	-0.02 $\pm$ 0.02	8.62 $\pm$ 0.07	A+S (MS)
	39.3 $\pm$ 5.5	61.69 $\pm$ 1.49	32.84 $\pm$ 2.03	-28.85 $\pm$ 2.41	-0.17 $\pm$ 0.07	9.32 $\pm$ 4.78	A+S (MS)
	73.5 $\pm$ 4.5	56.20 $\pm$ 4.30	32.94 $\pm$ 5.89	-23.26 $\pm$ 10.03	-0.39 $\pm$ 0.15	7.54 $\pm$ 0.24	A+S(MS)
	108.8 $\pm$ 3.0	62.03 $\pm$ 2.70	25.95 $\pm$ 0.58	-36.08 $\pm$ 3.28	-0.36 $\pm$ 0.17	7.16 $\pm$ 0.47	A+S
99PVA	52.8 $\pm$ 2.3	43.11 $\pm$ 0.46	36.90 $\pm$ 0.92	-6.21 $\pm$ 1.16	-0.30 $\pm$ 0.03	0.30 $\pm$ 0.04	A+S
	88.3 $\pm$ 4.6	43.15 $\pm$ 2.07	37.85 $\pm$ 1.83	-5.30 $\pm$ 0.65	-0.32 $\pm$ 0.02	0.35 $\pm$ 0.10	A+S
	129.7 $\pm$ 3.3	43.70 $\pm$ 1.15	39.00 $\pm$ 1.16	-4.70 $\pm$ 0.49	-0.32 $\pm$ 0.01	0.11 $\pm$ 0.04	A+S
	208.5 $\pm$ 2.2	44.77 $\pm$ 0.95	39.04 $\pm$ 1.25	-5.73 $\pm$ 0.97	-0.51 $\pm$ 0.12	0.18 $\pm$ 0.03	A+S
Plasticised 99PVA	33.1 $\pm$ 3.3	35.69 $\pm$ 0.81	21.00 $\pm$ 1.27	-14.69 $\pm$ 1.44	-0.37 $\pm$ 0.10	6.10 $\pm$ 1.05	A+S
	65.8 $\pm$ 3.0	33.13 $\pm$ 1.63	17.82 $\pm$ 0.57	-15.31 $\pm$ 1.66	-0.33 $\pm$ 0.10	6.53 $\pm$ 0.23	A+S
	119.8 $\pm$ 2.1	38.61 $\pm$ 1.08	26.69 $\pm$ 0.62	-11.91 $\pm$ 1.25	-0.38 $\pm$ 0.03	3.14 $\pm$ 0.44	A+S
	169.2 $\pm$ 4.1	40.62 $\pm$ 1.57	23.93 $\pm$ 1.17	-16.69 $\pm$ 1.17	-0.43 $\pm$ 0.08	4.72 $\pm$ 0.75	A+S

**Table 10.30.** CA evolution parameters for investigated compositions stored at 100% RH using water as the medium. Symbols represent:  $CA_0$  – initial CA,  $CA_e$  – contact angle at the end of the measurement,  $\Delta CA$  – difference between  $CA_0$  and  $CA_e$ ,  $\Delta V$  – change in the droplet volume,  $\Delta A$  – change in the liquid/solid contact area. For mechanisms, A+S stands for absorption and spreading, while S – for spreading (MS indicates mainly spreading). Shaded cells correspond to spin-coated films.

Sample	Thickness ( $\mu\text{m}$ )	$CA_0$ ( $^\circ$ )	$CA_e$ ( $^\circ$ )	$\Delta CA$ ( $^\circ$ )	$\Delta V$ ( $\mu\text{l}$ )	$\Delta A$ ( $\text{mm}^2$ )	Mechanism
87PVA	30.6 $\pm$ 1.9	71.18 $\pm$ 1.86	34.48 $\pm$ 1.43	-36.69 $\pm$ 2.98	-0.16 $\pm$ 0.18	4.32 $\pm$ 0.76	A+S
	44.5 $\pm$ 3.8	82.12 $\pm$ 3.43	28.85 $\pm$ 2.44	-53.27 $\pm$ 4.46	-0.66 $\pm$ 0.39	8.45 $\pm$ 1.35	A+S
	87.0 $\pm$ 3.3	76.57 $\pm$ 3.69	36.30 $\pm$ 2.08	-40.27 $\pm$ 2.55	-0.49 $\pm$ 0.26	4.00 $\pm$ 0.31	A+S
	129.7 $\pm$ 7.6	77.43 $\pm$ 0.94	33.37 $\pm$ 1.21	-44.06 $\pm$ 0.28	-0.32 $\pm$ 0.31	6.97 $\pm$ 1.26	A+S
Plasticised 87PVA	21.7 $\pm$ 2.7	71.24 $\pm$ 8.76	15.65 $\pm$ 1.65	-67.98 $\pm$ 19.49	-6.14 $\pm$ 4.51	28.73 $\pm$ 2.86	A+S
	39.3 $\pm$ 5.5	85.14 $\pm$ 9.13	33.83 $\pm$ 13.27	-51.31 $\pm$ 7.43	-1.04 $\pm$ 0.52	12.64 $\pm$ 4.82	A+S
	73.5 $\pm$ 4.5	74.27 $\pm$ 9.55	11.38 $\pm$ 1.94	-62.89 $\pm$ 7.78	-0.93 $\pm$ 0.43	24.89 $\pm$ 1.76	A+S
	108.8 $\pm$ 3.0	62.43 $\pm$ 1.39	17.36 $\pm$ 5.25	-45.07 $\pm$ 3.89	-1.16 $\pm$ 0.33	7.27 $\pm$ 0.08	A+S
99PVA	52.8 $\pm$ 2.3	42.69 $\pm$ 3.19	30.68 $\pm$ 7.35	-12.00 $\pm$ 10.40	-0.15 $\pm$ 0.07	0.17 $\pm$ 0.12	A+S
	88.3 $\pm$ 4.6	33.57 $\pm$ 2.11	29.57 $\pm$ 3.14	-4.00 $\pm$ 3.15	2.36 $\pm$ 0.45	4.76 $\pm$ 0.86	A+S

## Appendix E – Migration of molecules from adjacent media into PVA-based films

### E1. Introduction

In a single-dose detergents, PVA films containing multiple additives are exposed to complex, non-aqueous solution containing multiple surfactants and water.<sup>447</sup> Migration of these components into the polymer film are liable to cause detrimental changes in film properties over time, leading to consumer dissatisfaction and decreased product shelf-life.

The non-aqueous nature of the surfactant solution encapsulated in single-dose detergents prevents polymer dissolution before use. Other desired properties for the solvent include:

- low-polarity (to prevent PVA swelling or dissolution),
- reasonably high  $M_w$  (to prevent excess infiltration into the film),
- non-toxicity,
- commercial viability (reasonably low price, non-corrosive etc).

Single-dose detergent manufacturers (i.e. Monosol and P&G),<sup>81,447–449</sup> typically use a range of solvents including glycol molecules, their homologues and derivatives, and aliphatic fatty acids. Key to this chapter, these solvents must dissolve the two studied surfactants: anionic SDS and cationic CTAB. Nonionic  $C_{12}E_{10}$  was not considered due to the high surfactant concentrations required to alter film morphology compared to ionic surfactants (Chapter 5).

In this appendix, preliminary findings on z-migration from adjacent non-aqueous liquid media to PVA-based films are presented. First, solvent selection is performed to find compounds which will dissolve the studied surfactants while also fitting the criteria listed above. Then, preliminary investigation into the use of Raman spectroscopy and AFM to study surfactant infiltration are shown.

## **E2. Materials and methods**

2-ethoxyethanol, ethylene glycol, dipropylene glycol, PEG 200, butyl carbitol, 2-methyl-1-propanol, 2-butanone, 2-undecanone, oleic acid, and vegetable oil (Sainsbury's PLC, UK) were purchased and used as received. To prepare solution cast films to analyse z-migration from adjacent media to the PVA-based formulation, various volumes of solutions were used (up to 35 ml) that were prepared in the vacuum oven overnight (conditions as described in Chapter 2). The solvent library was chosen according to those used in references 447,448,450.

To test surfactant solubility (either SDS or CTAB, Chapter 2), 0.5 g of surfactant was mixed with 50 ml of solvent of choice. Upon complete dissolution detected by visual inspection, additional 0.5 g was added until the solubility limit was reached. AFM (procedure described in Chapter 2) and Raman spectroscopy (*vide infra*) were used.

### **E2.1. Raman spectroscopy**

#### **Operating principle**

Raman spectroscopy is a vibrational spectroscopy method similar to FTIR. However, unlike FTIR, Raman spectroscopy is not based on the changes in the dipole moments, but on the changes in a molecular bond polarizability. Therefore, Raman will show the presence of the samples with symmetric bonds only (i.e. homonuclear bonds).

The main difference in the operating principle of Raman spectroscopy compared to FTIR spectroscopy is the fact that the former looks at light scattering, not absorption. When light of a given frequency interacts with a sample, it is possible for the bonds to change their vibrational energy level, resulting in the emission of a photon of different energy compared to the photon that interacted with the sample (Figure 10.14). This difference in energies is called the Raman shift and results in the Raman spectrum. Therefore, it is possible to obtain



information about lower frequency modes, together with information about molecular backbone structure and crystal lattice.

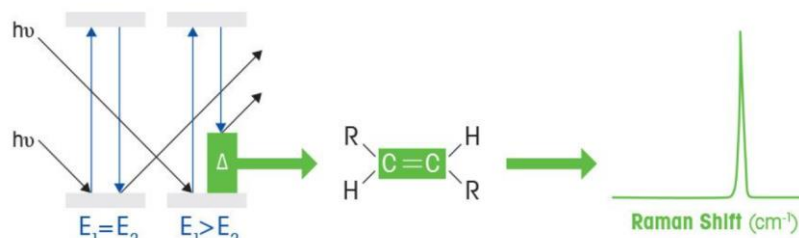


**Figure 10.14.** Raman spectroscopy operating principle. Reproduced from reference 451.

### Experimental procedure

Raman measurements were used for an investigation into surfactant migration from liquid adjacent medium to the PVA-based film, assessing the effectiveness of different experimental arrangements and technique spatial resolution. Raman measurements were performed on Renishaw inVia Qontor Raman Microscope. A 532 nm laser at 60% power was used, with spectra recorded from  $4000 \text{ cm}^{-1}$  to  $300 \text{ cm}^{-1}$  to identify the peaks characteristic for given species. Baseline correction was performed as described in Chapter 2 for FTIR spectrum analysis.

## E3. Results and discussion

### E3.1. Non-aqueous solvent selection

To investigate surfactant infiltration into PVA films from non-aqueous media, two criteria of each solvent were necessary: dissolving the surfactant, and not infiltrating into the PVA film itself. Based on a preliminary dissolution study (where dissolution was defined as a solubility equal or higher than 1 g/100 ml), the investigated solvents were divided into four groups:

- Dissolves both SDS and CTAB: 2-ethoxyethanol, ethylene glycol.

- Dissolves SDS: dipropylene glycol, poly(ethylene glycol) 200 (PEG 200), Butyl carbitol.
- Dissolves CTAB: 2-methyl-1-propanol.
- Dissolves neither CTAB nor SDS: 2-butanone, 2-undecanone, oleic acid, vegetable oil.

After initial identification of solvents, swelling tests were performed. Solution-cast PVA thick films (ca. 100  $\mu\text{m}$ ) were cut into rectangles and placed into a given solvent. Then, gravimetric analysis was performed to investigate film mass changes over time (Figure 10.15).

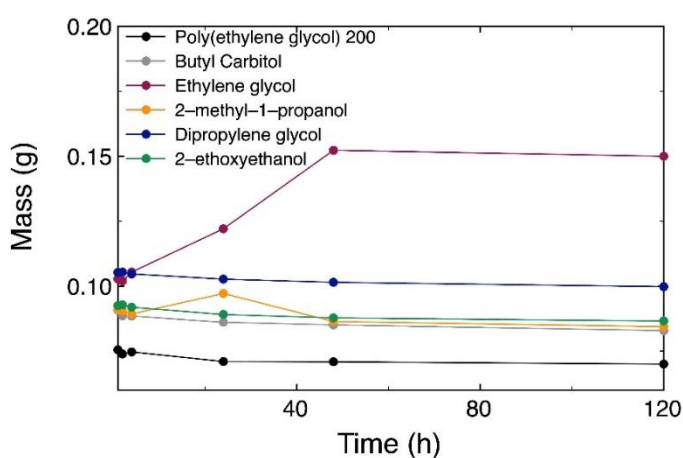


**Figure 10.15.** Mass change over time for PVA films stored at various solvents.

From the swelling tests, ethylene glycol was discarded as it was the only candidate solvent which led to a permanent increase in film mass (likely due to its smaller  $M_w$  than other solvents tested). For other solvents, a small decrease in film mass over time was recorded. This is either a consequence of slight dissolution of the film in the solvent or abrasion during drying with a tissue prior to weighing. Further, despite acceptable swelling behaviour, 2-ethoxyethanol was discarded as a candidate solvent due to safety concerns (i.e. toxicity upon inhalation).

From these initial tests, 2-methyl-1-propanol was chosen as the best solvent for CTAB (solubility ca. 3 g/100 ml), while PEG 200 was the best solvent for SDS (solubility ca. 19 g/100 ml), with butyl carbitol showing second best performance (solubility ca. 5 g/100 ml).

Films were proven to be in their original form after 9 months of storage in solvent of choice, despite smaller  $M_w$  of the solvent compared to some industrially applied counterparts.

### **Raman spectroscopy**

Following the identification of good solvents, measurements of surfactant infiltration into the film were performed using confocal Raman spectroscopy. Initial spectra of pure components (PVA, surfactant, and solvent) and surfactant solutions were recorded to identify characteristic peaks for each compound (Figure 10.16), with the intention of scanning the film at constant increments in the z-direction to identify surfactant presence.

From the spectra presented, there is a significant overlap between peaks corresponding to the surfactants, polymer, and solvents. It is suggested that using deuterated surfactant could address the challenge identified above by shifting its characteristic peak away from those of the solvent or polymer, enabling z-migration to be measured from adjacent solvent to the PVA film. However, due to the COVID-19 pandemic these measurements could not be continued.

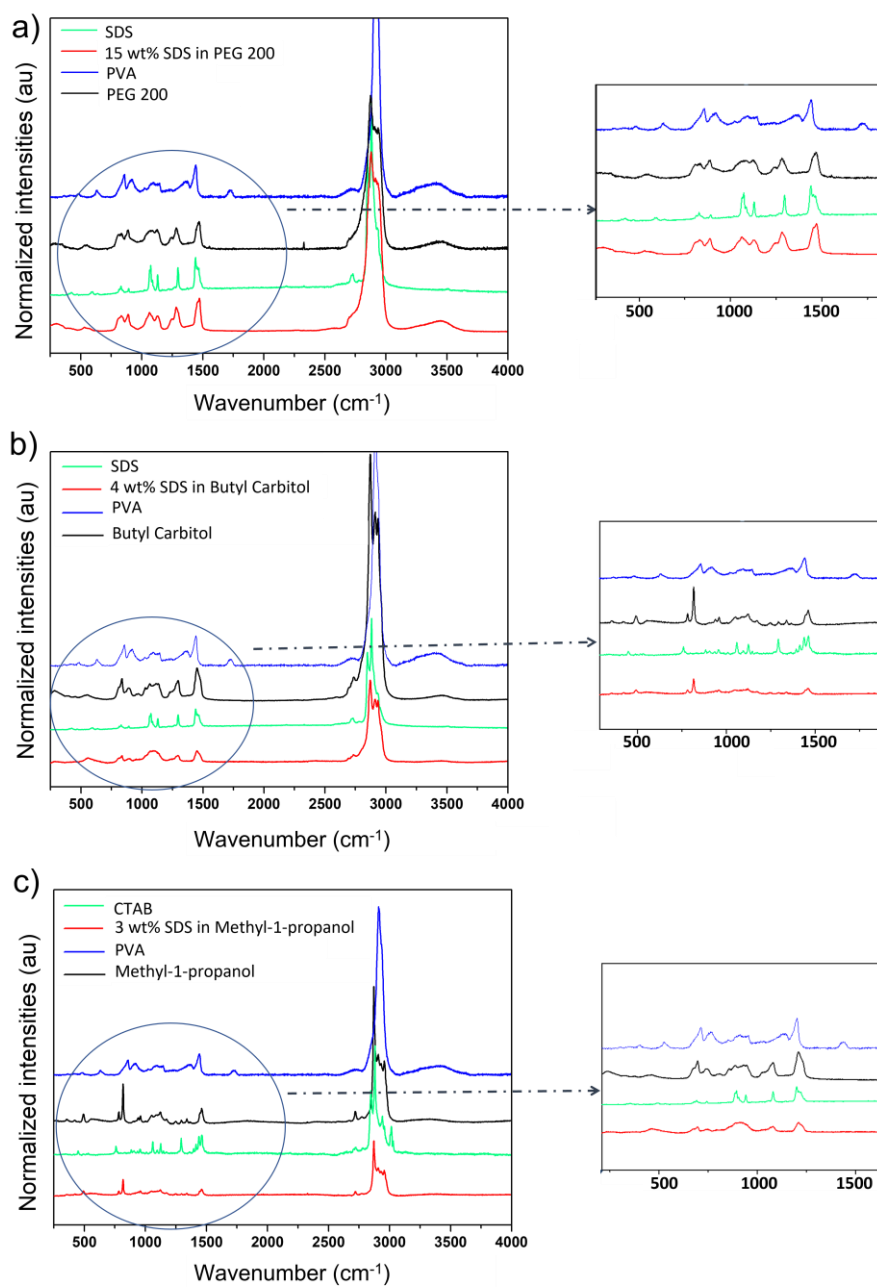


**Figure 10.16.** Raman spectra for pure components (solvent, PVA film and surfactant) and solutions of surfactant in non-aqueous solvent for investigated compositions.

### E3.2. AFM investigations of surfactant and solvent infiltration

Because of the described challenges to using confocal Raman spectroscopy, investigations were performed using AFM, with imaging as an indication of the surfactant migration. As shown in Chapters 5 and 6, it is possible to establish an insight into migration kinetics by

investigating morphology changes as a result of surfactant migration. To ensure constant contact of film and solvent, the film was fixed (using insulation tape) to one of four substrate geometries:

- 1. PVA-based film placed on glass slide** wetted with droplet (15  $\mu\text{l}$ ) of the non-aqueous surfactant solution. Because of the low fluid volume, liquid was nonuniformly distributed on the slide and tended to accumulate in one place, creating folds in the film.
- 2. PVA-based film placed on a concave glass slide** in contact with liquid (30  $\mu\text{l}$ ). In this case, an air bubble invariably formed when placing the film upon the slide, leading to uneven film surface hence nonuniform film-liquid contact. Moreover, the lack of a solid glass substrate for the film led to issues during AFM imaging, as pressure from the AFM tip would cause movement of the fluid underneath the film, spreading the liquid across the remainder of the glass slide.
- 3. PVA-based film placed on a Teflon well.** Similar in concept to the concave glass slide, here the well was deeper enabling more liquid to be used (500  $\mu\text{l}$ ). While the same problems were encountered as with the concave glass slide (bubble formation, non-uniform surface level), because of the larger liquid reservoir the bubble did not move during AFM imaging (and regions near the bubble could be avoided), leading to a more stable system.
- 4. PVA-based film placed on an upturned UV cuvette.** This geometry led to creation of liquid-solid interface without presence of bubbles and overall provided the best results. Before imaging, the film was removed from the cuvette and placed on glass slide, sealed with insulation tape and imaged.

Investigations were focused on the influence of sample thickness (films prepared from PVA solutions of various concentration and volume), and composition (fully- and partially

hydrolysed PVA, unplasticised or with the addition of plasticiser at weight ratios of 10 and 20 wt%). To control against infiltration of solvent molecules, control samples (PVA-based films in contact with non-aqueous solution without addition of surfactant) were prepared and investigated in parallel to samples adjacent to surfactant solution. As higher concentration of surfactant is expected to lead to faster migration, compositions with the addition of SDS were chosen (with SDS content equal to 15 wt%). Concentration of 3 wt% for CTAB required a long time for morphology changes to appear for thin, spin-coated films (Chapter 5), therefore, for thick films that time is likely to be further extended.

For all investigated geometries and compositions, no clear dependence of film thickness nor liquid volume adjacent to the film (for geometry with UV cuvette) on film morphology were observed despite the range of thicknesses investigated (from ca.  $17.0 \pm 0.5 \mu\text{m}$  to  $123.0 \pm 0.5 \mu\text{m}$ ). Changes were, however, dependent on the film composition – both DH and glycerol addition. Partially hydrolysed PVA created macroscopically uniform films, with a surface morphology similar to that reported for films cast on glass substrate (Chapter 7, Figure 7.1), with depressions created on some films (Figure 10.17m,n, also observed in thick films investigated in Chapter 7). However, from day 0, greater surface roughness was observed than was found in previously discussed formulations (e.g.  $R_q = 7.2 \pm 0.8 \text{ nm}$  compared to values below 1 nm for films described in Chapter 7). Given the lack of time for migration, it is expected that these changes in roughness are connected with any instability in the film surface that, in most cases, is in contact with liquid reservoir hence is sensitive to cantilever movement. Alternatively, it may be due to scaling up of the solution-casting procedure for these films – from a volume of 800  $\mu\text{L}$  to ca. 20 mL in this chapter.  $R_q$  values further increased upon contact with adjacent medium (Figure 10.17i-l).

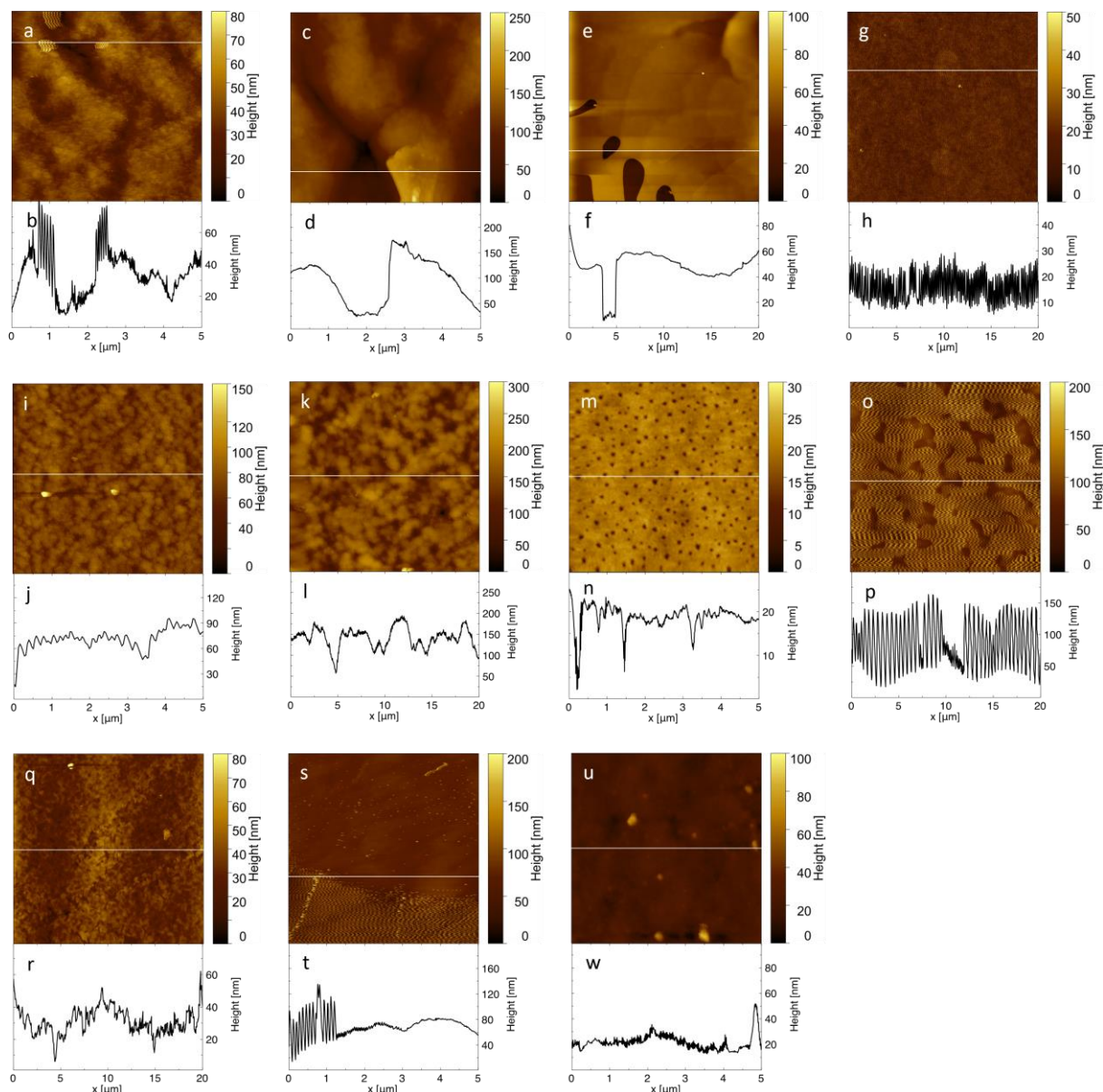


**Figure 10.17.** AFM images and surface profiles of 87PVA-based films in contact with non-aqueous solvent (control samples): (a,b) regions rich in non-aqueous solvent, day 3; (c,d) PVA plasticised with 20 wt% glycerol, day 4; (e,f) polymer film on glass slide following drying, day 7; 87PVA-based films in contact with non-aqueous surfactant solution: (g,h) regions rich in non-aqueous surfactant solution for sample on day 1; (i,j) modified background film structure of PVA+10% glycerol structure on day 2; (k,l) plasticised PVA structure visible on day 2 following drying; (m,n) depressions visible for some PVA films on day 6; (o,p) PVA plasticised with 10% glycerol on glass slide, day 6; (q,r,s,t) PVA sample on glass slide, day 7; (u,w) morphology of PVA films on day 21.

Investigations into migration kinetics of surfactant from adjacent medium to the film were hindered by the migration of the solvent through the film, leading to accumulation on the opposite surface. Indeed, this phenomenon was observed after 3 days for non-plasticised PVA control sample (Figure 10.18a, Figure 10.17a,b) and 4 days for sample in contact with surfactant

solution (Figure 10.17g,h). For plasticised samples, these changes were seen from day 2 (Figure 10.17c,d). After storage time of 6 days, for some investigated formulations wetting structures (Figure 10.17o,p) are seen which, have also been observed for formulations described in Chapter 6. Here, they correspond to the presence of PEG 200 on the film surface.

Following drying of the solvent from the surface, no significant morphology changes were observed at microscopic level (Figure 10.17k,l), although they would be expected from inspection of macroscopic images (Figure 10.18b). After drying, in some positions the solvent was still visible (striped pattern in Figure 10.17s,t), which in general did not enable imaging (due to the viscosity of the liquid and incomplete coverage of the surface). Even after drying the solvent from the surface and aging for 23 days, no evidence of surfactant migration (i.e. blooming) was observed (Figure 10.17u,w) for both plasticised and unplasticised PVA films. For some samples, changes correlated with surfactant presence were noted (bloom-like features in Figure 10.17o-r). However, it is not clear if this is a result of migration of surfactant itself or morphological changes as a result of contact with liquid (like these in Figure 10.17e,f).

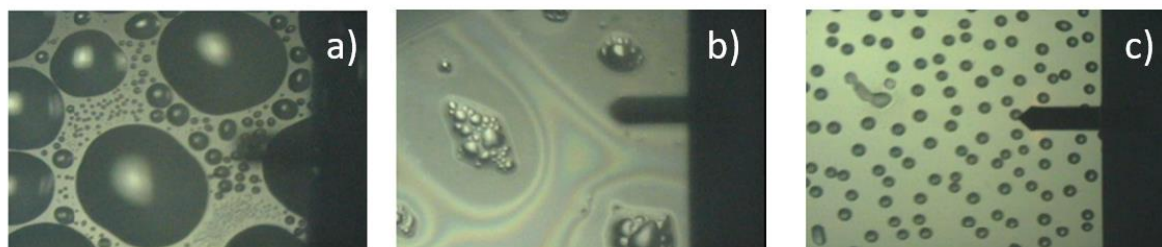


**Figure 10.18.** Images from the optical microscope connected to the AFM instrument: (a) solvent visible on the surface of the sample, (b) surface features after drying the film surface with compressed air, and (c) morphology of the film created from fully hydrolysed PVA. The length of the protruding cantilever is ca. 125  $\mu\text{m}$ .

Similar results were observed while imaging films prepared from fully hydrolysed PVA solutions. After two weeks, morphologies that can be correlated with surfactant presence were identified (Figure 10.19g,h). However, these could not be deconvoluted into surfactant migration or solvent migration. Further, these surface features were not consistent, only



appearing on some of the formulations. Films prepared from 99PVA can be characterised by wetting structures covering the macroscopic morphology (Figure 10.18c). They remained unchanged after drying the film, indicating that they are bubbles within the film structure rather than water droplets on the surface. Therefore, these microstructures were avoided during AFM imaging. Moreover, while removing cut films from the surface they were less opaque compared to counterparts of lower RH and were visibly wet regardless of drying times or temperature (always below  $T_m$  for plastic petri dish).

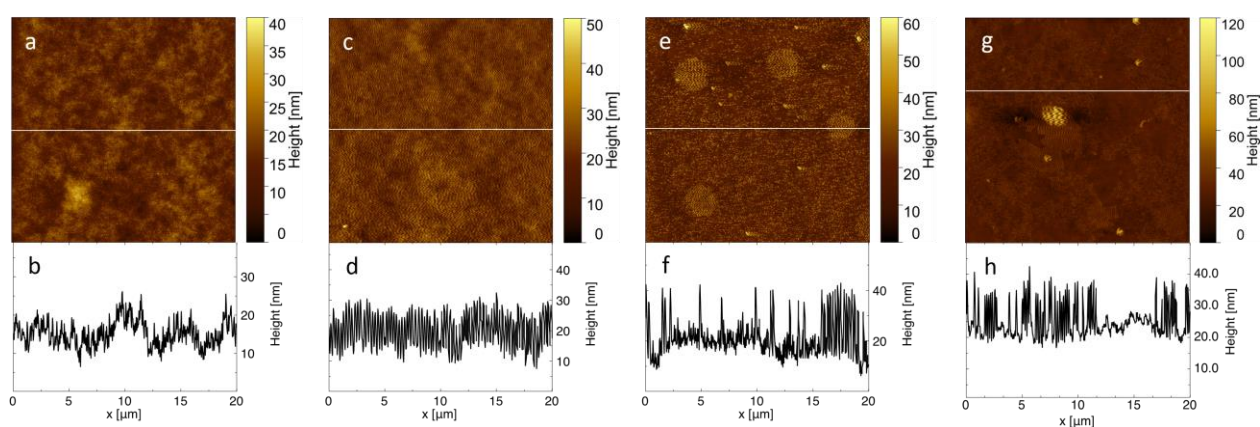


**Figure 10.19.** AFM images and surface profiles of 99PVA-based films in contact with non-aqueous solvent with 15 wt% SDS addition: (a,b) background plasticised PVA structure visible for samples without any morphological changes recorded after film drying on day 3; (c,d) background plasticised PVA morphology influenced by presence of non-aqueous solvent after film drying on day 3; (e,f) regions rich in non-aqueous solvent on day 7; (g,h) surface features visible for non-plasticised PVA after 2 weeks of aging (Teflon well).

Timescales for solvent diffusion in non-plasticised films prepared from fully hydrolysed PVA were more varied than those for partially hydrolysed PVA – the first changes in morphology appeared after 2 to 7 days of exposure for the former group compared to between 4 and 7 days for the latter. As entanglement and crystallinity are expected to be higher in the 99PVA system, this result is rather surprising. However, considering different behaviour of films after preparation, remaining water in the system for these formulations and surface features (representing differences in molecular arrangement) may be responsible for these changes. Upon introducing glycerol to the film, the solvent created a thin layer on the surface

of the film from day 2 for control sample and day 3 for samples containing SDS. Overall, after drying samples with compressed air, no morphology changes that were correlated with presence of surfactant (i.e. blooms) were noted (Figure 10.19a,b), while partial surface coverage of solvent molecules remained (Figure 10.19c,d). Similar to samples prepared from 87PVA, the presence of the solvent in the film is highlighted by regions with characteristic high-viscosity structures, observed for both control samples and samples with the addition of SDS in adjacent solvent (Figure 10.19e,f).

In general, samples in contact with solvent containing SDS show longer migration times (e.g. first changes visible on day 4 for unplasticised PVA film cf. day 3 for the control samples). This suggests that the main migrating species is the solvent. This can be explained as the solvent treating PVA as a weakly-interacting porous matrix of capillaries to flow through, while SDS diffusion through the film is affected by compatibility, surfactant-polymer interactions and free volume in the system. It is furthermore suggested that SDS (itself with a higher  $M_w$  than PEG 200) creates complex-like structures with PEG molecules, and because of its larger size compared to pure solvent (both complexed and uncomplexed), longer diffusion times are required. Finally, due to the high excess of solvent compared to SDS, no pure surfactant (e.g. through the formation of blooms) could be identified. These findings underline the importance of including reinforcement additives in PVA formulations and applying solvent of higher  $M_w$ , as solvent migration through the film is an undesired property for a consumer product.

#### **E4. Conclusions**

In this study, infiltration of surfactants into PVA films from non-aqueous solutions was studied to investigate migration timescales in systems mimicking the detergent solutions within a laundry pod. Solvents were selected based on their surfactant dissolution capability, retention

of PVA film structure, and safety. Accordingly, CTAB solutions in 2-methyl-1-propanol and SDS solutions in PEG 200 were used.

Infiltration in the z-direction was initially measured using confocal Raman spectroscopy, however it was impossible to deconvolute the individual components from the recorded spectra. To avoid these issues, it is suggested that confocal Raman measurements with deuterated surfactants (and possibly solvents) should be introduced in further studies. Moreover, as addition of glycerol significantly reduces migration time, continuous measurements may be necessary in future studies, accounting for uneven film surface (as a result of contact with liquid) and ensuring sealed connection with mould (e.g. a PDMS mould).

AFM imaging was then used to observe morphological changes on the film surface during infiltration. In all cases, the solvent migrated through the film, necessitating drying prior to imaging. From the resultant optical microscope images, it was concluded that surfactant migration occurred in parallel with solvent migration. Therefore, a complete understanding of infiltration cannot be gained by considering surfactant migration alone.

Lastly, presented results show the importance of reinforcements and other additives in the system. Given that PEG is used with satisfactory results in industrial formulations in contrast with the findings of this study (although usually of  $M_w$  of 300 or higher), more complex systems should be studied to avoid overly quick timescales of solvent migration.